
Aus der Klinik und Poliklinik für Orthopädie, Physikalische Medizin und Rehabilitation

der Ludwig-Maximilians-Universität München

Direktor: Prof. Dr. Dipl.-Ing. Volkmar Jansson

**Biomechanical Evaluation of Glenoid Component Stability
After ATSA Under Phasic Cyclic Loading**

Dissertation

zum Erwerb des Doktorgrades der Medizin

an der Medizinischen Fakultät der

Ludwig-Maximilians-Universität zu München

vorgelegt von

Mohamed Mahmoud

aus Sharkia/Ägypten

2018

Mit Genehmigung der Medizinischen Fakultät
der Universität München

Berichterstatter: Prof. Dr. med. Matthias Pietschmann

Mitberichterstatter: Prof. Dr. med. Rüdiger von Eisenhart-Rothe
Prof. Dr. med. Stefan Milz

Mitbetreuung durch
den promovierten Mitarbeiter: Dr. PhD. Yan Chevalier

Dekan: Prof. Dr. med. dent. Reinhard Hickel

Tag der mündlichen Prüfung: 20.12.2018

**قل إن صلاتي ونسكي ومحياي ومماتي لله رب
العالمين لا شريك له وبذلك أمرت وأنا أول
المسلمين**

To

*my dear parents, my dear brother Tariq, my
lovely sister Mayada and my beautiful niece
Mariam with my love and gratitude*



Prof. Dr. Themistocles Gluck (1853-1942)

The First Arthroplasty Surgeon & the Designer of First Shoulder Prothesis (DOI: 10.1007/s11999-011-1836-8) & (DOI: 10.1007/s11999-011-1837-7).

“...going through life, the surgeon is always motivated and guided by the wish to alleviate suffering and to avert danger and on occasion is encouraged, by means of a new interpretation of known scientific facts, usually not previously discussed and therefore not utilized for a long time and facts with meaning that should not be underestimated.”

T. Gluck

27 SECEC-ESSE
CONGRESS

EUROPEAN SOCIETY FOR SURGERY
OF THE SHOULDER AND THE ELBOW



BERLIN 2017 • GERMANY • SEPTEMBER 13-16

Berlin, 16th September 2017

The Scientific Committee of the **27th Congress of the European Society for Surgery of the Shoulder and the Elbow** held in Berlin, September 13-16, 2017

CERTIFIES THAT

the following eposter has been accepted and presented at the Congress

Biomechanical Evaluation In Cyclic Loading After Total Shoulder Athroplasty

Inês Santos, Mohamed Mahmoud, Christoph Thorwächter, Antoine Bourgeois, Peter E. Müller, Matthias F. Pietschmann, Yan Chevalier

Department of Orthopedic Surgery, Physical Medicine and Rehabilitation, University Hospital of Munich (LMU), Munich, Germany

Markus Scheibel
Congress President

Roger Emery
President of SECEC-ESSE



www.secec.org

BIOMECHANICAL EVALUATION IN CYCLIC LOADING AFTER TOTAL SHOULDER ARTHROPLASTY

Inês Santos (1), Mohamed Mahmoud (1), Christoph Thorwächter (1), Antoine Bourgeois (1), Peter E. Müller (1), Matthias F. Pietschmann (1), Yan Chevalier (1)

1. Department of Orthopedic Surgery, Physical Medicine and Rehabilitation, University Hospital of Munich (LMU), Germany

Introduction

While total shoulder arthroplasty (TSA) is a generally successful procedure, glenoid loosening remains a common complication. Though the occurrence of loosening was related to patient-specific factors [1], biomechanical factors related to implant features may also affect the fixation of the glenoid component [2, 3], in particular, increased glenohumeral mismatch that could result in eccentric loads and translations [4]. In this study, a novel test setup was used to quantify glenohumeral pressures for different motion patterns after TSA.

Methods

Six cadaveric human shoulders were implanted with total shoulder replacements (Exactech, Inc., USA) and subjected to cyclic internal-external (IE), flexion-extension (FE) and abduction-adduction (AA) rotations in a passive motion testing apparatus (Figure 1). The system was coupled to a pressure sensor system (Tekscan, Inc., USA) to acquire joint loads and to a Zebris system (Zebris Medical, GmbH, Germany) to measure joint kinematics. The pressure sensor was placed within the joint and sutured to the surrounding soft tissue to allow the mapping of pressure distribution along the glenoid surface during motion. The specimens were subjected to a total of 2160 cycles and peak pressures were compared for each motion pattern.

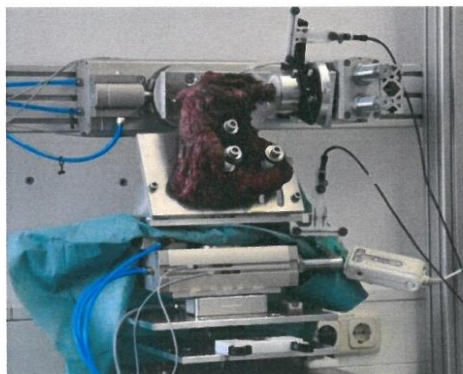


Figure 1: Passive motion testing apparatus: internal-external, flexion-extension and abduction-adduction motions are induced at the glenohumeral joint while maintaining passive muscle loads and glenohumeral contact force.

Results

It was shown that during abduction the contact area between the humeral head and the glenoid component shifts from a posterior to an anterior position, while also moving inferiorly (Figure 2). For IE rotation a mean peak pressure of 8.37 ± 0.22 MPa was registered, while for FE a pressure of 9.37 ± 0.38 MPa and for AA a pressure of 9.88 ± 0.07 MPa were obtained (Figure 3).

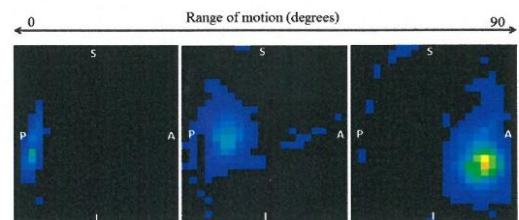


Figure 2: Abduction motion pattern in the glenoid surface recorded with the pressure sensor (A: anterior; P: posterior; S: superior and I: inferior positions).

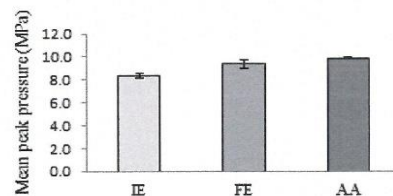


Figure 3: Mean peak pressures (MPa) for each motion.

Discussion

This study showed how glenohumeral pressures after TSA vary during simulated internal-external, flexion-extension and abduction-adduction rotations in a cyclic testing setup. It showed that peak loads are mainly obtained in abduction, and that these occurred mainly near the anterior part of the glenoid. Future steps involve implantation of other type of anatomical glenoid components to obtain different levels of glenohumeral mismatch and relating the 3D measurements of motion patterns to contact pressures.

References

1. Stroud et al, J Should El Surg, 22:1573-1579, 2013.
2. Terrier et al, Clin Biomech, 20:710-7, 2005.
3. Zhang et al, J Should El Surg, 22:350-356, 2013.
4. Patel et al, J Should El Surg, 23:1831-1837, 2014.



ABSTRACT

a. Background

Total shoulder arthroplasty (TSA) is considered a successful curative procedure for many stiff painful shoulder disorders. However, it may be associated with many complications. Glenoid loosening is thought to be the most common complication of anatomic total shoulder arthroplasty (ATSA); its underlying causes could be *mechanical* (*abnormal loading*), *septic* (*infections*) or *aseptic* (*autoimmune reaction*). This study discusses the mechanical glenoid component loosening after ATSA.

b. Hypotheses (Hi, Hii & Hiii)

(*Hi*) The recorded mean peak pressure values of the ATSA components are expected to vary greatly according to the motion type; (*Hii*) the recorded mean peak pressure values are expected to vary between the initial and final phases of each tested specimen; and (*Hiii*) the occurrence of glenoid component loosening and its degree of extension are expected to be related to the changes of the obtained mean peak pressure values.

c. Objectives

This study's aim was to conduct a comprehensive experimental biomechanical evaluation of the stability of ATSA components under phasic cyclic loading, as follows: (*i*) testing of the degree of artificial glenoid component stability under repetitive phasic cyclic loading; (*ii*) testing of the relation between the criteria of the applied cyclic loading according to our testing plan and the occurrence of glenoid component loosening; (*iii*) measurement and assessment of the values, patterns and magnitudes of the contact pressure between the joint components under cyclic loading; (*iv*) comparison between the obtained mean peak contact pressure values under cyclic loading in the initial and final phases to detect any relations and/or differences; (*v*) correlation of the measured pressure values during testing with the QCT findings with respect to glenoid component loosening.

d. Materials

A series of six fresh-frozen complete cadaveric shoulder joint specimens (*bones and soft tissues*) was used in this study. The specimens were implanted with ATSA components and tested successively by mounting them on the shoulder simulator. To measure the values mentioned above, we used a TekScan system with a group of two-headed pressure sensor foils, QCT, shoulder pointer and a digitalized 3D-imaging Zebris system with US, in addition to the routinely used surgical and lab instruments in such experiments.

e. Methodology

The specimens were scanned prior to experimentation to evaluate their articular surfaces morphology. Then the specimens were implanted with ATSA components and a pressure sensor was inserted within the joint cavity of each specimen and situated on the glenoid component surface. The six specimens were successively mounted on the shoulder simulator and each was tested through three phases of cyclic loading in the three directions of motion. The 1st and 3rd short phases took place for each specimen with insertion of a pressure sensor within the joint cavity, while the 2nd long phase took place without sensor insertion. After the completion of all experiments, the specimens were again scanned with QCT to evaluate the position of the implanted glenoids and any presence of radiolucency and/or loosening.

f. Findings (Observations & Examinations)

Two specimens were severely unstable during testing, even with the application of lower loads, particularly during abduction/adduction motion cycles. Provisional and/or subsequent controlling physical examinations revealed either a malposition of the glenoid component or a suspected abnormal glenoid morphology. The other four specimens were completely stable during testing in all motion directions with the application of different loading forces and stabilizing weights. Four specimens were radiologically determined to have a massive glenoid component loosening after the completion of testing.

g. Results

The recorded mean peak pressure values varied greatly between the testing phases, testing cycles and motion directions. The highest mean peak pressure values were recorded during AA testing episodes, followed by FE testing episodes. The lowest mean peak pressure values were recorded during IE testing episodes. However, high mean peak pressure values were also recorded during IE testing episodes, but with a low frequency. In seven testing episodes, the recorded mean peak pressure values were higher by 16.7 % in all directions of motion in the final testing phase than those recorded in the initial phase of all testing episodes (*42 testing episodes*). According to the computed t-test values between the initial and final phases per motion direction/per specimen, null hypothesis (*Hypothesis (Hii)*) was accepted in the whole AA & FE testing cycles with a percentage of 100%, while it was rejected in only one relation of IE testing cycles with a percentage of 5% and accepted in six relations of IE testing cycles with a percentage of 95%. In total, null hypothesis (*Hypothesis (Hii)*) was rejected in only one relation of the testing cycles, with a percentage of 5%, and accepted in twenty relations of the testing cycles with a percentage of 95%. According to the calculated t-test values between all initial and final phases for each specimen, null hypothesis (*Hypothesis (Hii)*) was rejected in two experiments with a percentage of 28.6% and accepted in five experiments with a percentage of 71.4%. Four specimens (*three keeled and one pegged*) were found to be loose, representing 66.7% of all specimens; one of them was unstable during the testing, representing 25% of the loose specimens and 16.7% of all specimens.

h. Conclusion

The recorded mean peak pressure values and load quantities of the tested shoulder joint varied greatly between motion phases, motion cycles and motion types. The resulting contact pressures across the shoulder joint during its action varied greatly according to the acting force, motion type, muscles status and pathologies within the joint and were directly proportional to the motion type, being higher during AA and FE motion cycles than during IE motion cycles. Also, they were directly proportional to the contact surface area and to the degree of compression between joint articulating surfaces during motion. The greatest degree of variability of SD and mean peak pressure values was seen during FE testing cycles.

Shoulder joint instability after ATSA could result from component malposition and/or the articular surface morphological abnormalities. Both glenoid loosening and joint instability could incite the occurrence of the other and could worsen its course in a devastating vicious circle. We concluded that glenoid component loosening could be related to joint stability, loads and the mode of load application in relation to the application duration, and to some extent to the component type, which was apparently evident in our study. The first and third hypotheses were approved, while the second hypothesis was statistically rejected (*according to the computed t-test values*), which may require a further evaluation in future studies.

i. Keywords

Shoulder joint, instability, component loosening, cyclic loading, shoulder simulator, ATSA, Zebris system, complications, Tekscan, pressure sensor, dynamic stabilizers, static stabilizers, biomechanics, articular surfaces, conformity, mismatch, radiolucency, loosening, t-test values, component failure, SD, mean peak pressure values, data analysis.

ACKNOWLEDGEMENT

Completion of this doctoral thesis and its submission to the dean's office of the faculty of medicine of LMU is the fruit of the unlimited help and support of many people, who have done their best during the last three years to make this research possible and real.

First of all, I would like to express my great gratitude and my deep thanks to my dear family: my father, my mother and my siblings (Tariq and Mayada), for their patience and continuous support. Really, their determination and support, following the help of my unique God (Allah), were the lone motive for me to overcome the successive obstacles and the great difficulties to complete this work!

I would like to express my great thanks and appreciation to my dear supervisor; Mr. Prof. Dr. M. Pietschmann, MD. Really, Prof. Pietschmann has given me all the possible support, advices, guidance and help to achieve my work. His unlimited help was always available for me at both ("personal and professional") levels. I'm extremely grateful for his great support and for his supervision during the duration of the research.

I would like to express my great thanks and appreciation to my colleagues in the lab who gave me the chance to work in their team. Really, their technical support during my work had a great influence on the completion of this project. Also, I'm grateful for the other colleagues in the lab who weren't involved in this project, but they were always ready to offer their support, when needed.

Also, I would like to thank the colleagues in the department of radiology for their help in scanning the scheduled specimens of our study before and after the trials.

Finally, my deep thanks and great appreciation to the working staff in the dean's office, in particular Mrs. Andrea Hinkelmann, for their advices and help during my enrollment and my research.

LIST OF CONTENTS

Item	Page
Cover page	I
Dedication	IV
Adage of Prof. Gluck	V
Certificate from the 27 th SECEC-ESSSE-Congress	VI
Citation published in the 23 rd Congress of the European Society of Biomechanics	VII
Abstract	VIII
<i>a. Background</i>	<i>VIII</i>
<i>b. Hypotheses</i>	<i>VIII</i>
<i>c. Objectives</i>	<i>VIII</i>
<i>d. Materials</i>	<i>VIII</i>
<i>e. Methodology</i>	<i>IX</i>
<i>f. Findings (Observations & Examinations)</i>	<i>IX</i>
<i>g. Results</i>	<i>IX</i>
<i>h. Conclusion</i>	<i>X</i>
<i>i. Keywords</i>	<i>X</i>
Acknowledgement	XI
List of Contents	XII
1. Introduction	1
1.1. Shoulder Complex Anatomy	1
1.1.1. Background	1
1.1.2. Proximal humerus anatomy	2
1.1.3. Glenoid fossa anatomy	3
1.1.4. Shoulder complex ligaments	4
1.1.5. Glenoid labrum	4
1.1.6. Glenohumeral joint capsule	5
1.1.7. Shoulder complex muscles	5
1.1.8. Rotator cuff anatomy	6
1.1.9. Glenohumeral joint motion	7
1.1.10. Scapulothoracic articulation	7
1.2. Shoulder Stability	8
1.2.1. Definition	8
1.2.2. Shoulder stabilizers	8
1.2.2.1. Shoulder static stabilizers	8
1.2.2.1.1. GHJ articular surfaces	8
1.2.2.1.2. Labrum-capsuloligamentous-complex (LCLC)	9
1.2.2.2. Shoulder dynamic stabilizers	9
1.2.3. Force couple concept	10
1.2.4. Concavity-compression mechanism	11
1.2.5. Rotator cuff biomechanics	11
1.2.6. Scapulothoracic articulation	12
1.2.7. Scapulohumeral rhythm (SHR)	12

1.3.	<i>Shoulder Chronic Pain Disorders</i>	13
1.3.1.	<i>Shoulder pain epidemiology</i>	13
1.3.2.	<i>Shoulder arthritis</i>	13
1.3.2.1.	<i>Glenohumeral osteoarthritis (GH OA)</i>	13
1.3.2.2.	<i>Glenohumeral rheumatoid arthritis (GH RA)</i>	14
1.3.3.	<i>Shoulder osteonecrosis (ON)</i>	14
1.3.4.	<i>Rotator cuff tears (RCTs)</i>	14
1.3.5.	<i>Calcific tendinitis of rotator cuff</i>	15
1.3.6.	<i>Impingement syndrome (rotator cuff tendinopathy)</i>	15
1.4.	<i>Shoulder Arthroplasty</i>	16
1.4.1.	<i>Background</i>	16
1.4.2.	<i>Arthroplasty history</i>	16
1.4.3.	<i>Shoulder arthroplasty types</i>	17
1.4.4.	<i>Anatomic total shoulder arthroplasty</i>	17
1.4.4.1.	<i>ATSA: indications</i>	17
1.4.4.2.	<i>ATSA: success requirements</i>	17
1.4.4.3.	<i>ATSA: design (components)</i>	18
1.4.4.3.1.	<i>Humeral component features</i>	18
1.4.4.3.2.	<i>Glenoid component features</i>	19
1.4.4.4.	<i>ATSA: postoperative imaging</i>	19
1.4.4.5.	<i>ATSA: complications</i>	20
2.	<i>Study Design & Hypotheses</i>	21
2.1.	<i>Introduction</i>	21
2.2.	<i>Study's problem definition</i>	23
2.3.	<i>Preliminary work</i>	24
2.4.	<i>Study objectives</i>	25
2.5.	<i>Hypotheses</i>	26
2.5.1.	<i>Hypothesis (Hi)</i>	26
2.5.2.	<i>Hypothesis (Hii)</i>	26
2.5.3.	<i>Hypothesis (Hiii)</i>	26
3.	<i>Study Materials & Instrumentation</i>	27
3.1.	<i>Specimens</i>	27
3.2.	<i>ATSA components</i>	27
3.3.	<i>Cement</i>	28
3.4.	<i>Metal bases</i>	28
3.5.	<i>Fixating screws</i>	28
3.6.	<i>Plastic template</i>	28
3.7.	<i>Surgical instruments</i>	28
3.8.	<i>Shoulder set-up (shoulder simulator)</i>	29
3.8.1.	<i>Simulator construction</i>	29
3.8.2.	<i>Simulator mechanics</i>	29
3.9.	<i>Shoulder pointer, Zebris system "US" & kinematics tripods</i>	33
3.10.	<i>TekScan pressure sensor</i>	34
3.11.	<i>Testing system operating programs</i>	35
3.11.1.	<i>Simulator operating program ("LabView-SchulterKinemator")</i>	35
3.11.2.	<i>TekScan operating program</i>	36
3.12.	<i>Quantitative computed tomography (QCT)</i>	37

4. Methodology & Testing Protocol	38
4.1. Stage I: Initial pre-testing radiological scanning using QCT	38
4.2. Stage II: Pre-experimental planning	38
4.3. Stage III: Preparatory stage	38
4.4. Stage IV: Arthroplasty (implantation stage)	39
4.5. Stage V: Specimen step-wise testing	40
4.5.1. Formulation of the cycling loading phases	41
4.5.2. Description of data recording using shoulder pointer	42
4.6. Stage VI: radiological evaluation using QCT	42
4.7. General testing procedure	45
4.7.1. Level I: Specimen step-wise testing	45
4.7.1.1. Pressure sensor insertion	45
4.7.1.2. Specimen mounting on the simulator	45
4.7.1.3. Shoulder pointer data recording	47
4.7.1.4. Initiation of the first phase of cyclic loading testing	47
4.7.2. Level II: Specimen step-wise testing	47
4.7.3. Level III: Specimen step-wise testing	47
4.7.4. Important technical remarks	47
5. Data Collection & Analysis	51
6. Results	53
6.1. Findings (observations & examinations)	53
6.2. Radiological results	54
6.3. TekScan results (statistical results & graph interpretation)	57
6.3.1. Graph interpretation	57
6.3.2. Statistical results	58
7. Discussion	71
7.1. Hypothesis (Hi)	71
7.2. Hypothesis (Hii)	72
7.3. Hypothesis (Hiii)	75
8. Conclusion	76
9. Study Limitations	78
8.1. Small number of specimens	78
8.2. Passive shoulder simulator system	78
8.3. Inability to evaluate shoulder kinematics	78
10. Recommendations	79
11. Zusammenfassung	80
11.1. Hintergrund	80
11.2. Hypothesen	80
11.3. Studienziel	80
11.4. Material	81
11.5. Methoden	81
11.6. Befunde (Beobachtungen & Untersuchungen)	81
11.7. Ergebnisse	82
11.8. Schlussfolgerung	82
11.9. Stichwörter	83
12. List of Abbreviations	84

13. List of Figures	86
14. List of Tables	91
15. List of Graphs	92
16. List of Diagrams	93
17. References	94
17.1. <i>References – (“Shoulder Anatomy”)</i>	94
17.2. <i>References – (“Shoulder Stability”)</i>	98
17.3. <i>References – (“Shoulder Pain Disorders”)</i>	99
17.4. <i>References – (“Total Shoulder Arthroplasty”)</i>	101
17.5. <i>References – (“Biomechanical Study”)</i>	103
Eidesstattliche Versicherung	106
<u>Appendix I: TekScan Graphs</u>	1-24
i. <i>Internal-External Rotation: Phase 1</i>	1
ii. <i>Internal-External Rotation: Phase 3</i>	5
iii. <i>Flexion-Extension Motion: Phase 1</i>	9
iv. <i>Flexion-Extension Motion: Phase 3</i>	13
v. <i>Abduction-Adduction Motion: Phase 1</i>	17
vi. <i>Abduction-Adduction Motion: Phase 3</i>	21
<u>Appendix II: Pioneers of Shoulder Arthroplasty</u>	25- 35
1. <i>Prof. Dr. Themistocles Gluck (1853–1942)</i>	25
1.1. <i>Biography</i>	25
1.2. <i>References</i>	28
2. <i>Dr. Jules-Émile Péan (1830 – 1898)</i>	29
2.1. <i>Biography</i>	29
2.2. <i>References</i>	30
3. <i>Dr. Charles S. Neer, II, MD (1917–2011)</i>	31
3.1. <i>Biography</i>	31
3.2. <i>References</i>	32
4. <i>Prof. Dr. Paul-Marie Grammont (1940-2013)</i>	33
4.1. <i>Biography</i>	33
4.2. <i>References</i>	35

1. Introduction

1.1. Shoulder Complex Anatomy

1.1.1. Background

The shoulder is classified structurally as a synovial joint with a further sub-classification as a ball and socket joint, because of the shape of its articulating surfaces “*humeral head (HH) is a hemisphere and the glenoid fossa is a shallow narrow hole*” and is classified functionally as a multi-axial joint ^{(5) (7)}, because it can offer long arches of motion in different directions ^{(3) (4) (5) (6) (9) (18) (36) (57)} in the three mutually perpendicular axes in space (*x & y & z coordinates*) to create a real tri-dimensional image of motion ⁽⁵⁾ of the hand and the opposing thumb ^{(6) (9)} (*Figure 2*). The shoulder girdle forms the link between spine, thorax and the ipsilateral shoulder, which consists of GHJ, ACJ, SCJ and the scapulothoracic articulation. These collectively perform the following motions: elevation, depression, upward rotation, downward rotation, anterior tilt, posterior tilt, protraction and retraction ⁽⁹⁾.

The shoulder complex is the most movable ^{(8) (9) (11) (15) (28) (29) (30) (31) (36) (44) (57)} and the least stable joint in human body ^{(3) (8) (9) (11) (36) (29) (30) (31) (50)}. These two characteristics of the shoulder arise from the deficiency of the effective osseous grip at its articulating surfaces ^{(3) (4) (5) (30) (31) (36)}. Therefore, the stability of the shoulder joint originates: **(i)** mainly from the surrounding soft tissues ^{(8) (9) (11) (18) (30) (36) (57)} ensured by the muscles ^{(30) (25) (29)}, which run transversely across the shoulder ⁽⁵⁷⁾, and **(ii)** additionally from the nearby articulations ⁽³⁾.

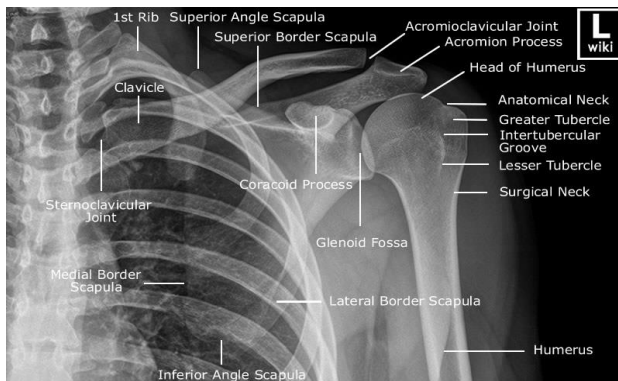


Figure (1): Shoulder-PXR “AP view” shows bones and joints of shoulder girdle in the adult (Wikiradiography shoulder).

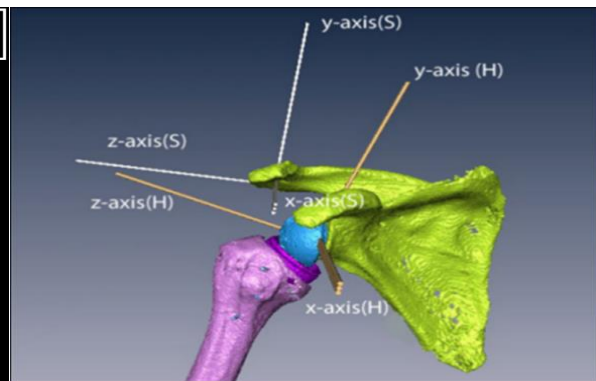


Figure (2): 3D shoulder model. Shoulder two coordinates system is defined (Scapula (S); Humerus (H) (DOI:10.1186/1749-799X-6-42).

The shoulder joint is a major joint of the human body ⁽⁵⁰⁾ and a highly specialized structure ⁽⁴⁴⁾. The constituting structures of the shoulder complex are: **(i)** three bones: proximal humerus, scapula and the distal third of the clavicle ^{(1) (2) (3) (20) (44)}; **(ii)** four articulations: glenohumeral, acromioclavicular, scapulothoracic and sternoclavicular joints ^{(1) (2) (3) (20) (29) (57)} (*Figure 1*); **(iii)** a surrounding muscular envelope ^{(1) (2) (3) (20)} (*about 20 muscles*) ⁽²⁰⁾; and **(iv)** additional specialized structures: labrum, joint capsule, ligaments, bursae, synovium & cartilage ^{(1) (2) (3)} (*Figure 7*).

1.1.2. Proximal humerus anatomy

The proximal humerus is composed of a hemispherical head, proximal shaft, humeral neck, bicipital groove, lesser tuberosity (*LT*) and greater tuberosity (*GT*)^{(1) (8) (10) (12) (33)} (*Figure 3*). The humeral head has a diameter between 37 and 57 mm (*average 46 mm*) and its height is about 8 mm superior to the greater tuberosity with an offset of about 3 mm posterior and 7 mm medial to the shaft⁽¹³⁾. The humeral head is inclined at the anatomical neck about 130° to 150° relative to the shaft and retroverted about 26° to 30° relative to the medial and lateral epicondylar planes^{(1) (8)} (*Figure 4*). The articular surface of the humeral head mostly forms a true sphere, bordered anteriorly by *LT* and laterally by *GT* with a tilting of its margin about 45° relative to the humeral shaft. The central portion of its hyaline cartilage is the thickest, in contrast to that at the center of the glenoid⁽⁸⁾.

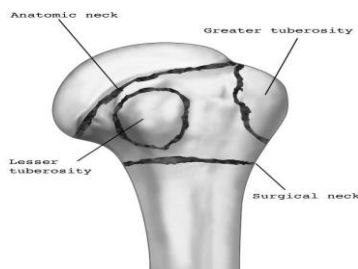


Figure (3): Proximal humerus portions (DOI:10.1053/j.ro.2005.01.012).

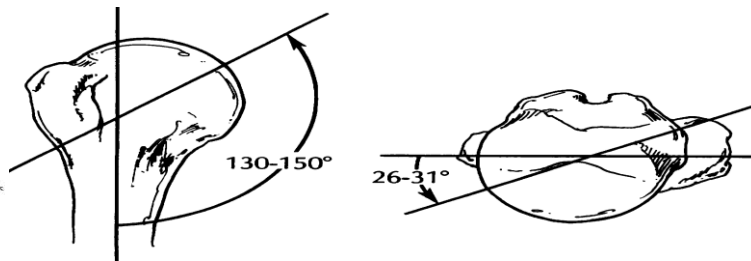


Figure (4): Humeral head shaft angle ranges from 130° to 150°; head is retroverted from 26° to 31° (Terry et al. *Journal of Athletic Training* 2000;35(3):248-255).

The humeral head coverage of hyaline cartilage^{(10) (48)} has an approximate thickness of about 1 mm⁽¹⁰⁾, which terminates laterally at a sulcus between the humeral head and the greater tuberosity with a bared area of cartilage^{(12) (48)}. The anterior and lateral borders of the articular surface with the medial surface of the surgical neck serve as attachments of a tendoligamentous ring, which acts to stabilize the joint by centering the humeral head within the glenoid by tightening around the prominent articular surface⁽⁸⁾.

The humeral head is described surgically and clinically to have two necks. **(i)** The anatomical neck (*AN*) forms the oblique circumference of the head⁽¹⁰⁾, separating the head and the tuberosities^{(10) (13)} and serving as an attachment site for the ligaments. Fracture healing prognosis in this region is poor, because of the disruption of blood supply to HH⁽¹³⁾. **(ii)** The surgical neck (*SN*) forms the axial circumference of the humerus. *SN* is located just distal to the tuberosities⁽¹⁰⁾ and is considered a common region of fractures^{(1) (10)}. The blood supply to the humeral head comes from its surrounding anastomosis, formed by branches of anterior and posterior humeral circumflex arteries (*AHCA and PHCA*). HH is vascularized mainly by *AHCH* and highly susceptible to *AVN* after proximal humerus fractures⁽¹⁴⁾ (*Figure 5*).

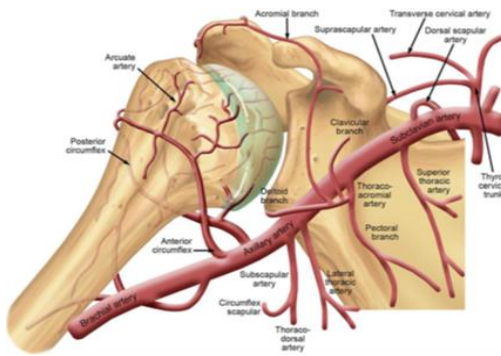


Figure (5): Vascular network of proximal humerus (DOI: 10.1007/978-3-319-08951-5_2/ Springer).

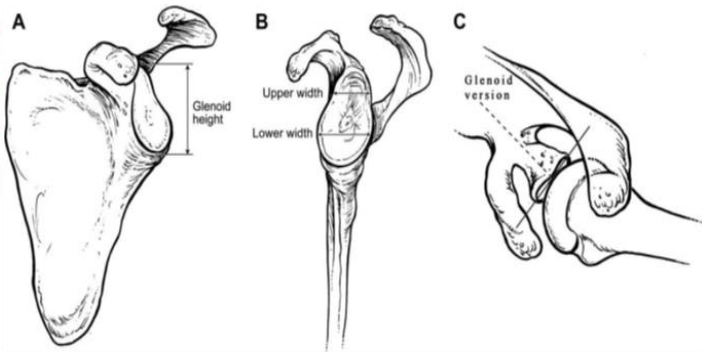


Figure (6): Parameters of glenoid anatomy include (A) glenoid height, (B) width, and (C) version (DOI: 10.1016/j.jse.2009.05.008).

1.1.3. Glenoid fossa anatomy

The glenoid is as a concave process⁽⁹⁾ or thickening of the scapula inferior to the acromion⁽⁸⁾, situated at the superolateral aspect of the scapula⁽¹⁷⁾ and described as pear-shaped, rounded, oval or having an inverted comma shape⁽¹⁸⁾⁽¹⁹⁾ in the coronal plane⁽¹⁰⁾ (*Figure 6*). The glenoid is tilted slightly cranially and directed anterolaterally⁽⁹⁾ with an upward inclination tilt of its face about 10° to 15° relative to the medial border of the scapula⁽²¹⁾. Glenoid fossa may have a notch called spinoglenoid notch⁽¹⁷⁾, which is located at the glenoid anterosuperior margin⁽¹⁷⁾⁽¹⁸⁾, separating the glenoid from the acromion base⁽⁸⁾. The glenoid surface is slightly concave with an anterior incision⁽⁸⁾ and is covered with a layer of hyaline articular cartilage⁽⁴⁾⁽¹²⁾⁽²¹⁾⁽²³⁾⁽³⁵⁾⁽⁴⁵⁾, which deepens its shallow surface by about additional 50% through the formation of the fibrocartilaginous labrum at its rim⁽⁴⁾⁽¹²⁾⁽²¹⁾⁽²³⁾⁽³⁵⁾. Maximal depths without the glenoid's labrum are approximately 2-4 mm transversely and 7-9 mm horizontally⁽²²⁾. In contrast to its edge, the glenoid shows a central portion of a thinned cartilage⁽⁸⁾. The supraglenoid tubercle is situated on the glenoid superior pole and provides attachment for the origin of the long head of biceps tendon (*LHBT*)⁽⁸⁾⁽¹⁰⁾, while the infraglenoid tubercle is situated on the glenoid inferior pole and provides attachment for the origin of the long head of triceps⁽⁸⁾.

The small and shallow⁽¹⁾⁽²²⁾⁽²⁶⁾⁽³⁵⁾⁽³⁶⁾ glenoid fossa articulates through the glenohumeral joint with the large hemispherical head of the humerus⁽¹⁾⁽²²⁾⁽²⁶⁾⁽³¹⁾⁽³⁵⁾⁽³⁶⁾⁽⁵⁰⁾. There is a disproportion between their sizes, so that the total surface area of the articular surface of the glenoid is about ¼ or ⅓ of the surface area of the articular surface of the humeral head⁽¹⁾⁽⁹⁾⁽²¹⁾⁽²³⁾⁽³⁶⁾⁽³⁸⁾⁽³⁹⁾⁽⁴⁸⁾. The glenoid vertical and transverse diameters are 75% and 60% of those of the humeral head, respectively⁽²⁴⁾, and as a result of this disproportion the stability of the shoulder is sacrificed⁽¹⁾⁽²³⁾ while the shoulder's range of motion (ROM) was maximized. Shoulder's ROM is further augmented by the scapula sliding on the posterior thoracic wall, as well as by the rotation of the ACJ and SCJ joints⁽³⁶⁾. However, Soslowky determined that the articular surfaces of the glenoid and humeral head have identical shapes and are highly congruent

⁽²²⁾. Glenoid version is defined as the angular orientation of the axis of the glenoid articular surface relative to the long “*transverse*” axis of the scapula, with the posterior angle denoted as a retroversion (*Figure 6*). Glenoid version was estimated by many studies to range normally between 2° anteversion and 9° retroversion, with noted changes in case of GHJ pathologies ⁽²⁰⁾, particularly GHJ instabilities ⁽³⁴⁾. The scapular plane lies 30°– 45° anterior to the coronal plane of the body ^{(1) (21) (27)}, because of the curve of the rib cage ⁽²¹⁾.

1.1.4. Shoulder complex ligaments

The ligaments of the shoulder complex are divided into capsular and extracapsular ligaments. Capsular ligaments are the glenohumeral ligaments (*GHLs*), the transverse humeral ligament and the coracohumeral ligament, while the extra-capsular ligaments are the ligaments of shoulder complex articulations “*the acromioclavicular joint (ACJ), the scapuloacromioclavicular joint (SCJ) and the scapulothoracic articulation*”. *GHLs* are classified as components of the labrocapsular ligamentous complex (*LCLC*). *GHLs* were described firstly by Flood in 1829 ⁽¹⁰⁾ and are composed of three ligaments: the superior and middle glenohumeral ligaments and the inferior glenohumeral ligament complex (*SGHL, MGHL and IGHLC*) ^{(30) (50)}. *GHLs* are described as band-like collagenous ⁽³⁰⁾ localized ⁽⁵⁰⁾ thickenings ^{(30) (43) (50) (51)} of the anterior ⁽⁵¹⁾ thin GHJ capsule ^{(30) (78) (51)} with different sizes, strengths and orientations ⁽⁴⁹⁾ (*Figure 7*). *GHLs* serve to stabilize and strengthen the GHJ capsule ⁽¹⁰⁾ and their function varies greatly according to the position of the shoulder and the direction of the translating forces ⁽⁴⁹⁾. *For more details, see the next chapter, Shoulder Stability.*

1.1.5. Glenoid labrum

The literatures describe the labrum as a dense fibrous ^{(1) (9) (15) (45) (48) (49)} and cartilaginous structure with chondrocytes ⁽⁴²⁾. The labrum is round ^{(36) (40) (43) (45)}, crescentic ⁽⁴⁵⁾ or triangular in cross-section ^{(1) (15) (40) (30) (43) (45)}. The labrum’s average thickness is about 4 mm ⁽⁴³⁾ and its depth ranges from 4.9 to 9 mm ^{(1) (41)}. The labrum consists of three layers: ***(i)*** a peripheral fibrous layer, which functions as an anchor to biceps tendon ^{(36) (37) (40) (42) (49)}; ***(ii)*** a fibrocartilaginous transitional zone ^{(22) (36) (37) (40) (42)}, which provides a firm attachment of the labral peripheral layer to the deep layer; and ***(iii)*** the central parts of the glenoid ^{(22) (37) (40) (42)}. For descriptive purposes, the labrum is divided into 6 zones based on clock face ^{(36) (40) (41)} (*Figure 8*), going from superior to inferior in clockwise direction on right shoulders and in anticlockwise direction on left shoulders ⁽³⁶⁾. The labrum encircles the glenoid rim, forming a collar or a cuff, which deepens the glenoid cavity and increases its functional contact area with the humeral head ^{(1) (3) (9) (15) (22) (30) (36) (40) (41) (42) (45) (48) (49)}.

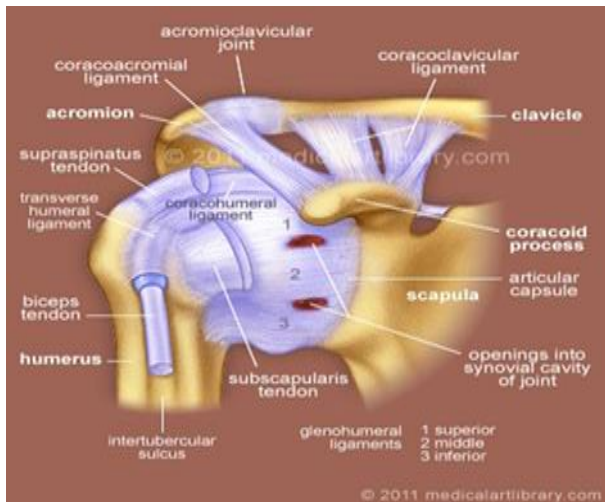


Figure (7): Shoulder joint ligaments (Medicalartlibrary.com/muskuloskeletal. 2011).

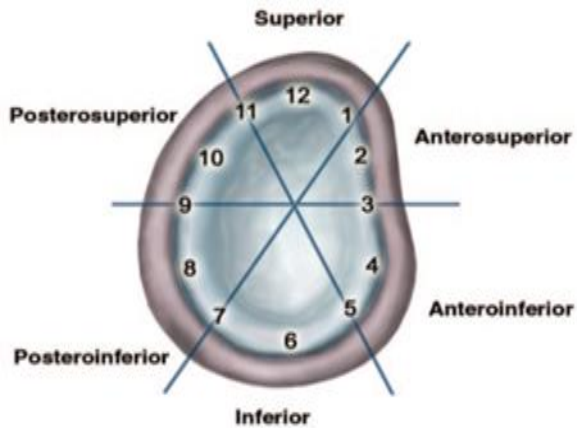


Figure (8): The glenoid labrum is compared with clock face (DOI:10.2214/AJR.10.7236).

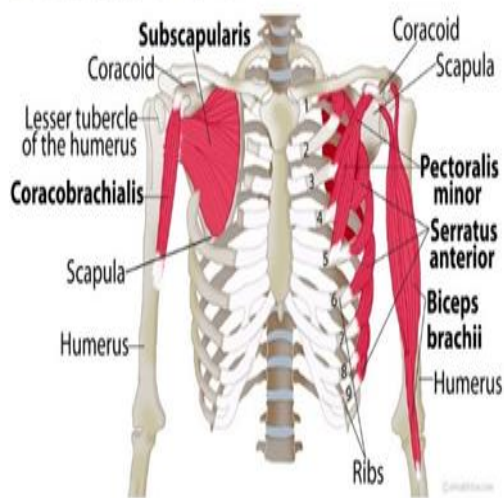
1.1.6. Glenohumeral joint capsule

The GHJ capsule is a dense fibrous connective tissue⁽³⁰⁾⁽⁴⁷⁾, lined with a synovium⁽⁸⁾⁽⁹⁾⁽⁴⁶⁾⁽⁴⁷⁾, attached to the labrum⁽⁹⁾ (Figure 7) and anchored to the bone of the glenoid neck⁽⁸⁾⁽³⁰⁾⁽⁴⁸⁾. The GHJ capsule inserts laterally⁽³⁰⁾ into the anatomical neck of the humerus⁽⁸⁾⁽³⁰⁾ close to the humeral head cartilage⁽⁸⁾, just medial to the tubercles and lateral to the humeral head⁽⁴⁹⁾. It encloses the joint margins⁽⁴⁾⁽⁴⁶⁾⁽⁴⁷⁾. The GHJ capsule is divided into three main regions: anterior, posterior and axillary pouches⁽⁴⁶⁾. It is completely reinforced exteriorly, except inferiorly⁽³⁾⁽⁸⁾, where dislocations are common⁽³⁾. The anterior and axillary pouches are reinforced by SGHL, MGHL and IGHL⁽⁹⁾⁽⁴⁶⁾. The capsule is loose⁽³⁾⁽⁴⁾⁽⁹⁾⁽³⁰⁾ and redundant⁽⁹⁾⁽³⁰⁾, having a large volume compared to that of the humeral head⁽⁸⁾⁽⁹⁾⁽¹⁵⁾⁽⁴⁸⁾, normally about 10-15 ml, and twice the surface area of the humeral head⁽¹⁾⁽⁸⁾, allowing for an extensive range of motion⁽¹⁾⁽³⁾⁽⁹⁾⁽¹⁵⁾⁽³⁰⁾ and also for potential instabilities of the GHJ⁽³⁰⁾.

1.1.7. Shoulder complex muscles

Shoulder girdle muscles originate from the axial skeleton, insert into the clavicle and scapula and act on the pectoral girdle⁽⁵⁾. Muscles of the shoulder girdle are divided anatomically into two large groups⁽⁵⁾⁽⁹⁾: **(i) anterior shoulder girdle muscles:** sternocleidomastoid, subclavius, pectoralis minor, pectoralis major, deltoid “anterior and lateral fibers”, biceps brachii and coracobrachialis muscles; and **(ii) posterior shoulder girdle muscles:** deltoid “posterior fibers”, levator scapulae, rhomboids minor, rhomboids major, serratus anterior, latissimus dorsi, teres major, subscapularis, infraspinatus, supraspinatus, teres minor, triceps brachii and trapezius muscles⁽⁵⁾⁽⁸⁾⁽⁹⁾⁽¹⁵⁾⁽³²⁾ (Figure 9).

Pectoral Girdle Muscles From the Front



Pectoral Girdle Muscles From Behind

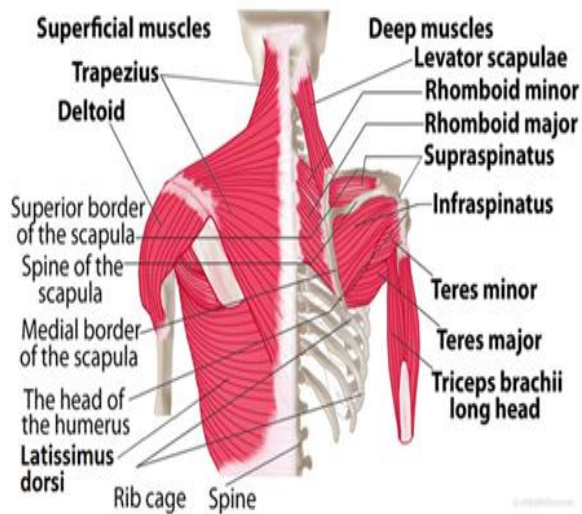


Figure (9): Anterior & posterior pectoral girdle muscles (Jan Modric, *shoulder blade muscles*, eHealthStar Dec 2014).

1.1.8. Rotator cuff anatomy

“Rotator cuff” refers to a myotendinous complex group of four flat, short, broad tendinous insertions that link the scapula to the humerus ^{(34) (52) (53) (55)}, including: supraspinatus (SSP), infraspinatus (ISP), teres minor (TM) and subscapularis (SSS) muscles and their tendons ^{(34) (52) (53) (54) (55) (56)} (Figure 10), which together form a multi-layered horseshoe-shaped flattened architecture ⁽⁵³⁾, the “musculotendinous cuff”, which fuses intimately with the GHJ capsule ⁽⁵²⁾ and inserts onto the humeral head ⁽⁵³⁾ (Figure 11). Rotator cuff muscles are vital for upper limb function and are the main component in both GHJ stability and mobility ^{(55) (56)}.

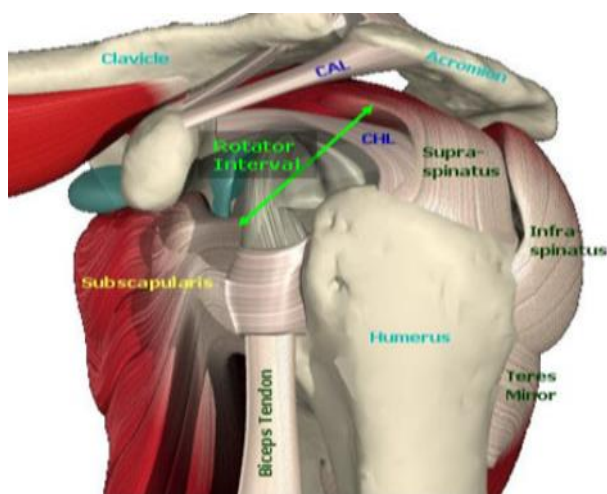


Figure (10): Rotator cuff muscles & rotator interval (Lennard Funk, *Rotator cuff biomechanics*, MSc Orthopaedic Engineering, 2005).

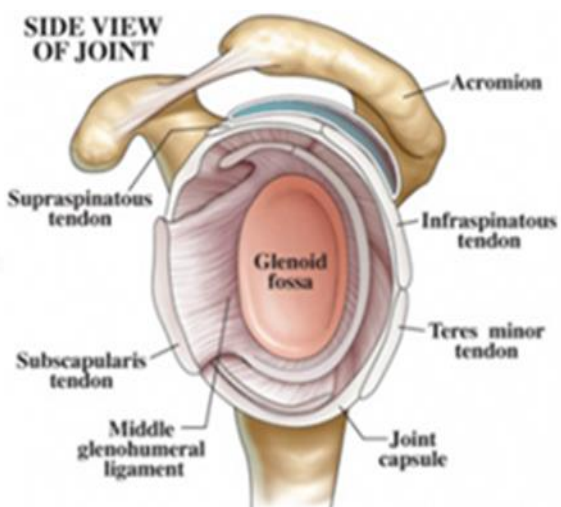


Figure (11): RC muscles overview (Phonex *shoulder and knee*, shoulder surgery 2013).

1.1.9. Glenohumeral joint motions

The GH joint is the most mobile joint in the body ⁽⁵⁷⁾, offering free motion on the three different axes, “transverse, sagittal and coronal axes” ^{(9) (57)}, which all traverse the head of the humerus ⁽⁹⁾ (Table 1). Shoulder motion is performed in a smooth action as a component of the whole motion of the shoulder girdle (Table 2) along with (i) scapular movements, (ii) the leverage action at the sternoclavicular joint, and (iii) the action of the costoclavicular ligament as a pivot ⁽³⁵⁾.

Motion Direction	GH joint	Shoulder girdle
Flexion - Extension	90°- 0°- 40°	170°- 0°- 40°
Abduction - Adduction	90°- 0°- 40°	180°- 0°- 40°
Int. Rotation - Ext. Rotation	60°- 0°- 70°	90°- 0°- 100°

Motion	Performing muscles
Abduction	Initiation by supraspinatus to 45°, continuation by deltoid up to 90° and completion up to 180° (elevation) by action of trapezius and serratus anterior through the upward rotation of the scapula. The movements of scapula occur reciprocally to the motions at sternoclavicular joint.
Adduction	Three medial rotators ; teres major, pectoralis major & latissimus dorsi and one lateral rotator ; teres minor.
Flexion	Pectoralis major, coracobrachialis & anterior fibers of deltoid.
Extension	Teres major, latissimus dorsi & posterior fibers of deltoid.
Int. Rotation	Teres major, pectoralis major, latissimus dorsi, subscapularis & anterior fibers of deltoid.
Ex. Rotation	Infraspinatus, teres minor & posterior fibers of deltoid.

1.1.10. Scapulothoracic articulation – (“scapulothoracic gliding”)

The scapulothoracic articulation is classified as a physiological joint ⁽⁵⁷⁾, because it lacks the normal features of joints ⁽¹⁵⁾. It is formed by the ventral concave surface of the scapula lying on the upper posterolateral convex aspect of the thorax. Between them, soft tissues such as muscles, neurovascular bundles and bursae are positioned ^{(9) (15)}. The scapula does not have any direct osseous or ligamentous connection with the thorax, but it is connected with it indirectly through the clavicle, ACJ and SCJ ⁽¹⁵⁾. This articulation is vital for shoulder motions, because it enables the scapula to tilt, rotate and glide. Any abnormalities in it, such as the irregularity of the posterior aspect of the thorax, result in painful motions of arm and scapula ⁽⁹⁾.

1.2. Shoulder Stability

1.2.1. Definition

Matsen III used the term glenohumeral joint stability to describe the ability to keep the humeral head centered within the glenoid fossa. The GH joint is unique, because it can maintain its stability despite its few restraints ⁽⁴⁾.

1.2.2. Shoulder stabilizers

The GHJ is minimally constrained, with a little inherent bony stability ^{(3) (4) (6)}. Constraint comes from the humeral head, which articulates directly with the glenoid cavity. It is related to glenoid depth, but independent of the articular congruence ⁽³⁾. Shoulder stability is a result of a complex interaction between static and dynamic shoulder restraints ^{(2) (3) (4) (6) (8) (9) (11) (12)} (*Table 3*). Other physiological factors, such as the negative intra-articular pressure and the adhesion-cohesion mechanisms, are thought to play a role in GHJ stability ^{(1) (8) (9) (11) (12)}. The role of any component of the GHJ stabilizing system varies according to the position of the shoulder and the direction of shoulder motion ^{(1) (9)}. Static and dynamic shoulder stabilizers react to the forces applied through GHJ to provide stability at different positions along the motion arc ⁽⁴⁾. Static restraints ensure joint stability well at rest and at end-ranges of motion, but they are ineffective for sustaining joint stability in mid-ranges of motion, which is characterized by a high velocity and large external loads. At these ranges the active stabilizers function ⁽¹²⁾.

Table (3): Static and Dynamic Shoulder Stabilizers <i>(Adapted from Ref. (1) & (3))</i>	
Static Stabilizers	
Capsuloligamentous: capsule, labrum, glenohumeral ligaments & coracohumeral ligament.	Articular: humeral head retroversion, scapular inclination, joint conformity, negative intraarticular pressure & articular cartilage.
Dynamic Stabilizers	
Scapulohumeral: supraspinatus, deltoid, teres minor infraspinatus, subscapularis, teres major, LHBT & coracobrachialis. Axioscapular: trapezius, rhomboids, serratus anterior & levator scapulae.	Axioclavicular: sternocleidomastoid & subclavius. Axiohumeral: latissimus dorsi & pectoralis major. Others: omohyoid, biceps brachii & triceps brachii.

1.2.2.1. Shoulder static stabilizers – (“passive stabilizers”)

Static stabilizers are the bony, cartilaginous, ligamentous and capsular structures of the GHJ ^{(4) (6) (9) (11)}.

1.2.2.1.1. GHJ articular surfaces

Jobe and Iannotti reported that the humeral head presented up to 160° of the articular cartilage in both transverse and coronal planes, apposed by 75° and 95° of the glenoid articular cartilage, respectively. Therefore, up to 85° and 65°, respectively, of humeral articular cartilage was unconstrained by the glenoid ⁽¹²⁾ (*Figure 12*). Also, only 25-30% of the humeral head at any given point through the long arc

of motion is in contact with the glenoid fossa, and the humeral head is constrained to within 1-2 mm of the center of the glenoid cavity in the whole motion arc in a normal shoulder ⁽⁸⁾. The glenohumeral index (*GHI*) is a ratio defined as the maximum glenoid diameter divided by the maximum humeral head diameter ⁽³⁾⁽⁷⁾. The *GHI* was determined by Saha et al. ⁽⁷⁾ to be 0.75 and (0.60 ⁽³⁾ or 0.76 ⁽⁷⁾) in the sagittal and transverse planes, respectively ⁽³⁾⁽⁷⁾. A low glenohumeral index is associated with recurrent anterior instability ⁽³⁾. Glenohumeral congruence (*conformity*) is the relationship between the radii of the curvatures of the humeral head and the glenoid ⁽¹⁾.

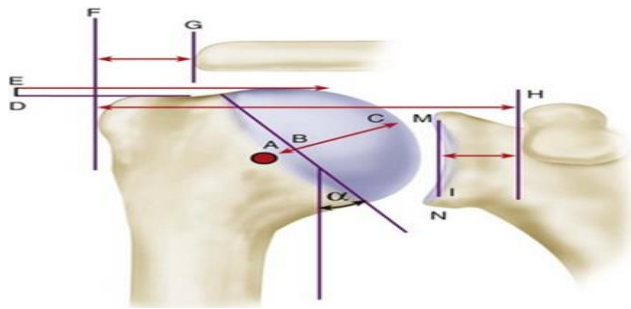


Figure (12): Normal glenohumeral relationships. Humeral offset is depicted by distance F to H, thickness of humeral head from B to C, and center of humeral head at C. Note superior position of humeral head proximal to greater tuberosity (D to E) (Throckmorton 2016, <http://musculoskeletalkey.com/shoulder-and-elbow-arthroplasty>).

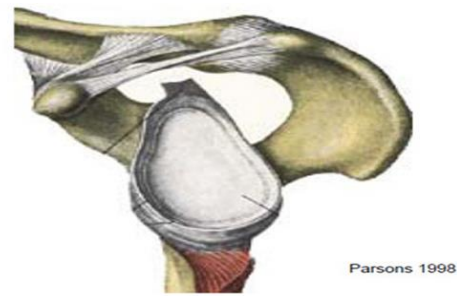


Figure (13): Normal shoulder articular surfaces with obvious deepening effect of labrum (originally from Parsons 1998, taken from Massimini's master's thesis 2005).

1.2.2.1.2. Labrum-Capsuloligamentous-Complex (LCLC)

As discussed before, the labrum functions: **(i)** to deepen the glenoid cavity ⁽¹⁾⁽³⁾⁽⁴⁾⁽⁷⁾⁽⁸⁾⁽¹¹⁾ (“contributes to about 50% of its depth”) ⁽¹⁾⁽⁴⁾ (Figure 13); **(ii)** to increase the congruity ⁽⁴⁾⁽⁷⁾ and the surface contact area of HH ⁽⁷⁾; **(iii)** to generate a suction effect enhancing GHJ stability ⁽⁴⁾⁽⁷⁾, by serving to bridge the bone to the GHJs and the biceps tendon ⁽¹⁾; **(iv)** acts as a link between the glenoid and capsule exerting a buttress effect, in which the labrum functions as a physical block ⁽¹⁾⁽⁹⁾ to prevent HH displacement ⁽¹⁾⁽⁴⁾. The labrum enables HH to resist the tangential, torsional and about 60% of the compressive loads ⁽¹⁾ and increases the efficiency of the compression effect of the muscles and the tightening effect of the capsuloligamentous complex, which are exerted to stabilize the GHJ by compressing the HH against the glenoid ⁽¹⁾⁽³⁾⁽⁴⁾⁽⁵⁾. This is termed the “concavity compression” mechanism ⁽⁴⁾⁽¹²⁾. The LCLC exerts a passive stabilization effect on the GHJ ⁽¹⁾. The GH capsule maintains the negative intra-articular pressure to support GHJ stability ⁽³⁾⁽¹²⁾ and also functions to limit the rotation, to prevent excessive translations, and to cause a cooption of the joint and to resist the translation of the humeral head on the glenoid at the end of the passive movements ⁽¹⁾⁽⁴⁾⁽⁸⁾ (Tables 3 & 4).

1.2.2.2. Dynamic stabilizers – (“muscle activity/active stabilizers”)

Active stabilizers are the surrounding musculatures of the GHJ ⁽⁴⁾, which are divided into primary dynamic stabilizers such as RCMs and LHBB and secondary dynamic stabilizers such as scapulothoracic muscles, pectoralis major and latissimus dorsi ⁽¹¹⁾.

Table (4): Function of GHJs in Shoulder Stability (Collected)	
Ligament	Function
SGHL	Resists inferior and anterior translations with the adducted arm in neutral rotation ⁽¹⁾⁽³⁾⁽⁴⁾⁽⁹⁾⁽¹⁰⁾ . Along with the anterior band of CHL, acts as a restraint against up to 50° of Abd and in ER of the adducted shoulder ⁽¹⁾⁽⁴⁾ .
MGHL	Anterior stabilizer when the arm is in Add, in up to 30°–45° Abd ⁽¹⁾⁽³⁾⁽⁴⁾ or in ER ⁽¹⁾⁽³⁾ . Provides a barrier against the anterior ⁽¹⁾⁽³⁾⁽⁴⁾⁽⁹⁾⁽¹⁰⁾ and anterosuperior displacements ⁽¹⁾ of HH.
IGHLC	Resists anterior, inferior and posterior humeral head translations, especially when the arm is in ER, Abd beyond 45°, and EX ⁽¹⁾⁽⁸⁾⁽⁴⁾⁽⁹⁾⁽¹⁰⁾ . The anterior band tightens with Abd and ER of GHJ ⁽¹⁾⁽⁴⁾⁽⁸⁾⁽¹⁰⁾ . At neutral position (0° Abd and 30° of horizontal EX), the anterior band becomes the primary static stabilizer of GHJ ⁽⁴⁾ . The posterior band is the primary static stabilizer when the arm is in FL and IR, providing posterior stability ⁽³⁾⁽⁴⁾⁽¹⁰⁾ .
CHL	Resists posterior and inferior translations in the suspended shoulder ⁽¹⁾ . Inferior stabilizer when the arm in Add, and tightens at ER ⁽¹⁾⁽⁴⁾⁽⁸⁾⁽¹⁰⁾ . Acts as a primary restraint of GHJ ⁽¹⁾ .
Remarks: GHJ: glenohumeral joint; FL: flexion; EX: extension; Abd: abduction; Add: adduction; IR: internal rotation; ER: external rotation; CHL: coracohumeral ligament; HH: humeral head.	

1.2.3. Force couple concept

Force couple is a term used to describe the rotatory motion brought about by forces, that are generally equal in magnitude and act in opposite directions at some distance from each other ⁽⁴⁾⁽⁸⁾⁽¹²⁾. Dynamic stabilizers function through two force couples; the first force couple originates mainly from the RC muscles with deltoid and the second force couple originates from the axio-scapular and axio-clavicular muscles to provide a dynamic symmetry of joint motions ⁽¹⁾⁽¹¹⁾ (Figures 14 & 15).

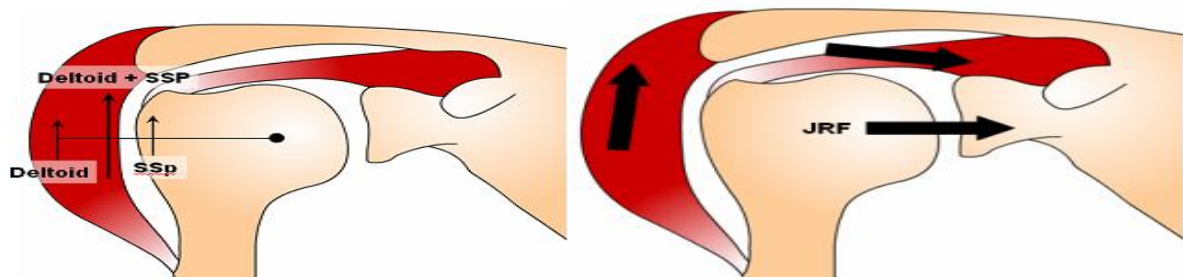


Figure (14): Deltoid and supraspinatus both contribute to abduction equally. As the arm is abducted, the resultant joint reaction force is directed towards the glenoid. This compresses the humeral head against the glenoid and improves the stability of the joint when the arm is abducted and overhead (Lennard Funk, Rotator cuff biomechanics, MSc Orthopaedic Engineering, 2005, originally, Parsons et al. J Orthop Res. 2002).

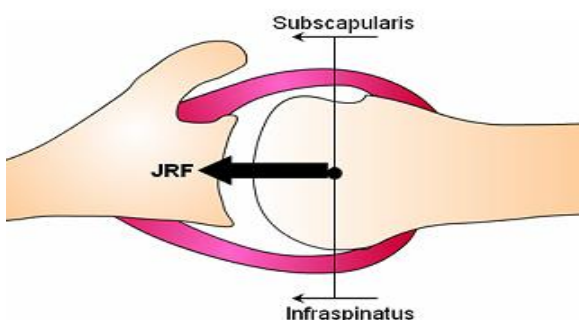


Figure (15): Throughout the range of motion, the compressive resultant joint reaction force in the transverse plane contributes to joint stability. This is the predominant mechanism resisting superior humeral head displacement with cuff tears. As long as the force couple between subscapularis and infraspinatus remains balanced, the joint remains centered (Lennard Funk, Rotator cuff biomechanics, MSc Orthopaedic Engineering, 2005, originally, Parsons et al. J Orthop Res. 2002).

1.2.4. Concavity-compression mechanism

Muscle forces acting on the shoulder joint can be divided into three components: compressive forces, superiorly-inferiorly directed forces and anteriorly-posteriorly directed forces ⁽¹⁾⁽⁵⁾. Compressive forces stabilize the GHJ, while the anteriorly, posteriorly, inferiorly, and superiorly directed forces, or translational forces, destabilize the joint ⁽⁵⁾. The applied compressive forces push the humeral head into the glenoid and allow concentric rotation of the humeral head on the glenoid “*concavity-compression*” mechanism (*Figure 17*), which depends on both shoulder muscle forces and articular surfaces shape, principally that of the glenoid ⁽¹⁾⁽⁴⁾. Glenohumeral joint stability through concavity-compression is greater in the neutral than in the abducted positions, which may contribute to anterior shoulder dislocation (*ASD*). Rotator cuff muscles and LHBBT actively compress HH into the glenoid cavity, along with the outer sleeve of shoulder muscles, such as deltoid, pectoralis major and latissimus dorsi. Shoulders with weakened or deficient rotator cuff mechanisms are likely to have compromised stability from impaired concavity-compression mechanism ⁽¹⁾.

1.2.5. Rotator cuff biomechanics

RCMs are well positioned closer to the center of GHJ rotation ⁽⁴⁾⁽⁸⁾ and act in association with the underlying capsular and ligamentous structures to resist glenohumeral shear stresses ⁽⁴⁾. RCMs usually function together ⁽¹⁰⁾ (*Table 5*); however, each RC muscle has its independent actions, which in combination contribute to the overall stability of the GHJ during mid- and end-ranges of motion ⁽⁴⁾. Subscapularis were described as the most important passive and active stabilizers among RCMs ⁽¹⁰⁾. RCMs exert compression force ⁽⁴⁾⁽⁸⁾⁽⁹⁾ on the GHJ as part of the “*concavity-compression*” mechanism ⁽⁴⁾⁽⁸⁾, through their organized contraction coordinated by their mechanoreceptors and resisting the shear forces ⁽⁴⁾ (*Figure 16*).

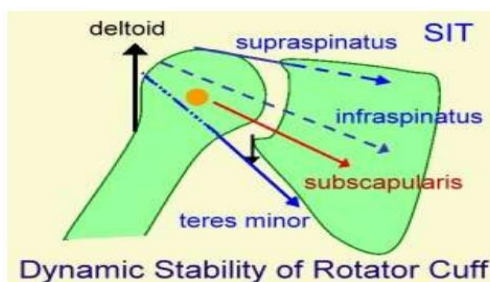


Figure (16): Rotator cuff dynamic stability with deltoid action; SITS; supraspinatus, infraspinatus, teres minor and subscapularis muscles. The net result of acting forces pulls the center of the humeral head towards the center of the GHJ to stabilize it (*KINESIOLOGY SHOULDER, by Hermizan Halihanafiah College of Allied Health and Science 2011, Malaysia*).

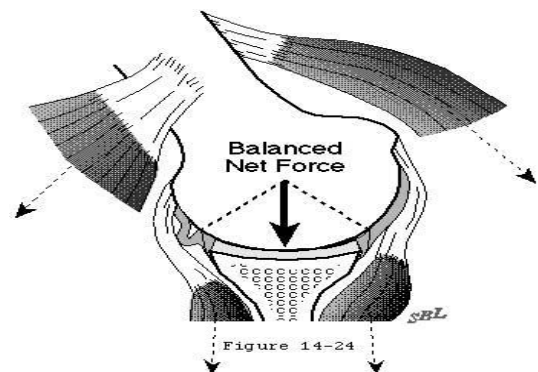


Figure (17): Balanced net force of the acting muscles to compress humeral head against glenoid fossa “*concavity-compression mechanism*” (*Masten et al., Mechanics of Glenohumeral Instability 2013*).

1.2.6. Scapulothoracic articulation

The scapulothoracic joint also provides shoulder movements beyond the initial 120° provided by the glenohumeral joint and contributes to the stability of the joint ^{(4) (8)}. In combination with the motion of the scapulothoracic joint, the range of motion of the human upper extremity covers about 65% of a sphere ⁽⁶⁾. The stability of the scapulothoracic joint is provided by the muscles and fasciae attached to the scapula ⁽¹⁰⁾. Scapular motion is based on its orientation, which is internally rotated by 30°, abducted 3°, and tilted anteriorly by 20°. The scapula moves in different planes to produce a combination of movements, that culminate in protraction or retraction. Scapulothoracic motion provides only 15° of internal rotation in daily activities. If the scapula is fused, limitations occur mostly with extension and internal rotation ⁽⁴⁾.

1.2.7. Scapulohumeral rhythm (SHR)

Scapulothoracic or scapulohumeral rhythm is defined by Wallace ^{(13) (14)} as the coordinated movement between scapulothoracic and glenohumeral joints ^{(4) (7) (10)}. SHR describes the ratio between the motion at the GH joint and the synchronous scapular rotation, which is about 2:1, meaning that the scapula rotates 1° for each 2° of the GH joint motion ^{(4) (10) (13) (14)}. These synchronous movements can be observed clinically during the elevation of the arm ^{(13) (14)}. Shoulders with multidirectional instability have an increased SHR, whereas shoulders with impingement or rotator cuff tears tend to have a decreased SHR. A disruption of this ratio could predispose to GHJ pathologies such as RC tendinitis according to published studies ^{(4) (10)}.

Muscle	Description	Function
Supraspinatus	Circumpennate muscle Average width at midportion of tendinous insertion is 14.7 mm Mean surface area of its insertion is 1.55 cm ²	Initializes humeral abduction to 90° Deficiency can be compensated by the remaining rotator cuff muscles
Infraspinatus	Circumpennate muscle Mean surface area of infraspinatus insertion is 1.76 cm ²	Resists posterior and superior translations Generates 60% of external rotation force
Teres minor	Circumpennate muscle	Resists posterior and superior translations Generates 40% of the external rotation forces
Subscapularis	Multicircumpennate muscle	Contributes to the floor of the bicipital sheath Resists anterior and inferior translations Strong internal rotator

1.3. Shoulder Chronic Pain Disorders

1.3.1. Shoulder pain epidemiology

Shoulder disorders are the most common musculoskeletal problems ⁽⁵⁾, with an incidence rate of about 16% of all musculoskeletal disorders ⁽²⁾. It has been reported, that one third of the population suffer from shoulder symptoms during their lifetime ⁽⁷⁾. Shoulder disorders manifest with pain ⁽¹⁾⁽³⁾⁽⁵⁾⁽⁶⁾ and disabling ⁽³⁾ functional loss ⁽⁵⁾⁽³⁾ (“*shoulder stiffness*”) ⁽⁶⁾. Shoulder pain is a very common musculoskeletal manifestation ⁽¹⁾⁽³⁾⁽⁷⁾ with a rate of incidence of about 18-20% in the adult population. It can strike at any age, making the shoulder one of the most common structure of regional pain syndromes ⁽³⁾. Shoulder pain may be acute, or it may be chronic, which is when it persists for longer than six months ⁽²⁾ in spite of vigorous conservative treatment. **Chronic shoulder pain** is caused by tumors, AVN, Paget’s disease, RCTs, impingement syndrome, FSS, SLAP injury, RCA, calcific tendinitis, biceps tendinitis, GH joint instability, OA, RA, fibrositis, metabolic disorders or infections ⁽¹⁾⁽³⁾⁽⁵⁾⁽⁶⁾.

1.3.2. Shoulder arthritis

Shoulder arthritis can be primary, of unknown aetiology or secondary, which could be atraumatic, post-inflammatory, post-surgical, post-traumatic or due to AVN ⁽²⁵⁾.

1.3.2.1. Glenohumeral osteoarthritis (GH OA)

OA is a degenerative disorder ⁽²³⁾⁽²⁸⁾, that affects the GHJ and is characterized by gradual wearing ⁽²⁵⁾ of the articular cartilage and the subchondral bone with narrowing of the GHJ space ⁽²⁵⁾⁽²⁸⁾, resulting in loss of joint sphericity and congruity ⁽²⁵⁾ (*Figure 18*). OA may be primary or secondary ⁽²²⁾⁽²⁵⁾⁽²⁷⁾ and can be classified arthroscopically or radiologically according to the extent of the cartilage damage ⁽²⁵⁾⁽²⁷⁾. According to the patient’s age, symptom severity, activity level, radiographic findings and medical co-morbidities ⁽²²⁾, OA can be treated conservatively or surgically ⁽²²⁾⁽²⁵⁾⁽²⁷⁾⁽²⁸⁾.



Figure (18): PXR shows a typical shoulder with advanced glenohumeral OA. There is joint space narrowing with marginal osteophytes and subchondral sclerosis present (www.learnorthopaedics.com).

1.3.2.2. Glenohumeral rheumatoid arthritis (GH RA)

RA is defined as an autoimmune mediated synovitis of multiple joints ⁽¹⁹⁾⁽²⁰⁾, which commonly affects the small joints in feet and hands. The shoulder is considered to be the seventh or eighth most frequently affected joint ⁽¹⁸⁾. RA is treated initially with conservative measures, but surgery ⁽¹⁾⁽¹⁸⁾⁽²¹⁾ is indicated in case of advancing articular damage and increasing symptoms ⁽²⁰⁾.

1.3.3. Shoulder osteonecrosis (ON)

Shoulder ON refers to humeral head osteonecrosis ⁽¹⁾, causing shoulder pain, but it isn't a common condition ⁽¹⁶⁾. The humeral head remains the second most common site of osteonecrosis following the femoral head ⁽¹⁷⁾. AVN of HH leads to bone necrosis ⁽⁴⁾⁽¹¹⁾, fractures ⁽¹¹⁾, head collapse and degenerative arthritic changes ⁽⁴⁾⁽¹¹⁾⁽¹⁴⁾ (*Figures 19 & 20*). AVN of HH can be traumatic or atraumatic ⁽⁴⁾⁽¹¹⁾⁽¹⁵⁾⁽¹⁶⁾⁽¹⁷⁾, which could be caused by the use of corticosteroids, vasculitis, Gaucher's disease, hypercoagulability, haemoglobinopathy, CTDs, radiation injury or can be spontaneous ⁽¹⁵⁾⁽¹⁷⁾. ON is treated by the correction of the PDFs ⁽¹⁾⁽¹⁵⁾⁽¹⁷⁾, but surgery in the form of arthroscopy and/or arthroplasty to re-vascularize or replace the necrotic collapsed head could be needed if the pathology continues to progress ⁽¹⁾⁽¹⁴⁾⁽¹⁵⁾⁽¹⁷⁾.

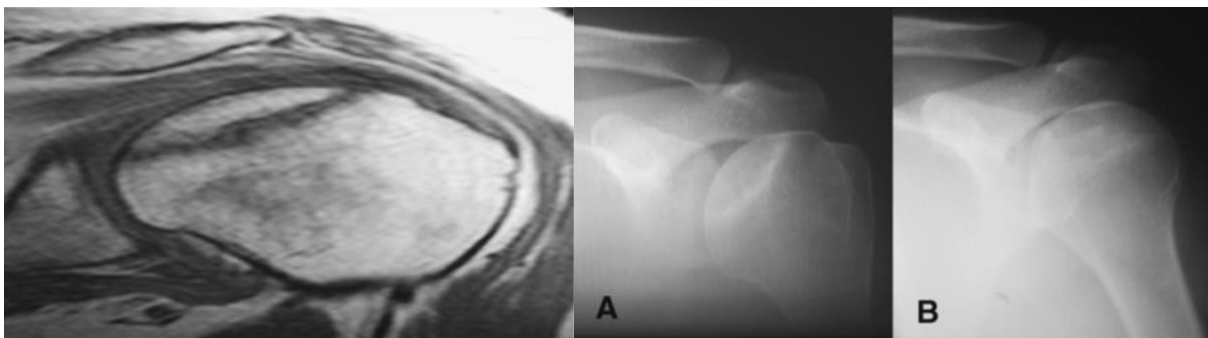


Figure (19): MRI of stage 2 humeral head ON disease. Note the characteristic involvement of a significant portion of the superior articular surface, as well as the clear demarcation between the relatively normal distal bone and the ischaemic subchondral bone (*Bulletin of the NYU Hospital for Joint Diseases 2009;67(1):6-14*).

Figure (20): Radiographs of late stage 2 humeral head osteonecrosis. AP views in (A) external and (B) internal rotation demonstrate areas of sclerosis involving a major portion of the humeral head (*Bulletin of the NYU Hospital for Joint Diseases 2009;67(1):6-14*).

1.3.4. Rotator cuff tears (RCTs)

RC tendons are the most common degenerative tendons ⁽⁸⁾ and RCTs are a common cause of shoulder pain, especially in the elderly ⁽⁷⁾⁽⁸⁾. Two mechanisms have been described: **(i)** intrinsic tendinopathy ⁽⁷⁾⁽⁸⁾⁽⁹⁾, which adopts a degenerative process ⁽⁷⁾⁽⁸⁾⁽⁹⁾⁽¹³⁾ involving the hypo-vascularised tendon ⁽⁷⁾⁽⁸⁾⁽⁹⁾, and **(ii)** extrinsic tendinopathy ⁽⁷⁾⁽⁸⁾⁽⁹⁾, which adopts a pathological process outside the tendon ⁽⁷⁾⁽⁸⁾ and is related to trauma and impingement ⁽⁸⁾. RCTs are classified using MRI or at surgery ⁽⁷⁾⁽⁸⁾ according to their **size** (*partial or full thickness*), **site** (*ventral or dorsal*) and **shape** (*crescentic, L-shaped, reverse L-shaped or trapezoid*) ⁽⁷⁾⁽⁸⁾⁽⁹⁾⁽¹⁰⁾ (*Figure 21*). The acute partial RCTs may be treated conservatively with

good results according to DePalma ⁽¹⁾ or surgically using open or arthroscopic techniques, depending on the criteria of both the patient and the RC defect ⁽¹⁾ ⁽⁷⁾ ⁽⁸⁾.



Figure (21): MRI of full thickness RCT (Dr Brian Badman, American health network, www.Indyshoulder.com).



Figure (22): Shoulder PXR (AP view) shows calcific tendinitis of the supraspinatus tendon causing shoulder impingement (red arrow) (Homepage, Dr G. Goudelis, 2015).

1.3.5. Calcific tendinitis of rotator cuff

Calcific tendinitis of RC is a common ⁽¹⁾ ⁽¹²⁾ ⁽²⁶⁾ ⁽²⁴⁾ and painful shoulder disorder ⁽¹⁾ ⁽²⁴⁾ of unknown aetiology ⁽²⁶⁾ and characterized by either single or multiple calcium deposits in RC tendons ⁽¹⁾ ⁽²⁴⁾ and/or subacromial bursa ⁽²⁴⁾ (Figure 22). PXR, US, CT ⁽¹⁾ ⁽¹²⁾ ⁽²⁴⁾ and MRI ⁽¹²⁾ ⁽²⁴⁾ are used to detect the calcium deposits. Initially, conservative treatment could work ⁽¹⁾ ⁽¹²⁾ ⁽²⁴⁾ ⁽²⁶⁾; otherwise surgical removal of the calcium deposits is indicated in refractory and long-lasting cases ⁽¹²⁾ ⁽²⁴⁾ ⁽²⁶⁾.

1.3.6. Impingement syndrome – (“rotator cuff tendinopathy”)

RC tendinopathy was described by Dr Neer in 1972 and is defined as the encroachment of the acromion, coracoacromial arch, coracoid process or ACJ on the rotator cuff as it passes beneath them during GHJ motion. The degree of mechanical impingement depends on the shape and the slope of the acromion (Figure 23). Impingement syndrome manifests with sudden rotator cuff tears or dull ache pain in chronic cases. It is initially treated with conservative methods, but in advanced cases open or arthroscopic surgical interventions are preferred ⁽¹⁾.



Figure (23): Rotator cuff arthropathy in an elderly patient. Note the obliteration of the subacromial space and the roundedness of the humeral head, which is subluxated superiorly resting on the acromion and forming a new “joint” at this location (Foruria et al., *Rev. esp. cir.ort op. traumatol.* 2008; 52:392-402).

1.4. Shoulder Arthroplasty

1.4.1. Background

The scientific term “*arthroplasty*” was first introduced by Prof. Gluck in 1902 ⁽¹⁾. Gluck designed the first shoulder prosthesis, but it wasn’t reported that he implanted it ⁽²⁾. Arthroplasty can be defined as a surgical orthopedic intervention; which is done either by replacing the joint with an artificial one, realigning the joint or remodelling the joint to relieve the disabling pain and/or to restore the restricted function of the joint after structural damage. Shoulder arthroplasty is indicated and was developed initially for the treatment of shoulder arthroses (“*stiff painful shoulder*”) ^{(1) (2) (8) (10) (27)}.

1.4.2. Arthroplasty history

The first excisional joint replacement was performed by Dr Anthony White in 1822 in London, and the first artificial shoulder joint replacement was performed by the French surgeon Dr Jules Emile Pean in 1893 ^{(1) (2) (5) (6) (8) (10) (11) (24) (25) (26) (27)} on a 37-year-old baker ⁽²⁾ whose shoulder was affected by T.B arthritis ^{(2) (8) (10) (11) (24) (27)}. The implanted joint was manufactured by a Parisian dentist, Dr Porter Michaels ⁽²⁴⁾, from natural biological materials ⁽¹⁾: **(i)** stem from platinum and leather ^{(2) (6) (8) (11) (24) (26) (27)} and **(ii)** head from a hardened ⁽¹⁰⁾ rubber ^{(2) (6) (8) (10) (11) (24) (26) (27)} coated with paraffin ^{(2) (6) (8)} with two deep grooves arranged at right angles ⁽¹⁰⁾, each containing a metal loop, one that fixes the ball to the scapula and the tube ^{(8) (10)} and the other that terminates in the shaft of the proximal humerus ⁽¹⁰⁾ (*Figure 24*). Although the patient postoperatively reported an improved function of the operated shoulder ^{(2) (8)}, Pean had to remove it after two years because of the severe infection ^{(1) (2) (8) (10) (24) (26)} in form of “*recurrent tuberculous arthritis and fistulae*” ⁽¹⁰⁾.

In 1914 Dr Koenig did a second trial using a prosthesis made of ivory, but thereafter a deep silence covered the field of shoulder arthroplasty for over 40 years, till the beginning of Neer’s era ⁽²⁶⁾. Neer introduced the first modern, anatomic, adjustable and durable shoulder prosthesis, the Neer type 2 prosthesis, in 1974 and manufactured it as a humeral head component from vitallium and a polyethylene glenoid component ⁽⁸⁾. The shoulder prosthesis designed by Dr Neer was successful ^{(8) (11)} except for the high failure rates due to glenoid loosening ⁽⁸⁾. Henceforth, surgeons began to think about the development of reverse total shoulder arthroplasty (RTSA) as a solution ^{(2) (3) (8) (16)}.

Unfortunately, the early clinical results of RTSA were disappointing, because of the high rates of mechanical loosening and revisions ^{(3) (16)}, but in 1987 Prof. Paul Grammont developed a very successful prosthesis ^{(3) (8) (16) (22) (27)} to shift the center of rotation ⁽³⁾ at the shoulder medially to compensate for the deficient RCMs ^{(8) (16)}. His prosthesis is still used nowadays ⁽³⁾ (*Figure 25*). Subsequently, arthroplasty interventions (*materials, implant designs, approaches, surface coating etc.*) developed rapidly ^{(1) (5) (9) (10)} to the extent that about 70 modifications of shoulder prostheses have appeared in the last decades ⁽⁸⁾ allowing patients to live an active lifestyle with the modern prostheses ⁽¹⁰⁾.



Figure (24): Photograph taken at Smithsonian National Museum of History shows first shoulder replacement placed by Jules E. Pean in patient with tuberculous arthritis (DOI:10.2214/AJR.12.8854).

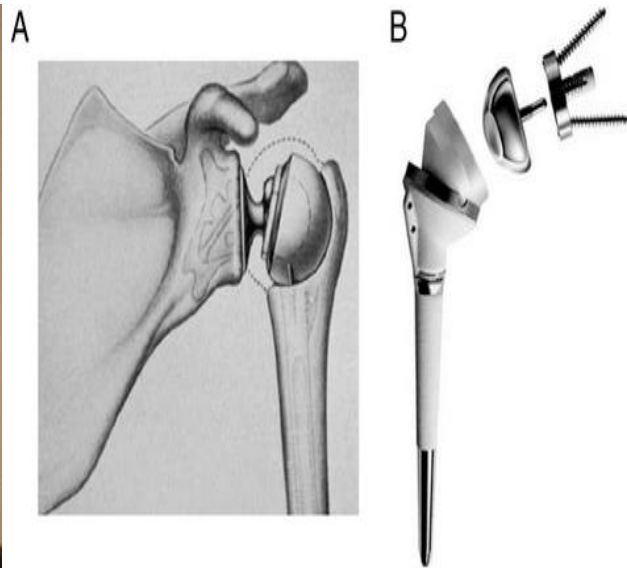


Figure (25): Neer's constrained reverse shoulder prosthesis concept (a) and the Delta III reverse shoulder prosthesis based on Grammont's original design (b) (DOI.org/10.1186/s13018-015-0244-2).

1.4.3. Shoulder arthroplasty types ^{(2) (3) (4) (5) (7) (8) (9) (10) (24) (25) (27)}

The shoulder joint is the third joint in the body to be replaced after the hip and knee joints ^{(27) (28)}. Four main successive designs of shoulder arthroplasty have been introduced and used widely in practice ⁽⁷⁾. These are ^{(7) (8) (9) (10)}: **(i)** hemiarthroplasty (*HA*); **(ii)** anatomic total shoulder arthroplasty (*ATSA*); **(iii)** reverse total shoulder arthroplasty (*RTSA*); and **(iv)** shoulder resurfacing arthroplasty. The outcome of shoulder arthroplasty depends on the type of prosthesis and the criteria of patient selection ⁽¹⁰⁾. Total shoulder replacement (*TSR*) leads to better results regarding pain relief, range of motion (*ROM*) and patient satisfaction than hemiarthroplasty ⁽²⁸⁾.

1.4.4. Anatomic total shoulder arthroplasty

1.4.4.1. ATSA: indications

ATSA is indicated for OA, inflammatory arthritis, revision of failed partial joint replacements and advanced AVN with secondary OA ⁽²⁷⁾.

1.4.4.2. ATSA: success requirements

To be successful, ATSA requires intact rotator cuff muscles and an adequate glenoid bone stock ⁽²⁷⁾.

1.4.4.3. ATSA: design (components)

ATSA prostheses have two components, humeral and glenoid components ⁽⁷⁾⁽⁸⁾⁽⁹⁾⁽¹¹⁾⁽²⁴⁾, which articulate together.

1.4.4.3.1. Humeral component features

The humeral component is a minimally constrained ⁽⁷⁾⁽⁸⁾ or unconstrained anatomic implant ⁽¹¹⁾⁽²⁴⁾ composed of two parts: **(i)** a metal spherical head with a smooth articular surface ⁽⁸⁾ and **(ii)** a metal cemented or press-fit stem ⁽⁷⁾⁽⁸⁾⁽⁹⁾⁽¹³⁾⁽²⁶⁾. Cofield claims that the press-fit components are adequate and stable in HA, while the cemented components are better in TSA ⁽²⁴⁾ (*Figure 26*). The humeral prosthesis designed by Neer was a monobloc ⁽⁹⁾⁽¹¹⁾⁽¹³⁾⁽²⁶⁾ with a smooth contour ⁽⁸⁾⁽⁹⁾⁽¹¹⁾ and was fixed initially by PMMA ⁽⁹⁾⁽¹¹⁾. **The advantages of cementing** are very low mechanical failure rates ⁽⁸⁾⁽⁹⁾, a lower incidence of radiolucent lines between cement and bone ⁽²⁶⁾, more stability ⁽⁸⁾ and better positioning ⁽⁹⁾ of the prosthesis in the patients with poor bone stock ⁽⁸⁾⁽⁹⁾, deformity and/or proximal humeral fractures ⁽⁹⁾ and the ability to mix the antibiotics with the cement to guard against infection as a prophylactic measure ⁽⁸⁾⁽⁹⁾. **The disadvantages of cementing** are the difficulty of prosthesis removal for revisions ⁽⁸⁾⁽⁹⁾⁽²⁶⁾ and the incidence of iatrogenic radial palsy secondary to cement extrusion ⁽⁸⁾⁽⁹⁾ through the nutrient artery foramen ⁽⁹⁾, which is rare but has been reported ⁽⁸⁾⁽⁹⁾. On the other hand, **the disadvantages of the cementless components** are the high incidence (*over 50%*) of progressive radiolucent lines and/or the migration of the component ⁽⁹⁾.

Development of the design of the anatomic humeral components has passed through three generations ⁽⁷⁾⁽⁹⁾. **1st generation prostheses** were monoblocs ⁽⁷⁾⁽⁹⁾⁽¹³⁾, manufactured in a very limited number of mid-range sizes ⁽⁷⁾⁽⁹⁾⁽²⁶⁾ and didn't precisely reproduce the proximal humerus geometry ⁽¹¹⁾. **2nd generation prostheses** are characterized by modular heads and an ingrowth coating on the stem ⁽⁷⁾⁽⁹⁾⁽¹¹⁾⁽¹³⁾⁽²⁴⁾⁽²⁶⁾. **3rd generation prostheses** are referred to as adaptable or anatomic and have modular heads ⁽⁷⁾⁽⁹⁾⁽¹¹⁾⁽¹³⁾⁽²⁴⁾, which facilitate the selection of the ideal head size for each particular patient to balance the soft tissues ⁽⁹⁾⁽¹¹⁾⁽²⁴⁾. Also, humeral bipolar prostheses were introduced to reduce the risk of glenoid wear ⁽²⁴⁾⁽²⁶⁾.



Figure (26): Different humeral components of HA (left: Stryker homepage) & TSA (right: www.foundation.shoulder.com).

Figure (27): Photograph of the SMR system glenoid, Castanga et al. (SMR System, Lima Corporate, Villanova, Italy) (DOI: 10.1302/0301-620X.92B10).

1.4.4.3.2. Glenoid component features

The glenoid component is a radiolucent ^{(7) (27)} polyethylene component (*PE-component*) ^{(7) (9) (27)}, which is either keeled or pegged with two or more ⁽⁹⁾ pegs on its inferior aspect ^{(7) (9) (24)} that contain radio-opaque markers ^{(7) (27)} (*Figures 27, 28 & 29*). According to some authors, keeled glenoids are old-fashioned and should be replaced by the pegged glenoids ^{(7) (9)}, which can currently be introduced in multiple configurations ⁽⁹⁾. Pegged-glenoids have advantages over keeled glenoids such as, better and more equal distribution of the applied stresses over the glenoid, removal of a little amount of bone during the implantation, easier to be revised ⁽⁷⁾, more accurate preparation of the bone socket, lower rates of translucency lines in the immediate postoperative radiographs ⁽⁹⁾, and better resistance against the tilting motions ⁽²⁴⁾. However, the keeled components are still indicated for patients with bone loss, inadequate bone structure ^{(7) (9)} and inadequate space for the pegged glenoids ⁽⁷⁾.

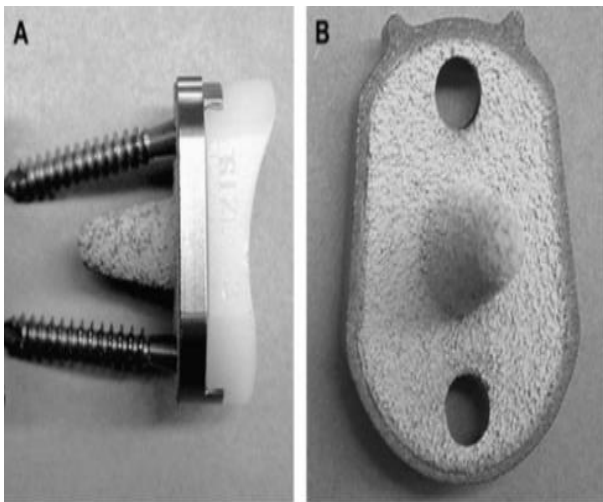


Figure (28): An example of an uncemented glenoid design where (A) initial fixation is achieved with 2 peripheral screws and (B) the component is press-fit into position using a central peg (*BMC Musculoskelet Disor* 2007; 8:76).

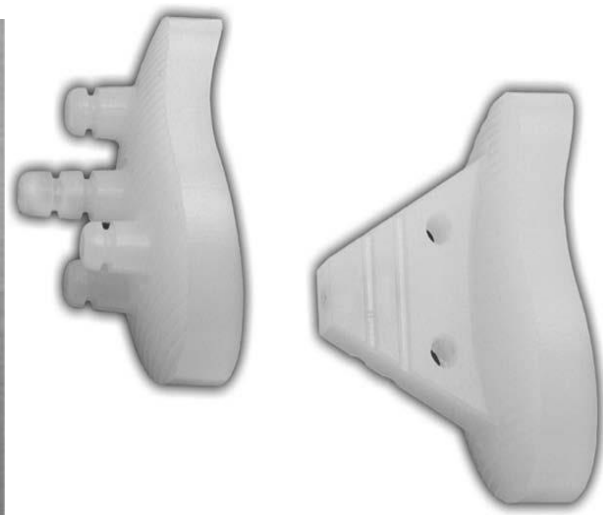


Figure (29): Cemented keeled (right) and pegged (left) glenoid designs for total shoulder arthroplasty (DOI: 10.1016/j.jse.2009.05.008).

1.4.4.4. ATSA: postoperative imaging

The postoperative radiographic criteria of ATSA success are: **(i)** glenoid component should demonstrate 0° version and 0° inclination with respect to the scapula on axillary views; **(ii)** humeral head component should be centered within the glenoid component; and **(iii)** humeral stem component should be centered within the humeral shaft, without translucency around either component ⁽²⁷⁾ (*Figure 30*).



Figure (30): The four standard projections for standard radiographic evaluation show a patient with ATSA. **(a)** AP view with the patient rotated approximately 45° towards the abnormal side; **(b)** AP view with the forearm in neutral position; **(c)** Cross-table view; **(d)** Neer's (Y) view with the radiographic beam parallel to the scapula and tilted craniocaudally by 15° (DOI: 10.1007/s00330-008-1093-8).

1.4.4.5. ATSA: complications

Many complications of ATSA have been reported ^{(4) (10) (18)}, such as instability ^{(10) (12) (14) (17) (19) (20) (21) (23)}, rotator cuff tears ^{(4) (10) (25) (27)}, periprosthetic fractures ^{(4) (8) (9) (10) (25) (26)} (*intraoperative and postoperative*), neural injury ^{(4) (9)}, stiffness ⁽⁹⁾, hematomas, deltoid injury and VTE ⁽⁴⁾, heterotopic ossification ⁽⁹⁾, periprosthetic infections ^{(8) (9) (10) (25) (27)}, humeral component complications such as subsidence, medial or lateral translation, anterior or posterior subluxation, superior migration ⁽⁸⁾, radiolucency/loosening ^{(2) (4) (8) (10) (25) (26)} and glenoid component complications such as glenoid loosening ^{(4) (7) (9) (10) (15) (24) (27)}, glenoid component failure and glenoid component wear ^{(3) (4) (10) (15) (16)}.

2. Study Design & Hypotheses

2.1. Introduction

Although total shoulder arthroplasty is considered a successful curative procedure for many chronic pain and stiffness disorders of the shoulder, it may be complicated by many problems, such as instability, component loosening, infection, periprosthetic fractures ^{(5) (6) (7)} etc. It has a complication rate of 10% to 15% ⁽⁷⁾. Glenoid component loosening ^{(10) (24) (27)} is still the most common complication of ATSA ^{(13) (14) (15) (17) (18)}, with a rate of incidence of up to 39% or 40% of operated shoulders ^{(7) (14) (16) (27)}. Hasan et al. found that 59% of failed TSRs exhibited loosening of the glenoid component ⁽⁷⁾. Glenoid loosening may be associated with GHJ instability ⁽¹⁶⁾ with a risk of frank dislocation ⁽¹⁸⁾ and frequently results in TSA failure ^{(13) (15)}, followed by humeral component loosening ^{(14) (18)}.

Glenoid loosening aetiology is multifactorial ⁽²²⁾. It could be **mechanical** (*abnormal loading* ^{(7) (8) (9) (12)} ⁽²²⁾, *rotator cuff insufficiency and/or soft tissues instability* ^{(13) (15) (22)}) (*Figures 32, 33 & 34*), **septic** (*infections*) ^{(9) (22)} or **aseptic** (*autoimmune reactions/osteolysis*) ^{(9) (10) (11) (22)}.

Sperling, Cofield and Rowland identified radiolucent lines adjacent to 59% of glenoid components, while the overall prevalence of these radiolucent lines is reported to range from 22% to 95% ⁽⁷⁾. A literature review showed, that the incidence of the radiological loosening of glenoid components varies between 0% and 15% after a follow-up of three years, rising to between 24% and 44% after nine years (*Figure 31*). Lazarus et al. have classified the pegged glenoid radiolucency, while Franklin et al. have classified the keeled glenoid radiolucency ⁽¹⁴⁾ (*Table 6*). The presence of radiolucency at bone-cement-interface ^{(14) (16) (19)} or cement-implant-interface ⁽¹⁶⁾ of the glenoid more than 2 mm in width in association with clinical manifestations including; increased pain level during follow-up, that appeared to be related to the implant, with restriction of external rotation to under 20° and abduction to under 60° ⁽¹⁹⁾ indicates glenoid loosening and/or failure ^{(14) (16) (19)}. The loose glenoid component can be corrected through a revision to a new component, in addition to bone grafting, using an autologous graft or an allograft, to preserve a sufficient bone socket and an adequate glenoid version ^{(20) (21) (22)}.

Classification	Lazarus et al.	Franklin et al.
Type of component	Pegged glenoid	Keeled glenoid
Grade 0	Absent	No radiolucency
Grade I	Incomplete radiolucency around one or two pegs	Radiolucency at superior and/or inferior flange
Grade II	Complete radiolucency (< 2 mm wide) around one peg only with or without incomplete radiolucency around one other peg	Incomplete radiolucency at keel
Grade III	Complete radiolucency (< 2 mm wide) around two or more pegs	Complete radiolucency ≤ 2 mm around keel
Grade IV	Complete radiolucency (> 2 mm wide) around two or more pegs	Complete radiolucency > 2 mm around keel
Grade V	Gross loosening	Gross loosening

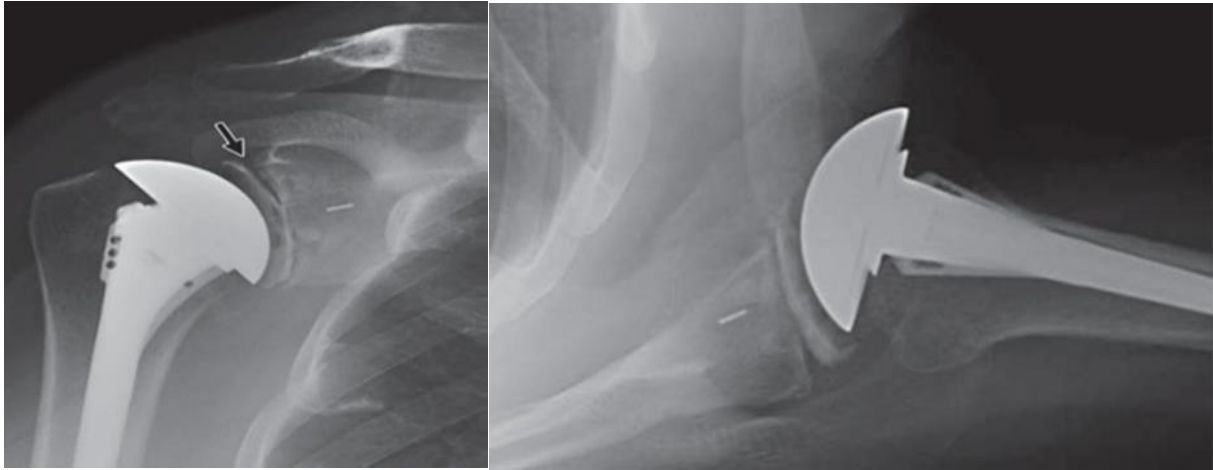


Figure (31): Glenoid component loosening in a 72-year-old woman with an anatomic total shoulder arthroplasty. Grashey (left) and axial (right) radiographs show frank loosening of glenoid component, with several millimeters of space between bone and polyethylene face (arrow, left) (DOI:10.2214/AJR.12.8855).

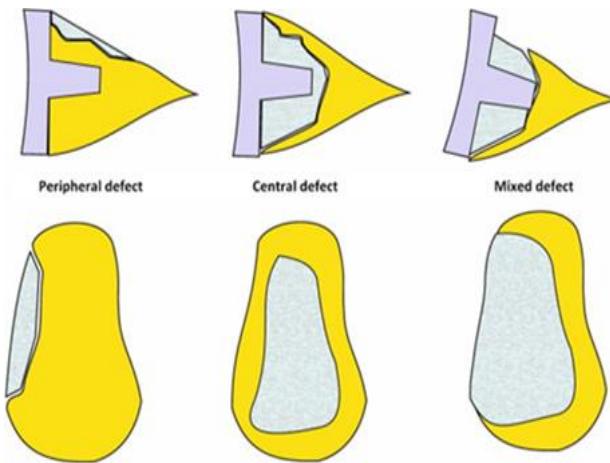


Figure (32): Three types of glenoid component loosening according to Walch et al. (DOI: 10.1016/j.otsr.2012.11.010).

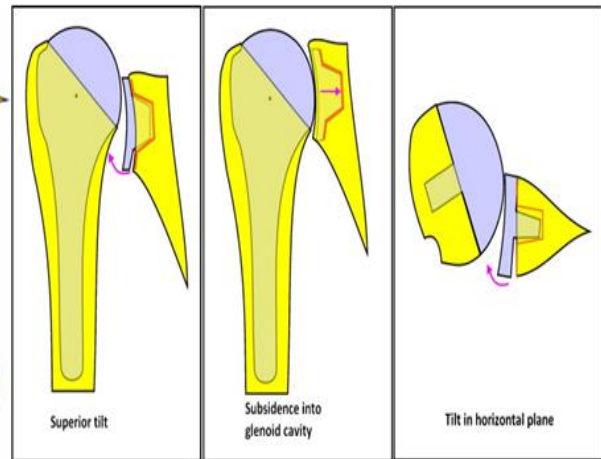


Figure (33): Evaluation of glenoid bone stock (DOI: 10.1016/j.otsr.2012.11.010).

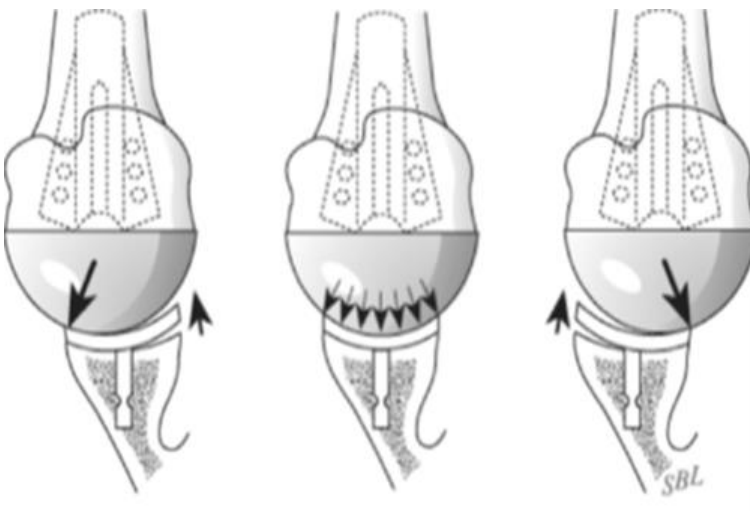


Figure (34): Rocking-horse loosening. Glenoid component is stable, but when the load applied by the humeral head is centered (middle), anterior (left) or posterior (right), translation of the head of the glenoid causes eccentric loading and lifting up of the opposite, unloaded glenoid rim (Masten III et al. 2008. DOI: 10.2106/JBJS.G.01263).

2.2. Study's problem definition

The submitted study discusses the mechanical aetiology of glenoid loosening after ATSA, which may be predisposed by abnormal glenoid morphology, implant design, inadequate surgical techniques ^{(9) (13)}, poor bone stock, poor cementing techniques ⁽¹⁸⁾, bone stock osteolysis or resorption ⁽¹⁵⁾ and/or rotator cuff deficiency ^{(9) (13) (18)}, which leads to superior humeral migration with “*eccentric loading*” ^{(9) (18)} (*Figure 33*). The glenoid fixation mechanism seems to play an important role in loosening occurrence. The early implanted glenoid prostheses were cemented all-polyethylene components. Following the poor results of these implants, metal-backed uncemented glenoids were gradually introduced (*Figure 28*). However, the results using all-polyethylene components were better than those using metal-backed components according to Neer's experience ⁽⁷⁾. Franklin et al. have suggested that the cyclic eccentric loading of the humeral head on the glenoid was responsible for loosening ⁽⁸⁾. This mechanism termed “*rocking-horse effect*”, has become the gold standard explanation of glenoid failure ^{(8) (9) (23)} (*Figure 34*). The rocking horse phenomenon can occur anterior to posterior as a result of increased glenoid retroversion or superior to inferior in the setting of rotator cuff tear and disruption of the dynamic force couple ⁽²³⁾.

2.3. Preliminary work

In our laboratory, experimental setups were previously built to allow the repaired shoulder joint to be tested in simplified and complex cyclic tests. Fixation stability studies of the glenoid investigated the effects of bone microarchitecture through state-of-the-art numerical analysis to evaluate the contribution of bone quality to the resulting stresses in the periprosthetic zone (*Figure 35*), especially, in relation to fixation designs and glenohumeral mismatch, which may lead to bone resorption and poor long-term fixation ⁽¹⁾. The first setup is adapted from previous studies of the glenoid ^{(2) (3)}. Tests were conducted on glenoid components to study the rocking-horse mechanisms, during which micromotions were recorded. This was done on extracted scapulae using components implanted into either synthetic or cadaveric specimens ⁽⁴⁾. However, the contribution of glenohumeral conformity, component designs and surgical implantation techniques to the joint stability and the contribution of the variations of the applied load quantities to the occurrence of glenoid loosening after ATSA in complete cadaveric shoulder specimens (*bone & soft tissues*) under cyclic loading in the three motion directions through prolonged successive phases using TeckScan and pressure data sensors haven't been fully investigated yet.

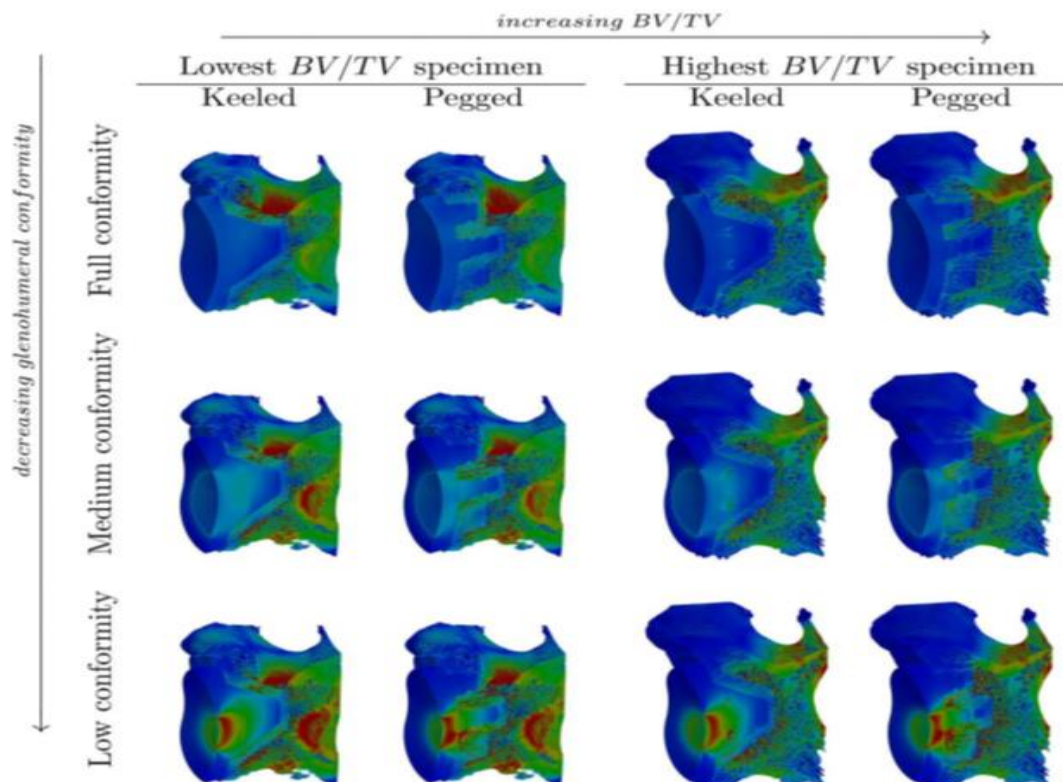


Figure (35): State-of-the-art numerical analysis showing the effects of fixation design on periprosthetic stresses in cement and bone (Chevalier et al., 2015a).

2.4. Study objectives

The submitted study aimed at a comprehensive experimental biomechanical evaluation of glenoid component stability of ATSA under repeated phasic cyclic loading, as follows:

- Evaluation of the biomechanical behavior of the artificially implanted shoulder under cyclic loading using TekScan system and pressure data sensors.
- Measurement and assessment of the quantity, pattern, mode of transmission and magnitude of the contact pressure between the joint's artificial articulating components under cyclic loading.
- Evaluation of the ability of the implanted glenoid component to maintain its stability without failure under continuous loading while transferring through the successive phases of cyclic loading.
- Understanding of the correlations between the measured mean peak pressure values of the successive testing phases to the CT findings with regard to glenoid component stability under cyclic loading.
- Statement of the correlation between glenoid component loosening, the experimentally observed joint instability or stability and the computed pressure values of the implanted joints under cyclic loading.
- Evaluation of the hypotheses.

2.5. Hypotheses

- 2.5.1.** Hypothesis (**Hi**): the recorded mean peak pressure values of the tested specimens are expected to vary greatly according to motion type.
- 2.5.2.** Hypothesis (**Hii**): the recorded mean peak pressure values are expected to vary between the initial (1st) and the final (3rd) testing phases.
- 2.5.3.** Hypothesis (**Hiii**): the occurrence of glenoid component loosening and its degree of extension are related to the changes in the obtained peak pressure values during testing.

3. Study Materials & Instrumentation

3.1. Specimens

In this experimental study, six “three paired” fresh-frozen complete cadaveric shoulder specimens were used (Table 7). Each specimen consists of a scapula, a complete humerus and complete soft tissues (*muscles, ligaments, labrum & capsule*), in addition to the ACJ. The specimens were supplied by the responsible governmental authority and were labeled with serial numbers providing the general features of their donors, such as age, sex, weight and body size, but without any specifically identifying data, such as place of residency, social status or medical history.

Table (7):		Specimens				
Serial	Specimen ID	Specimen Characteristics				
		Side (left or right)	Size (cm)	Weight (kg)	Age (y)	Sex (m/f)
1	SG04/14	RT	162	81	71	F
2	SG04/14	LT	162	81	71	F
3	SG02/15	RT	181	113	58	M
4	SG02/15	LT	181	113	58	M
5	1214/12	RT	179	87	76	M
6	1214/12	LT	179	87	76	M

Remarks:
 The total number of specimens is 6.
 Sex: Male> 3 specimens & Female> 3 specimens.
 Side: RT.....> 3 specimen & LT.....> 3 specimens.
 The RT and LT shoulders were extracted from 3 human cadavers.
 The body sizes of the donors of specimens ranged between 162 cm and 181 cm (mean body size is 174 cm).
 The body weights of the donors of specimens ranged between 81 kg and 113 kg (mean weight is 93.666 kg).
 The ages of the donors of specimens ranged between 58 and 76 years (mean age is 68.333 years).
 We don't have any information on the medical history of the donors.

3.2. ATSA components (Exactech, Inc., USA)

Two types of prostheses were implanted. **(i) Glenoid components:** seven glenoid components, three pegged and four keeled, were used in this study. The joint of each of the right-sided specimens was replaced with a keeled-glenoid component, while the joint of each of the left-sided specimens was replaced with a pegged-glenoid component. One of the left-sided specimens failed severely during the experiments, as will be described later, due to extreme instability under cyclic loading, so it was revised to a new keeled-glenoid component to be retested later. **(ii) Humeral components (adapters):** these were designed and manufactured in our laboratory and functioned as short-stemmed humeral components. The adapters were six cuboid-shaped metal pieces with dimensions of about 0.5 cm x 0.5 cm x 1.5 cm. Each adapter was drilled centrally from its upper small surface through its whole length to its lower small surface to make a longitudinal toothed hole for the fixating screw. For each adapter, a plastic cylindrical piece (“connector”) was fixed firmly to the metal piece with a suitable screw and a

metal washer was positioned between them. The metal head of the humeral component was fixed to the adapter with the press-fit method on the above-described plastic piece (*Figure 36*).

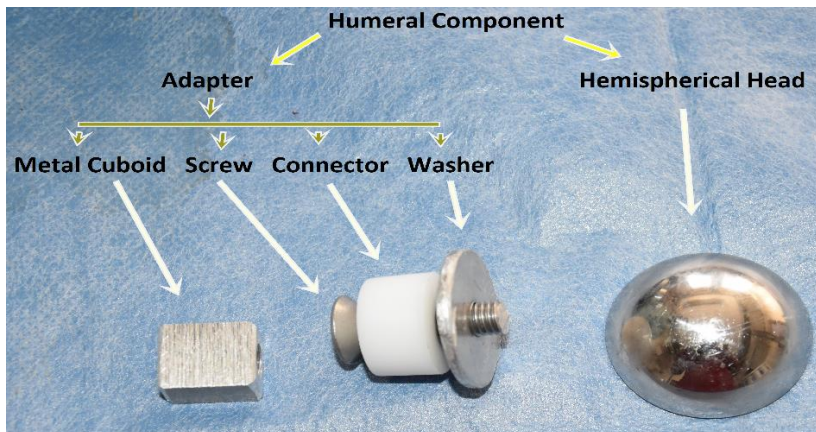


Figure (36): The parts of the humeral component (an adapter & a hemispherical head). The parts of the adapter are: a metal cuboid, a screw, a washer and a plastic cylinder (“Connector”).

3.3. Cement

Surgical bone cement was used for the fixation of the artificial components (*Refobacin® Plus Bone Cement 2x20, Biomet*). Additionally, ordinary lab cement was used for specimens embedding.

3.4. Metal bases

Two metal bases were used, one a flat broad plate for the fixation of the scapular portion and the other a cylindrical cup for the fixation of the humerus portion. Both were used to fix and mount the tested specimen to the shoulder simulator with screws (*Figures 53 & 54*).

3.5. Fixating screws

Numerous screws of different lengths and sizes and with suitable washers were used to fix each specimen to the metal bases and then to mount the specimen with its two metal bases on the simulator (*Figures 53 & 54*).

3.6. Plastic template

A plastic template was used as a reference to make accurate holes through the bone of the scapular portion of each specimen, which should correspond to the holes of the metal bases and the holes of the simulator to be fixed to them.

3.7. Surgical instruments

The ordinary surgical instruments such as saws, screwdrivers, scalpels, suture needles, scissors, retractors etc. were used to prepare the specimens for mounting on the setup. Also, the special surgical instruments of arthroplastic surgery were used for the implantation of the prostheses.

3.8. *Shoulder setup – (“shoulder simulator”)*

The simulator used is a novel setup (*Figure 41*), which was built especially for our laboratory to be used in the biomechanical experiments of shoulder specimens. It offers free passive motions of the tested joints in the three anatomical axes: abduction-adduction (AA), flexion-extension (FE) and internal rotation-external rotation (IE) in vitro (AA: 90° - 0° - 0° / FE: 40° - 0° - 40° / IE: 30° - 0° - 30°).

3.8.1. *Simulator construction*

The shoulder rig is composed of **(i) a large metal frame** (*Figure 41*) with dimensions about 180 cm (*height*) x 116 cm (*length*) x 66 cm (*width*), which carries a central moving metal part composed of successive metal plates and a metal abducting arm; and **(ii) a central moving metal part** (*Figure 38*) composed of three parallel separate supportive metal plates and an additional upper movable plate. The three metal plates are connected together through movable bridges/connectors to allow a flexible independent free single-planed motion of each plate. When these plates of the central part are enumerated from bottom to top, the lowest plate (*4th plate*) is fixed with its inferior surface to the central pillars of the simulator and connected at its upper surface with the following plate, the 3rd plate, through flexible bridges which allow the 3rd plate to move from side to side. The 3rd plate is connected at its inferior surface to the 4th plate and at its upper surface with the second plate by flexible bridges. The 2nd /middle plate is the thickest plate and is connected at its inferior surface with the 3rd plate through flexible bridges and at its superior surface with the lower surface of the uppermost plate, the 1st plate, through a central axis, which allows the rotatory motion of the 1st plate. The 1st plate (*movable plate*) is connected at its inferior surface to the upper surface of the 2nd plate through a joint with a central axis. Its upper surface carries two pyramidal metal projections (*Figures 39 & 40*) for the fixation of the metal base of the scapula to carry the tested specimen. Finally, the setup has **(iii) a moving (abducting) metal arm** (*Figure 37*): when facing the simulator, the metal arm is located on the right side of the observer. This arm originates from the middle horizontal posterior pillar of the simulator frame through a jointed root that enables the metal arm to move in a rotatory/circular pattern around the central axis of the hinge in a motion arc of 90° to simulate the Abd-Add motion in vivo (*Figure 43*). The moving metal arm consists of four connected parts: hinged-root, long longitudinal portion located parallel to the posterior aspect of the simulator frame, short transverse part located parallel to the left side of the simulator frame on the right hand of the observer, and a very short part located parallel to the anterior aspect of the simulator frame and to which the metal base of the humerus stump of the tested specimen were fixed with screws.

3.8.2. *Simulator mechanics*

The motions of the simulator parts can be described as follows: **(i) the 4th metal plate (lowest plate)** of the central part of the simulator is completely fixed and non-movable. **(ii) The 3rd plate** can move freely from side to side through the flexible bridges that connect it with the 2nd and the 4th plates. Stabilizing weights can be hung on its left side (*observer’s right side*) with a metal wire during testing (*Figure 42*).

(iii) The 2nd plate can move freely in an anterior to posterior direction and in a posterior to anterior direction through the flexible bridges between it and the 3rd plate, but during its motion the 2nd plate carries the 1st plate as well as the mounted specimen with it to move together as one block. The stabilizing weights can be hung on its posterior surface with a metal wire during testing of the right-sided specimens and hung on its anterior surface during testing of the left-sided specimens (*Figure 42 & Table 12*). **(iv) The 1st plate** carries the scapular portion of the tested specimen, which is fixed with screws to two metal pyramidal pieces lying on the upper surface of the 1st plate. These two metal pyramidal pieces are apparent and seen during testing of the left-sided specimens, whereas they become hidden posteriorly when testing right-sided specimens (*Figures 39, 40 & 43*).

The 1st plate can move freely in a rotatory/circular pattern within an arc of half a circle around the central axis to create the FL-EX motion simulation of the setup, which connects it with the underlying 2nd plate. The 1st plate starts its motion from the neutral point at the middle line and moves posteriorly in a circular fashion to simulate extension in right-sided specimens or flexion in left-sided specimens. From the neutral point, it moves anteriorly in a circular fashion to simulate flexion in right-sided specimens or extension in left-sided specimens.

It is important to note that while the simulated FL-EX (40° - 0° - 40°) motion is produced by the 1st plate of the central metal part, the simulated IR-ER (30° - 0° - 30°) and Abd-Add (90° - 0° - 0°) motions are produced through the moving abducting arm (*Figure 43*). The expressed motions from the 2nd and the 3rd plates with the attached weights function together to adjust, neutralize and stabilize the produced motions of the 1st plate of the central part and the produced motions of the moving arm, and also to optimize the biomechanical function of the setup.

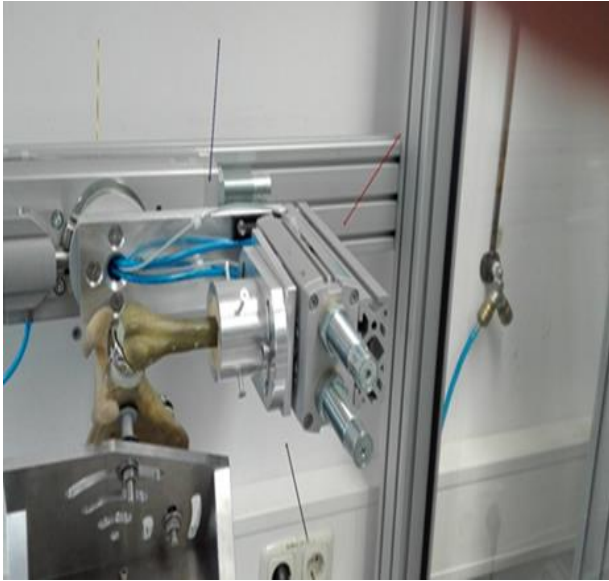


Figure (37): The simulator with a mounted LT-sided Sawbone synthetic specimen shows the moving metal arm of the simulator (oblique view from above) and its four parts: the movable jointed-root with central axis (yellow arrow), the longitudinal part (blue arrow), the transverse part (red arrow) and the attaching part with the humeral stump (black arrow).

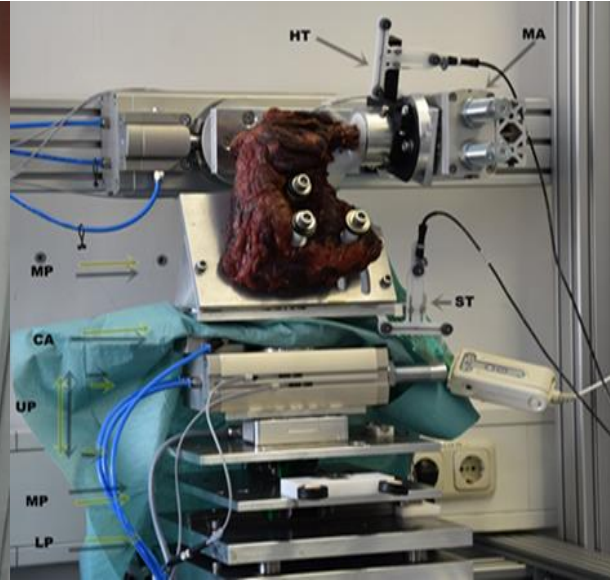


Figure (38): The central part of the simulator with a mounted RT-sided specimen, moving arm of simulator, tripods from Zebris, TekScan and an inserted pressure sensor within the GHJ of a right-sided mounted shoulder specimen (MP: moving plate; CA: central axis; UP: upper plate; MP: middle plate; LP: lower plate; ST: scapular tripod; HT: humeral tripod; MA: moving arm).

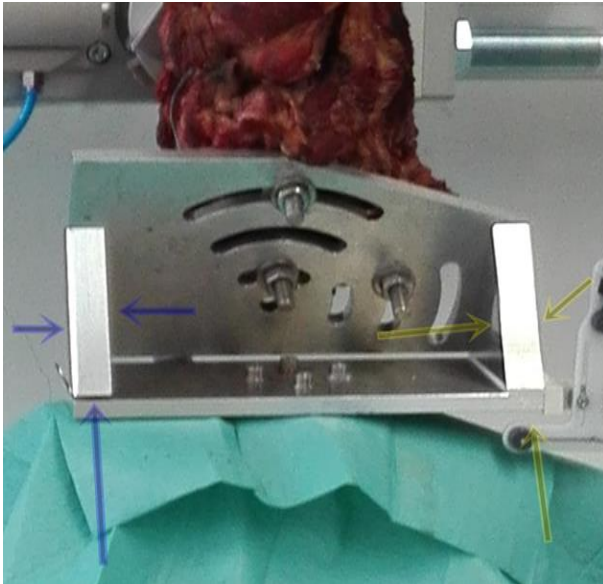


Figure (39): The orientation of the two metal pyramids in the resting position with a mounted LT-sided shoulder specimen. Both pyramids face anteriorly with their small surfaces; blue arrows point to the RT pyramid of the simulator on the LT of the observer and yellow arrows point to the LT pyramid of the simulator on the RT of the observer.

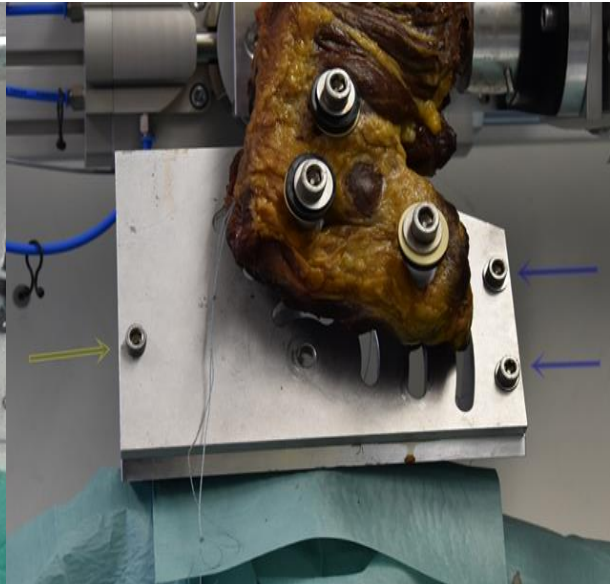


Figure (40): The mounting of a RT-sided shoulder specimen, in which two screws (blue arrows) are fixed to the posteriorly situated and hidden LT metal pyramid of the simulator on the RT of the observer and one screw (yellow arrow) is fixed to the posteriorly situated and hidden RT metal pyramid of the simulator on the LT of the observer.

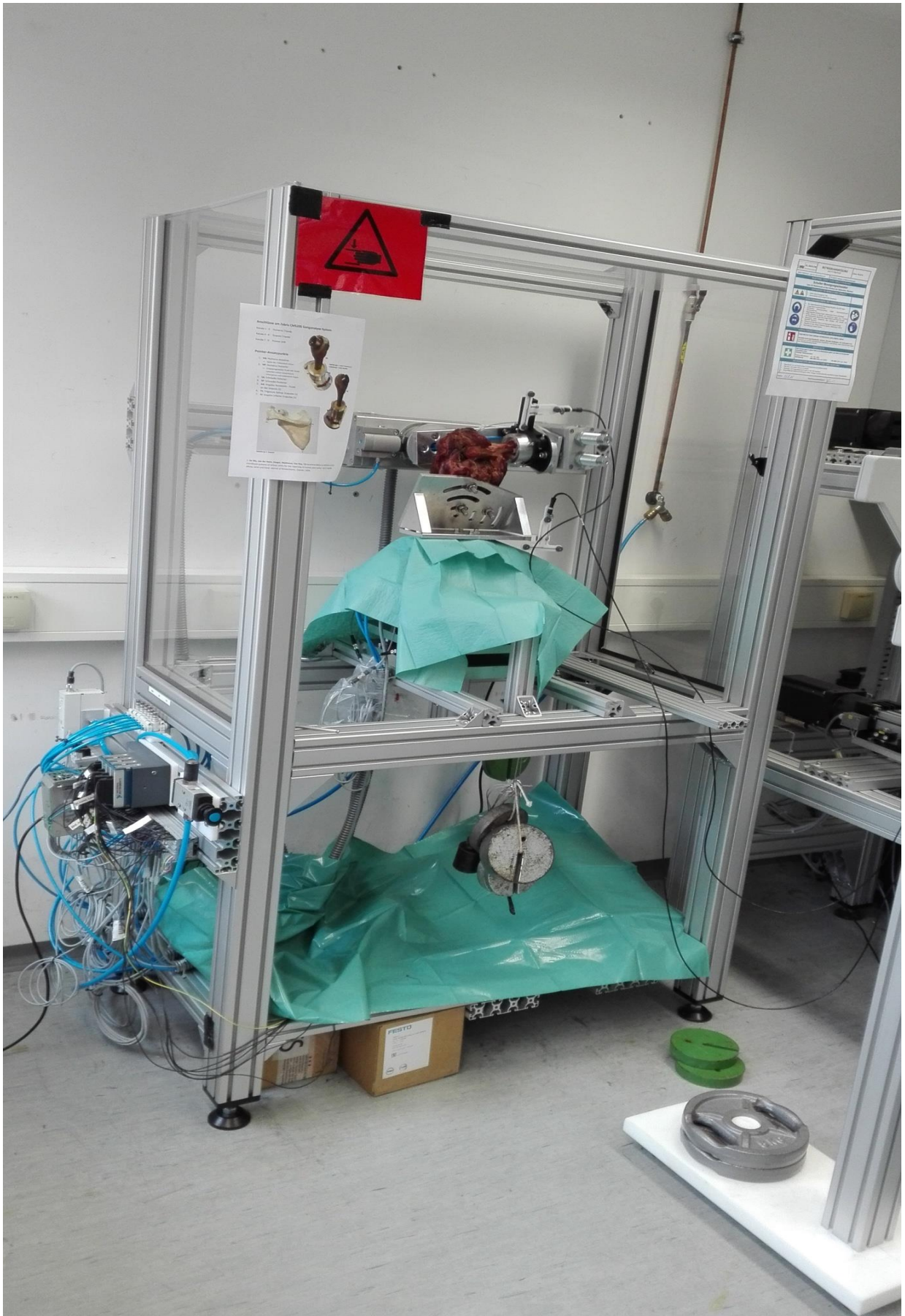


Figure (41): General view of the simulator with a mounted left-sided shoulder specimen.



Figure (42): The pattern of hanging of the stabilizing weights during testing of a left-sided mounted shoulder specimen on shoulder rig. Black arrows refer to the stabilizing weights of scapula, which is attached to the 2nd plate and hung on the anterior aspect of shoulder rig when testing a left-sided specimen, while the yellow arrows refer to the stabilizing weights attached to the 3rd plate and usually hung on the left side of the simulator during testing of LT- or RT-sided specimens.

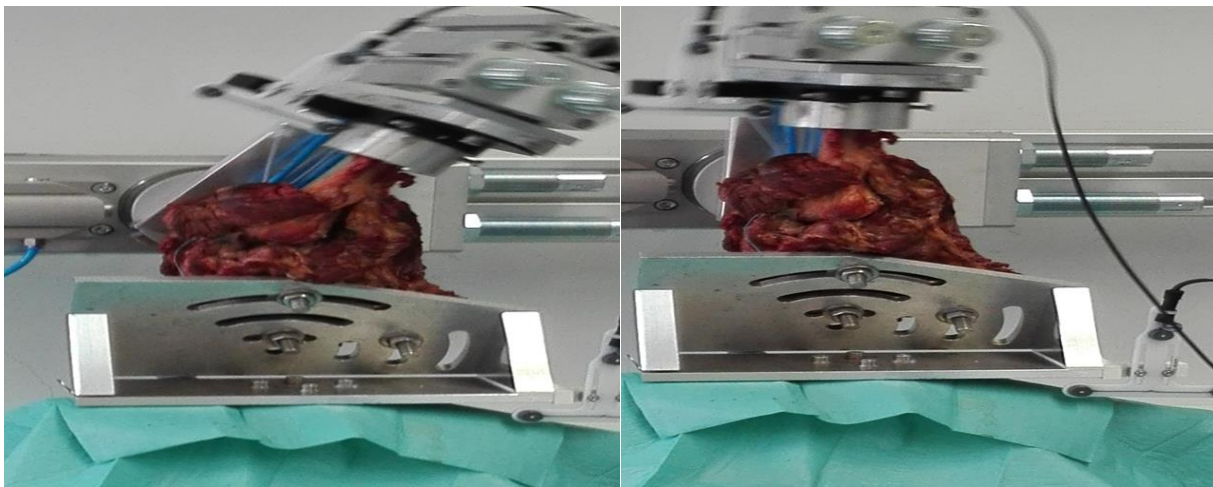


Figure (43): A mounted left-sided shoulder specimen on the simulator at mid-abduction (left) & at full abduction (right) motions during cyclic loading testing (the haziness/cloudiness at the upper part of the two images around the moving metal arm of the simulator is evidence of the motion).

3.9. Shoulder pointer, Zebris system with “US” & kinematic tripods

The shoulder pointer is a plastic stick measuring about 25 cm that is connected proximally with a cable and distally with a metal pointer measuring about 5 cm (Figure 44). The cable connects the whole pointer with the Zebris system (Zebris Medical, GmbH, Germany). The shoulder pointer is used to localize the position of the tested specimen after its mounting on the simulator as an initial step before the starting of any testing phases. This is carried out by outlining the dimensions of the specimen by defining three landmarks on the scapula and four landmarks on the humerus, as will be described later. With ultrasound, the Zebris system can determine the accurate position of the specimen and can follow it during its simulated motion in the space to give the examiners an idea about the joint kinematics during testing (Figure 44). This function of the Zebris system is achieved with the assistance of two T-shaped plastic parts (kinematic tripods); one of these is fixed to the right side of the lower part of the central metal part of the simulator and functions as a scapular tripod, while the other is fixed to the black plastic connector, which in turn is fixed around the metal cup of the humeral stump and functions as a humeral tripod. The two tripods function as guides for the Zebris system (Figure 45).

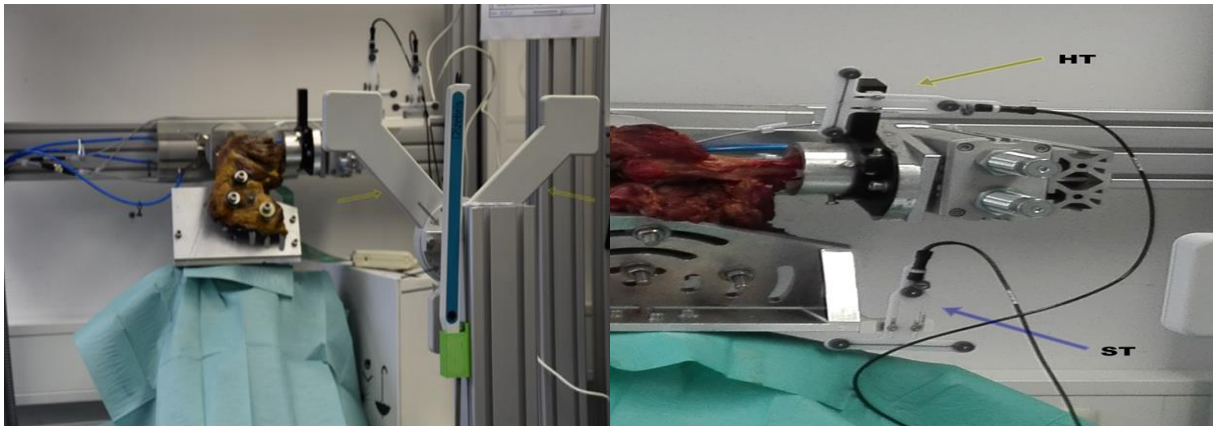


Figure (44): Zebris system from behind (yellow arrows) and shoulder pointer (black arrows), in addition to a right-sided shoulder specimen mounted on the simulator.

Figure (45): The humeral tripod above (HT/yellow arrows) and the scapular tripod below (ST/blue arrow) with a left-sided shoulder specimen mounted on the simulator.

3.10. TekScan pressure sensor (Tekscan, Inc., USA)

Double-headed and single-tailed pressure-sensitive foils (Figure 46) were used to measure the contact pressure between the articular surfaces during the testing of each specimen under cyclic loading. Each pressure sensor has two ends and a body; the proximal end is two-headed, in that it has two identical heads with an option to use only one of them during the testing. The body is slender, elongated and flat, while the distal end “tail” is single and should to be pushed through a cleft within a small apparatus, which is connected to the operating computer to measure the transferred data. The heads of each pressure sensor are rich with highly sensitive cells, and from each cell originates a sensitive fiber, which crosses the whole length of the sensor to end within another sensitive cell at the tail, which appear as rounded dots on the surface of the sensor. The head sensitive cells (*collecting cells*) collect the data in form of impulses during the motion of the joint under cyclic loading and these impulses are then transferred through the sensitive fibers (*transferring neurons*) to be imported to the tail sensitive cells (*delivering cells*), which then send them across the connected apparatus to the computer to appear as one round colored signal to be evaluated (Figure 49). This indicates the pattern, value and magnitude of the contact pressure during joint motion according to the references of the installed program.

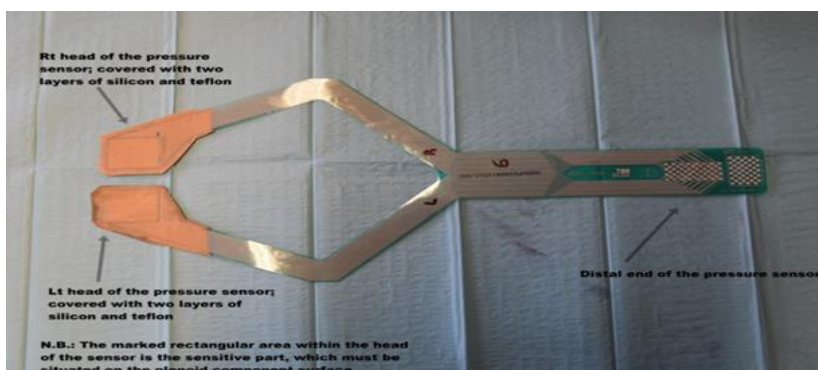


Figure (46): The TekScan pressure sensor foil. It consists of a proximal end with two RT & LT heads and a distal end. The two heads are covered with silicon & Teflon layers for protection during joint motion under loading testing.

3.11. Testing system operating programs

Two computer programs were installed to control the work during this study through two interconnected devices. The evaluator should work on both simultaneously.

3.11.1. Simulator operating program – (“LabView-SchulterKinemator”)

This program is considered the main program (Figures 47 & 48), because it controls the function of the simulator locally, initiates the whole test and then helps in controlling the whole test during the course of the experiment with each specimen. After the installation of the program, the specimen is attached to the shoulder rig. Firstly, the scapular portion of the tested specimen should be mounted at 0 volts, then the applied forces should be increased gradually up to 2.5 volts, at which point the humeral portion can be mounted. Then the appropriate weights should be hung according to the side of the subjected specimen. The evaluator must then position the joint of the specimen optimally to avoid the presence of dislocations or subluxations.

At this stage, and when everything functions well, the applied forces should be increased gradually up to 3.5 or 3.7 volts and the stabilizing weights should also be increased and adjusted to obtain an optimally stable joint before the initiation of the cyclic loading testing. At this stage, the evaluator should go to the other side of the operation room to install the other programs. After the installation of the other co-operating programs as discussed below, the evaluator returns to this computer to give the order to start testing. The evaluator has the option to perform a pretest before the main test, i.e. five or ten cycles in each motion direction to check the efficiency of the simulator and the whole integrated operating system. Ordinarily, the evaluator saves the specimen ID, the direction of the intended motion (*IR-ER*, *FL-EX* or *Abd-Add*) and the number of the planned testing cycles. Then the experiment can be initiated.

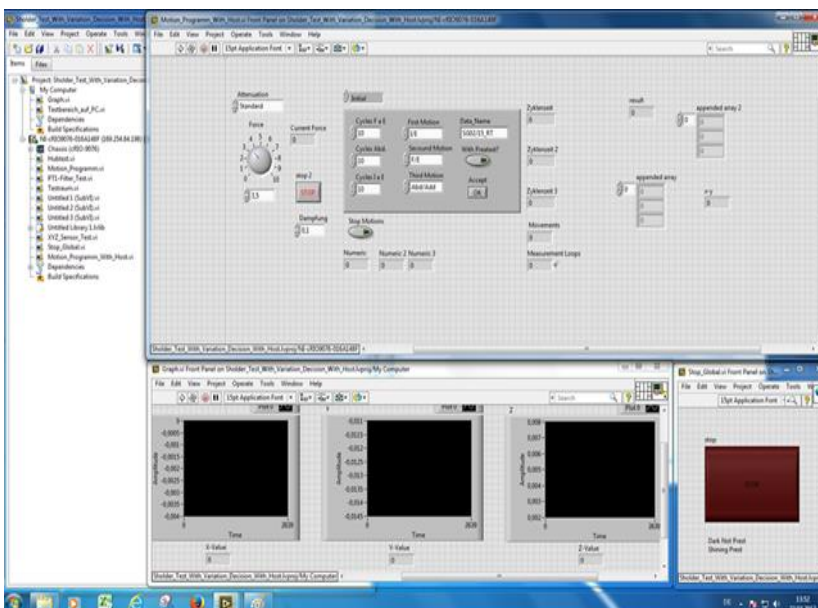


Figure (47): The operating program of the simulator. Firstly, the ID of the specimen, the number of cycles, the direction of cycles and their sequence are entered, in addition to the amount of the force. Then the evaluator presses “Accept”. The red Stop button is designed for urgent stoppage. The black windows below show the graphs of motion, but this wasn’t a part of our study.

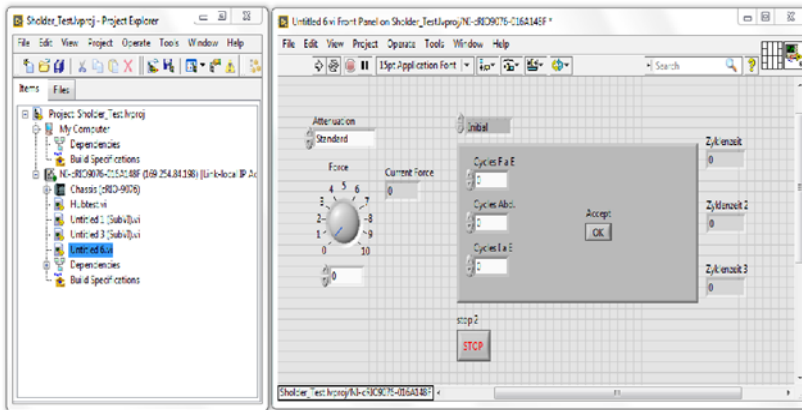


Figure (48): The second window of the operating program of the simulator. When everything is in order, the evaluator presses “Accept” to start the phase of cyclic loading.

3.11.2. TekScan operating program

The evaluator should then install the TekScan program and check the presence of the signal from the inserted sensor head on the corresponding screen, its quality and its matching with the position of the inserted pressure sensor head. The sensor is composed of two heads, which can be used separately, so the computer screen is also divided into two halves, each one representing one of the two heads. The signal of the used sensor head will appear on the corresponding half of the computer screen. The outer and inner sides of the displayed signal correspond to those of the joint surface (*RT to RT, LT to LT*), while the upper and lower sides are reversed (*upside-down mirror image*): the upper side of the joint corresponds to the lower side of the signal and the lower side of the joint to the upper side of the signal. Furthermore, the site of the signal within its screen half indicates the position of the sensor head within the joint cavity and the stability of the joint, so that any shifting of the site of the displayed signal within the screen indicates abnormal head sensor insertion/position within the joint cavity and/or subluxation or dislocation of the implanted joint of the subjected specimen (*Figure 49*).

The evaluator should then routinely evaluate the following parameters of the quality of the signal (*Figure 49*): **(i) signal site**: the position of the displayed signal within its screen half; **(ii) signal size**: large or small; **(iii) signal shape**: rounded, oval, elongated or irregular; **(iv) signal intensity**: according to the color reference of the program; **(v) signal abnormalities**, such as the presence of transverse or longitudinal, single or multiple, complete or incomplete black lines, which run across the corpus substance of the signal in superoinferior or mediolateral directions. The displayed signal is a reflected image of the quality of the contact (*the contact pressure and the contact pattern*) between the articulating prosthetic components within the joint at the resting phase and then during testing phases.

The presence of black lines within the displayed signal (*Figure 50*) indicates either: **(i)** defect in the contact between the two articulating surfaces of the joint of the specimens due to dislocation, subluxation, or failure to properly adjust the joint position after the installation of the LabView program of the simulator; **(ii)** technical defect within the sensor head itself at the time of its fabrication; or **(iii)** damage/disruption of the sensor head due to shear forces which have separated the two layers of the

sensor head from each other, if the inserted sensor was used in a previous testing session. **The optimal signal should be** rounded in shape and large, medium or small in size according to the size of the tested specimen and the implanted joint components, and the intensity of the signal increases in outwards-inwards direction. This means that the most intense point of the signal is its center, which indicates the highest contact pressure value between the two articulating surfaces of the artificial joint. In the TekScan program, the specimen ID and motion direction are saved routinely after the termination of each cyclic motion phase.

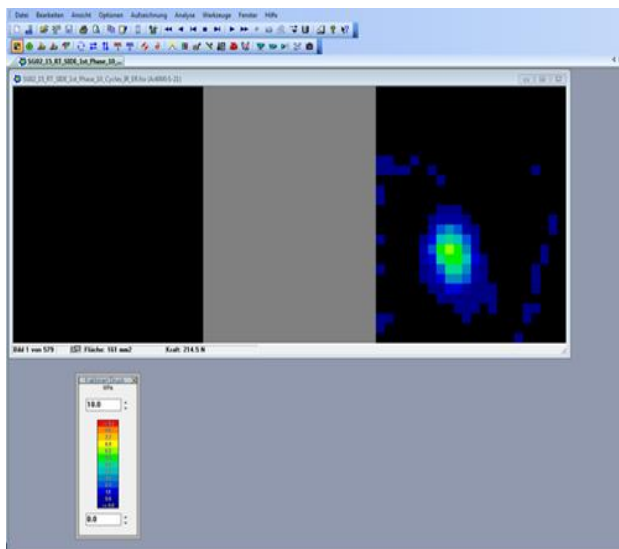


Figure (49): An optimally displayed TekScan signal at the resting phase according to the described criteria (complete, rounded & corresponding to the colors reference at the lower part of the photo).

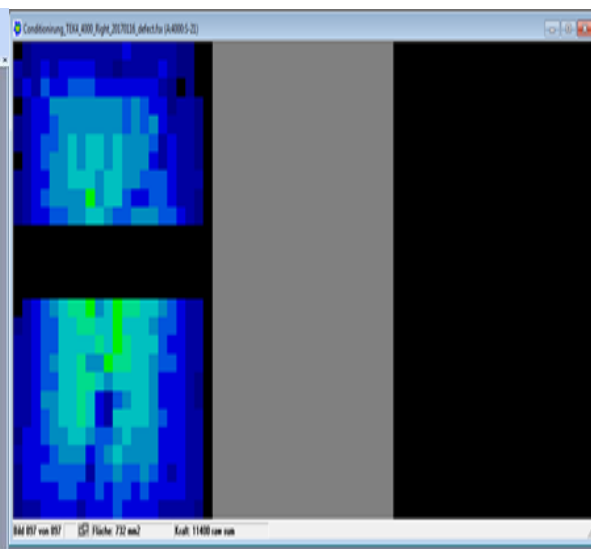


Figure (50): A bad TekScan signal, because there is a central black line running from side to side, which indicates damage within the sensor head substance. The whole signal was enlarged for clarity.

3.12. Quantitative computed tomography (QCT)

Prior to the experiments and upon their completion, the shoulder specimens were sent to the radiology department of the university hospital to be scanned by QCT.

4. Methodology

4.1. Stage I: Initial pre-testing radiological scanning using QCT

The six shoulder specimens were sent on 17/09/2015 to the radiological department of the university hospital to be scanned by QCT to evaluate the versions and superior-inferior lengths of their native glenoids, and additionally to evaluate the humeral head size, bone socket quality, and presence of diseases and/or implants (*Figures 51 & 52*). According to the provisional evaluation, the six specimens were mostly free of the arthritic changes and/or congenital malformations, except the glenoid of one specimen (ID: 1214/12/RT), which was suspected to be slightly elongated in the coronal sections (*Figure 51*).

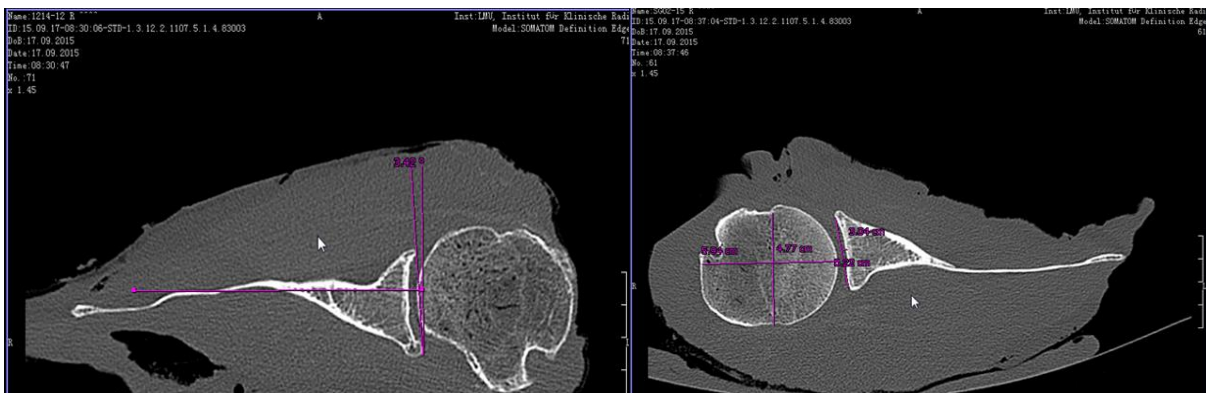


Figure (51): An example of glenoid version evaluation using QCT (coronal section). Specimen ID: 1214/12 RT with measured retroversion about 3.4° & SI length about 39 mm.

Figure (52): An example of evaluation of glenoid size (superior-inferior length) and humeral head size (superoinferior (SI) and mediolateral (ML) diameters) using QCT (coronal section) (specimen ID: SG02/15 RT).

4.2. Stage II: Pre-experimental planning

According to the macroscopically evaluated size of each specimen and the radiologically evaluated/measured superior-inferior length of the glenoid of each specimen using QCT coronal sections, the scheduled three pairs of specimens were categorized as follows (*Table 8*): a small-sized pair (SG04/14/RT & LT), a medium-sized pair (1214/12/RT & LT) and a large-sized pair (SG02/15/RT & LT). The initial plan was to implant the three right-sided specimens with keeled-glenoids and the three left-sided specimens with pegged glenoids, but one pegged specimen (LT-sided) was unstable under cyclic loading and was revised to a new keeled glenoid.

4.3. Stage III: Preparatory stage

Each specimen was prepared as follows: the humerus was resected at the elbow and the distal 5 cm of the resected humeral shaft was cleaned from soft tissue coverage. Then the scapula was drilled to make three holes for its fixation using the plastic template as a reference (*Figures 53 & 54*). The previously

prepared distal portion of the humerus was positioned within the metal cup and fixed with the laboratory cement and an additional four screws while the scapula was fixed to the metal base through the previously prepared three holes (Figures 53 & 54).



Figure (53): Dorsal aspect of a LT-sided shoulder specimen prepared with the fixation of the humeral and scapular metal bases for subsequent mounting on the simulator.



Figure (54): Ventral aspect of a LT-sided shoulder specimen prepared with the fixation of the humeral and scapular metal bases for subsequent mounting on the simulator.

4.4. Stage IV: Arthroplasty (implantation stage)

After the preparation of the specimens, the joints were approached through the DP approach to implant the prosthetic components. The humeral heads were resected and drilled for the adapters, and then the glenoids were debrided, reamed and drilled for either pegged or keeled glenoid components according to the stated plan (Table 8). The prosthetic components were cemented in each specimen directly before its testing (Figures 55, 56, 57 & 58).



Figure (55): The drilled hole for humerus adapter component within the rest of the humeral head after its resection in a RT-sided shoulder specimen.



Figure (56): The drilled native glenoid for a subsequent implantation of a pegged glenoid component in a LT-sided shoulder specimen.

Table (8): Plan of Glenoid Implantation					
Serial	Specimen ID	Specimen Side	Component Size	Type of Glenoid Component	Test Date
1	SG04/14	RT	Small	Keeled	12/01/2017
2	SG04/14	LT	Small	Pegged	23/01/2017
3	1214/12	RT	Medium	Keeled <i>Deviation:</i> Testing failed and repeated on 19/01/2017	16/01/2017
4	1214/12	LT	Medium	Pegged	02/02/2017
5	SG02/15	RT	Large	Keeled	17/01/2017
6	SG02/15	LT	Large	Pegged <i>Deviation:</i> Testing failed and the specimen was revised to a new keeled component and retested on 08/02/2017	24/01/2017
Remarks: After revision of the LT-sided specimen ID: SG02/15 to a new keeled glenoid component the total number of tested keeled specimens became four and the total number of tested pegged specimens became two.					



Figure (57): A RT-sided shoulder specimen with an implanted keeled glenoid component (according to the plan of study) and the metal part of the humeral adapter (upper side of the figure corresponds to the upper glenoid pole).



Figure (58): A cemented humeral adapter with its complete parts within the resected humeral head in a RT-sided shoulder specimen.

4.5. Stage V: Specimen step-wise testing

Each specimen was tested after the completion of the implantation of ATSA components through a three-level experiment. Each of these three levels was further subdivided into four major steps (Table 9).

Table (9): Levels of Specimen Step-Wise Testing		
Level	Steps	Description
Level I	Step A	Insertion of the TekScan pressure sensor within the GHJ of the specimen
	Step B	Mounting of the specimen on the simulator with adjustment of the involved devices & installation of the operating programs
	Step C	Recording of the data of the shoulder pointer
	Step D: (1 st Phase)	Launching of the “First Phase of Cyclic Loading”
Level II	Step A	Temporary stoppage – “Tactical Pause” of the simulator
	Step B	Removal of the TekScan pressure sensor from the GHJ of the specimen
	Step C	Remounting of the specimen on the simulator with re-adjustment of the involved devices & re-installation of the operating programs
	Step D: (2 nd Phase)	Launching of the “Second Phase of Cyclic Loading”
Level III	Step A	Temporary stoppage – “Tactical Pause” of the simulator
	Step B	Reinsertion of the TekScan pressure sensor within the GHJ of the specimen
	Step C	Remounting of the specimen on the simulator with re-adjustment of the involved devices & re-installation of the programs
	Step D: (3 rd Phase)	Launching of the “Third Phase of Cyclic Loading”

4.5.1. Formulation of the cyclic loading phases

The plan was to test each specimen through three successive phases of cyclic loading with different loading forces and different number of cycles in one day (*Table 10*). Two phases, the 1st and the 3rd, were short, while the second phase was long. The motions of each of the three phases are in the three directions of the anatomical axes (*Abd-Add, FL-EX and IR-ER*) under cyclic loading. It was planned to measure the contact pressure values and the contact pattern between the articulating surfaces of humeral and glenoid components of each specimen under cyclic loading using the TekScan pressure sensor foil only in the first and third phases of cyclic loading. The measurements recorded by the TekScan pressure sensor system in the first and third phases would then be compared.

The Zebris system and the tripods were used during the three testing phases for better controlling of the testing course as they gave the evaluator an idea about the joint kinematics (*Figure 71*). The first and third phases consist of ten cycles for each motion direction, starting with IR-ER (*10 cycles*), followed by FL-EX (*10 cycles*) and ending with Abd-Add (*10 cycles*). The total number of motion cycles for the first and third phases for each specimen is 60 cycles, while the second phase consists of 700 cycles for each motion direction, starting with IR-ER (*700 cycles*), followed by FL-EX (*700 cycles*) and ending with Abd-Add (*700 cycles*). The total number of motion cycles of the second phase for each specimen was 2,100 cycles and the whole number of testing cycles in the three motion directions per specimen was 2,160 motion cycles (*Table 10*).

The described testing sequence of motion direction IR-ER -> FL-EX -> Abd-Add was scheduled for two reasons:

Firstly, to protect the sensitive sensor head inserted between the articulating hard surfaces of the ATSA prosthetic components, because IR-ER motion shows the least destructive effect, while Abd-Add motion shows the most destructive effect on the inserted sensors. However, many sensors were unfortunately

damaged during the experiments, due to the following causes: **(i)** complete sensor head damage because of sudden dislocations of the tested specimens; **(ii)** tearing and squeezing of the sensor head under the loading of the prosthetic components; **(iii)** linear cutting of the sensor head at the edges of the glenoid component in the large sized specimens particularly during FL-EX and/or IR-ER, because the sensor head was incised between the edge of the glenoid component and the outer surface of the moving humeral head component; **(iv)** shear forces, which could be borne between the two layers of the head sensor leading to their separation, because of the adhesion-cohesion between the lower surface of the sensor head and the glenoid component surface and between the upper surface of the sensor head and the humeral head component surface. During joint motion, each layer is pulled with the related joint component in two dissociative/reversed directions leading to their separation.

Secondly, it was planned to create an organized programmed step-wise ascending pattern of the applied cyclic loading to evaluate the whole characteristics of the contact pressure (*such as: values, magnitudes, patterns, modes of propagation over glenoid surface etc.*) and to correlate this sequence with the recorded values to the incidence of glenoid loosening, if it occurred in any one of the scheduled specimens.

4.5.2. Description of data recording using shoulder pointer

The shoulder pointer was used before the beginning of the testing of each specimen for the localization of the specimen and to define its dimensions. This data was recorded three successive times at once for the same points (*kinematic references*) of the humerus and the scapula (*Figure 59 & Table 11*). The four points of the humerus were taken first, then the three points of the scapula, and then this cycle was repeated three consecutive times. The purpose of the data recorded by the shoulder pointer is to give the Zebris system an accurate and detailed idea about the position of the humerus and scapula of the tested specimen, about its dimension, about its size, and to localize the specimen to enable Zebris system to follow it during its motion with the guidance of the kinematic tripods (*Figure 60*).

4.6. Stage VI: Radiological evaluation using QCT

After the completion of the experiments on 27/02/2017 the specimens were sent to the radiology department of the university hospital to be re-scanned by QCT.

Table (10): Phases of Cyclic Loading Testing				
Phases	Cycles Direction	Cycles Number	TekScan	Recorded Measurements
1st Phase (Initial short phase)	IR-ER	10	With pressure sensor insertion	Contact pressure values; contact pressure magnitude; contact pressure pattern; component stability under cyclic loading
	FL-EX	10		
	Abd-Add	10		
	Sum (i)	30		
2nd Phase (Transitional prolonged phase)	IR-ER	700	Without pressure sensor insertion	NONE
	FL-EX	700		
	Abd-Add	700		
	Sum (ii)	2,100		
3rd Phase (Final short phase)	IR-EX	10	With pressure sensor insertion	Contact pressure values; contact pressure magnitude; contact pressure pattern; component stability under cyclic loading
	FL-EX	10		
	Abd-Add	10		
	Sum (iii)	30		
	Total summation	2,160		

Remarks:

The sequence of the motion cycles is the same as the above-described sequence. Time period is 1.4 seconds per IR-EX motion cycle & 14 seconds per phase. Time period is 4.5 seconds per FL-EX motion cycle & 45 seconds per phase. Time period is 4.5 seconds per Abd-Add motion cycle & 45 seconds per phase. Total number of motion cycles for the 1st phase per specimen is 30 cycles. Total number of motion cycles for the 2nd phase per specimen is 2,100 cycles. Total number of motion cycles for the 3rd phase per specimen is 30 cycles. Total number of IR-ER motion cycles for each specimen is 720 cycles and for the whole study is 4,320 cycles. Total number of FL-EX motion cycles for each specimen is 720 cycles and for the whole study is 4,320 cycles. Total number of Abd-Add motion cycles for each specimen is 720 cycles and for the whole study is 4,320 cycles. Total number of motion cycles for the entire testing of one specimen is 2,160 cycles. Total number of motion cycles for the entire testing of all specimens is 12,960 cycles. The measurements of the 1st and 3rd phases were compared with each other to detect the effect of the prolonged application of cyclic loading on the artificial joint of each specimen during the 2nd phase.

Table (11): Shoulder Pointer References			
Specimen Portion	Points Number	Landmarks (Points/References)	
A) Humerus	4 Points	A	1) HA
		B	2) HP
		C	3) SA
		D	4) SP
B) Scapula	3 Points	A	5) AA
		B	6) TS
		C	7) AI

Remarks:

The points were taken three successive times at once in the same demonstrated sequence from 1 to 7. **HA** is humerus anterior and represented by LT. **HP** is humerus posterior and represented by the point between GT, SN and AN. **SA** is screw anterior and represented by the anterior screw of the base of the metal cup of humeral shaft which is connected to the moving arm of simulator. **SP** is screw posterior and represented by the posterior screw of the base of the metal cup of humeral shaft which is connected to the moving arm of the simulator. **AA**: angulus acromialis, which is represented by the tip of acromion process of scapula. **TS**: trigonum spinae, which is represented by the termination of the scapular spine at the medial border of the scapula. **AI**: angulus inferior and represented by the inferior angle of the scapula.



Figure (59): Humeral and scapular kinematic references for shoulder pointer on humerus (left) & on scapula (right) (**HA**: humerus anterior, **HP**: humerus posterior, **AA**: angulus acromialis, **AI**: angulus inferior, **TS**: trigonum spinae).

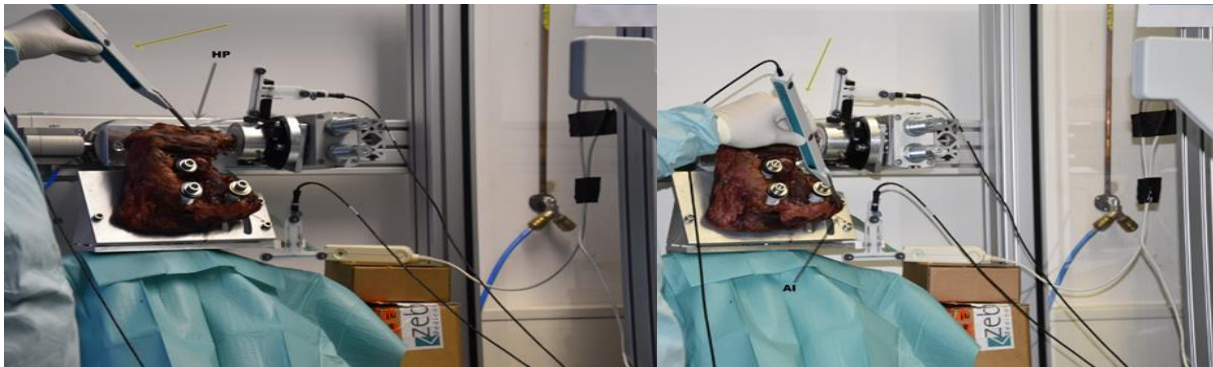


Figure (60): A mounted RT-sided shoulder specimen. Examples of the application of shoulder pointer before the initiation of the 1st phase of cyclic loading: **Left**: humerus; 2nd point (**HP**: humerus posterior) & **Right**: scapula; 7th point (**AI**: angle inferior).

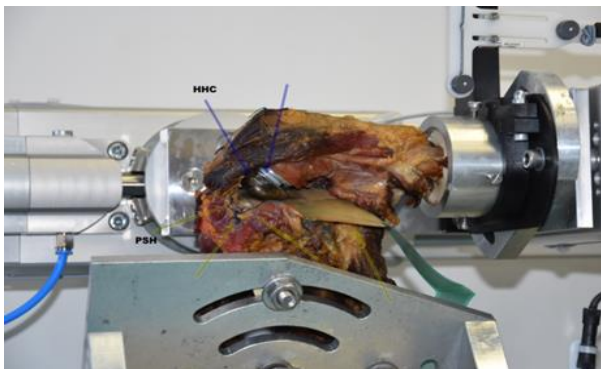


Figure (61): A left-sided specimen mounted on the simulator during the 1st phase of cyclic loading. The GH joint of the specimen is clearly visible and the inserted pressure sensor is also obvious where it comes out of the joint.

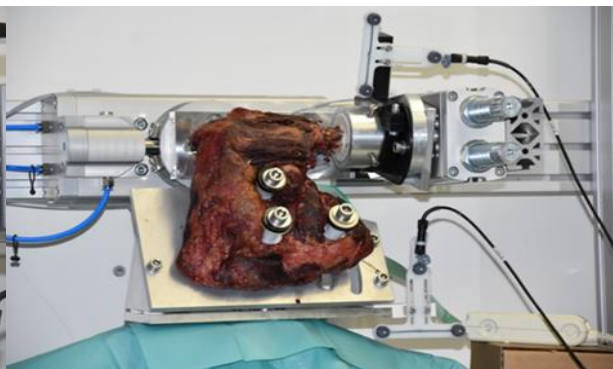


Figure (62): A RT-sided shoulder specimen. The observer can't see the joint during motion, because the joint opening faces posteriorly and the pressure sensor is hanging on the posterior aspect of the simulator (the anterior surface of the specimen).

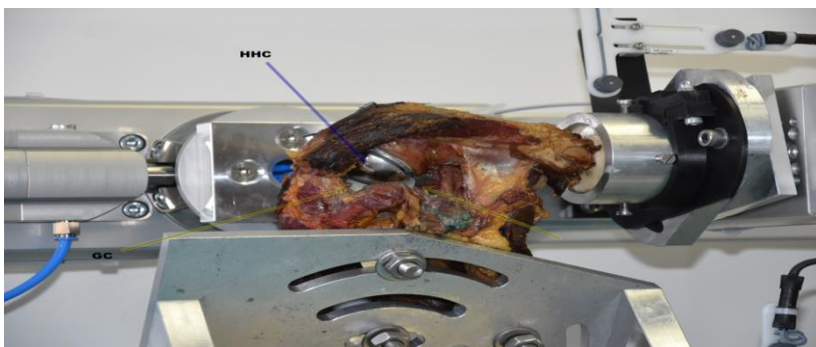


Figure (63): A mounted LT-sided shoulder specimen on the simulator during the 2nd prolonged phase of cyclic loading, without the insertion of the pressure sensor. “**GC**”: glenoid component (yellow arrow) & “**HHC**”: humeral head component (blue arrow).

4.7. General testing procedure

After the cementing of the glenoid and humeral prosthetic components in the specimen, the head of the pressure sensor foil was then inserted within the joint between the articulating surfaces of the prosthetic components.

4.7.1. Level I: Step-wise testing of the specimen

4.7.1.1. Pressure sensor insertion

Firstly, to protect the inserted sensor head against damage during joint motion under cyclic loading, it was covered with two isolating layers (*upper and lower*) of silicon and then with a further two upper and lower protective layers of Teflon tape. The method used was to insert the sensor head within the joint of the tested specimen and to suture it with the surrounding musculatures and soft tissues, mainly the rotator cuff (*Figures 64 & 65*). The joint was exposed to gain access to the glenoid, and then the sensor head was situated on the glenoid component surface and adjusted properly to cover the glenoid surface completely, without displacement in any direction, as if the sensor was displaced in any direction the signals originating from the uncovered portion of the glenoid surface would be lost. Then, the sensor edges were sutured circumferentially to the surrounding soft tissues of the glenoid, especially the rotator cuff insertion around the glenoid, and superiorly to the coracoacromial arch. After the insertion of the sensor head, the humeral head component was fixed on the humeral adapter by pressing (*press-fit fixation*) (*Figure 64*). Then the soft tissues were re-sutured and the approach was closed completely with sutures. Sometimes we released some sutures to create a window to watch the joint motions and/or to palpate it in the resting phase before re-suturing it.

4.7.1.2. Specimen mounting on the simulator

The scheduled specimen was then taken to the testing room, where the simulator is located. Firstly, the central part of the simulator and the floor under the simulator and around it were covered with protective surgical towels to guard them against dropping tissue fluids from the tested specimen. Then the tested specimen was mounted on the simulator. The metal base, which was fixed to the scapula, was mounted first at a loading force value of 0.0 volts with the two pyramidal-shaped metal pieces of the upper surface of the central part with two screws with the right piece and with one screw to the left piece. Then the metal cup, which was fixed to the humeral stump, was mounted at a loading force value of 2.5 volts with two screws through its base to the top of the moving arm of the simulator. These two screws also function as two defining points of the four humeral references of the shoulder pointer.

Then the kinematic tripods were fixed, each to the corresponding portion of the specimen (*Figure 62*). The distal end of the inserted pressure sensor was inserted into a slot of the TekScan apparatus.

The simulator was then switched on and connected to the operating computers. The operating programs were then installed as previously described. The joint of the tested specimen was positioned and then palpated before initiation of the testing to detect if any dislocations or subluxations were present. When the joint was well positioned, the loading force was then increased gradually up to 3.5 volts and the stabilizing weights also were adjusted according to the stabilization demands of the joint of the tested specimen and according to the specimen side (*Table 12*). Any sudden increase or decrease of the applied forces or the stabilizing weights of the shoulder simulator could lead to sudden movements of the scapular portion of the specimen (*upward jumping from increasing the loading forces or downward falling from decreasing the stabilizing weights*), which may have led to fractures of the scapula and/or humerus of the mounted specimen. Afterwards, the evaluator would take a general look at the TekScan to check the quality of the displayed signal, which initially indicated the degree of the contact pressure and the extent of the contact surface area between the two articulating surfaces of the implanted joint.



Figure (64): A RT-sided specimen after the insertion of the pressure sensor head over the glenoid and fixing it with circumferential sutures with the surrounding soft tissues (arrows), (LT: dislocated joint; RT: reduced joint).

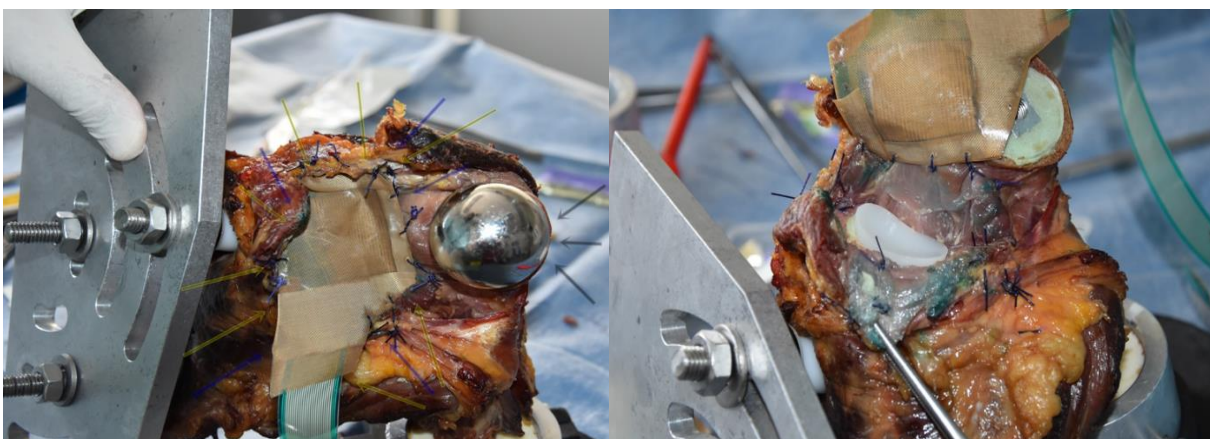


Figure (65): A LT-sided specimen with metal bases. **Left:** dislocated joint shows a well inserted pressure sensor situated over the hidden glenoid (arrows) after specimen testing. The sensor appears shiny because of the specimen's tissue fluids. **Right:** the release of the sutures to remove the pressure sensor head.

4.7.1.3. Shoulder pointer data recording

After the specimen was mounted on the simulator and everything was ideal, the shoulder pointer data was taken three consecutive times at once to define the specimen position references (*Figure 60*).

4.7.1.4. Initiation of the first phase of cyclic loading testing

At the beginning of the testing, a pretest of five cycles in each motion direction was performed to check the quality of the function of the whole integrated system. Then the first testing phase was initiated with ten cycles in IR-EX, followed by ten cycles in FL-EX and finally ten cycles in Abd-Add motion directions with simultaneous saving of the streaming data of the pressure sensor TekScan system. When the loading testing in the three motion directions of the first phase was completed, the second level of the experiment could be initiated.

4.7.2. Level II: Specimen step-wise testing

The applied loading forces were then lowered to 2.5 volts and some weights were concurrently removed with great caution to avoid any sudden dislocation of the joint, which could lead to fractures of the scapula and/or the humerus of the specimen. The humeral and the scapular tripods were first removed and the pressure sensor was then pulled out from the apparatus. Afterwards, the humeral portion metal base was removed first at a loading force value of 2.5 volts, then the loading forces were gradually reduced to zero volts with elimination of some weights to remove the scapular portion metal base of the simulator. Then the whole specimen was removed from the simulator. The pressure sensor was then taken out from the joint by releasing the fixating sutures (*Figure 65*). The second testing phase was planned without insertion of the pressure data sensor because the large number of the motion cycles of this phase in the three motion directions (*2,100 cycles*) would have destroyed it (*Figure 63*). The 2nd phase started with 700 cycles in IR-ER motion direction, then with 700 cycles in FL-EX motion direction and finally with 700 cycles in Abd-Add motion direction. Then the specimen was removed again as described for the end of the 1st phase.

4.7.3. Level III: Specimen step-wise testing

After the removal of the specimen from the simulator, the pressure sensor was re-inserted and the specimen was re-mounted on the simulator as described for the 1st testing phase. Then, the third testing phase was conducted like the 1st testing phase. After the testing was completed and the tested specimen removed, the operating programs were uninstalled and the controlling computers were switched off, in addition to checking and saving the collected data and measurements.

4.7.4. Important technical remarks

The simulator has two different configurations for the right-sided and left-sided shoulder specimens, so the simulator was adjusted firstly for RT-sided specimen testing and then for LT-sided specimen testing.

When a right-sided shoulder specimen was subjected to the simulator, the anterior aspect of the shoulder specimen faced posteriorly and the posterior aspect of the specimen faced anteriorly, so the approach and the potential observation window for joint access during the testing were located on the anterior aspect of the shoulder specimen. Thus, when the specimen was subjected to the simulator, the left window faced posteriorly, so the joint space and the articulating surfaces were hidden and invisible during the experiments and the only way to check the position of the joint and the articulating surfaces was palpation with the index finger in the resting phase (*Figure 62 & Table 13*). When a left-sided shoulder specimen was subjected to the simulator, the anterior aspect of the shoulder specimen faced anteriorly and the posterior aspect of the shoulder specimen faced posteriorly, so the approach of the implantation and the left window for joint access during the cyclic loading testing were located as mentioned on the anterior aspect of the shoulder so that when the specimen was subjected to the simulator the left window faced anteriorly and the joint space and the articulating surfaces were accessible to the evaluator during the experiments for both visual inspection and palpation in the resting phase (*Table 13 & Figures 61 & 63*).

Table (12): Sequence of the Testing Course and Simulator Configuration		
Mode of Simulator Configuration		Position of the Applied Stabilizing Weights
A) Testing plan 1st part		
Simulator	Adjusted for the RT-sided specimens	<i>Hanging posteriorly</i> “on the posterior aspect of the simulator” from the middle plate of the central part of simulator, which carries the scapula portion of the specimen
Specimens	Testing of the RT-sided specimens successively	
B) Testing plan 2nd part		
Simulator	Re-adjusted for the LT-sided specimens	<i>Hanging anteriorly</i> “on the anterior aspect of the simulator” from the middle plate of the central part of simulator, which carries the scapula portion of the specimen
Specimens	Testing of the LT-sided specimens successively	

Table (13): Tested Specimen Orientation on Simulator					
Specimen Side	Anterior Aspect (Surface)	Posterior Aspect (Surface)	DP Approach and Controlling Window	Accessibility to the Implanted joint (TSA) of the Tested Specimen	
				Palpation	Visibility
RT-sided Specimens	Faces posteriorly	Faces anteriorly	Located posteriorly	palpable	invisible
LT-Sided Specimens	Faces anteriorly	Faces posteriorly	Located anteriorly	palpable	visible

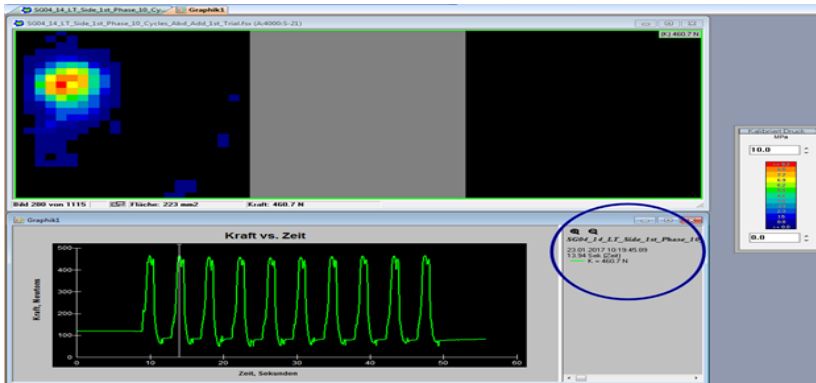


Figure (66): A TekScan signal during the Abd of an Abd/Add motion cycle of a mounted LT-sided shoulder specimen, which is large, rounded and lies at the upper outer side of the demonstrating window. The signal shows a large contact area between joint articulating surfaces and a medium contact pressure (the red center of the signal). The top of the graph below represents the Abd.

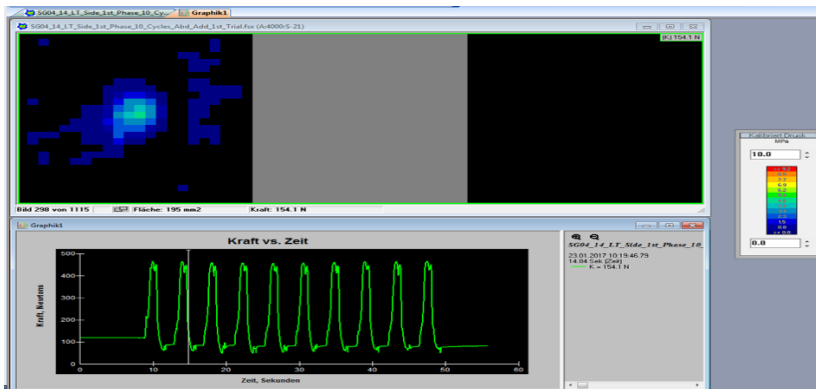


Figure (67): A TekScan signal during a mid-abduction motion of a mounted LT-sided shoulder specimen, which is represented by the slope between the Abd & Add on the graphic wave below. The signal center is completely blue, indicating a very low contact pressure value.

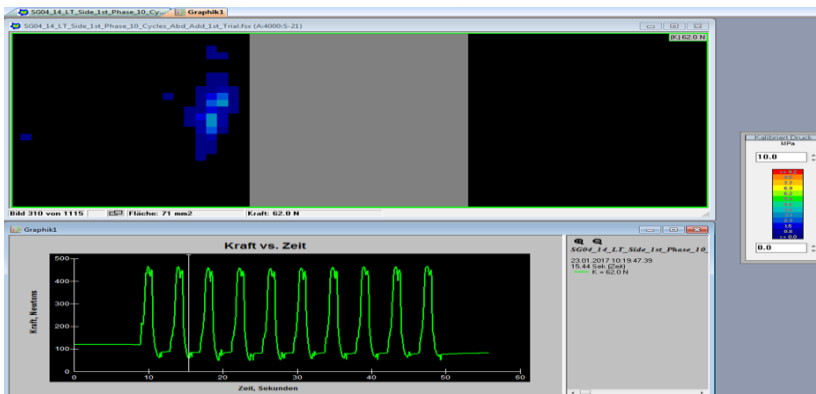


Figure (68): A TekScan signal during an Add motion of a mounted LT-sided shoulder specimen, which is small, elongated, lying at the inner side of the window and represented by the baseline (bottom) of the graphic wave below. The signal center is completely blue, indicating a very low contact pressure value.

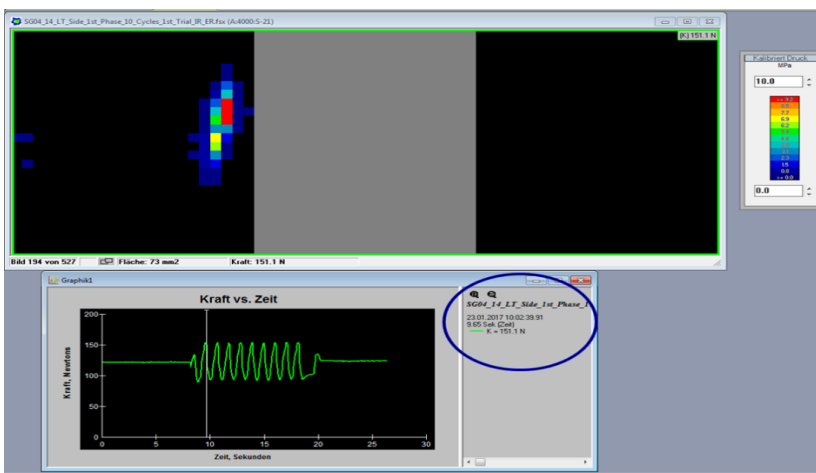


Figure (69): TekScan signal during an external rotation motion of a mounted LT-sided shoulder specimen (blue circle). TekScan signal is small, elongated and situated at the inner side of the demonstrating window, indicating a small contact surface area between joint articulating surfaces. The graph top represents the ER.

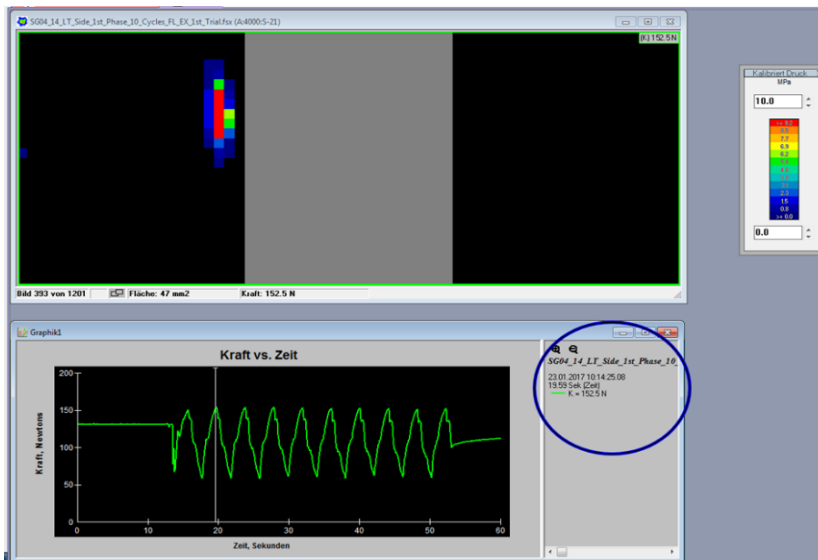


Figure (70): TekScan signal during an extension motion of a mounted LT-sided shoulder specimen. TekScan signal is small, elongated and situated at the inner side of the demonstrating window, indicating a small contact surface area between joint articulating surfaces. The top of the graph situated at the lower part of the window represents the extension motion. Signal center is red, indicating a high contact pressure value.

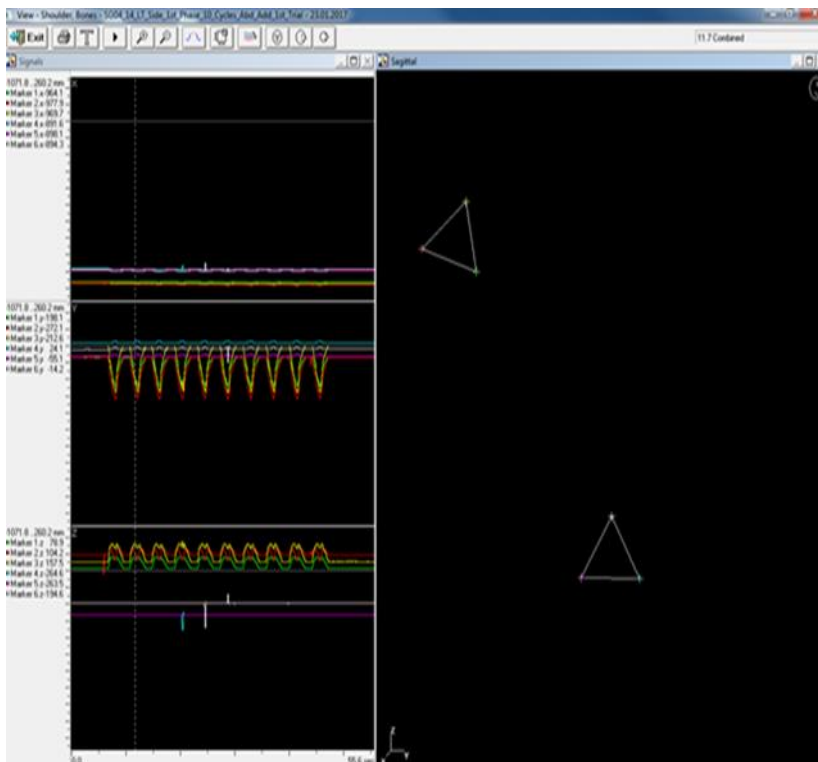


Figure (71): Zebris system program during the abduction of an Abd/Add motion cycle of the tested specimen ID: SG04/14 LT. The upper triangle refers to the humerus (humeral tripod), whereas the lower triangle refers to the scapula (scapular tripod). The upper triangle moves during Abd/Add & IR/ER motions and the lower triangle moves during FL-EX motions. The graph situated at the left side of the window is similar to that of the TekScan. At the RT part of the figure, the distance between the two triangles is clearly wide and the upper triangle moves in a circular pattern towards the LT side indicating an Abd. motion.

5. Data Collection & Analysis

The following methods were used to collect the data:

- Physical examination of the specimens.
- Observation during the experiments.
- Radiological evaluation of the joints of the specimens pre- & post-experimentally using QCT.
- Data collection using TekScan & pressure data sensors

To evaluate the motion of the tested joint, two indicators needed interpretation: **(i)** the displayed signal (*Table 16 & Figures 66, 67, 68, 69 & 70*): signal shape, signal motion direction and signal size, which reflects the contact surface area between the articulating surface and the contact pressure values; and **(ii)** the demonstrated graphs (*Tables 14 & 15 & Graphs 1, 2 & 3*): reflects the contact pattern and the contact pressure between the articulating surfaces in each motion direction. **The collected TekScan data** was in two forms: **(I)** the demonstrated graphs (*Tables 14 & 15 & Graphs 1, 2 & 3*) and **(II)** the recorded peak pressure values of each motion cycle for the three motion directions (*AA, FE & IE*) during both the initial and final phases for each specimen, which were analyzed statistically (*Table 19*).

Table (14): TekScan Graph Description				
Motion Direction	Wave Width	Wave Height	Configuration	Explanation
Abd/Add	Wide at the base and narrow at the top	The highest	Motion occurs only above the baseline	Motion occurs only in one side of the motion arc, from the resting position (Add) towards the abduction (90°) and back towards the adduction (0°). This motion has the widest ROM (Abd/Add: 90°- 0°- 0°).
FL/EX	The widest	Medium	Motion occurs above and below the baseline	Motion occurs on both sides of the resting position. Firstly, in the direction of extension (45°), then back to resting position at the central line, then in the direction of flexion (45°). This motion has a wide ROM (FL/EX: 45°- 0°- 45°).
IR/ER	Narrow	Short	Motion occurs above and below the baseline	Motion occurs on both sides of the resting position. Firstly, in the direction of IR (30°), then back to resting position at the central line, then in the direction of ER (30°). This motion has a short ROM (IR/ER: 30°- 0°- 30°).

Table (15): Correlations Between Specimen Side, Simulator Mechanics & TekScan Graphs					
Specimen Side	Motion Cycle	Motion Direction Sequence		TekScan Graphic Representation	
		1 st Motion	2 nd Motion	Graph Top	Graph Bottom
RT-sided Specimens	IR/ER	IR	ER	IR	ER
	FL/EX	FL	EX	FL	EX
	Abd/Add	Abd	Add	Abd	Add (graph baseline)
LT-sided Specimens	IR/ER	ER	IR	ER	IR
	FL/EX	EX	FL	EX	FL
	Abd/Add	Abd	Add	Abd	Add (graph baseline)

Remarks:
 The directions of FL/EX and IR/ER motion cycles are reversed in the LT- & RT-sided specimens, because the LT- & RT-sided specimens are mounted on the simulator in a reversed configuration, while the directions of the Abd/Add motion cycles are the same for both LT- & RT-sided specimens.
 The slope between Abd and Add on the graphs represents the mid-abduction motion.

Table (16): TekScan Signal Description					
Motion Direction	Signal Shape (reflects articular surfaces conformity)	Signal Size (reflects contact surface area between the articulating surfaces)	Signal Motion Pattern (reflects motion direction and range)	Contact Surface Area (between the articulating surfaces)	Contact Pressure (between the articulating surfaces)
Abduction	Completely rounded	The largest	Abd-Add: The largest motion arc Circular pattern	The largest & round	Medium
Mid-Abd	Rounded	Large		Large & round	Low
Adduction	Less rounded	Medium		Small & elongated	Low
FL/EX	Elongated & thick/wide	Small to medium	Average-sized motion arc Semi-circular pattern	Small & elongated	The highest
IR/ER	Elongated & thin/narrow	The smallest	Short motion arc Straight pattern from side to side	Small & elongated	High
Remarks: Contact pressure value is reflected by the intensity of the red center of the TekScan displayed signal. Contact surface area is reflected by the size of the TekScan displayed signal. Contact pattern “conformity” is reflected by the shape of the TekScan displayed signal.					

6. Results

6.1. Findings (observations & physical examinations)

During the experiments under cyclic loading, four specimens were completely stable, while two specimens exhibited extreme degrees of instability. The first specimen was extremely unstable under testing, especially during AA testing cycles; from the pre-experimental CT sections, the specimen was suspected to be slightly elongated in the superior-inferior dimension (*Figure 51*), which was confirmed by the physical examination during implantation, in addition to the detection of the presence of a narrow anterior-posterior diameter, which resulted in a mismatch between the native and prosthetic glenoids of about 10 mm (*Figures 72 & 73*). During the implantation trials, the implantation of a larger glenoid component wouldn't have solved the problem, because the prosthetic glenoid was larger in the anteroposterior diameter than the native glenoid and bridged over the sides and didn't covered the whole superior-inferior length of the native glenoid. Furthermore, the glenoid bone stock in the anterior-posterior diameter wasn't able to carry a keel or pegs of a large-sized component. After testing, signs of component substance damage in the form of serrations at the component's anterior and anteroinferior edges were detected (*Figure 74*), which indicates the violent oscillation of the humeral head component over the glenoid component before dislocation (*pendulum-like motion*). The specimen was retested with a modification to the applied stabilizing weights and loading forces and the second trial succeeded.

The other specimen was extremely unstable under cyclic loading, especially during AA testing cycles, and dislocated severely after the 8th AA motion cycle of the final phase. Physical examination revealed a glenoid component malposition in form of a superior displacement of about 5 mm (*Figure 75*). The specimen was revised to a new keeled glenoid, and upon re-testing exhibited absolute stability under testing (*Figure 76*).



Figure (72): The specimen ID: 1214/12/RT with a mismatch in the superior-inferior length between the native and the prosthetic glenoids of about 10 mm.

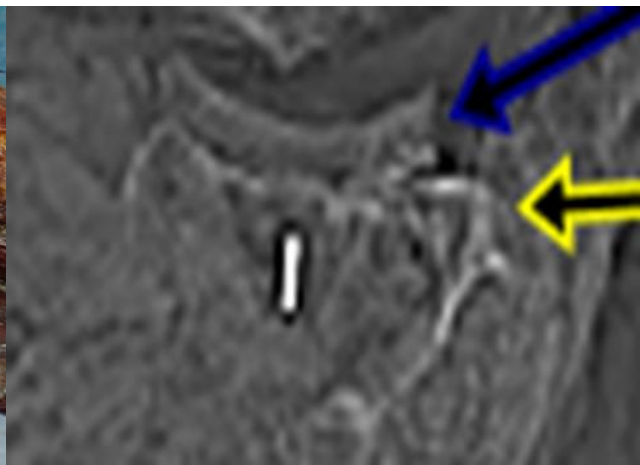


Figure (73): The specimen ID: 1214/12/RT; post-experimental CT coronal section shows the mismatch between the native glenoid (yellow arrow) and the prosthetic glenoid (blue arrow).

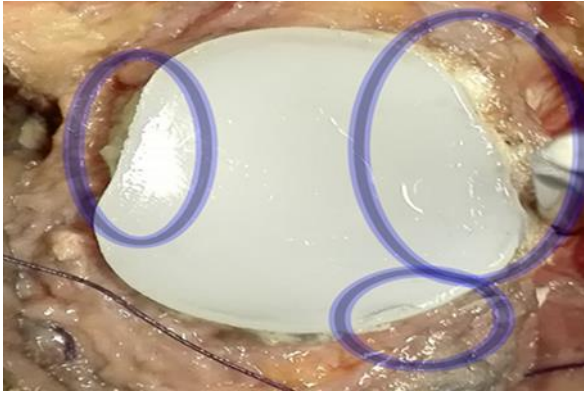


Figure (74): The specimen ID: 1214/12/RT shows damage marks (within the blue circles) mainly at the anterior and anteroinferior edges of the glenoid due to the violent oscillation of the humeral head over the glenoid component.



Figure (75): The LT-sided specimen ID: SG02/15 with an evident mismatch between the native and the prosthetic glenoids of about 5 mm in the superior-inferior diameter due to superior displacement of the implanted prosthetic glenoid.

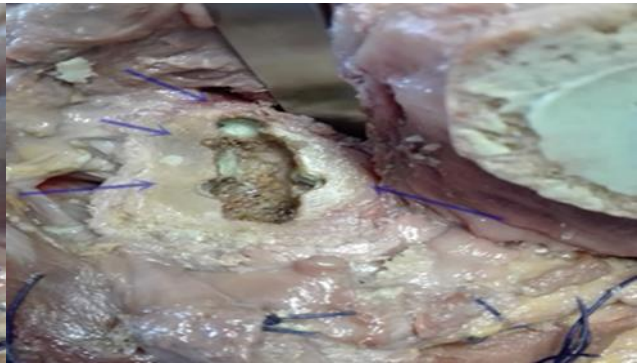
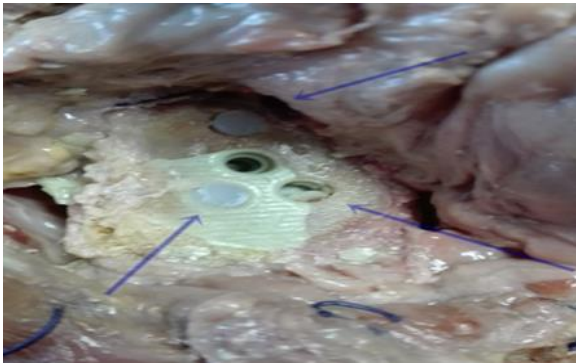


Figure (76): The native glenoid of the LT-sided specimen ID: SG02/15 after removal of the failed prosthetic glenoid component (left) & after drilling to implant the new keeled component (right).

6.2. Radiological results

The evaluation of the post-experimental CT scans (*mainly coronal section*) of the tested specimens revealed that glenoid loosening has occurred in four specimens of the total six specimens, a percentage of 66.7%. In addition, a hairy radiolucent line was detected in one of the unloose specimens (*Table 17 & Figures 77, 78, 79 & 80*).

To determine the extent of the loosening (*Tables 17 & 18*), it was suggested to divide the surface of the native glenoid (*prosthetic glenoid-cement-native glenoid interface*) into nine compartments (*SA, SM, SP, MA, MM, MP, IA, IM & IP*) to enumerate how many compartments were loose using successive coronal CT scans. It was found, according to the suggested criteria, that the loosening was massive in all four affected specimens with inferior and anterior predominance in both keeled and pegged glenoids, as follows: one specimen was completely loose in the whole nine compartments; one specimen exhibited loosening in seven compartments; one specimen showed loosening in six compartments; and the last specimen was loose in five compartments, with a percentage of more than 50% of affection of the surface area of the loose components in all of the loose specimens.

Regarding the size of the loosening line, three loose specimens exhibited a loosening line size greater than 2 mm in the loosest compartments, while the loosening line size was < 2 mm in only one loose specimen. Three of the loose glenoids were keeled, while only one of the loose specimens was pegged. The percentage of the loose keeled specimens was 75% of all keeled specimens and 50% of all specimens. The percentage of the loose pegged specimens was 50% of all pegged specimens and 16.7% of all specimens (*Tables 32, 33 & 36*).

Three of the loose specimens were RT-sided, representing 100% of RT-sided specimens and 50% of all specimens. One of the loose specimens was extremely unstable under cyclic loading, representing 25% of loose specimens, while the other three loose specimens were completely stable under cyclic loading. The recorded total load quantities (*during the whole testing course for each specimen*) of the loose specimens were arranged separately in *Tables 21 & 32*.

The implanted humeral adapters/stems were completely stable with an excellent radiological appearance of a firm fixation without any signs of loosening or radiolucency in all specimens, or 100% of all specimens (*Figure 78*). By comparing the loose specimens to their obtained peak pressure values and with the calculations of the total mean peak pressure of the whole testing course during the entire testing phase in the three directions of motion for each specimen, it was found that the mean peak pressure values of three loose specimens were between 5 and 10 MPa, while in only one specimen did the total mean peak pressure exceed the level of 10 MPa (*a keeled RT-sided specimen*). The calculated total mean peak pressure values of the loose specimen are shown in *Tables 21 & 32*.

Table (17): Detection of Glenoid Component Loosening Using QCT Sections of the Tested Specimens			
Specimen ID	Presence of loosening	Extent of loosening on QCT coronal sections from ant. to post. glenoid rims and from sup. to inf. glenoid poles <i>(nine descriptive compartments)</i>	Size of the loosening line
1214/12/RT	Present	SA, SM, MA, IA, PS, PM & PI (Loose surface area ---→ 77.8% of glenoid surface area)	>2 mm
1214/12/LT	Present	SA, SM, SP, MA, MM, MP, IA, IM & IP (Loose surface area ---→ 100% of glenoid surface area)	>2 mm
SG02/15/RT	Present	IM, SP, MP, MI & IP (Loose surface area ---→ 55.6% of glenoid surface area)	<2 mm
SG02/15/LT	Absent	-----	-----
SG04/14/RT	Present	SA, SM, SP, IA, IM & IP (Loose surface area ---→ 66.7% of glenoid surface area)	Anteriorly >2mm Inferiorly >2 mm Superiorly >2 mm Posteriorly <1 mm
SG04/14/LT	Absent	IM (only a very thin hairy radiolucent line)	-----
Remarks: <i>For descriptive & evaluative purposes, it was suggested to divide the glenoid surface area into nine compartments: SA: superior anterior; SM: superior middle; SP: superior posterior; MA: middle anterior; MM: middle middle; MP: middle posterior; IA: inferior anterior; IM: inferior middle; IP: inferior posterior.</i>			

Table (18): Evaluation of Loosening by Glenoid Type				
Glenoid Loosening		Keeled specimens	Pegged specimens	Total
Absent		1	1	2
Present		3	1	4
Extension		Extensive and predominant antero-inferiorly	Extensive and predominant inferiorly	
Percentage	Absent	25 % of specimens	50 % of specimens	33.33% of specimens
	Present	75 % of specimens	50% of specimens	66.66% of specimens

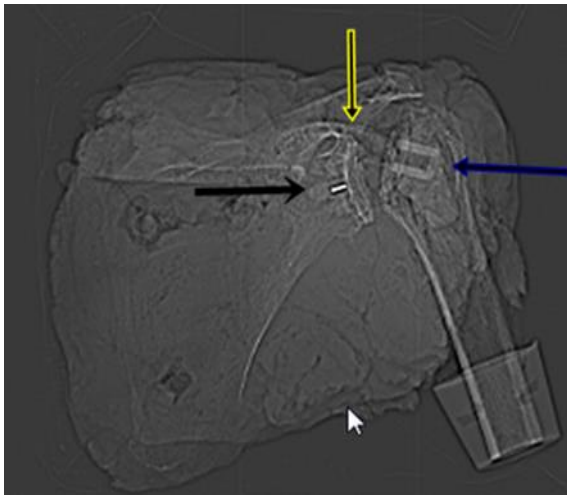


Figure (77): Post-experimental CT coronal section of specimen ID: 1214/12 LT shows the radiopaque humeral adapter (blue arrow), the radiopaque marker in the keel of the glenoid component (black arrow) and the radiolucent glenoid component (yellow arrow).



Figure: (78): CT coronal section of specimen ID: SG02/15/LT. The glenoid component seems to be well-positioned and the cement has a good amount and a good distribution around the prosthetic glenoid (a sticky thick cement mantle) without radiolucency; also, the humeral adapter seems to be well-positioned and completely surrounded with cement without radiolucency.



Figure (79): CT coronal section shows loosening (blue arrows) around the glenoid component of specimen ID: 1214/12/LT with a separation line of more than 2 mm in width, particularly inferiorly.

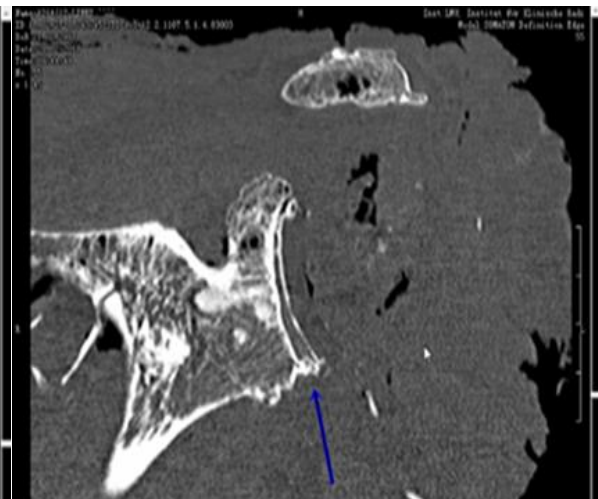
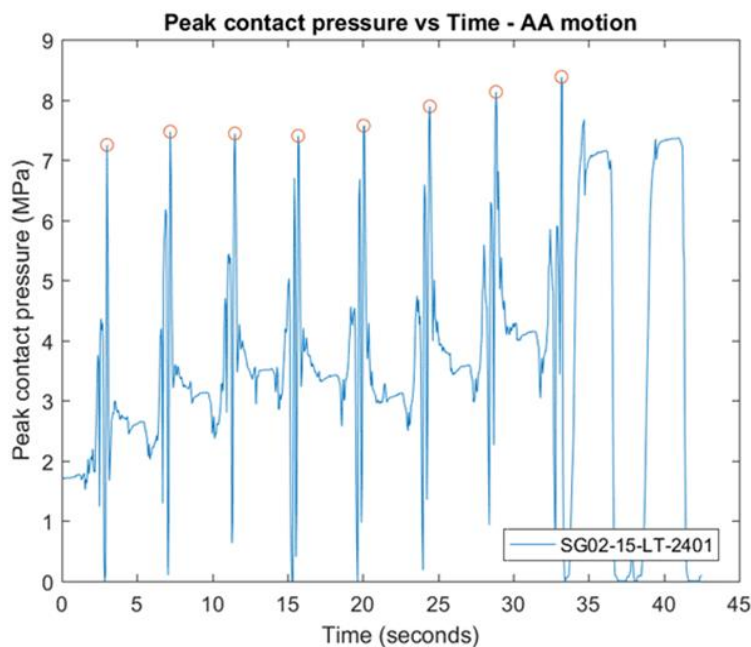


Figure (80): CT coronal section shows loosening (blue arrow) around the glenoid component of specimen ID: 1214/12/LT with a separation line of more than 2 mm in width, particularly inferiorly.

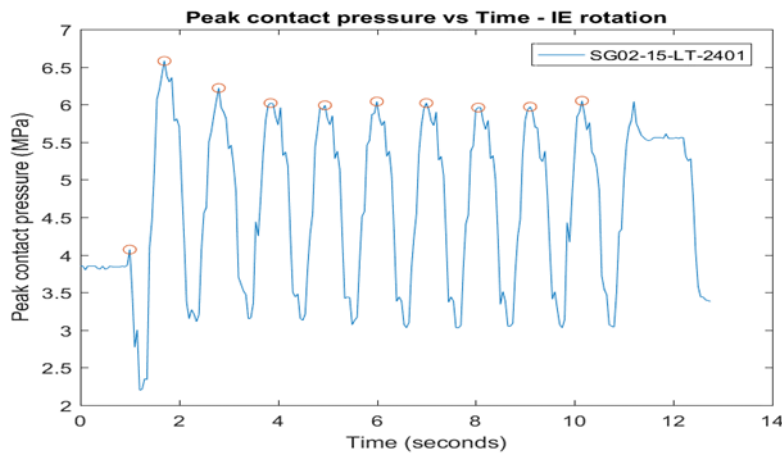
6.3. TekScan results (statistical results & graph interpretation)

6.3.1. Graph interpretation

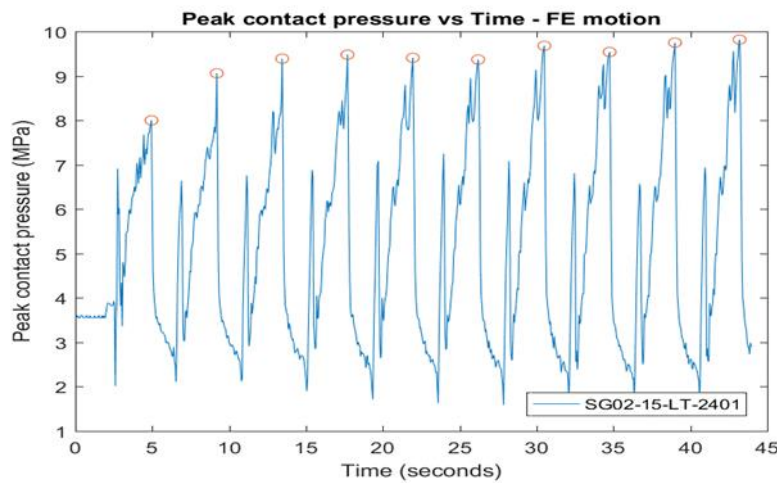
The obtained graphs demonstrate the relation between the successive values of peak contact pressure versus time. Each graph exhibits ten values/relations of ten motion cycles in one motion direction (AA, FE or IE) during one testing phase (1st or 3rd phase) of one specimen (Graphs 1, 2 & 3). Each graph gives an idea about the pattern and the mode of the pressure propagation over the glenoid component surface (steady or hesitating; ascending or descending or straight; random) according to the changes of the plotted ten contact pressure peaks versus time. The obtained graphs were studied to understand the relation between the mean peak pressure values, the cycle time and the pattern of pressure propagation over the glenoid component surface per motion cycle/per motion direction/per specimen during the initial and the final testing phases and to correlate the contact pressure values and patterns with the occurrence of glenoid component loosening. The description of the normal and abnormal variations of the graph pattern according to motion direction can be found below beside each graph (Graphs 1, 2 & 3). It wasn't possible to include all the graphs of the three motion directions during both the initial and the final phases of all specimens in the thesis, because we had about 42 graphs (see appendix I, pages 1-24).



Graph (1): Demonstrates peak pressure value per motion cycle versus time in AA motion direction during the final testing phase of specimen ID: SG02/15/LT. Testing duration in AA motion direction/per phase is 45 seconds for ten cycles (4.5 seconds/cycle). Motion waves are absent between 35 & 45 seconds, because the specimen joint dislocated between the 8th & the 9th Abd/Add motion cycles at second 35. The graphic wave is wide, high and Abd motion is represented by the top of the graphic wave, while the Add motion is represented by the bottom of the graph & mid-abduction motion by the slope of the graphic wave.



Graph (2): Demonstrates peak pressure value per motion cycle versus time in IE motion direction during the final testing phase of specimen ID: SG02/15/LT. Testing duration in IE motion direction per phase is 14 seconds for ten cycles (1.4 seconds/cycle). The graphic wave is narrow, short and lies on both sides (upper and lower sides) of the baseline of the graphic wave. ER motion is represented by the top of the graphic wave & IR motion by the bottom of the graphic wave.



Graph (3): Demonstrates peak pressure value per motion cycle (ten cycles) versus time in FE motion direction during the final testing phase of specimen ID: SG02/15/LT. Testing duration in FE motion direction per phase is 45 seconds for ten cycles (4.5 seconds/cycle). The graphic wave is wide, medium-sized and lies on both sides (upper and lower sides) of the graphic baseline. FL motion is represented by the bottom of the graphic wave and EX motion by the top of the graphic wave.

6.3.2. Statistical results

The data collected with the pressure sensor and the software (TekScan) was analyzed statistically using an analytical program. The program, which is available currently in the lab, can function in an automatic fashion to give the results of the analysis rapidly and accurately, and can also function manually to confirm the automatically obtained results. Microsoft Excel sheets were also used to plot the results. With the used software, the peak contact pressure values versus time for each motion direction/per testing phase/per specimen were exported to an Excel file, then a Matlab software was used to select from each Excel file the data corresponding only to the 10 motion cycles and their 10 pressure peaks. Finally, those 10 peaks per phase of motion/per specimen were saved in the Excel files for further analysis. Hence, we had a total of about 420 peak pressure values for the whole study trials (60 pressure peaks per trial/7 trials/6 specimens), 60 peak pressure values for the whole testing course per specimen, 140 peak pressure values for each motion direction (AA, FE & IE) for the whole testing course (20 peak pressure values/motion direction/7 trials/6 specimens).

Table (19): Statistical Calculations	
1)	Total mean peak pressure per phase per motion direction for the whole study (all specimens as one unit) (<i>Table 20</i>)
2)	Total loads applied on each specimen separately during testing (collectively) (<i>Table 21</i>)
3)	Total mean peak pressure per specimen for its whole testing course (collectively) (<i>Table 21</i>)
4)	Total mean peak pressure per phase per motion direction per specimen (<i>Tables 22, 23 & 24</i>)
5)	Total mean peak pressure per phase per specimen for all three motion directions (<i>Table 25</i>)
6)	t-Test values (p-values) between initial & final phases per specimen per motion direction (<i>Tables 22, 23 & 24</i>)
7)	t-Test values (p-values) between initial & final phases per specimen (<i>Table 25</i>)
8)	SD values per phase per motion direction for all specimens as one unit (<i>Table 20</i>)
9)	SD values per specimen for its whole testing course (collectively) (<i>Table 21</i>)
10)	SD values per phase per motion direction per specimen (<i>Tables 22, 23 & 24</i>)
11)	SD values per phase per specimen for all three motion directions (collectively) (<i>Table 25</i>)
12)	Arrangement & summations of the calculated SD values according to our selected criteria with their percentage values (<i>Tables 26, 29 & 30</i>)
13)	Arrangement & summation of the computed mean peak pressure values according to our selected criteria with their percentage values (<i>Tables 26, 27, 28 & 30</i>)
14)	Hypothesis (Hi) evaluation (<i>Tables 26, 27, 28, 29, 30 & 34</i>)
15)	Hypothesis (Hii) evaluation (<i>Table 26, 27, 28, 29, 30, 31, 34 & 35</i>)
16)	Hypothesis (Hiii) evaluation (<i>Tables 32, 33 & 36</i>)

Firstly, the total mean peak pressures during the whole study per motion direction (AA, FE & IE) were computed using Excel sheets to have a general view about the peak pressure values (*Table 20*).

Table (20): Total Mean Peak Pressure per Motion Direction for the Whole Study		
Motion Direction	Total mean peak pressure of the whole phases of the whole scheduled specimens of the whole study for each motion direction	
	Initial Phase	Final Phase
Abd/Add	9.2 ±1.8	9.23 ±3.6
FL/EX	8.06 ±3.12	7.8 ±2.5
IR/ER	5.9 ±1.8	6.4 ±2.8

Secondly, the total loads, total mean peak pressure and SD values during the whole testing course (*in total, two testing phases & three motion directions*) per specimen, under which each one of the scheduled specimens was tested separately, were computed and correlated with the degree of specimen stability during the experiment and also with the presence of glenoid component loosening (*Table 21*). Subsequently, the obtained results were demonstrated in the form of diagrams (*Diagrams 1 & 2*).

Table (21): Relation Between Applied Loads, Joint Stability & Component Loosening					
Specimen ID	Total Loads (MPa)	Total Mean Peak Pressure (MPa)	Stability	Component Type	Glenoid Loosening
1214/12/RT	456.44	7.6 ±2.7	Unstable	Keeled	Present
1214/12/LT	310.68	5.2 ±1.7	Stable	Pegged	Present
SG02/15/RT	457.64	7.6 ±2.8	Stable	Keeled	Present
SG02/15/LT	440.71	7.34 ±3.14	Stable	Keeled	Absent
SG04/14/RT	626.18	10.43 ±2.0	Stable	Keeled	Present
SG04/14/LT	547.22	9.12 ±0.8	Stable	Pegged	Absent

Thirdly, the peak pressure values [ten peak pressure values/per phase (two phases)/per motion direction (three motion directions)/per trial/specimen (seven trials/six specimens)] obtained for the whole study were classified on separate Excel sheets in columns according to motion direction (AA, FE & IE) per phase/per specimen to compute the mean peak pressure values per phase (initial & final phases) for each motion direction/per specimen and to calculate SD values (standard deviation) between the recorded peak pressures of each phase/per motion direction/per specimen. Then, t-test values (p-values) between the initial and final testing phases per motion direction/per specimen were computed to detect statistically the changes in mean peak pressure values between the two phases/per motion direction/per specimen, in order to test the hypothesis (Tables 22, 23, 24 & 31 & Diagrams 3, 4, 5, 6, 7 & 8). **A hypothesis should be rejected** (null hypothesis/H0) when the calculated p-value of t-test is < 0.05, hence the difference between the two compared groups is undetectable. **A hypothesis should be accepted** (research hypothesis (H1)/alternative hypothesis (Ha)) when the calculated p-value of t-test is > 0.05, and hence the difference between the two compared groups is detectable.

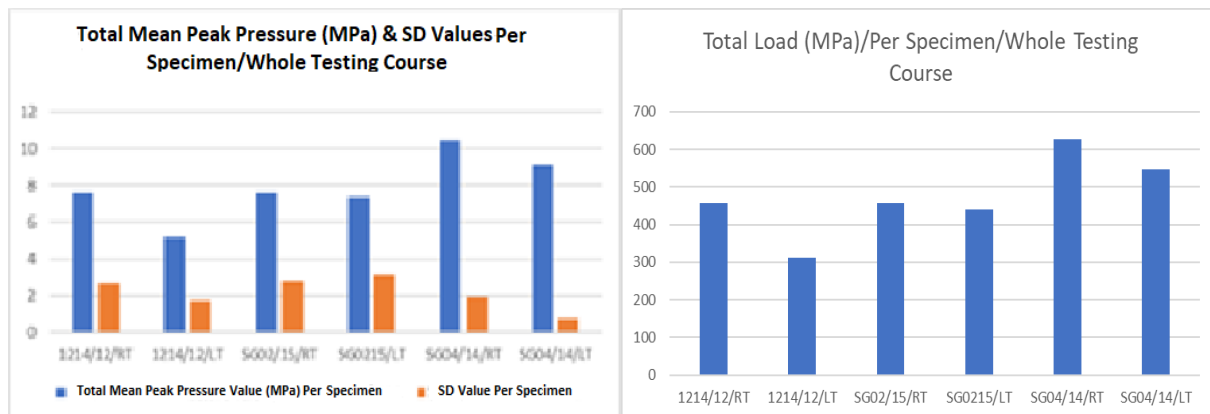


Diagram (1): Shows total mean peak pressure values & SD values during the whole testing course of each specimen (two phases & three motion directions).

Diagram (2): Shows the total load under which each specimen was tested during the whole testing course (two phases & three motion directions).

Table (22): Statistical Calculations during AA Testing Episodes Per Phase/Per Specimen					
Specimen ID	Hypothesis State (Hii)				
	Mean peak pressure values		Statistically		
	Initial Phase (MPa)	Final Phase (MPa)	t-Test (p-value)	Critical Value	Hypothesis State (H1/Ha: p-value > 0.05 & H0: p-value < 0.05)
1214/12/LT	7.9 ±0.77	4.2 ±0.11	3.35137E-08	0.05	H0
1214/12/RT	11.32 ±0.0	11.32 ±0.0	#DIV/0!	0.05	H0/invalid
SG02/15 /LT /Ja	7.7 ±0.4	13 ±0.3	2.87453E-08	0.05	H0
SG02/15 /LT /Fe	6.6 ±0.3	3.9 ±1.5	3.47526E-10	0.05	H0
SG02/15 /RT	11.6 ±0.3	10.4 ±0.23	1.10561E-05	0.05	H0
SG04/14/LT	9.9 ±0.2	9.0 ±0.7	0.008205709	0.05	H0
SG04/14/RT	9.0 ±0.3	12.8 ±0.3	1.17926E-09	0.05	H0

Remarks: see (Table 23)
AA: Abduction/Adduction.

Table (23): Statistical Calculations during FE Testing Episodes Per Phase/Per Specimen					
Specimen ID	Hypothesis State (Hii)				
	Mean Peak Pressure Values		Statistically		
	Initial Phase (MPa)	Final Phase (MPa)	t-Test (p-value)	Critical Value	Hypothesis (H1: p-value > 0.05 & H0: p-value < 0.05)
LT/1214/12	6.5 ±1.9	4.1 ±0.4	0.00921873	0.05	H0
RT/1214/12	5.5 ±0.3	6.0 ±0.5	0.012178409	0.05	H0
LT/SG02/15/Fe	12.1 ±1.5	10.5 ±0.91	0.000232438	0.05	H0
LT/SG02/15/Ja	3.6 ±0.34	9.4 ±0.52	3.08674E-12	0.05	H0
RT/SG02/15	7.9 ±1.4	5.1 ±0.12	0.000191448	0.05	H0
LT/SG04/14	9.4 ±0.51	9.7 ±0.7	0.006365623	0.05	H0
RT/SG04/14	11.5 ±0.14	9.8 ±0.11	2.12133E-13	0.05	H0

Remarks:
This table demonstrates the following statistical values: mean peak pressure, SD & p-values for both phases per specimen for the mentioned motion direction.
t-Test values were calculated between mean peak pressure values of the initial & final phases per specimen. Hypothesis state means that a hypothesis should be rejected (*null hypothesis (H0)*) when the calculated p-value of t-test is < 0.05 or should be accepted (*research hypothesis (H1)/alternative hypothesis (Ha)*) when the calculated p-value of t-test is > 0.05.
t-Test (p-value: #DIV/0!): means invalid test, because the testing cycles have the same mean peak pressure values during the initial and final testing phases, and also SD values between them are zeroes.
Specimen (SG02/15/LT) was tested in January (Ja) & retested in February (Fe) after its revision, because of its dislocation during the initial testing due to glenoid component malposition.
FE: Flexion/Extension

Table (24): Statistical Calculations during IE Testing Episodes Per Phase/Per Specimen					
Specimen ID	Hypothesis State (Hii)				
	Mean peak pressure values		Statistically		
	Initial Phase (MPa)	Final Phase (MPa)	t-Test (p-value)	Critical Value (p-value = 0.05)	Hypothesis (H1: p-value > 0.05 & H0: p-value < 0.05)
LT/1214/12	4.2 ±0.05	3.9 ±0.15	0.000819905	0.05	H0
RT/1214/12	6 ±0.2	5.9 ±0.22	1.88719E-09	0.05	H0
LT/SG02/15/Fe	6.3 ±0.4	4.6 ± 0.18	7.43457E-08	0.05	H0
LT/SG02/15/Ja	2 ±0.3	5.9 ±0.7	2.30681E-10	0.05	H0
RT/SG02/15	6.7 ±0.5	4.0 ±0.2	2.14218E-09	0.05	H0
LT/SG04/14	8.4 ±0.4	8.3 ±0.06	0.866713076	0.05	H1
RT/SG04/14	7.3 ±0.4	12.2 ±0.23	1.72588E-12	0.05	H0

Remarks: see Table 23 **IE:** Internal rotation/External rotation

Table (25): Statistical Calculations: Mean Peak Pressure Value per Phase per Specimen & t-Test Values between Initial & Final Phases per Specimen					
Specimen ID	Hypothesis State (Hii)				
	Total Mean Peak Pressure		Statistically		
	Initial Phase (MPa)	Final Phase (MPa)	t-Test (p-value)	Critical value (p-value = 0.05)	Hypothesis (H1: p-value > 0.05 & H0: p-value < 0.05)
RT/1214/12	7.6 ±2.7	7.6 ±2.7	0.905541654	0.05	H1
LT/1214/12	6.2 ±2	4.1 ±0.3	1.62081E-06	0.05	H0
RT/SG02/15	8.7 ±02.3	6.5 ±2.9	1.1826E-11	0.05	H0
LT/SG02/15/Fe	8.4 ±2.9	6.3 ±3.1	1.71938E-14	0.05	H0
LT/SG02/15/Ja	4.1 ±2.3	9.3 ±3.0	1.02223E-22	0.05	H0
RT/SG04/14	9.3 ±1.8	11.6 ±1.3	0.000169191	0.05	H0
LT/SG04/14	9.2 ±0.73	9.0 ±0.8	0.227735458	0.05	H1
	Research hypothesis /Alternative hypothesis (H1)			Null hypothesis (H0)	
Total (7 t-test values/14 phases)	2			5	
Percentage (%)	28.6%			71.4%	
Remarks: see Table 23					

Fourthly, the obtained statistical values (*SD & mean peak pressure values*) were illustrated in the form of diagrams, which show the mean peak pressure values per phase/per specimen/per motion direction of the specimens and also the SD values per phase/per specimen/per motion direction for all specimens separately (*Diagrams 3, 4, 5, 6, 7, 8, 9 & 10*).

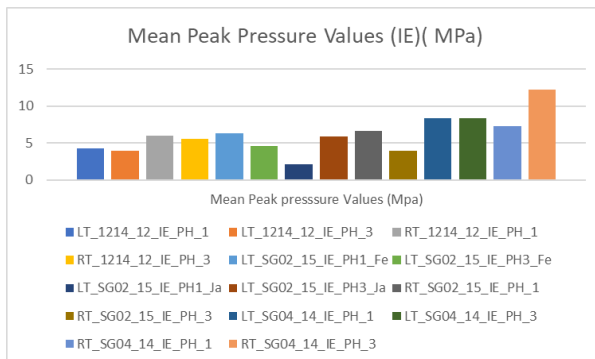


Diagram (3): Shows mean peak pressure values per phase/per specimen during IE testing episodes for the whole study.

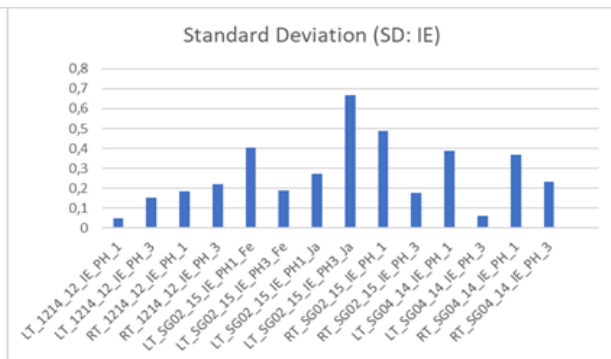


Diagram (4): Shows SD values per phase/per specimen during IE testing episodes for the whole study.

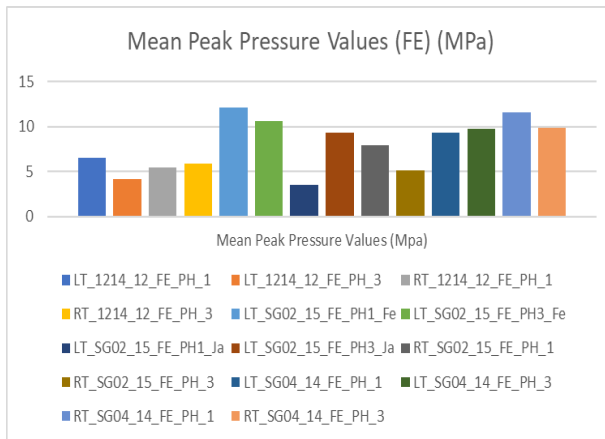


Diagram (5): Shows mean peak pressure values per phase/per specimen during FE testing episodes for the whole study.

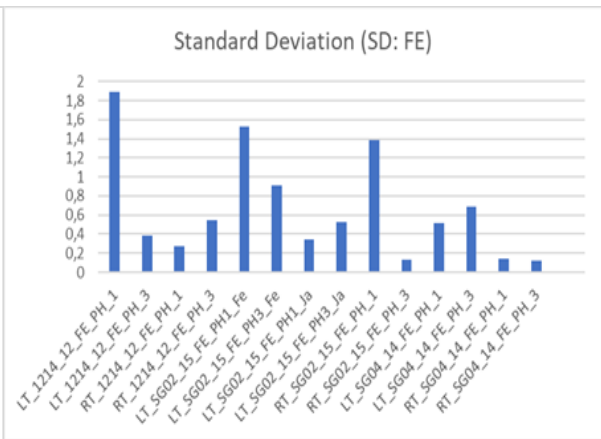


Diagram (6): Shows SD values per phase/per specimen during FE testing episodes for the whole study.

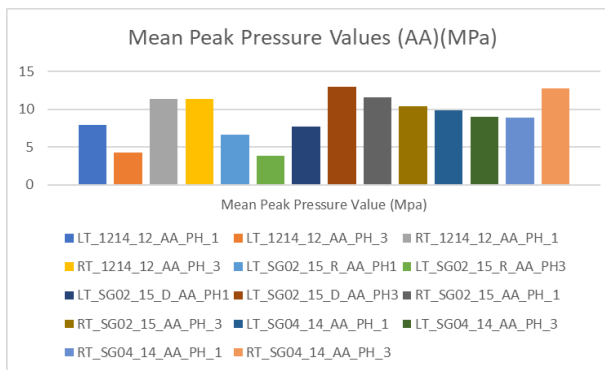


Diagram (7): Shows mean peak pressure values per phase/per specimen during AA testing episodes for the whole study.

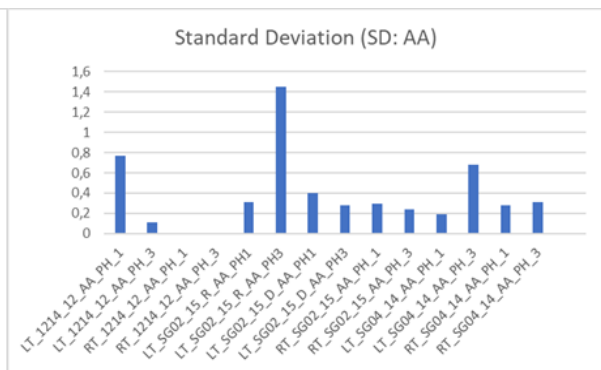


Diagram (8): Shows SD values per phase/per specimen during AA testing episodes for the whole study.

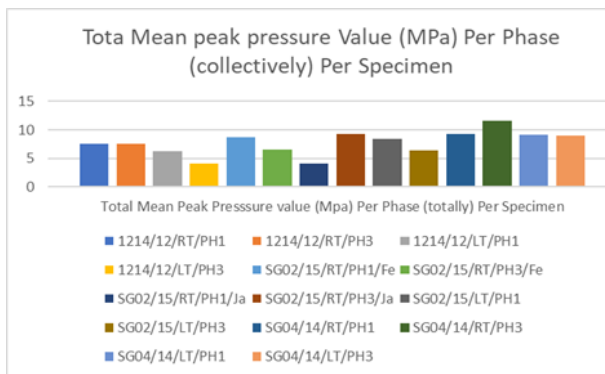


Diagram (9): Shows total mean peak pressure values per testing phase collectively (AA, FE & IE) per specimen for all specimens.

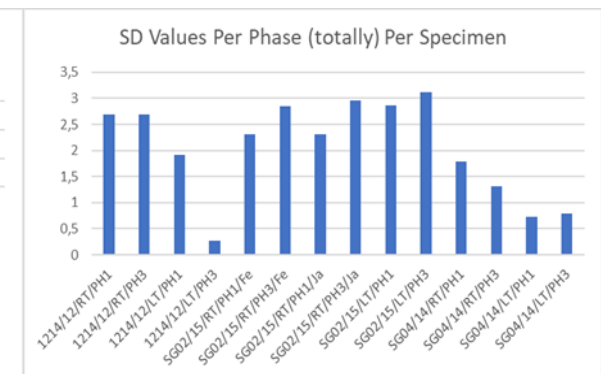


Diagram (10): Shows SD values per testing phase collectively (AA, FE & IE) per specimen for all specimens.

Fifthly, three standard values (<5, 5-10 and >10) MPa were selected as criteria to detect the differences between the recorded mean peak pressure values for different motion directions and their correlation to the motion type, and also to test the study hypothesis (*Hi* & *Hii*). Therefore, it was applied to classify the obtained mean peak pressure values per phase/per motion direction/per specimen (Table 26) and the

calculated total mean peak pressure values per phase/per specimen into three categories (Table 28), with their percentage values related to the total number of the testing episodes for their motion directions and related to the total number of testing phases in the three motion directions for the whole study (Tables 27, 28 & 29).

Additionally, three standard values (<0.5 , $0.5-1.0$ and >1.0) were selected as criteria to detect the rate of changes/variations between these values during the whole study to test the study hypothesis (Hi & Hii). The selected standard values were applied to classify the computed SD values per phase/per motion direction/per specimen (Tables 26, 29 & 30) with their percentage values related to the total number of the testing episodes for their motion directions and related to the total number of the testing phases in the three motion directions for the whole study.

Table (26): State of Hypothesis (Hi & Hii) According to the Selected Criteria (1)												
Specimen ID	Mean peak pressure variations (MPa) Standard values: (<5 , $5-10$ & >10) (MPa)						Differences (SD) within initial & final phases Standards values: (<0.5 , $0.5-1.0$ & 1.0)					
	Initial Phase			Final Phase			Initial Phase			Final Phase		
	AA	FE	IE	AA	FE	IE	AA	FE	IE	AA	FE	IE
1214/12/RT	>10	5-10	5-10	>10	5-10	5-10	= 0.0	<0.5	<0.5	<0.5	=0.5	<0.5
1214/12/LT	5-10	5-10	<5	<5	<5	<5	0.5-1.0	>1.0	<0.5	<0.5	<0.5	<0.5
SG02/15/RT	>10	5-10	5-10	>10	=5	<5	<0.5	>1.0	=0.5	<0.5	<0.5	<0.5
SG02/15/LT/Fe	5-10	>10	5-10	<5	>10	<5	<0.5	>1.0	<0.5	<0.5	0.5-1.0	<0.5
SG02/15/LT/Ja	5-10	<5	<5	>10	5-10	5-10	<0.5	<0.5	<0.5	<0.5	=0.5	0.5-1.0
SG04/14/RT	5-10	>10	5-10	>10	=10	>10	<0.5	<0.5	<0.5	<0.5	<0.5	<0.5
SG04/14/LT	=10	5-10	5-10	5-10	=10	5-10	<0.5	=0.5	<0.5	0.5-1.0	0.5-1.0	<0.5

Remarks (evaluative criteria):
The three standard values (<5 , $5-10$ & >10) MPa were selected to sort the recorded mean peak pressures per phase/per motion direction/per specimen into three categories to detect the extent of variations of these values during the study and also to test the study hypothesis (Hi & Hii).
In the same way, three standard values (<0.5 , $0.5-1.0$ & >1.0) were selected to classify the SD values per phase/per motion direction/per specimen into three categories to detect the extent of variations of these values during the whole study and also to test the study hypothesis (Hi & Hii).

Sixthly, according to the previously selected criteria, the number of changes in SD values between study testing phases was added with their percentages. Also, the changes in the mean peak pressure values within phases in total and per motion direction were added with their percentages and correlated with the motion directions (AA, FE & IE) to find out if there was a relation (*an inverse proportion, a direct proportion or no proportion*) between the motion type and the value of the recorded mean peak pressure values (Table 27).

Seventhly, the validity of hypothesis (Hii) for the whole study was evaluated statistically. t-Test values were computed between the total mean peak pressure values for all motion directions in the initial and final phases for each specimen (Tables 25 & 31).

Table (27): State of Hypothesis (Hi & Hii) According to the Selected Criteria (2)												
Motion Direction	Testing episodes number sorted by values of MPa											
	Initial Phase			Final Phase			Total			Percentage: (14 phases = 100%)		
	<5	5-10	>10	<5	5-10	>10	<5	5-10	>10	<5	5-10	>10
AA	---	4	3	2	1	4	2	5	7	14.3%	35.7%	50%
FE	1	4	2	1	3	3	2	7	5	14.3%	50%	35.7%
IE	2	5	---	3	3	1	5	8	1	35.7%	57.14%	7.14%
Total							9	20	13			
Percentage: (42 episodes = 100%)									AA	4.8 %	11.9%	16.7%
(Total episodes number of the study according to motion direction is 42 episodes = 100%)									FE	4.8 %	16.7%	11.9%
(6 testing episodes/7 trials/6 specimen)									IE	11.9%	19%	2.4%
Remarks:												
Specimen ID: SG02/15/LT was tested two times.												
Total number of testing episodes for each motion direction is 7 testing episodes.												
Total number of testing episodes of all motion directions of the whole study is 42 testing episodes.												

Table (28): State of Hypothesis (Hi & Hii) According to the Selected Criteria (3)			
Specimen ID	Mean peak pressure values per phase per specimen		
	Initial Phase (MPa)		Final Phase (MPa)
1214/12/RT	5-10		5-10
1214/12/LT	5-10		<5
SG02/15/RT	5-10		5-10
SG02/15/LT/Fe	5-10		5-10
S02/15/LT/Ja	<5		5-10
SG04/14/RT	5-10		5-10
SG04/14/LT	5-10		5-10
Standard values of the selected criteria			
	<5 MPa		5-10 MPa
	>10 MPa		>10 MPa
Total (14 phases) (2 phases X 7 trials)	2		12
Percentage (14 phases = 100%)	14.3%		85.7%
Remarks: Specimen ID: SG02/15/LT was tested two times in January (Ja) & in February (Fe)			

Eighthly, each one of the loose specimens was correlated separately with the values of its collectively recorded and computed total mean peak pressure values during the whole testing episodes and to the degree of its functional stability, which was observed during the testing episodes to find out the in-between relations (Tables 32, 33 & 36).

Ninthly, hypothesis (Hiii) supposed that the occurrence of the glenoid component loosening and its extension could be related collectively to many factors: component type, joint stability after implantation and quantity/value and quality/pattern of the applied loads across the implanted component surface in vitro and subsequently in vivo. So, the mentioned factors were correlated with each other to find out the in-between relations (Tables 32, 33 & 36).

Tenthly, and finally, the whole study was evaluated through the separate evaluation of each of the three stated hypotheses according to the specific indicated parameters of each one (Tables 34, 35 & 36).

Table (29): State of Hypothesis (Hi & Hii) According to the Selected Criteria (4)													
Motion Type	Testing phases number sorted by SD values												
	Initial Phase			Final Phase			Total			Percentage (14 phases = 100%)			
	< 0.5	0.5-1.0	> 1.0	< 0.5	0.5-1.0	> 1.0	<0.5	0.5-1.0	> 1.0		<0.5	0.5-1.0	>1.0
AA	5	2	---	6	1	---	11	3	---		78.6%	21.4%	0.0%
FE	3	1	3	3	4	---	6	5	3		42.9%	35.7%	21.4%
IE	6	1	---	6	1	---	12	2	---		85.7%	14.3%	0.0%
Total							29	10	3				
Percentage (42 episodes = 100%)							69%	23.8%	7.1%	AA	26%	7.1%	0.0%
<i>(6 specimens/7 trials/14 phases/42 testing episodes/14 testing episodes in each motion direction)</i>										FE	14.3%	12%	7.14%
										IE	28.6%	4.8%	0.0%
Remarks:													
Total number of testing episodes for each motion direction is 14 testing episodes.													
Total number of testing episodes for all motion directions of the whole study is 42 testing episodes.													
SD values higher than 1.0 were recorded only in FE testing cycles.													
SD values during AA & FE testing cycles had nearly the same variations for both initial and final phases.													
In the whole study, the larger number of variations of SD values was lower than 0.5 with a percentage of 69%, while a smaller number of SD values variations was higher than 1.0 with a percentage of 7.1%.													
The larger number of variations of SD values for every motion direction separately was lower than 0.5.													

Table (30): State of Hypothesis (Hi & Hii) According to the Selected Criteria (5)										
	(1) Mean peak pressure variations within phases (MPa)			(2) SD variations between phases						
	<5	5-10	>10	<0.5	0.5-1.0		>1.0			
Total testing episodes number	9	20	13	29	10		3			
Percentage (42 episodes = 100%)	21.4%	47.6%	30.95%	69%	23.8%		7.1%			
	(3) Relation between mean peak pressure values (MPa) & motion type									
	<5			5-10			>10			
	AA	FE	IE	AA	FE	IE	AA	FE	IE	
Total testing episodes number	2	2	5	5	7	8	7	5	1	
Percentage (42 episodes = 100%)	4.8%	4.8%	11.9%	11.9%	16.7%	19%	16.7%	11.9%	2.4%	
Remarks:										
In this table, according to the previously selected criteria, the numbers of changes in SD values between study testing episodes were added with their percentages, and the changes in the mean peak pressure values within phases in total and per motion direction were also added with their percentages. They were correlated with the motion direction (AA, FE & IE) to find out if there was a relation (<i>an inverse proportion, a direct proportion or no proportion</i>) between the motion direction and the recorded mean peak pressure values and with the differences of these values according to the motion type as it was previously hypothesized.										

Table (31): State of Hypothesis (Hii) (Statistically: t-Test Values)							
(1) t-test values between mean peak pressure values of the initial & final phases per motion direction/per specimen (21 t-test values /42 testing cycles/2 testing phases & 7 t-test values/14 testing cycles/2 testing phases/per motion direction)		Null Hypothesis (H0)			Research Hypothesis (H1/Ha)		
		AA	FE	IE	AA	FE	IE
Number (7 t-test values/per motion direction)		7	7	6	0	0	1
Sum (21 t-test values/42 testing cycles)		20			1		
Percentage (7 values = 100%)	All testing cycles per motion direction (7 t-test values/14 testing episodes for each motion direction)	100 %	100 %	85.7 %	0.0 %	0.0 %	14.3 %
(21 values = 100%)	Whole study (21 t-test values/42 testing episodes)	95%			5%		
(2) t-test values between total mean peak pressure values of the three motion directions of the initial & final phases/per specimen/per trial: 7 t-test values/14 testing phases/7 trials/6 specimens		Null Hypothesis (H0)			Research Hypothesis (H1/Ha)		
Number: 7 values (7 t-test values/ 14 testing phases)		5			2		
Percentage (7 values =100%) (7 t-test values/14 testing phases)		71.4%			28.6%		
Remarks: Null hypothesis (H0); Research Hypothesis (H1) or Alternative hypothesis (Ha). H0: p-value < 0.05; H1/Ha: p-value > 0.05							

Table (32): State of Hypothesis (Hiii): Relation Between Glenoid Component Loosening, Joint Stability & Recorded Pressure Data

Specimen ID	Loosening		Mean Peak Pressure (MPa)							Joint Stability Under Loading	
			Initial Phase			Final Phase			TMPP		
	Detection	Degree	AA	FE	IR	AA	FE	IR	AA, FE & IE	Stab	Unstab
1214/12/RT	Present	Ext	11.3 ±0.0	5.5 ±0.3	6.0 ±0.19	11.3 ±0.0	5.9 ±0.5	5.6 ±0.22	7.6 ±2.7	----	Unstab
1214/12/LT	Present	Ext	7.9 ±0.8	6.5 ±1.9	4.3 ±0.04	4.2 ±0.11	4.1 ±0.4	4.0 ±0.15	5.2 ±1.7	Stab	----
SG02/15/RT	Present	Ext	10.6 ±0.3	7.9 ±1.4	6.7 ±0.5	10.4 ±0.2	5.1 ±0.12	4.0 ±0.18	7.6 ±2.8	Stab	----
SG02/15/LT	Absent	-----	6.6 ±0.4	12.1 ±1.5	6.3 ±0.4	3.8 ±0.3	10.6 ±0.9	4.6 ±0.19	7.3 ±3.1	Stab	-----
SG04/14/RT	Present	Ext	8.9 ±0.3	11.5 ±0.14	7.3 ±0.4	12.8 ±0.3	9.8 ±0.11	12.2 ±0.23	10.4 ±2.0	Stab	----
SG04/14/LT	Absent	-----	9.9 ±0.18	9.4 ±0.52	8.4 ±0.4	9.0 ±0.7	9.7 ±0.69	8.3 ±0.06	9.1 ±0.08	Stab	----

Remarks:

TMPP: total mean peak pressure value per specimen for its whole testing episodes.

Ext: extensive; **Stab:** stable; **Unstab:** unstable

Table (33): State of Hypothesis (Hiii): Loosening & Mean Peak Pressure Values

Glenoid Loosening	Specim. No.	Glenoid Type		Joint Stability of Loose Specim.		Loosening Extent		TMPP Value (MPa)		
		Keel	Pegg	Stab	Unstab	Keel	Pegg	5 -10	>10	
Present	4	3	1	3	1	Ext	Ext	3	1	
Absent	2	1	1	2	---	---	---	2	---	
Present (Percent. %)	Whole Study Specim.	66.7%	50%	16.7 %	50%	16.7%	---	---	50%	16.7 %
	Glenoid Type	75% keel & 50% pegg	75%	50%	50% keel & 50% pegg	25% keel	100%	100%	50% for either keel or pegg	25% keel
	Loose Specim.	-----	75%	25%	75%	25%	100%	100%	75%	25%
Absent (Percent. %)	Whole Study Specim.	33.3%	16.7 %	16.7 %	40%	-----	-----	-----	33.3%	0.0%
	Glenoid Type	25% keel & 50% pegg	50%	50%	-----	-----	-----	-----	25% keel & 50% pegg	0.0% keel& 0.0% pegg

Remarks:

Total number of specimens was six specimens (*three keeled & three pegged*)

After revision of the unstable specimen (*SG02/15/LT*) to a new keeled glenoid, the scheduled specimens became *four keeled & two pegged specimens*.

Keel: keeled; **Pegg:** pegged; **Percent.:** percentage; **TMPP:** total mean peak pressure; **Specim.:** specimen; **No.:** number; **Ext.:** extensive; **Stab.:** stable; **Unstab.:** unstable; **MPa:** megapascal

Table (34): Study Evaluation: Hypothesis (Hi & Hii)	
Indicators	Applicability
(i) Variability of mean peak pressure values within each testing phase	40 episodes from 42 testing episodes per motion cycle exhibited great variability of mean peak pressure values, or 95.2%.
	Two episodes from 42 testing episodes per motion cycle exhibited no variability of mean peak pressure values, or 4.8%.
(ii) Variability of mean peak pressure values between testing phases	Recorded mean peak pressure values during 9 episodes per motion cycle from 42 testing episodes were lower than 5 MPa, or 21.4%.
	Recorded mean peak pressure values during 20 episodes from 42 testing episodes ranged between 5 and 10 MPa, or 47.6%.
	Recorded mean peak pressure values during 13 episodes per motion cycle from 42 testing phases were higher than 10 MPa, or 31%.
	Recorded total mean peak pressure values during 12 testing phases per specimen from 14 testing phases ranged between 5-10 MPa, or 85.7%, and in two testing phases per specimen were lower than 5 MPa, or 14.3%, while no testing phases per specimen recorded total mean peak pressure higher than 10 MPa, or 0.0%.
(iii) Variability of SD values between testing phases	SD values during 29 episodes from 42 testing episodes per motion cycle were lower than 0.5, or 69%.
	SD values during 10 episodes from 42 testing episodes per motion cycle ranged between 0.5 and 1.0, or 23.8%.
	SD values during 3 episodes from 42 testing episodes per motion cycle were higher than 1.0, or 7.1%.
(iv) Relation between the recorded mean peak pressure values and motion type	<u>AA Cycles:</u> 7 AA episodes from 14 AA cycles recorded mean peak pressure values >10 MPa, or 50% of the total AA episodes & 16.7% of the total testing episodes (42 episodes). 5 AA episodes from 14 AA episodes recorded mean peak pressure values between 5 and 10 MPa, or 35.7% of total AA testing episodes (14 episodes) & 11.9% of total testing episodes (42 episodes). 2 AA episodes from 14 AA testing episodes recorded mean peak pressure values <5 MPa, or 14.3% of total AA testing episodes & 4.8% of total episodes (42 episodes).
	<u>FE cycles:</u> 5 FE episodes from 14 FE testing episodes recorded mean peak pressure values >10 MPa, or 37.5% of total FE testing episodes & 11.9% of total episodes (42 episodes). 7 FE episodes from 14 FE episodes recorded mean peak pressure values between 5 and 10 MPa, or 50% of total FE episodes & 16.7% of total episodes (42 episodes). 2 FE episodes from 14 FE episodes recorded mean peak pressure values <5 MPa, or 14.3% of total FE episodes & 4.8% of total study episodes (42 episodes).
	<u>IE cycles:</u> One IE episode from 14 IE episodes recorded mean peak pressure values >10 MPa, or 7.14% of total IE episodes & 2.4% of total study testing episodes (42 episodes). 8 IE episodes from 14 IE episodes recorded mean peak pressure values between 5 and 10 MPa, or 57.14% of total IE episodes & 19% of total study episodes (42 episodes). 5 IE episodes from 14 IE episodes recorded mean peak pressure values <5 MPa, or 37.5% of total IE episodes number & 11.9% of total study testing episodes (42 episodes).
	<u>In total:</u> AA cycles exhibited the highest mean peak pressure values and a large number of the high mean peak pressure values, followed by the FE cycles. Although IE cycles exhibited the largest number of cycles with low mean peak pressure values, they also exhibited cycles with high mean peak pressure values, but at a lower frequency.

Table (35): Study Evaluation: (Hypothesis (Hii))	
Indicators	Applicability
Significant differences between mean peak pressure values of the initial & final phases were hypothesized to be detected per testing phase/per motion direction/per specimen (according to the computed t-test values)	(1) <u>According to the computed t-test values between the initial & final phases per motion direction per specimen:</u>
	<i>AA cycles:</i> null hypothesis (Hypothesis (Hii)) was accepted for all testing cycles with a percentage of 100%.
	<i>FE cycles:</i> null hypothesis (Hypothesis (Hii)) was accepted for all testing cycles with a percentage of 100%.
	<i>IE cycles:</i> null hypothesis (Hypothesis (Hii)) was rejected in one relation of testing cycles with a percentage of 5% and accepted in six relations of testing cycles with a percentage of 95%.
	<i>In Total:</i> null hypothesis (Hypothesis (Hii)) was rejected only in one relation of testing cycles with a percentage of 5% & accepted in twenty relations of testing cycles with a percentage of 95%.
(2) <u>According to the computed t-test values between all initial & final phases per specimen:</u>	
	Null hypothesis (Hypothesis (Hii)) was rejected in two experiments with a percentage of 28.6% & accepted in five experiments with a percentage of 71.4 %.

Table (36): Study Evaluation: (Hypothesis (Hiii))	
Indicators	Applicability
(i) Glenoid component loosening under loading	66.7% of all specimens (four specimens from six specimens) were loose.
(ii) Glenoid component type	75% of loose specimens were keeled (three specimens).
	75% of keeled specimens were loose.
	Loose keeled specimens represent 50% of the total specimens.
	25% of loose specimens were pegged (one specimen).
	50% of pegged specimens were loose (one specimen). Loose pegged specimen represents 16.7% of all specimens.
(iii) Glenoid component loosening & specimen instability	Only one specimen was unstable during the testing under cyclic loading and its glenoid component was also massively loosened.
(iv) Mean peak pressure values, loosening occurrence & loosening extension	25% of loose specimens exhibited radiological signs of an extensive loosening and recorded high mean peak pressure values.
	66.7% of all specimens (four specimens) were loose and recorded high mean peak pressure values.
	33.3% of all specimens (two specimens) exhibited no signs of loosening and recorded high mean peak pressure values.

7. Discussion

7.1. Hypothesis (Hi)

The recorded total mean peak pressure values per motion direction (*AA*, *FE* & *IE*) did not exceed the limit of 10 MPa for both initial and final testing phases. *AA* motion direction recorded the highest values (*around 9 MPa*), *FE* motion direction exhibited medium values (*around 8 MPa*), while *IE* motion direction recorded the lowest values (*around 6 MPa*). The highest recorded mean peak pressure value during all testing episodes was 13.0 ± 0.3 MPa, which was recorded during an *AA* testing episode, while the lowest recorded mean peak pressure value during all testing episodes was 3.6 ± 0.34 MPa, which was obtained during a *FE* testing episode. It was noticed that the highest mean peak pressure values were obtained during *AA* testing cycles, but less frequently; high mean pressure values were obtained during *FE* testing cycles at a higher rate of frequency.

The recorded mean peak pressure values during the *IE* testing cycles tended to be lower than those of *AA* and *FE* motion cycles. However, some *IE* testing episodes exhibited mean peak pressure values as high as those of *AA* and *FE* testing episodes, but at a much lower frequency. This may indicate that the obtained mean peak pressures could be related to the motion type, ROM ($AA > FE > IE$), the compression degree between the articulating surfaces of the tested joint ($IE > FE > AA$) and the size of the contact surface area between the articulating surfaces of the tested joint ($AA > FE > IE$). These conclusions could be confirmed by a retrospective inspection of the size of the red center of the TekScan signals obtained during *AA*, *FE* and *IE* testing episodes, which was larger in size and intensified in *IE*, medium in *FE* and small in Abduction, while the signal center was completely blue in adduction and mid-adduction cycles, which indicates a very low contact pressure value (*Figures 66, 67, 68, 69 & 70 & Table 16*).

It was expected that the recorded total mean peak pressure values and the recorded total load quantities of each specimen would be directly proportional to the size of each specimen. Although the obtained total load quantities varied greatly, these variations were random without a controlling rule, so that the two small-sized specimens recorded load quantities between 300 and 457 MPa and the two large-sized specimens recorded load quantities between 440 and 458 MPa, while the two medium-sized specimens recorded load quantities between 447 and 626 MPa (*Table 21*). It is clear that the obtained load quantities were nearly the same in the large and small specimens, while the highest load quantity was recorded in one of the medium-sized specimens. The calculated total mean peak pressure values during the whole testing course per specimen were nearly the same in the small and large specimens and ranged between 5.2 ± 1.7 and 7.6 ± 2.7 MPa, while they were higher in the medium-sized specimens and ranged between 9.12 ± 0.8 and 10.43 ± 2 MPa. This may indicate that the size of the shoulder joint doesn't play a great role in the peak pressure values obtained during its motion, but may contribute to the degree of compression between the articulating surfaces of the joint, which in turn depends on the degree of their conformity and the efficiency of the surrounding muscle activity.

7.2. Hypothesis (Hii)

It was hypothesized that the obtained mean peak pressure values are expected to vary between the initial and final testing phases per motion direction per specimen and between the initial and final testing phases per specimen for all motion directions collectively. It was found that according to the computed t-test values between the initial and final phases per motion direction per specimen, null hypothesis (*hypothesis (Hii)*) was accepted in the entire AA and FE testing cycles with a percentage of 100%, while it was rejected in only one relation of IE testing cycles with a percentage of 5% and accepted in six relations of testing cycles with a percentage of 95%. In total, null hypothesis (*hypothesis (Hii)*) was rejected in only one relation of testing cycles with a percentage of 5% and accepted in twenty relations of testing cycles with a percentage of 95%, while according to the calculated t-test values between all initial and all final phases per specimen, null hypothesis (*hypothesis (Hii)*) was rejected in two experiments with a percentage of 28.6% and accepted in five experiments with a percentage of 71.4%.

Additionally, the recorded mean peak pressure values were compared with each other. It was found that the obtained mean peak pressure values were apparently higher in the final testing phase than those recorded in the initial testing phase in all motion directions in seven testing episodes with a percentage of 16.7% related to total testing episodes (*42 testing episodes of the whole study*), while two testing episodes related to total testing episodes (*42 testing episodes of the whole study*) exhibited no variability of the obtained mean peak pressure values between the initial and final phases, or 4.8%. This may indicate that the recorded mean pressure values could vary from phase to phase, from specimen to specimen, from motion direction to motion direction and from motion cycle to motion cycle of the same motion direction, but these variations couldn't be ruled to be in the favor of the final testing phase.

The variations in the recorded mean peak pressure values could be related to the motion direction. To test this hypothesis, three standard values (<5 ; $5-10$; >10) MPa were selected as criteria to sort the total number (*42 mean peak pressure values*) of recorded mean peak pressure values per motion direction per specimen (*Tables 26 & 27*) and to sort the total number (*14 total mean peak pressure values*) of the calculated total mean peak pressure values per phase per specimen (*Table 28*). It was found that 40 of 42 testing episodes per motion cycle exhibited a great variability of mean peak pressure values, or 95.2%. Two of 42 testing episodes per motion cycle exhibited no variability of mean peak pressure values, or 4.8%. The recorded mean peak pressure values during 9 testing episodes per motion cycle were lower than 5 MPa, a percentage of 21.4%. The recorded mean peak pressure values during 20 of 42 testing episodes ranged between 5 and 10 MPa, a percentage of 47.6%. The recorded mean peak pressure values during 13 testing episodes per motion cycle from 42 testing episodes were higher than 10 MPa, a percentage of 31%. The recorded total mean peak pressure values during 12 testing phases out of 14 testing phases per specimen ranged between 5 and 10 MPa, a percentage of 85.7%, and in two testing phases per specimen were lower than 5 MPa, a percentage of 14.3%. No testing phases per specimen recorded a total mean peak pressure value higher than 10 MPa, a percentage of 0.0%. These

results could indicate the great variability of the recorded mean peak pressure values within and between the testing phases and from testing cycle to cycle of the same motion direction.

The larger number of recorded mean peak pressure values were between 5 and 10 MPa, while a smaller number was lower than 5 MPa. Additionally, the majority of recorded high values ($> 10 \text{ MPa}$) of mean peak pressure were in the AA motion direction, while the IE cycles recorded the larger number of mean pressures with the lowest value ($> 5 \text{ MPa}$). Only one IE motion cycle recorded a high mean peak pressure value ($> 10 \text{ MPa}$). FE motion was found to be the motion direction with the highest variability regarding the recorded mean peak pressure values: both phases of FE cycles exhibited a great variability in the mean peak pressure values. They fell into all three categories, as they exhibited mean peak pressure values < 5 , $5\text{-}10$ and $>10 \text{ MPa}$, while AA cycles in the initial phase didn't exhibit mean peak pressure values below 5 MPa and the IE testing cycles in the initial phase didn't exhibit mean peak pressure values higher than 10 MPa.

The final testing phase showed a greater variability in the mean peak pressure values for each motion direction than those recorded in the initial phase. Also, most calculated total mean peak pressures per phase per specimen were between 5 and 10 MPa, while none of the total mean peak pressure values per phase exhibited a value above 10 MPa.

To detect the degree of the variability in the recorded mean peak pressure values, three standard values (< 0.5 ; $0.5\text{-}1.0$; > 1.0) were selected to sort the calculated SD values in three categories to detect the number and the value of the changes of the obtained mean peak pressures (Tables 26 & 29). It was found that in 29 of 42 testing episodes per motion cycle, or 69%, SD values were lower than 0.5, and in 10 of 42 testing episodes per motion cycle, or 23.8%, SD values ranged between 0.5 and 1.0. In 3 of 42 testing episodes per motion cycle, or 7.1%, SD values were higher than 1.0.

The final testing phase didn't exhibit SD values higher than 1.0 in all motion directions, and the initial phase didn't exhibit SD values higher than 1.0 in AA and IE motion directions. It was noticed that the number and the value of the variability in SD values in IE and AA motion directions were nearly the same in both the initial and the final testing phases. The highest calculated SD value during all testing phases was ± 1.9 and was computed between FE initial and final testing phases, while the lowest calculated SD value during all testing phases was ± 0.05 and was computed between IE initial and final testing phases. However, the greatest variability in SD and mean peak pressure values was observed during FE testing cycles, with a percentage of 71.4%, while the variability in SD and mean peak pressure values during AA and IE testing cycles had a percentage of 14.2% each. These values may indicate the high degree of variability of the recorded mean peak pressure values between motion phases, motion directions and between motion cycles of the same motion direction. Additionally, the greatest degree of variability could be detected in FE motion cycles.

Two specimens were unstable during testing. However, low total mean peak pressure values were measured for them in comparison with the other specimens, which were stable. Additionally, the medium-sized specimen, which recorded the highest total mean peak pressure value and the highest total load quantity, was absolutely stable under loading testing. Furthermore, one of the two unstable specimens exhibited a slight morphological abnormality and the other exhibited a glenoid component malposition, which may indicate that the applied loads on shoulder joints do not play an absolute or an independent role in the creation of instability, but may play a role in the worsening of an already present instability due to component malposition, defective shoulder stabilizers, morphological abnormalities etc. It is also thought that the manner of load application could play a role in the creation of the instability: when the loads are applied on the joint in a regular and homogeneous pattern, parallel with the action axis of the muscular envelope of the shoulder joint, they stabilize the joint, but when they are applied in a random/heterogeneous pattern, they destabilize the joint.

7.3. Hypothesis (Hiii)

Four specimens out of six were detected radiologically to have glenoid component loosening, or 66.7% (Tables 17, 18, 32, 33 & 36). It was found that 75% of the loose specimens are keeled (*three specimens*) and in turn 75% of the keeled specimens are loose (*3 from 4 specimens*), while 25% of the loose specimens are pegged (*one specimen from four loose specimens*), which in turn represents 50% of all pegged specimens and 16.7% of total specimens. These results could intensify the thinking about the relation between the type of glenoid component design and the incidence rate of glenoid loosening, which is thought to be higher with keeled components. However, the extension of the detected glenoid loosening was massive (*according to the interpretation of the results of this study*) in both loose pegged and loose keeled components. Nonetheless, it is still believed that the pegged components are more stable than the keeled ones, because when the keel becomes loose, the entire component could be pulled out easily, whereas if one peg becomes loose, the other pegs could remain stable. This could be tested further in a wider study.

Only one of the loose specimens was unstable during testing and its glenoid component, a keeled component, was detected to be massively loose. This represents 25% of all loose specimens and 16.7% of all specimens. This result could highlight the relation between joint instability and glenoid component loosening. We believe that each of them could cause and worsen the other. Instability can cause glenoid loosening through micromotions (*minor subluxations*) and/or major subluxations and frank dislocations. In this case the severe joint instability causes severe eccentric loading on the edges of the components with attacks of violent hits, because of the violent oscillations of the humeral component head over the glenoid component surface, which would cause the loosening. Once the loosening has occurred, it will worsen the instability and vice versa in a vicious circle.

The loose specimens recorded pressure ranging between 310 and 626 MPa and the unloose specimens recorded comparative high-pressure values. Additionally, the recorded total mean pressure values in the loose specimens ranged between 5.2 ± 1.7 and 10.43 ± 2 MPa, while the total mean peak pressure values of the two unloose specimens were 7.34 ± 3.14 and 9.12 ± 0.8 MPa. This could indicate that the main factor in the relation between the loosening and the applied loads may be the mode of the application and the mode of load propagation over the glenoid component surface, not the load itself. However, the variations of SD values may play a significant role in loosening occurrence, because the high degree of variability in peak pressure values (*SD values*) between testing cycles in different motion directions and between testing phases could subject the implanted component to a series of successive strikes, which could loosen it. By reviewing SD values (*7 values*) between the initial and final phases (*collectively*) per specimen, they ranged between (± 1.7 and ± 2.8). The calculated SD values (*42 values*) per phase per motion direction per specimen ranged between ± 0.0 and ± 1.9 ; this could indicate that the application of greatly variable pressures on the implanted component leads over time, through unequal repetitive loading, to component loosening.

8. Conclusion

From the observations and examinations of this study it can be concluded that shoulder is one of the most dynamic joints in the human body. It can exhibit a huge range of biomechanical behavior under cyclic loading testing in vitro, which in turn could reflect the variability in shoulder biomechanics in vivo with and without arthroplasty.

The recorded mean peak pressure values and the imported load quantities of the shoulder joint could vary greatly between motion phases and motion cycles, which would reflect the changes in the controlling and functioning mechanisms and components of shoulder biomechanics. The resulting pressures across the shoulder joint during its action vary greatly according to the acting forces. The resulting contact pressures within the shoulder could be directly proportional to the motion direction, being higher during AA and FE motion cycles than during IE motion cycles. However, these obtained contact peak pressure values could be directly proportional to the size of the contact surface area between joint articulating surfaces during motion and also to the degree of compression of these surfaces against each other, which were both found to decrease gradually with the continuation of AA motion cycles. The AA motion direction is the most destabilizing motion of the shoulder joint, while the two articulating surfaces of the moving shoulder can be better compressed and pushed against each other during FE and IE motion cycles because of their relatively shorter and absolutely shorter motion arcs, respectively, in comparison with that of AA motion direction.

We found that the size of the shoulder has no great role in determining the value of the obtained peak pressure during its motion, but it could contribute to the degree of compression between the articulating surfaces of the joint, which in turn depends on the degree of their conformity and the efficiency of the surrounding muscle activity. The obtained mean peak pressure values could vary greatly from motion phase to motion phase, from shoulder to shoulder, and from motion direction to motion direction, but these variations could not be found to be clearly more present in any one of the motion cycles or phases. However, the greatest degree of variability was seen during FE motion cycles.

Shoulder joint instability after ATSA could result from component malposition, which absolutely requires revision surgery to be corrected; but it may also be caused by the morphological abnormalities of the joint articular surface, which could cause severe instability due to the loss of joint conformity between the articulating surfaces. Shoulder joint instability after ATSA is considered, together with glenoid component loosening, to be the most devastating complication after ATSA, potentially leading to the complete failure of the whole procedure. Both glenoid loosening and joint instability could incite the occurrence of the other and worsen its course through a devastating vicious circle. This study found that glenoid component loosening is related to joint stability, the applied loads and the mode of load application and propagation over the component surface in relation to the application duration and

degree of variability of the applied loads over time. It could also be related to the component design type, which was apparent in this study.

The study hypothesis (*Hii*) about the potentially detected difference between the recorded mean peak pressure values between the initial and final phases was not confirmed statistically, which may require more testing and evaluation trials using the Zebris system to record joint kinematics in a subsequent study. Hypothesis (*Hi & Hiii*) about the variations in the obtained mean peak pressure values within tested shoulders in different testing episodes and their contribution to both joint instability and glenoid component loosening were confirmed by the obtained results, and were also comprehensively discussed in correlation with the statistical calculations and the radiological and experimental findings.

9. Study Limitations

9.1. Small number of specimens

The study hypotheses were tested on a small specimen number (six specimens). It may be possible to get more detailed results and to detect additional variations if the hypotheses were tested in a wider study with a larger number of specimens.

9.2. Passive shoulder simulator system

The used setup was designed to test shoulder specimens passively, without giving any role in stability maintenance to the shoulder's muscular envelope during testing. As a consequence, we could evaluate only the relation of the characteristics of the prosthetic components and the articular surfaces to joint stability, but this could be evaluated comprehensively in another future study using a shoulder dynamic setup.

9.3. Inability to evaluate shoulder kinematics

The Zebris system used to measure shoulder kinematics couldn't be employed in this study, because the analytical program for shoulder kinematics is still in the building stage.

10. Recommendations

We strongly recommend a wider future study with a larger number of specimens in which the stability of the glenoid component after ATSA could be tested under cyclic loading using the Zebris system with US to measure joint kinematics and a dynamic shoulder setup to evaluate the function of the surrounding muscles in shoulder stability during testing. The results of that study could be combined with the results of this thesis to provide a wider understanding of the biomechanical behavior of the prosthetic glenoid component under cyclic loading.

11. Zusammenfassung

11.1. Hintergrund

Die Schultertotalendprothesen (*Schulter-TEPs*) gelten als erfolgreiche kurative Maßnahme für zahlreiche mit Steifigkeit und Schmerzen einhergehende Schultererkrankungen. Bei dem Verfahren können jedoch vielfältige Probleme auftreten. Die Lockerung der Schulterpfannenkomponenten (*Glenoid Komponenten*) gehört zu den häufigsten Komplikationen bei den anatomischen Schultertotalendprothesen; die zugrundeliegenden Ursachen können **mechanisch** (*abnorme Belastung*), **septisch** (*Infektionen*) oder **aseptisch** (*Autoimmunreaktionen*) sein. Die eingereichte Studie diskutiert die mechanisch bedingte Lockerung der Schulterpfannenkomponenten nach der Implantation von anatomischen Schultertotalendprothesen.

11.2. Hypothesen (*Hi, Hü & Hiii*)

(Hi) Es wird erwartet, dass die gemessenen mittleren Spitzendruckwerte der getesteten Schulterpräparate stark in Abhängigkeit von der Bewegungsart variieren, **(Hii)** dass die gemessenen mittleren Spitzendruckwerte zwischen der Anfangs- (Frühphase) und End- (Spätphase) der Messungen eines Schulterpräparates variieren und, **(Hiii)** dass das Auftreten und das Ausmaß der Lockerung der implantierten Schulterpfannenkomponenten (*Glenoid Komponenten*) mit den Veränderungen der gemessenen mittleren Spitzendruckwerten zusammenhängen.

11.3. Studienziel

Das Ziel der Studie ist eine umfassende experimentelle biomechanische Evaluation der Stabilität von anatomischen Schulterendprothesen (*Glenoid Komponenten*) unter phasenweiser zyklischer Belastung. Dazu zählen **(i)** die Analyse des Ausmaßes der Stabilität der künstlichen Schulterpfanneprothesen (*Glenoid Komponenten*) unter wiederkehrender zyklischer Belastung, **(ii)** die Analyse des Zusammenhangs zwischen den nach dem Prüfplan variierten Parametern der zyklischen Belastung und dem Auftreten der Schulterpfannenlockerung, **(iii)** die Messung und Beurteilung der Werte, Muster und des Ausmaßes des Kontaktdruckes zwischen den implantierten Gelenkkomponenten unter zyklischer Belastung, **(iv)** der Vergleich der Spitzenwerte des Kontaktdruckes unter zyklischer Belastung in der Anfangs- (Frühphase) und End- (Spätphase) der Messungen, um Zusammenhänge und/oder Unterschiede darzustellen, **(v)** die Analyse des Zusammenhangs zwischen den gemessenen Druckwerten während der Tests und den Daten der quantitativen Computertomographie (QCT) bezüglich der Lockerung der Schulterpfannenprothesen.

11.4. Material

Für die Studie wurden sechs frisch eingefrorene, komplette Schultergelenkspräparate (*Leichenschultern*) mit Knochen und Weichgeweben von drei verschiedenen Individuen verwendet. Nach der Implantation der Schultertotalendprothesen wurden die Präparate nacheinander mit Hilfe einer speziellen Testvorrichtung (*Schulter Simulator*) getestet. Für die geplanten Messungen wurden ein TekScan-System (*eine Computersoftware*) mit zweiköpfigen Drucksensorfolien, QCT, ein Schulter-Pointer und ein Schulterkinemator (*digitalisiertes 3D-Bilderfassungssystem (Zebris) mit Ultraschall (US)*), zusätzlich zu den routinemäßig bei derartigen Experimenten verwendeten Operations- und Laborinstrumenten, benutzt.

11.5. Methoden

Vor den Experimenten wurden die Schultergelenkspräparate mittels QCT gescannt, um die Oberflächenmorphologie des Gelenkes darzustellen. Dann wurden die Schulter-TEPs (*Glenoid- und Schafthkomponenten*) in die Präparate implantiert und die Drucksensoren in die Gelenkhöhle eingebracht und auf der Schulterpfannenprothese platziert und mit umlaufenden Nähten an den umliegenden Weichgeweben befestigt. Die sechs Präparate wurden nacheinander in den Schulter Simulator eingespannt und in drei aufeinanderfolgenden Testphasen einer unterschiedlichen dynamischen zyklischen Belastung bei unterschiedlichen simulierten Bewegungsmustern in die drei Bewegungsrichtungen [*Abduktion/Adduktion (AA), Flexion/Extension (FE), Innen-/Außenrotation (IA)*] ausgesetzt. Die kurzen erste und dritte Phasen (*Früh- und Spätphase*) fanden mit einem Drucksensor in der Gelenkhöhle statt, bei der zweiten längeren Phase (*Ermüdungs-/Übergangsphase*) wurde kein Drucksensor inseriert. Nach Beendigung des gesamten Experimentes wurden die Präparate erneut mit dem QCT gescannt, um die Lage der implantierten Schulterpfannenprothesen (*Glenoid Komponente*) und die potentiell auftretenden Radioluzenzen bzw. Lockerungen zu evaluieren.

11.6. Befunde (Beobachtungen & Untersuchungen)

Zwei Schulterpräparate erwiesen sich – *auch unter geringer Belastung* – als extrem instabil während der Testungen, besonders während der Lastzyklen mit Abduktions- und Adduktionsbewegungen (AA) und zeigten während der morphologisch-anatomischen Eingangs- und Abschlusskontrolle entweder eine ungewöhnliche Pfannenmorphologie oder eine Fehlstellung der implantierten Schulterpfannenkomponente. Dagegen waren die anderen vier Schulterpräparate während der Testungen in allen Bewegungsrichtungen [*Abduktion/Adduktion (AA), Flexion/Extension (FL), Innen-/Außenrotation (IA)*] unter verschiedenen Belastungskräften und mit Anwendung verschiedener Stabilisierungsgewichten stabil. Bei vier Präparaten wurde nach Beendigung der Tests radiologisch eine massive Pfannenimplantatlockerung nachgewiesen.

11.7. Ergebnisse

Die gemessenen mittleren Spitzendruckwerte und Belastungsmengen variierten erheblich zwischen den Testphasen, den Testzyklen und den Bewegungsrichtungen. Die höchsten mittleren Spitzendruckwerte traten in den AA-Testphasen auf, gefolgt von FE-Testphasen. Die geringsten Spitzendruckwerte wurden in den IA-Testphasen gemessen. Jedoch kam es auch in den IA-Testepisoden vereinzelt zu hohen Spitzendruckwerten. Die gemessenen Spitzendruckwerte lagen in sieben von 42 Tests (16,7%) mit verschiedenen Bewegungsrichtungen in der Abschlusstestphase höher als in der Eingangstestphase.

Die Nullhypothese (*bei Arbeitshypothese: Hii*) wurde laut der errechneten t-Test-Werte beim Vergleich der Eingangs- und Abschlusstestphase der verschiedenen Bewegungsrichtungen für alle AA- und FE-Testzyklen zu 100% bestätigt. Dagegen wurde die Nullhypothese (*bei Arbeitshypothese: Hii*) beim Vergleich von nur einem IA-Testzyklus mit einem Prozentsatz von 5% verworfen und beim Vergleich von sechs IA-Testzyklen mit einem Prozentsatz von 95% akzeptiert. Insgesamt wurde die Nullhypothese (*bei Arbeitshypothese: Hii*) nur für den Vergleich von einem Testzyklus mit einem Prozentsatz von 5% verworfen und für zwanzig Testzyklus-Vergleiche mit einem Prozentsatz von 95% akzeptiert. Laut der kalkulierten t-Test-Werte aller Eingangs- und Abschlussphasen eines Schulterpräparates wurde die Nullhypothese (*bei Arbeitshypothese: Hii*) in zwei Experimenten (28,6%) verworfen und in fünf Experimenten (71,4%) akzeptiert.

Bei vier Schulterpräparaten (*drei Präparate mit keilförmigen Glenoidkomponenten/keeled-Glenoidkomponenten und ein Präparat mit angenagelter Glenoidkomponente/Pegged-Glenoidkomponente*) wurde eine Lockerung entdeckt, das entspricht einem Anteil von 66,7% an allen in der Studie untersuchten Schulterpräparaten. Eines dieser Präparate (*mit einem Prozentsatz von 25% der gelockerten Präparate bzw. von 16,7% aller Präparate*) erwies sich während der Testung als instabil.

11.8. Schlussfolgerung

Die gemessenen Spitzendruckwerte und das Belastungsausmaß der getesteten Schultergelenke variieren teilweise erheblich zwischen den Bewegungsphasen, Bewegungszyklen und Bewegungsarten. Der resultierende Kontaktdruck in dem sich bewegenden Schultergelenk unterschied sich zum Teil stark in Abhängigkeit von der Kraftkomponente, der Bewegungsart, dem Status der Muskulatur und den Gelenkpathologien und hing direkt mit der Bewegungsrichtung zusammen. Bei den AA- und FE-Bewegungszyklen war der Kontaktdruck höher als während der IA-Bewegungszyklen. Weiter veränderte sich der Kontaktdruck proportional zur Kontaktfläche und zum Ausmaß der Kompression zwischen den artikulierenden Gelenkflächen während der Bewegung.

Die größte Variabilität der mittleren Spitzendruckwerte trat in den FE-Testzyklen auf. Die Schultergelenksinstabilität nach anatomischen Schultertotalendprothesen resultierte aus einer

Fehlposition der Implantatkomponenten und/oder aus morphologischen Gelenkoberflächenanomalien. Lockerung der Schulterpfannenkomponenten und Gelenkinstabilitäten konnten sich gegenseitig bedingen und die Entwicklung im Sinne eines Circulus vitiosus verschlechtern. Aus den Befunden lässt sich schließen, dass die Lockerung des Schulterpfannenimplantats mit der Gelenkinstabilität, dem Belastungsausmaß und der Art der Belastung in Relation zur Belastungsdauer in Zusammenhang stehen kann und offensichtlich –wie die Studie zeigt– auch im gewissen Maße mit dem Schulterpfannen-Implantattyp. Die erste und dritte Studienhypothesen (*Hi & Hiii*) wurden bestätigt, während die zweite Studienhypothese (*Hii*) aufgrund der statistischen Analyse (*t-Test-Werte*) verworfen werden musste. Daher sind weitere Evaluationen in zukünftigen Studien notwendig.

11.9. Stichwörter

Schulter, Instabilität, Prothesenlockerung, zyklische Belastung, Schulter Simulator, Schulter-TEP, Zebris-System, Komplikationen, Tekscan-System, Drucksensor, dynamische Stabilisatoren, statische Stabilisatoren, Biomechanik, Gelenkoberfläche, Übereinstimmung/Konformität, Diskrepanz/Mismatch, Radioluzenz, Verlust, Prothesenversagen, Standardabweichung, Spitzendruckwerte, Datenanalyse.

12. List of Abbreviations

Abbreviations List	
Abbreviation	Term
Abd-Add (AA)	Abduction-Adduction (<i>English</i>) / Abduktion-Adduktion (<i>German</i>)
AI	Acromial index
ACJ	Acromioclavicular joint
ACL	Acromioclavicular ligament
AC	Adhesive capsulitis
ATSA	Anatomic total shoulder arthroplasty
AN	Anatomical neck
AHCA	Anterior humeral circumflex artery
ASD	Anterior shoulder dislocation
ASI	Anterior shoulder instability
ASCL	Anterior sternoclavicular ligament
AP view	Anterior-posterior view
AVN	Avascular necrosis
BLC	Biceps-labral complex
BG	Bicipital groove
BV/TV	Bone volume/total volume
CT-scans	Computed tomography scans
CTDs	Connective tissue disorders
CAA	Coracoacromial arch
CAL	Coracoacromial ligament
CCL	Coracoclavicular ligament
CHL	Coracohumeral ligament
DP approach	Deltopectoral approach
FL/EX (FE)	Flexion/Extension
FSS	Frozen shoulder syndrome
GHJ	Glenohumeral joint
GHLs	Glenohumeral ligaments
GI	Glenoid inclination
GT	Greater tuberosity
HA	Hemiarthroplasty
HH	Humeral head
HS	Humerus shaft
IGHLC	Inferior glenohumeral ligament complex
ISI	Inferior shoulder instability
ISP	Infraspinatus
IR/AR (IA)	Innenrotation/Außenrotation (<i>German</i>)
IR/ER (IE)	Internal rotation/ External rotation (<i>English</i>)
JRF	Joint resistance force
LCLC	Labrocapsular ligamentous complex
LT	Left
LT	Lesser tuberosity
LHBBT	Long head of biceps brachii tendon
ML-Diameter	Mediolateral diameter
MPa	Megapascal
MGHL	Middle glenohumeral ligament
MDSI	Multidirectional shoulder instability
OA	Osteoarthritis
ON	Osteonecrosis
PXRs	Plain X-rays
PMMR	Poly (methyl methacrylate)
PE	Polyethylene (<i>Industry</i>)
PDFs	Predisposing factors
PHCA	Posterior humeral circumflex artery
PSD	Posterior shoulder dislocation

PSI	Posterior shoulder instability
PSCL	Posterior sternoclavicular ligament
PE	Pulmonary embolism (Medicine)
QCT	Quantitative computed tomography
ROM	Range of motion
RTSA	Reverse total shoulder arthroplasty
RA	Rheumatoid arthritis
RF	Rheumatoid factor
RT	Right
RFs	Risk factors
RC	Rotator cuff
RCA	Rotator cuff arthropathy
RCMs	Rotator cuff muscles
RCTs	Rotator cuff tears
RI/RCI	Rotator interval/Rotator cuff interval
SHR	Scapulohumeral rhythm
SA	Shoulder arthroplasty
SD	Shoulder dislocation
SCJ	Sternoclavicular joint
SSS	Subscapularis
SACL	Superior acromioclavicular ligament
SGHL	Superior glenohumeral ligament
SLAP Injury	Superior labrum anterior posterior injury
SI-Axis	Superior-inferior axis
SI-Diameter	Superoinferior diameter
SSP	Supraspinatus
SN	Surgical neck
TM	Teres minor
TE	Thromboembolism
TSA	Total shoulder arthroplasty
THL	Transverse humeral ligament
T.B.	Tuberculosis
TSR	Total shoulder replacement
US	Ultrasound
VTE	Venous thromboembolism

13. List of Figures

List of Figures		
Serial	Description	Page
Figure: 1	Shoulder-PXR “AP view” shows bones and joints of shoulder girdle in adult (Wikiradiography shoulder).	1
Figure: 2	3D shoulder model. Shoulder two coordinates system (Scapula (S); Humerus (H)) were defined (DOI: 10.1186/1749-799X-6-42).	1
Figure: 3	Proximal humerus portions (DOI:10.1053/j.ro.2005.01.012).	2
Figure: 4	Humeral head shaft angle ranges from 130° to 150°; head is retroverted from 260° to 310° (Terry et al. Journal of Athletic Training 2000;35(3):248-255).	2
Figure: 5	Vascular network of proximal humerus (DOI 10.1007/978-3-319-08951-5_2/ Springer).	3
Figure: 6	Parameters of glenoid anatomy include (A) glenoid height, (B) width, and (C) version (DOI: 10.1016/j.jse.2009.05.008).	3
Figure: 7	Shoulder joint ligaments (medicalartlibrary.com/muskuloskeletal. 2011).	5
Figure: 8	Glenoid labrum is compared with clock face (DOI:10.2214/AJR.10.7236).	5
Figure: 9	Anterior & posterior pectoral girdle muscles (Jan Modric, shoulder blade muscles, eHealthStar Dec 2014).	6
Figure: 10	Rotator cuff muscles & rotator interval (Lennard Funk, Rotator cuff biomechanics, MSc Orthopaedic Engineering, 2005).	6
Figure: 11	RC muscles overview (Phonex shoulder and knee, shoulder surgery 2013).	6
Figure: 12	Normal glenohumeral relationships. Humeral offset is depicted by distance F to H, thickness of humeral head from B to C, and center of humeral head at C. Note superior position of humeral head proximal to greater tuberosity (D to E) (Throckmorton 2016, http:// musculoskeletalkey.com/shoulder-and-elbow-arthroplasty).	9
Figure: 13	Normal shoulder articular surfaces with obvious deepening effect of labrum (Originally from Parsons 1998, taken from Massimini master thesis 2005).	9
Figure: 14	Deltoid and supraspinatus both contribute to abduction equally. As the arm is abducted, the resultant joint reaction force is directed towards the glenoid. This compresses the humeral head against the glenoid and improves the stability of the joint when the arm is abducted and overhead (Lennard Funk, Rotator cuff biomechanics, MSc Orthopaedic Engineering, 2005, originally, Parsons et al. J Orthop Res. 2002).	10
Figure: 15	Throughout the range of motion, the compressive resultant joint reaction force in the transverse plane contributes to joint stability. This is the predominant mechanism resisting superior humeral head displacement with cuff tears. As long as the force couple between subscapularis and infraspinatus remains balanced, the joint remains centered (Lennard Funk, Rotator cuff biomechanics, MSc Orthopaedic Engineering, 2005, originally, Parsons et al. J Orthop Res. 2002).	10
Figure: 16	Rotator cuff dynamic stability with deltoid action; SITS; supraspinatus, infraspinatus, teres minor and subscapularis muscles. The net result of acting forces pulls the center of the humeral head towards the center of the GHJ to stabilize it (KINESIOLOGY SHOULDER, by Hermizan Halihanafiah College of Allied Health and Science 2011, Malaysia).	11
Figure: 17	Balanced net force of acting muscles to compress humeral head against glenoid fossa “concavity compression”. (Masten et al., Mechanics of Glenohumeral Instability 2013).	11
Figure: 18	PXR shows a typical shoulder with advanced glenohumeral OA. There is joint space narrowing with marginal osteophytes and subchondral sclerosis present (www.learnorthopaedics.com).	13
Figure: 19	MRI of stage 2 ON disease. Note the characteristic involvement of a significant portion of the superior articular surface, as well as the clear demarcation between the relatively normal distal bone and the ischemic subchondral bone (Bulletin of the NYU Hospital for Joint Diseases 2009;67(1):6-14).	14
Figure: 20	Radiographs of late stage 2, humeral head osteonecrosis. AP views in (A) external and (B) internal rotation demonstrate areas of sclerosis involving a major portion of the humeral head (Bulletin of the NYU Hospital for Joint Diseases 2009;67(1):6-14).	14
Figure: 21	MRI of full thickness RCT (Dr Brian Badman, American health network).	15
Figure: 22	Shoulder PXR (AP view) shows calcific tendinitis of the supraspinatus tendon is the cause of shoulder impingement (red arrow) (Homepage Dr G. Goudelis 2015).	15

Figure: 23	Rotator cuff arthropathy in an elderly patient. Note the obliteration of subacromial space and roundedness of the humeral head, which is subluxated superiorly resting on the acromion and forming a new “joint” at this location (Foruria et al, Rev. esp. cir. ortop. traumatol.2008;52:392-402).	15
Figure: 24	Photograph taken at Smithsonian National Museum of History shows first shoulder replacement placed by Jules E. Pean in patient with tuberculous arthritis (DOI:10.2214/AJR.12.8854).	17
Figure: 25	Neer’s constrained reverse shoulder prosthesis concept (a) and the Delta III reverse shoulder prosthesis based on Grammont’s original design (b) (DOI.org/10.1186/s13018-015-0244-2).	17
Figure: 26	Different humeral components of HA (left; Stryker homepage) & TSA (right; www.Foundation.shoulder.com).	18
Figure: 27	Photograph of the SMR System glenoid, Castanga et al., (SMR System, Lima Corporate, Villanova, Italy) (Doi:10.1302/0301-620X.92B10).	18
Figure: 28	Example of an uncemented glenoid design where (A) initial fixation is achieved with 2 peripheral screws and (B) the component is press-fit into position using a central peg (BMC Musculoskelet Disor.2007;8:76.)	19
Figure: 29	Cemented keeled (right) and pegged (left) glenoid designs for total shoulder arthroplasty (DOI: 10.1016/j.jse.2009.05.008).	19
Figure: 30	The four standard projections for standard radiographic evaluation show a patient with ATSA. (a) AP view with the patient rotated approximately 45° towards the abnormal side; (b) AP view with the forearm in neutral position; (c) Cross-table view; (d) Neer’s (Y) view with the radiographic beam parallel to the scapula and tilted craniocaudally by 15° (DOI 10.1007/s00330-008-1093-8).	20
Figure: 31	Glenoid component loosening in 72-year-old woman with anatomic total shoulder arthroplasty. A and B, Grashey (A) and axial (B) radiographs show frank loosening of glenoid component, with several millimeters of space between bone and polyethylene face (arrow, A) (DOI:10.2214/AJR.12.8855).	22
Figure: 32	Three types of glenoid component loosening according to Walch et al., (DOI: 10.1016/j.otsr.2012.11.010)	22
Figure: 33	Evaluation of glenoid bone stock (DOI: 10.1016/j.otsr.2012.11.010).	22
Figure: 34	Rocking-horse loosening. Although the glenoid component is stable when the load applied by the humeral head is centered (middle), anterior (left) or posterior (right), translation of the head of the glenoid causes eccentric loading and lifting up of the opposite, unloaded glenoid rim. (Masten III et al.2008) (DOI:10.2106/JBJS.G.01263)	22
Figure: 35	State-of-the-art numerical analysis showing the effects of fixation design on periprosthetic stresses in the cement and bone (Chevalier et al, 2015a).	24
Figure: 36	The metal humeral components (head & adapter). The adapter parts are; a metal cuboid, a screw, a washer and a plastic cylinder.	28
Figure: 37	The simulator with a mounted LT-sided Sawbone synthetic specimen shows the moving metal arm of the simulator (oblique view from above) and its four parts four parts: the movable jointed-root with central axis (yellow arrow), the longitudinal part (blue arrow), the transverse part (red arrow) and the attaching part with the humeral stump (black arrow).	31
Figure: 38	The central part of the simulator with a mounted RT-sided specimen, moving arm of simulator, tripods from Zebris, TekScan and an inserted pressure sensor within the GHJ of a right-sided mounted shoulder specimen (MP: moving plate; CA: central axis; UP: upper plate; MP: middle plate; LP: lower plate; ST: scapular tripod; HT: humeral tripod; MA: moving arm).	31
Figure: 39	The orientation of the two metal pyramids in the resting position with a mounted LT-sided shoulder specimen. Both pyramids face anteriorly with their small surfaces; blue arrows point to the RT pyramid of the simulator on the LT of the observer and yellow arrows point to the LT pyramid of the simulator on the RT of the observer.	31
Figure: 40	The mounting of a RT-sided shoulder specimen, in which two screws (blue arrows) are fixed to the posteriorly situated and hidden LT metal pyramid of the simulator on the RT of the observer and one screw (yellow arrow) is fixed to the posteriorly situated and hidden RT metal pyramid of the simulator on the LT of the observer.	31
Figure: 41	General view of the simulator with a mounted left-sided shoulder specimen.	32
Figure: 42	The pattern of hanging of the stabilizing weights during testing of a left-sided mounted shoulder specimen on shoulder rig. Black arrows refer to the stabilizing weights of	33

	scapula, which is attached to the 2 nd plate and hung on the anterior aspect of shoulder rig when testing a left-sided specimen, while the yellow arrows refer to the stabilizing weights attached to the 3 rd plate and usually hung on the left side of the simulator during testing of LT- or RT-sided specimens.	
Figure: 43	A mounted left-sided shoulder specimen on the simulator at mid-abduction (left) & at full abduction (right) motions during cyclic loading testing (the haziness/cloudiness at the upper part of the two images around the moving metal arm of the simulator is evidence of the motion).	33
Figure: 44	Zebris system from behind (yellow arrows) and shoulder pointer (black arrows), in addition to a right-sided shoulder specimen mounted on the simulator.	34
Figure: 45	The humeral tripod above (HT/yellow arrows) and the scapular tripod below (ST/blue arrow) with a left-sided shoulder specimen mounted on the simulator.	34
Figure: 46	The TekScan pressure sensor foil. It consists of a proximal end with two RT & LT heads and a distal end. The two heads are covered with silicon & Teflon layers for protection during joint motion under loading testing.	34
Figure: 47	The operating program of the simulator. Firstly, the ID of the specimen, the number of cycles, the direction of cycles and their sequence are entered, in addition to the amount of the force. Then the evaluator presses “Accept”. The red Stop button is designed for urgent stoppage. The black windows below show the graphs of motion, but this wasn’t a part of our study.	35
Figure: 48	The second window of the operating program of the simulator. When everything is in order, the examiner presses “Accept” to start the phase of cyclic loading.	36
Figure: 49	An optimally displayed TekScan signal at the resting phase according to the described criteria (complete, rounded & corresponding to the colors reference at the lower part of the photo).	37
Figure: 50	A bad TekScan signal, because there is a central black line running from side to side, which indicates damage within the sensor head substance. The whole signal was enlarged for clarity.	37
Figure: 51	An example of glenoid version evaluation using QCT (coronal section). Specimen ID: 1214/12 RT with measured retroversion about 3.4° & SI length about 39 mm.	38
Figure: 52	An example of glenoid size (superior-inferior length and humeral head size (AP and mediolateral diameters) evaluation using QCT (coronal section) (specimen ID: SG02/15 RT).	38
Figure: 53	Dorsal aspect of a LT-sided shoulder specimen prepared with the fixation of the humeral and scapular metal bases for subsequent mounting on the simulator.	39
Figure: 54	Ventral aspect of a LT-sided shoulder specimen prepared with the fixation of the humeral and scapular metal bases for subsequent mounting on the simulator.	39
Figure: 55	The drilled hole for humerus adapter component within the rest of the humeral head after its resection in a RT-sided shoulder specimen.	39
Figure: 56	The drilled native glenoid for a subsequent implantation of a pegged glenoid component in a LT-sided shoulder specimen.	39
Figure: 57	A RT-sided shoulder specimen with an implanted keeled glenoid component (according to the plan of study) and the metal part of the humeral adapter (upper side of the figure corresponds to the upper glenoid pole).	40
Figure: 58	A cemented humeral adapter with its complete parts within the resected humeral head in a RT-sided shoulder specimen.	40
Figure: 59	Humeral and scapular kinematic references for shoulder pointer on humerus (left) & on scapula (right) (HA: humerus anterior, HP: humerus posterior, AA: angulus acromials, AI: angulus inferior, TS: trigonum spinae).	44
Figure: 60	A mounted RT-sided shoulder specimen. Examples of the application of shoulder pointer before the initiation of cyclic loading: Left: humerus; 2 nd point (HP: humerus posterior) & Right: scapula; 7 th point (AI: angle inferior), before the initiation of the 1st phase of cyclic loading testing.	44
Figure: 61	A left-sided specimen mounted on the simulator during the 1st phase of cyclic loading. The GH joint of the specimen is clearly visible and the inserted pressure sensor is also obvious where it comes out of the joint.	44
Figure: 62	A RT-sided shoulder specimen. The observer can’t see the joint during motion, because the joint opening faces posteriorly and the pressure sensor is hanging on the posterior aspect of the simulator (anterior surface of the specimen).	44

Figure: 63	A mounted LT-sided shoulder specimen on the simulator during the 2 nd prolonged phase of cyclic loading, without the application of the pressure sensor. “GC”: glenoid component (yellow arrow) & “HHC”: humeral head component (blue arrow).	44
Figure: 64	A RT-sided specimen after the insertion of the pressure sensor head over the glenoid and fixing it with circumferential sutures with the surrounding soft tissues (arrows), (LT: dislocated joint; RT: reduced joint).	46
Figure: 65	A LT-sided specimen with metal bases. Left: dislocated joint shows a well inserted pressure sensor situated over the hidden glenoid (arrows) after specimen testing. The sensor appears shiny because of the specimen tissue fluids. Right: the release of the sutures to remove the sensor head.	46
Figure: 66	A TekScan signal during the Abd of an Abd/Add motion cycle of a mounted LT-sided shoulder specimen, which is large, rounded and lies at the upper outer side of the demonstrating window. The signal shows a large contact area between joint articulating surfaces and a medium contact pressure (the red center of the signal). The top of the graph below represents the Abd.	49
Figure: 67	A TekScan signal during a mid-abduction motion of a mounted LT-sided shoulder specimen, which is represented by the slope between the Abd & Add on the graphic wave. The signal center is completely blue, indicating a very low contact pressure value.	49
Figure: 68	A TekScan signal during an Add motion of a mounted LT-sided shoulder specimen, which is small, elongated, lying at the inner side of the window and represented by the baseline (bottom) of the graphic wave below. The signal center is completely blue, indicating a very low contact pressure value.	49
Figure: 69	TekScan signal during an external rotation motion of a mounted LT-sided shoulder specimen (blue circle). TekScan signal is small, elongated and situated at the inner side of the demonstrating window, indicating a small contact surface area between joint articulating surfaces. The top of the graph below represents the ER.	49
Figure: 70	TekScan signal during an EX motion of a mounted LT-sided shoulder specimen. TekScan signal is small, elongated and situated at the inner side of the demonstrating window, indicating a small contact surface area between joint articulating surfaces. The top of the graph situated at the lower part of the window represents the extension motion. Signal center is red, indicating a high contact pressure value.	50
Figure: 71	Zebris system program during the abduction of an Abd/Add motion cycle of the tested specimen ID: SG04/14 LT. The upper triangle refers to the humerus, whereas the lower triangle refers to the scapula. The upper triangle moves during Abd/Add & IR/ER motions and the lower triangle moves during FL-EX motions. The graph situated at the left side of the window is similar to that of the TekScan. At the RT part of the figure, the distance between the two triangles is clearly wide and the upper triangle moves in a circular pattern towards the LT side indicating an Abd. motion.	50
Figure: 72	The specimen ID: 1214/12/RT with a mismatch in the superior-inferior length between the native and the prosthetic glenoids of about 10 mm.	53
Figure: 73	The specimen ID: 1214/12/RT; post-experimental CT coronal section shows the mismatch between the native glenoid (yellow arrow) and the prosthetic glenoid (blue arrow).	53
Figure: 74	The specimen ID: 1214/12/RT shows damage marks (within the blue circles) mainly at the anterior and antero-inferior edges of the glenoid due to the violent oscillation of the humeral head over the glenoid component.	54
Figure: 75	The LT-sided specimen ID: SG02/15/LT with an evident mismatch between the native and the prosthetic glenoids of about 5 mm in the superior-inferior diameter due to superior displacement of the implanted prosthetic glenoid.	54
Figure: 76	The native glenoid of the LT-sided specimen ID: SG02/15 after removal of the failed prosthetic glenoid component (left) & after drilling to implant the new keeled component (right).	54
Figure: 77	Post-experimental CT coronal section of specimen ID: 1214/12 LT shows the radiopaque humeral adapter (blue arrow), the radiopaque marker in the keel of the glenoid component (black arrow) and the radiolucent glenoid component (yellow arrow).	56
Figure: 78	CT coronal section of specimen ID: SG02/15 LT. The glenoid component seems to be well-positioned and the cement has a good amount and a good distribution around the prosthetic glenoid (a sticky thick cement mantle) without radiolucency; also, the humeral adapter seems to be well-positioned and completely surrounded with cement without radiolucency.	56

Figure: 79	CT coronal section shows loosening (blue arrows) around the glenoid component of specimen ID: 1214/12 LT with a separation line of more than 2 mm in width, particularly inferiorly.	56
Figure: 80	CT coronal section shows loosening (blue arrow) around the glenoid component of specimen ID: 1214/12 LT with a separation line of more than 2 mm in width, particularly inferiorly.	56

14. List of Tables

List of Tables		
Serial	Table Description	Page
Table: 1	Shoulder's range of motion (ROM)	7
Table: 2	Acting Muscles of GH joint	7
Table: 3	Static and Dynamic Stabilizers of Shoulder	8
Table: 4	Function of GHs in Shoulder Stability	10
Table: 5	Function of RCMs in Shoulder Stability	12
Table: 6	Glenoid Loosening Radiographic Classification	21
Table: 7	Specimens	27
Table: 8	Plan of Glenoid Implantation	40
Table: 9	Levels of Specimen Step-Wise Testing	41
Table: 10	Phases of Cyclic Loading Testing	43
Table: 11	Shoulder Pointer References	43
Table: 12	Sequence of Testing Course in Reference to Simulator Configuration	48
Table: 13	Tested Specimen Orientation on Simulator	48
Table: 14	TekScan Graph Description	51
Table: 15	Correlations Between Specimen Side, Simulator Mechanics & TekScan Graphs	51
Table: 16	TekScan Signal Description	52
Table: 17	Detection of Glenoid Component Loosening using QCT in the Tested Specimens	55
Table: 18	Evaluation of Loosening by Glenoid Type	56
Table: 19	Statistical Calculations	59
Table: 20	Total Mean Peak Pressure per Motion Direction for the whole Study	59
Table: 21	Relation Between Applied Loads Quantity, joint Stability & Component Loosening	59
Table: 22	Statistical Calculations during AA Testing Episodes Per Phase/Per Specimen	60
Table: 23	Statistical Calculations during FE Testing Episodes Per Phase/Per Specimen	61
Table: 24	Statistical Calculations during IE Testing Episodes Per Phase/Per Specimen	61
Table: 25	Statistical Calculations: Mean Peak Pressure value per Phase per Specimen & t-Test value between initial & final phases per specimen	62
Table: 26	State of Hypothesis (Hi & Hii) According to the Selected Criteria (1)	64
Table: 27	State of Hypothesis (Hi & Hii) According to the Selected Criteria (2)	65
Table: 28	State of Hypothesis (Hi & Hii) According to the Selected Criteria (3)	65
Table: 29	State of Hypothesis (Hi & Hii) According to the Selected Criteria (4)	66
Table: 30	State of Hypothesis (Hi & Hii) According to the Selected Criteria (5)	66
Table: 31	State of Hypothesis (Hii) (Statistically: t-Test Values)	67
Table: 32	State of Hypothesis (Hiii): Relation Between Glenoid Component Loosening, Joint Stability & Recorded Pressure Data	68
Table: 33	State of Hypothesis (Hiii): Loosening & Mean Peak Pressure Values	68
Table: 34	Study Evaluation: Hypothesis (Hi & Hii)	69
Table: 35	Study Evaluation: (Hypothesis (Hii))	70
Table: 36	Study Evaluation: (Hypothesis (Hiii))	70

15. List of Graphs

List of Graphs		
Serial	Graph Description	Page
Graph: 1	Demonstrates peak pressure value per motion cycle versus time in AA motion direction during the last testing phase of specimen ID: SG02/15/LT. Testing duration in AA motion direction/per phase is 45 seconds for ten cycles (4.5 seconds/cycle). Motion waves are absent between 35 & 45 seconds, because the specimen joint dislocated between the 8 th & the 9 th Abd/Add motion cycles at second 35. The graphic wave is wide, high and Abd motion is represented by the top of the graphic wave, while the Add motion is represented by the bottom of the graph & mid-abduction motion by the slope of the graphic wave.	57
Graph: 2	Demonstrates peak pressure value per motion cycle versus time in IE motion direction of specimen ID: SG02/15/LT. Testing duration in IE motion direction per phase is 14 seconds for ten cycles (1.4 seconds/cycle). The graphic wave is narrow, short and lies on both sides (upper and lower sides) of the baseline of the graphic wave. ER motion is represented by the top of the graphic wave & IR motion by the bottom of the graphic wave.	58
Graph: 3	Demonstrates peak pressure value per motion cycle (ten cycles) versus time in FE motion direction during the last testing phase of specimen ID: SG02/15/LT. Testing duration in FE motion direction per phase is 45 seconds for ten cycles (4.5 seconds/cycle). The graphic wave is wide, medium-sized and lies on both sides (upper and lower sides) of the graphic baseline. FL motion is represented by the bottom of the graphic wave and EX motion by the top of the graphic wave.	58

16. List of Diagrams

List of Diagrams		
Serial	Description	Page
Diagram: 1	Shows total mean peak pressure values & SD values during the whole testing course of each specimen (two phases & three motion directions).	60
Diagram: 2	Shows the total load under which each specimen was tested during the whole testing episodes (two phases & three motion directions).	60
Diagram: 3	Shows mean peak pressure values per phase/per specimen during IE testing episodes for the whole study.	62
Diagram: 4	Shows SD values per phase/per specimen during IE testing episodes for the whole study.	62
Diagram: 5	Shows mean peak pressure values per phase/per specimen during FE testing episodes for the whole study.	63
Diagram: 6	Shows SD values per phase/per specimen during FE testing episodes for the whole study.	63
Diagram: 7	Shows mean peak pressure values per phase/per specimen during AA testing episodes for the whole study.	63
Diagram: 8	Shows SD values per phase/per specimen during AA testing episodes for the whole study.	63
Diagram: 9	Shows total mean peak pressure values per testing phase collectively (AA, FE & IE) per specimen for all specimens.	63
Diagram: 10	Shows SD values per testing phase collectively (AA, FE & IE) per specimen for all specimens.	63

17. References

17.1. References – (“Shoulder Anatomy”)

- 1) Terry GC, Chopp TM. *Functional Anatomy of the Shoulder*. Journal of Athletic Training 2000 Sep; 35(3): 248-255.
- 2) Bickels J, Wittig JC, Kollender Y, Kellar-Graney K, Meller I, Malawer MM. *Limb-Sparing Resections of the Shoulder Girdle*. J AM Coll Surg 2002 April; 194(4): 422-435.
- 3) Chaudhary H, Aneja S. *MRI Evaluation of Shoulder Joint: Normal Anatomy & Pathological Finding: A Pictorial Essay and Review*. IOSR Journal of Dental and Medical Sciences (JDMS) 2012 Nov/Dec; 2(2): 01-09.
- 4) Gupta H, Robinson P. *Normal Shoulder Ultrasound: Anatomy and Technique*. Semin Musculoskelet Radiol 2015 July; 19(3): 203-2011.
- 5) Saladin KS, McFarland RK. *Human Anatomy*. 2008; (2): 234-261. ISBN-13: 978-0072943689.
- 6) Sanders TG, Jersey SL. *Conventional Radiography of Shoulder*. Seminars in Roentgenology; 2005 Jul; 40(3): 207-222.
- 7) Clippinger KS. *Dance Anatomy and Kinesiology: Principles and Exercises for Improving Techniques and avoid common Injuries*. ISBN: 9781450469289. 2007; (2): 1-28.
- 8) Halder AM, Itoi E, An KN. *Conservative Management of the Shoulder Injuries: Anatomy and Biomechanics of the Shoulder*. Orthop Clin North Am. 2000 Apr; 31(2): 159-176.
- 9) Ombregt L. *A System of Orthopaedic Medicine: Section 3; Applied Anatomy of Shoulder, and Section 4; Applied Anatomy of Shoulder Girdle*. 2013 Mar; (3): 205-274. ISBN: 9780702031458.
- 10) Cook TS, Stein JS, Simonson S, Kim W. *Normal and Variant Anatomy of Shoulder on MRI*. Magn Reson Imaging Clin N Am. 2011 Aug; 19(3): 581-594.
- 11) Shellock FG, Powers CM. *Kinematic MRI of the Joints: Functional Anatomy, Kinesiology and Clinical Application*. 2001 Mar; (1): 206-217. ISBN: 9780849308079.
- 12) Jacobson JA. *Radiology: Shoulder US; Anatomy, Techniques and Scanning Pitfalls*. Radiology 2011 Jul; 260(1): 6-16.

- 13) Crosby LA, Neviasser RJ. *Proximal Humerus Fractures: Evaluation and Management* by Twiss T. 2015 Jan; Pages 23-41. ISBN: 978-3-319-08951-5, Springer International Publishing.
- 14) Harrison JWK, Howcroft DWJ, Warner JG, Hodgson SP. *Internal Fixation of Proximal Humeral Fractures*. Acta Orthop. Belg., 2007; 73(1): 1-11.
- 15) Dreborowicz M, Dreborowicz E, Walecka J. *Anatomy of Scapula and Shoulder Girdle: Review of the Current Literature*. Issue Rehabil. Orthop. Neurophysiol. Sport Promot. 2016; 16: 61-70.
- 16) Paulsen, F., Waschke, J., *Sobotta Atlas der Anatomie des Menschen Band 1: Allgemeine Anatomie und Bewegungsapparat*. 2010 Sep; (23); 160-190. Elsevier Health Sciences, Germany, ISBN: 9783437594571.
- 17) Chhbara N, Prakash S, Mishra BK. *An Anatomical Study of Glenoid Cavity: Its Importance in Shoulder Prosthesis*. Int J Anat Res 2015; 3(3): 1419-1424.
- 18) Herscovici D, Fiennes AGT, Allgöwer M, Rüedi TP. *The Floating Shoulder: Ipsilateral Clavicle and Scapular Neck Fractures*. J Bone Joint Surg 1992 May; 74-B (3): 362-364.
- 19) Inui H, Sugamoto K, Miyamoto T, Machida A, Hashimoto J, Nobuhara K. *Evaluation of the Three-Dimensional Glenoid Structure Using MRI*. J. Anat. 2001 Sep; 199(Pt 3): 323-328.
- 20) Nagarchi K, Pillai J, Saheb SH, Brekeit K, Alharbi M. *Morphometry of Clavicle*. J. Pharm. Sci. & Res. 2014; 6(2): 112-114.
- 21) Frank RM, Ramirez J, Chalmers PN, McCormick FM, Romeo AA. *Review Article: Scapulothoracic Anatomy and Snapping Scapula Syndrome*. Anatomy Research International, Article ID: 635628, 2013; 2013: 1-9. DOI: 10.1155/2013/635628
- 22) Hurov J. *Scientific clinical Article: Anatomy and Mechanics of the Shoulder; Review of the Current Concepts*. J HAND THER 2009 Oct/Dec; 22(4): 328-343.
- 23) Sizer PS, Phelps V, Gilbert K. *Diagnosis and Management of Painful Shoulder: Part 1; Clinical Anatomy and Pathomechanics*. Pain Practice 2003 Jun; 3(1): 39-57.
- 24) Deepali K, Ashutosh A, Ajay C, Bahetee BH, Ashish B. *Osseous Anatomy of Glenoid: Cadaveric Study*. Int J Anat Res 2016; 4(2): 2473-2497.
- 25) Cutti AG, Veeger HEJ. *Shoulder Biomechanics: Today's Consensus and Tomorrow's Perspectives*. Med Biol Eng Comput 2009 May; 47(5): 463-466.
- 26) Ozaki J, Kawamura I. *"Zero Position" Functional Shoulder Orthosis*. Prosthetics and Orthotics International 1984 Dec; 8: 139-142.

- 27) Scibek JS, Carpenter JE, Hughes RE. *Rotator Cuff Tear Pain and Tear Size and Scapulohumeral Rhythm*. Journal of Athletic Training 2009 Mar/Apr; 44(2): 148-159.
- 28) Jones L. *The Shoulder Joint: Observations on Comparative Anatomy, Physiology and Treatment*. California Medical Association 1956 Mar; 84(3): 185-192.
- 29) Jayesh PN, Muragod AR, Motimath B. *Open Kinematic Chain Exercise for Sick Scapula in Competitive Asymptomatic Overhead Athletes for 3 Weeks*. Int J Physiother Res 2014; 2(4): 608-615.
- 30) Nakata W, Katou S, Fujita A, Nakata M, Lefor A, Sugimoto A. *Biceps Pulley: Normal Anatomy and Associated Lesions at MR Arthrography*. RG 2011 May/June; 31(3): 791-810.
- 31) Marconi GF, Macedo TAA. *Artifacts and Pitfalls in Shoulder Magnetic Resonance Imaging*. Radiol Bras. 2015 Jul/Aug; 48(4): 242-248.
- 32) Yuliana L. *Review Article: Anatomical Aspect of Shoulder Joint Dislocation for Volleyball Players*. Folia Medica Indonesiana 2009 Dec/Oct; 45(4): 308-314.
- 33) Arunkumar KR, Manoranjitham R, Delhi Raji U, Shalini R. *Morphometric Study of Bicipital Groove in South Indian Population and its Clinical Implication*. Int J Anat Res 2016; 4(2): 2187-2191.
- 34) Lebaschi A, Deng XH, Zong J, Cong GT, Carballo CB, Album ZM, Camp C, Rodeo SA. *Animal Model for Rotator Cuff Repair*. Ann. N.Y. Acad. Sci. 2016 Nov; 1383(1): 43-57.
- 35) Ellis H. *Clinical Anatomy: Applied Anatomy for Students and Junior Doctors*. 2006; (11): 168-184. ISBN-13: 978-1-4051-3804-8.
- 36) Krzyzanowski W. *The Use of Ultrasound in Assessment of the Glenoid Labrum of the Glenohumeral Joint: Part I; Ultrasound Anatomy and Examination Techniques*. J Ultrason 2012 Jun; 12(49): 164-177.
- 37) Kanatli U, Ozturk BY, Bolukbasi S. *Anatomical Variations of the Anterosuperior Labrum; Prevalence and Association with Type II Superior Labrum Anterior-Posterior (SLAP) Lesions*. J Shoulder Elbow Surg 2010 Dec; 19(8): 1199-1203.
- 38) Sager M, Herten M, Ruchay S, Assheuer J, Kramer M, Jäger M. *The Anatomy of the Glenoid Labrum: A Comparison between Human and Dog*. Comparative Medicine, by the American Association for Laboratory Animal Science 2009 Oct; 59(5): 465-475.
- 39) Hata Y, Nakatsuchi Y, Saitoh S, Masato HM, Uchiyama S. *Anatomy Study of the Glenoid Labrum*. J Shoulder Elbow Surg 1992 Jul-Aug; 1(4): 207-214.

- 40) Chang D, Mohana-Borges A, Borso M, Chung CB. *Review: SLAP Lesions; Anatomy, Clinical Presentation, MR Imaging Diagnosis and Characterization*. *European Journal of Radiology* 2008 Feb; 68: 72-87.
- 41) Smith CD, Masouros SD, Hill AM, Wallace AL, Amis AA, Bull AM. *Tensile Properties of the Human Glenoid Labrum*. *J. Anat.* 2008 Jan; 212(1): 49-54.
- 42) Hill AM, Hoerning EJ, Brook K, Smith CD, Moss J, Ryder T, Wallace AL, Bull AM. *Collagenous Microstructures of the Glenoid Labrum and Biceps Anchor*. *J. Anat.* 2008; 212: 853-862.
- 43) De Maeseneer M, Von Roy F, Lenchik L, Shahabpour M, Jacobson J, Ryu KN, Handelberg F, Osteaux M. *CT and MRI Arthrography of the Normal and Pathologic Anterosuperior Labrum and Labral-Bicipital Complex*. *Radiographics (RG), Special Issue*, 2000 Oct; 20: Spec. No: 67-S81.
- 44) Donnelly TD, Ashwin S, MacFarlane RJ, Wassem M. *Clinical Assessment of the Shoulder*. *The Open Orthopaedics Journal* 2013; 7(Suppl 3:M3): 310-315.
- 45) Massengill AD, Seeger LL, Yao L, Gentili A, Shnier RC, Shapiro MS, Gold RH. *Labrocapsular Ligamentous Complex of the Shoulder: Normal Anatomy, Anatomic Variations and Pitfalls of MR Imaging and MR Arthrography*. *Radio Graphics* 1994 Nov; 14(6): 1211-1223.
- 46) Dashottar A, Borstad J. *Posterior Glenohumeral Joint Capsule Contracture*. *Shoulder Elbow* 2012 Oct; 4(4): 01-13.
- 47) Ralphs JR, Benjamin M. *Review: The Joint Capsule; Structure, Composition, Ageing and Disease*. *J. Anat.* 1994 Jun; 184(Pt 3): 503-509.
- 48) Lajtai A, Synder SJ, Applegate GR, Aitzetmüller G, Gerber C. *Shoulder Arthroscopy and MRI Techniques: CH07; Arthroscopy Anatomy and Normal Variants*. 2003; (1): 101-116. ISBN:978-3-624-62771-2.
- 49) Wilk KE, Arrigo CA, Andrews JR. *Current Concepts: The Stabilizing Structures of the Glenohumeral Joint*. *Jospt* 1997 Jun; 25(6): 364-379.
- 50) Ogul H, Karaca L, Can CE, Pirimoglu B, Tuncer K, Topal M, Okur A, Kantarci M. *Anatomy, Variants and Pathologies of the Superior Glenohumeral Ligament: Magnetic Resonance Imaging with Three-Dimensional Volumetric Interpolated Breath Hold Examination Sequence and Conventional Magnetic Resonance Arthrography*. *Korean J Radio* 2014; 15(2): 508-522.
- 51) KasK K, Poldoja E, Lont T, Norit R, Merila M, Busch LC, Kolts I. *Anatomy of the Superior Glenohumeral Ligament*. *J Shoulder Elbow Surg* 2010 Sep; 19(6): 908-916.

- 52) DePalma AF. *Surgical Anatomy of the Rotator Cuff and the Natural History of Degenerative Periarthritis*. Clin Orthop Relat Res 2008 Mar; 466(3): 543-551.
- 53) Matthewson G, Beach CJ, Nelson AA, Woodmass JM, Ono Y, Boorman RS, Lo IKY, Thornton GM. *A Review Article: Partial Thickness Rotator Cuff Tears; Current Concepts*. Hindawi publishing Corporation, Advances in Orthopaedics, Volume 2015, Article ID: 458786, 11 Pages.
- 54) Czynny Z. *Diagnostic Anatomy and Diagnostics of Enthesal Pathologies of the Rotator Cuff*. Journal of Ultrasonography 2012 Jun; 12(49): 178-187.
- 55) Edwards P, Ebert J, Joss B, Bhabra G, Ackland T, Wang A. *Clinical Commentary: Exercise Rehabilitation in the Non-Operative Management of Rotator Cuff Tears; A Review of Literature*. The International Journal of Sports Physical Therapy. 2016 April; 11(2): 279-301.
- 56) Smith MA, Smith WT. *Rotator Cuff Tears: An Overview*. Orthopaedic Nursing 2010 Sep/Oct; 29(5): 319-322.
- 57) McCullagh PJJ. *Biomechanics and Design of Shoulder*. Proc Instn Mech Engrs 1995; 209: 207-213.

17.2. References – (“Shoulder Stability”)

- 1) Wilk KE, Reinold MM, Andrews JR. *The Athletes Shoulder: CH02; Clinical Biomechanics of the Shoulder Complex*, by Kelley MJ, Eckenrode BJ. 2009; (2): 17-41. ISBN: 978-0-443-06701-3.
- 2) Hayes K, Callanan M, Walton J, Paxinos, Murrell GAC. *Shoulder Instability: Management and Rehabilitation*. J Orthop Sports Phys Ther 2002 Oct; 3(10): 497-509.
- 3) Lam F, Bhatia DN, Mostofi SB, Van Rooyen K, DE Beer JF. *Biomechanical Considerations of the Normal and Rotator Cuff Deficient Shoulders and the Reverse Shoulder Prosthesis*. Current Orthopaedics 2007 Feb; 21(1): 40–46.
- 4) Lugo R, Kung P, Ma CB. *Shoulder Biomechanics*. European Journal of Radiology 2008 Oct; 68(1): 16-24.
- 5) Frankle M, Marberry S, Pupello D, Hermann S. *Reverse Shoulder Arthroplasty: Biomechanics, Clinical Techniques and Current Technologies*, by Hermann S. Springer International Publishing. 2016; (1): 21-30. ISBN:978-3-319-20839-8.

- 6) Zheng M, Zou Z, Bartolo PD, Peach C, Ren L. *Finite Element Models of the Human Shoulder Complex: A Review of their Clinical Implications and Modelling Techniques*. Int. J. Numer. Meth. Biomed. Engng. (2017); e02777: 2-24.
- 7) Kjær M, Krogsgaard MR, Magnusson P, Engebretsen L, Roos H, Timo T, L-Y Woo S. *Textbook of Sports Medicine Basic Science and Clinical Aspects of Sports Injury and Physical Activity: CH06.6: Shoulder*, by Debski RE, Norlin R, Rydqvist L. Blackwell Publishing company 2003; (1): 684-738. ISBN:0-632-06509-05.
- 8) Terry GC, Chopp TM. *Functional Anatomy of Shoulder*. Journal of Athletic Training 2000Jul/Sep; 35(3): 248-255.
- 9) Omoumi P, Teixeira P, Lecouvet F, Chung CB. *Review: Glenohumeral Joint Instability*. JOURNAL OF MAGNETIC RESONANCE IMAGING 2011 Jan; 33(1): 2-16.
- 10) Hadler AM, Itoi E, An KN. *Anatomy and Biomechanics of the Shoulder*. 2000 April; 31(2): 159-176.
- 11) Wilson F, Gormley J, Hussey J. *Exercise Therapy in the Management of Musculoskeletal Disorders: Part 07; The Shoulder Complex*, by Viser AS, Reinold MM, Rodenhi KJ, Gill TJ. Blackwell Publishing Ltd. 2011; (1): 94-112. ISBN: 978-1-4051-6938-7.
- 12) Hurov J. *Anatomy and Mechanics of the Shoulder: Review of Current Concepts*. J HAND THER. 2009 Oct/Dec; 22: 328–43.
- 13) Dreborowicz M, Dreborowicz E, Walecka J. *Anatomy of Scapula and Shoulder Girdle: Review of the current Literature*. Issue Rehabil. Orthop. Neurophysiol. Sport Promot. 2016; 16: 61-70.
- 14) Ombregt L. *A system of Orthopaedic Medicine: Section 3; Applied Anatomy of Shoulder, and Section 4; Applied Anatomy of Shoulder Girdle*. 2013 Mar; (3): 205-274.

17.3. References – (“Shoulder Pain Disorders”)

- 1) Firestein GS, Budd RC, Gabriel SE, Mcinnes IB, O’dell JR. *Kelley’s Textbook of Rheumatology: Part 06; Differential Diagnosis of Regional and Diffuse Musculoskeletal Pain; CH46; Shoulder Pain*, by Martin SD, Thornhill TS. 2012 Aug; (9): 639-664. ISBN: 9781437717389.
- 2) Burbank KM, Czarnecki GR, Stevenson JH, Dorfman J. *Chronic Shoulder Pain: Part I; Evaluation and Diagnosis*. Am Fam Physician 2008 Feb; 77(4): 453-460.
- 3) Linaker CH, Walker-Bone K. *Shoulder Disorders and Occupation*. Best Pract Res Clin Rheumatol. 2015 June; 29(3): 405–423.

- 4) Kumar V, White AD, Venkateswaran B. *Case Report: Atraumatic Osteonecrosis of the Humeral Head Associated with Pregnancy*. *Shoulder & Elbow* 2010; 2: 188-190.
- 5) McClure PW, Michener LA. *Staged Approach for Rehabilitation Classification: Shoulder Disorders (STAR-Shoulder)*. *American Physical Therapy Association* 2015 May; 95(5): 791-800.
- 6) Van der Windt DAWM, Kose BW, De Jong BA, Bouter LM. *Shoulder Disorders in General Practice: Incidence, Patient Characteristics and Management*. *Annals of the Rheumatic Diseases* 1995 Dec; 54(12): 959-964.
- 7) Haviv B. *Rotator Cuff Tears, Evaluation and Treatment: A Critical Review*. *OA Sports Medicine* 2013 Oct; 1(2): 20.
- 8) Herrmann SJ, Izadpanah K, Südkamp NP, Strohm PC. *Tears of the Rotator Cuff: Causes, Diagnosis and Treatment*. *ACTA CHIRURGIAE ORTHOPAEDICAE ET TRAUMATOLOGIAE ČECHOSL* 2014; 81: 256–266.
- 9) Pandey V, Willems WJ. *Rotator Cuff Tear: A Detailed Update*. *Asia-Pacific Journal of Sports Medicine, Arthroscopy, Rehabilitation and Technology* 2015 Jan; 2(1): 1-14.
- 10) Ellman H. *Diagnosis and Treatment of Incomplete Rotator Cuff Tears*. *Clin Orthop Relat Res* 1990 May; (254): 64–74.
- 11) Schoch BS, Barlow JD, Schleck C, Cofield RH, Sperling JW. *Shoulder Arthroplasty for Atraumatic Osteonecrosis of the Humeral Head*. *J Shoulder Elbow Surg* 2016 Feb; 25(2): 238-245.
- 12) El Shewy MT. *Calcific Tendinitis of Rotator Cuff*. *World J Orthop* 2016 Jan; 7(1): 55-60.
- 13) Gückel C, Nidecker A. *Diagnosis of Tears in Rotator-Cuff Injuries*. *European Journal of Radiology* 1997 Jan; 25: 168-176.
- 14) Hattrup SJ, Cofield RH, Scottsdale A, Rochester M. *Osteonecrosis of Humeral Head: Results of Replacement*. *J Shoulder Elbow Surg* 2000; 9: 177-182.
- 15) Hasan SS, Romeo AA. *Review Article: Nontraumatic Osteonecrosis of Humeral Head*. *J Shoulder Elbow Surg* 2002 May/Jun; 11(3): 281-298.
- 16) Byun JW, Shim JH, Shin WJ, Cho SY. *Case Report: Rapid Progressive Atypical Atraumatic Osteonecrosis of Humeral Head*. *Korean J Anesthesiol* 2014 May; 66(5): 398-401.
- 17) Gruson KI, Kwon YW. *Atraumatic Osteonecrosis of Humeral Head*. *Bulletin of the NYU Hospital for Joint Diseases* 2009; 67(1): 6-14.
- 18) Bennett WF, Gerber C. *Operative Treatment of Rheumatoid Shoulder*. *Current Opinion in Rheumatology* 1994 Mar; 6(2): 177-182.

- 19) Holcomb JO, Hebert DJ, Mighell MA, Dunning PE, Derek R. Pupello DR, Pliner MD, Frankle MA. *Reverse Shoulder Arthroplasty in Patients with Rheumatoid Arthritis*. J Shoulder Elbow Surg 2010 Oct; 19(7): 1076-1084.
- 20) Wasserman AM. *Diagnosis and Management of Rheumatoid Arthritis*. Am Fam Physician. 2011 Dec; 84(11): 1245-1252.
- 21) Barlow JD, Yuan BJ, Schleck CD, Harmsen WS, Cofield RH, Sperling JW. *Shoulder Arthroplasty for Rheumatoid Arthritis: 303 Consecutive Cases with Minimum 5-Year Follow-up*. J Shoulder Elbow Surg 2014 Jun; 23(6): 791-799.
- 22) Chillemi C, Franceschini V. *Review Article: Shoulder Arthroplasty*. Hindawi Publishing Corporation, Arthritis, 2013, Article ID: 370231, 7 pages.
- 23) Yucesoy B, Charles LE, Baker B, Burchfiel CM. *Occupational and Genetic Risk Factors for Osteoarthritis: A Review*. Work. 2015 Jan; 50(2): 261–273.
- 24) Merolla G, Singh S, Paladini P, Porcellini G. *Calcific Tendinitis of the Rotator Cuff: State of the Art in Diagnosis and Treatment*. J Orthopaed Traumatol 2016 Mar; 17(1): 7–14.
- 25) Millett PJ, Gobezie R, Boykin RE. *Shoulder Osteoarthritis: Diagnosis and Management*. Am Fam Physician. 2008 Sep; 78(5): 605-611.
- 26) Kachewear SG, Kulkarni DS. *Calcific Tendinitis of the Rotator Cuff*. Journal of Clinical and Diagnostic Research. 2013 Jul; 7(7): 1482-1485.
- 27) George MS. *Arthroscopic Management of Shoulder Osteoarthritis*. The Open Orthopaedics Journal 2008 Feb; 2(1): 23-26.
- 28) Thomas M, Bidwai A, Rangan A, Rees JL, Brownson P, Tennent D, Connor C, Kulkarni R. *BESS/BOA Patient Care Pathways: Glenohumeral Osteoarthritis*. Shoulder & Elbow 2016 Jul; 8(3): 203–214.

17.4. References – (“Total Shoulder Arthroplasty”)

- 1) Trebše R, Mihelič A. *Infected Total Joint Arthroplasty: The Algorithmic Approach; CH02; Joint Replacement; Historical View*. 2012; (1): 7-11. ISBN: 978-1-4471-6230-8, Springer-Verlag London.
- 2) Flatow EL, Harrison AK. *A History of Reverse Total Shoulder Arthroplasty*. Clin Orthop Relat Res 2011 Sep; 469(9): 2432-2439.
- 3) Hatzidakis AM, Norris TR, Boileau B. *Reverse Shoulder Arthroplasty: Indications, Techniques and Results*. Techniques in Shoulder and Elbow Surgery 2005; 6(3): 135-149.

- 4) Bohsali KI, Bois AJ, Wirth MA. *Current Concepts Review: Complications of Shoulder Arthroplasty*. J Bone Joint Surg Am. 2017 Feb; 99-A (3): 256-269.
- 5) Boileau P, Sinnerton RJ, Chuinard C, Walch G. *Review Article: Arthroplasty of Shoulder*. J Bone Joint Surg (Br) 2006 May; 88-B (5): 562-575.
- 6) Katz D, O'Toole G, Cogswell L, Sauzieres P, Valenti P. *Review Article: A History of the Reverse Shoulder Prosthesis*. Int J Shoulder Surg IJSS 2007 Oct; 1(4): 108-113.
- 7) Ha AS, Petscavage JM, Chew FS. *Current Concepts of Shoulder Arthroplasty for Radiologists: Part 2; Anatomic and Reverse Total Shoulder Replacement and Nonprosthetic Resurfacing*. AJR 2012 Oct; 199(4): 768-776.
- 8) Petscavage JM, Ha AS, Chew FS. *Current Concepts of Shoulder Arthroplasty for Radiologists: Part 1; Epidemiology, History, Preoperative Imaging and Hemiarthroplasty*. AJR 2012 Oct; 199(4): 757-767.
- 9) Sanchez-Sotelo J. *Total Shoulder Arthroplasty*. The Open Orthopaedics Journal 2011 Mar; 5: 106-114.
- 10) Buck FM, Jost B, Hodler J. *Shoulder Arthroplasty*. Eur Radiol 2008 Dec; 18(12): 2937-2948.
- 11) Petriccioli D, Bertone C, Marchi G. *Stemless Shoulder Arthroplasty: A Literature Review*. JOINTS 2015 Jan; 3(1): 38-41.
- 12) Bohsali KI, Wirth MA, Rockwood CA. *Complication of Total Shoulder Arthroplasty*. JBJS 2006 Oct; 88-A (10): 2279-2292.
- 13) Hawi N, Tauber M, Messina MJ, Habermeyer P, Martetschläger F. *Anatomic Stemless Shoulder Arthroplasty and Related Outcomes: A Systematic Review*. BMC Musculoskeletal Disorders 2016 Dec; 17(376): 1-10.
- 14) Warren RF, Coleman SH, Dines JS. *Instability after Arthroplasty: The Shoulder*. The Journal of Arthroplasty 2002 Jun; 17(4) (Suppl-1): 28-32.
- 15) Matsen III FA, Clinton J, Lynch J, Bertelsen A, Richardson ML. *Current Concepts Review: Glenoid Component Failure in Total Shoulder Arthroplasty*. J Bone Joint Surg Am. 2008 Apr; 90-A (4): 885-896.
- 16) Mahmood A, Malal JJG, Waseem M. *Reverse Shoulder Arthroplasty: A Literature Review*. The Open Orthopaedics Journal 2013 Sep; 7(Suppl 3: M13): 366-372.
- 17) Moorman III CT, Warren RF, Dines DM, Moeckel BH, Altchek DW. *Total Shoulder Arthroplasty: Revision for Instability*. Operative Techniques in Orthopaedics 1994 Oct; 4(4): 237-242.

- 18) Petersen SA, Hawkins RA. *Revision of Failed Total Shoulder Arthroplasty*. Orthopaedic Clinics of North America 1998 Jul; 29(3): 519-533.
- 19) Karduna AR, Williams GR, Williams JL, Iannotti JP. *Joint Stability After Total Shoulder Arthroplasty in a Cadaver Model*. J SHOULDER ELBOW SURG 1997 Nov/Dec; 6(6): 506-511.
- 20) Endres NK, Warner JJP. *Anterior Instability after Total Shoulder Replacement: Salvage with Modified Latarjet Procedure; A Report of 2 Cases*. J Shoulder Elbow Surg 2010; 19: e1-e5.
- 21) Eichinger JK, Galvin JW. *Management of Complications After Total Shoulder Arthroplasty*. Curr Rev Musculoskelet Med 2015 Mar; 8(1): 83–91.
- 22) Ackland DC, Patel M, Knox D. *Prosthesis Design and Placement in Reverse Total Shoulder Arthroplasty*. Journal of Orthopaedic Surgery and Research 2015 Jul; 10: 101-110.
- 23) Wirth MA, Rockwood CA. *Current Concepts Review - Complications of Total Shoulder-Replacement Arthroplasty*. The Journal of Bone and Joint Surgery 1996 Apr; 78-A (4): 603-616.
- 24) McCullagh PJJ. *Biomechanics and Design of Shoulder*. Proc Instn Mech Engrs 1995; 209: 207-213.
- 25) Windall JC, Dheerendra SK, MacFarlane RJ, Waseem M. *The Use of Shoulder Hemiarthroplasty and Humeral Head Resurfacing: A Review of Current Concepts*. The Open Orthopaedics Journal 2013 Sep; 7(Suppl 3: M7): 334-337.
- 26) Foruria AM, Antuña Sand Rodríguez-Merchán EC. *Shoulder Hemiarthroplasty: Review of Basic Concepts*. Rev. esp. cir. ortop. traumatol. 2008; 52: 392-402.
- 27) Lin DJ, Wong TT, Kazam JK. *Shoulder Arthroplasty from Indications to Complications: What the Radiologist Needs to Know*. Radiographics 2016 Jan/Feb; 36(1): 192-208.
- 28) Castagna A, Randelli M, Garofalo R, Maradei L, Giardella A, Borroni M. *Mid-Term Results of a Metal-Backed Glenoid Component in Total Shoulder Replacement*. J Bone Joint Surg [Br]2010 Oct; 92-B (10): 1410-15.

17.5. References – (“Biomechanical Study”)

- 1) Chevalier Y, Santos I, Mueller PE, Pietschmann MF. *The Effects of Bone Quality, Implant Fixation Design, Glenohumeral Conformity and Eccentric Instability on*

Periprosthetic Cement and Bone Tissue Stresses: A Micro Finite Element Analysis.
Submitted to J Biomech 2015a.

- 2) Anglin, C., Wyss, UP., Pichora, DR. *Mechanical Testing of Shoulder Prostheses and Recommendations for Glenoid Design.* J Shoulder Elbow Surg 2000 Jul/Aug; 9(4): 323–331.
- 3) Gunther SB, Lynch TL, O'Farrell D, Calyore C, Rodenhouse A. *Finite Element Analysis and Physiologic Testing of a Novel, Inset Glenoid Fixation Technique.* J Shoulder Elbow Surg. 2012 Jun; 21(6): 795-803. DOI: 10.1016/j.jse.2011.08.073.
- 4) Chevalier Y, Knoblauch M, Mueller PE, Pietschmann MF. *A New Testing Set-up for Assessment of Loosening at the Glenoid Component in Total Shoulder Replacements.* Submitted to J Applied Biomech 2015b.
- 5) Buck FM, Jost B, Hodler J. *Shoulder Arthroplasty.* Eur Radiol 2008 Dec; 18(12): 2937-2948.
- 6) Nagela J, Valstar ER, Stokdijk M, Rozing PM. *Patterns of Loosening of the Glenoid Component.* J Bone Joint Surg [Br] 2002 Jan ;84-B (1): 83-7.
- 7) Castagna A, Randelli M, Garofalo R, Maradei L, Giardella A, Borroni M. *Mid-Term Results of a Metal-Backed Glenoid Component in Total Shoulder Replacement.* J Bone Joint Surg [Br]2010 Oct;9 2-B (10): 1410-15.
- 8) Gregory T, Hansen U, Taillieu F, Baring T, Brassart N, Mutchler C, Amis A, Augereau B, Emery R. *Glenoid Loosening after Total Shoulder Arthroplasty: An In Vitro CT-Scan Study.* J Orthop Res 2009 Dec; 27(12): 1589–1595, DOI: 10.1002/jor.20912.
- 9) Matsen III FA, Clinton J, Lynch J, Bertelsen A, Richardson ML. *Current Concepts Review: Glenoid Component Failure in Total Shoulder Arthroplasty.* J Bone Joint Surg Am. 2008 Apr; 90-A (4): 885-896.
- 10) Hallab NJ, PhD, Jacobs JJ., MD. *Biologic Effects of Implant Debris.* Bul NYU Hosp Joint Dis. 2009; 67(2): 182-188.
- 11) Ren PG, Irani A, Huang Z, Ma T, Biswal S, Goodman SB. *Continuous Infusion of UNMWPE Particles Induces Increased Bone Macrophages and Osteolysis.* Clin Orthop Relat Res 2011 Jan; 469: 113-122.
- 12) Strauss EJ, Roche C, Flurin PH, Wright T, Zuckerman JD. *The Glenoid in Shoulder Arthroplasty.* J Shoulder Elbow Surg 2009 Sep/Oct; 18(5): 819-833.
- 13) Bohsali KI, Bois AJ, Wirth MA. *Current Concepts Review: Complications of Shoulder Arthroplasty.* J Bone Joint Surg Am. 2017 Feb; 99-A (3): 256-269.

- 14) Ha AS, Petscavage JM, Chew FS. *Current Concepts of Shoulder Arthroplasty for Radiologists: Part 2 Anatomic and Reverse Total Shoulder Replacement and Nonprosthetic Resurfacing*. AJR 2012 Oct; 199(4): 768-776.
- 15) Sanchez-Sotelo J. *Total Shoulder Arthroplasty*. The Open Orthopaedics Journal 2011 Mar; 5: 106-114.
- 16) Ellman H. *Diagnosis and Treatment of Incomplete Rotator Cuff Tears*. Clin Orthop Relat Res 1990 May; (254): 64–74.
- 17) McCullagh PJJ. *Biomechanics and Design of Shoulder*. Proc Instn Mech Engrs 1995; 209: 207-213.
- 18) Lin DJ, Wong TT, Kazam JK. *Shoulder Arthroplasty from Indications to Complications: What the Radiologist Needs to Know*. Radiographics 2016 Jan/Feb; 36(1): 192-208.
- 19) Wallace AL, Walsh WR, Sonnabend DH. *Dissociation of The Glenoid Component in Cementless Total Shoulder Arthroplasty*. J Shoulder Elbow Surg 1999 Jan/Feb; 8(1): 81-84.
- 20) Raphael BS, Dines JS, Warren RF, Figgie M, Craig EV. *Symptomatic Glenoid Loosening Complicating Total Shoulder Arthroplasty*. HSSJ 2010 Feb; 6(1): 52-56.
- 21) Namdari S, Gel DP, Wrner JJ. *Managing Glenoid Bone Loss in Revision Total Shoulder Arthroplasty: A Review*. UPOJ 2010; 20:44-49.
- 22) Flurin PH, Janout M, Roche CP, Wright TW, Zuckermann. *Revision of the Loose Glenoid Component in Anatomic Total Shoulder Arthroplasty*. Bulletin of the Hospital for Joint Diseases 2013; 71(Suppl 2): S68-76.
- 23) Eichinger JK, Galvin JW. *Management of Complications After Total Shoulder Arthroplasty*. Curr Rev Musculoskelet Med. 2015 Mar; 8(1): 83–91.

Eidesstattliche Versicherung

MAHMOUD, Mohamed Magdi Bayoumi

Name, Vorname

Ich erkläre hiermit an Eides statt,
dass ich die vorliegende Dissertation mit dem Thema

Biomechanical Evaluation of Glenoid Component Stability After ATSA Under Phasic Cyclic Loading

selbständig verfasst, mich außer der angegebenen keiner weiteren Hilfsmittel bedient und alle Erkenntnisse, die aus dem Schrifttum ganz oder annähernd übernommen sind, als solche kenntlich gemacht und nach ihrer Herkunft unter Bezeichnung der Fundstelle einzeln nachgewiesen habe.

Ich erkläre des Weiteren, dass die hier vorgelegte Dissertation nicht in gleicher oder in ähnlicher Form bei einer anderen Stelle zur Erlangung eines akademischen Grades eingereicht wurde.

München, den 20.12.2018

Ort, Datum

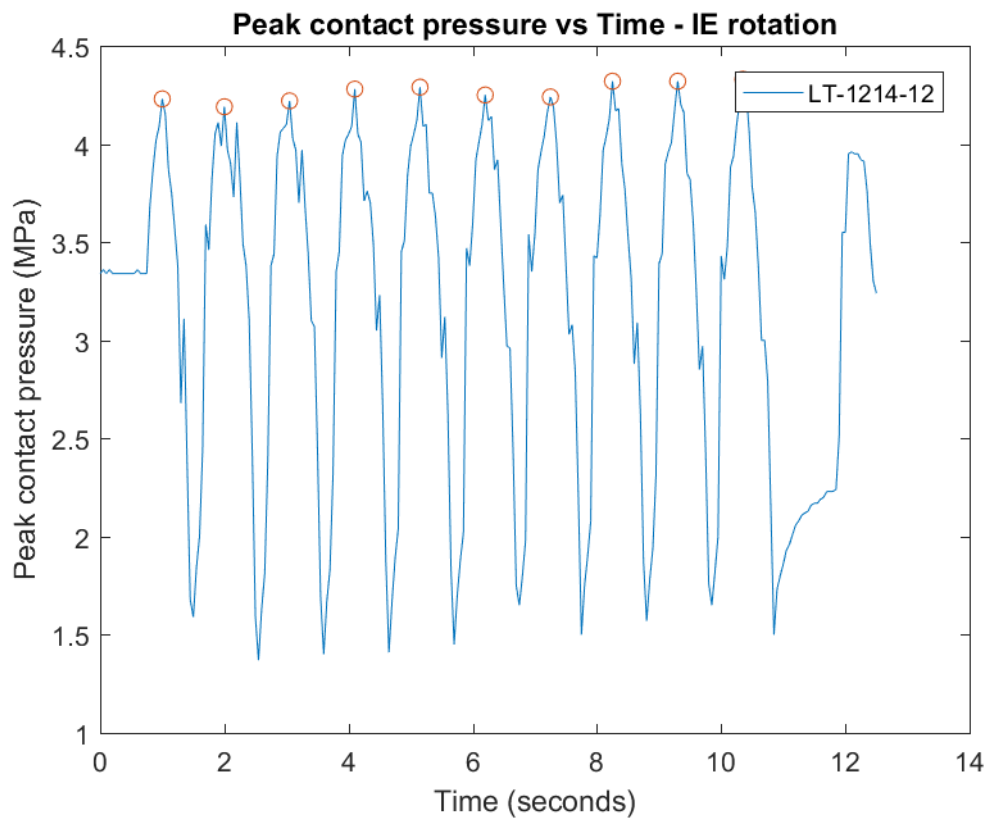
Mohamed Mahmoud

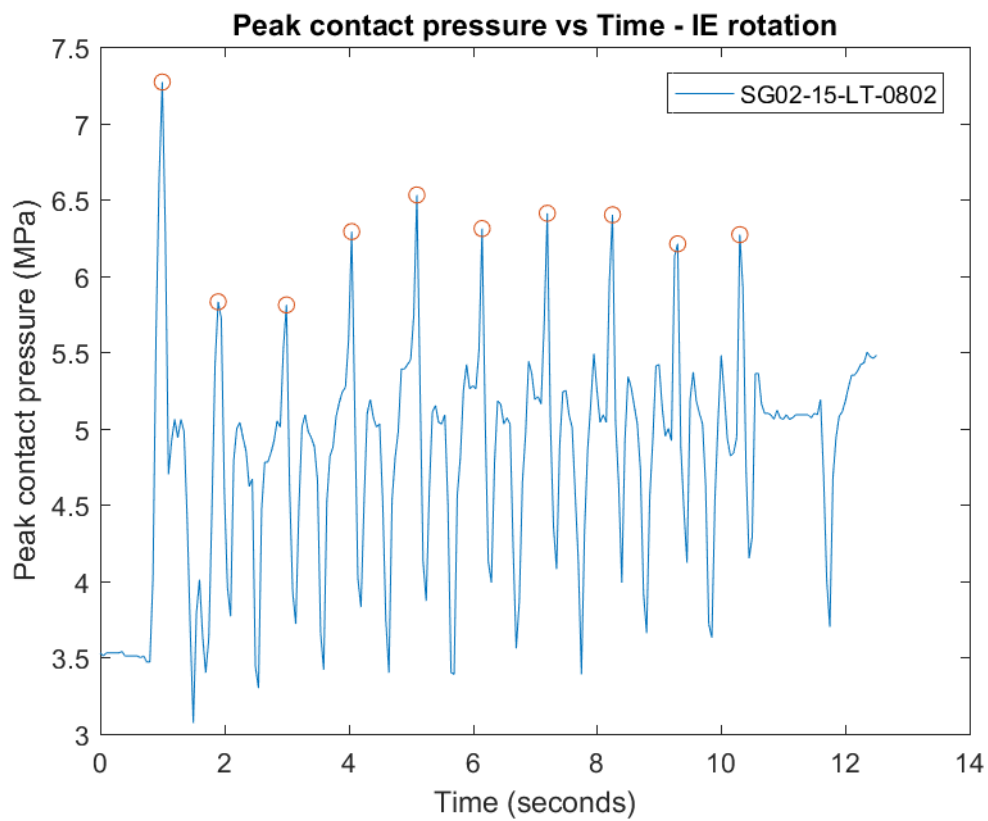
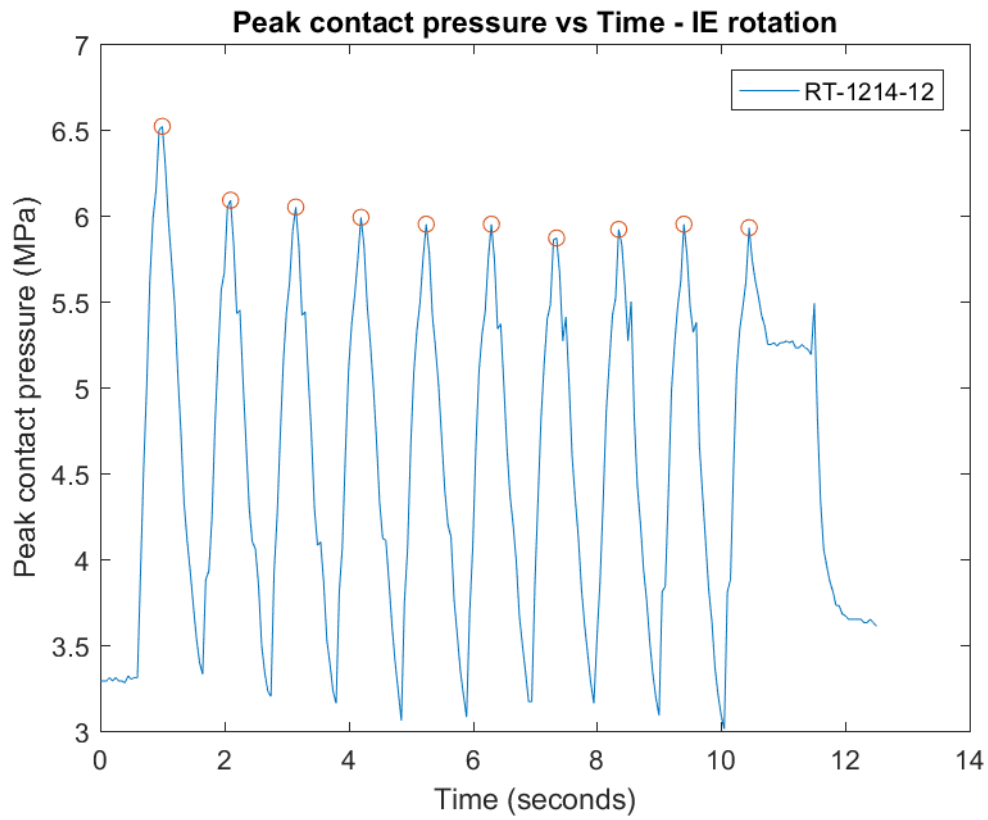
Unterschrift Doktorand

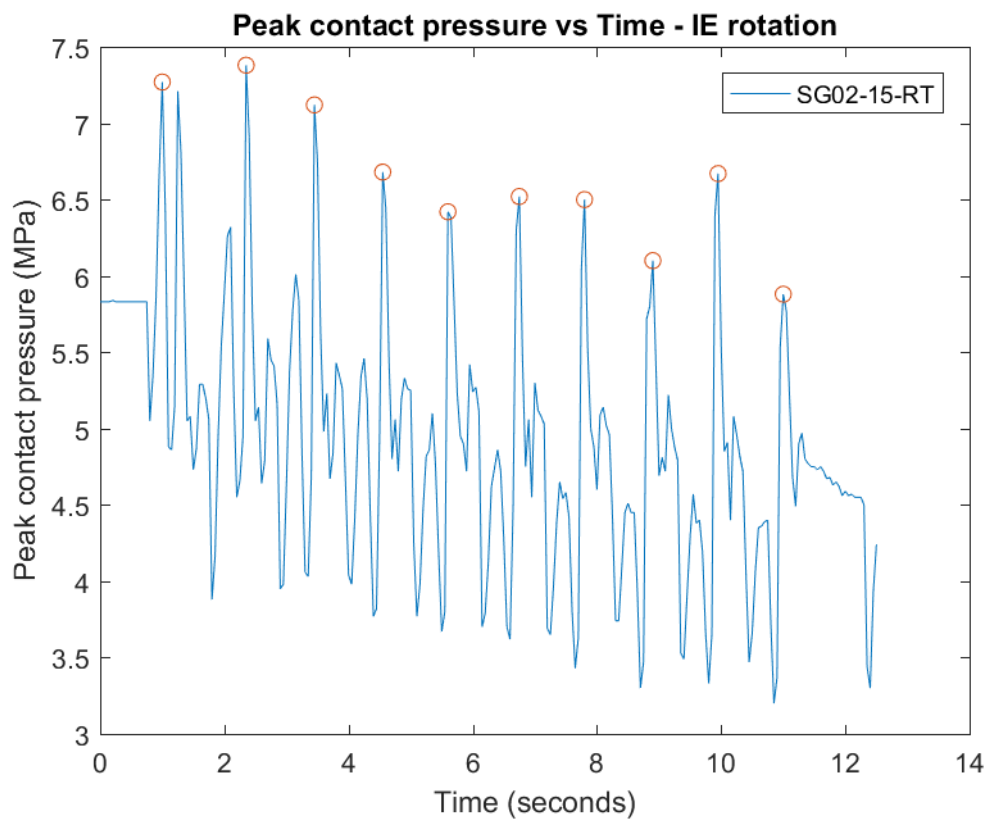
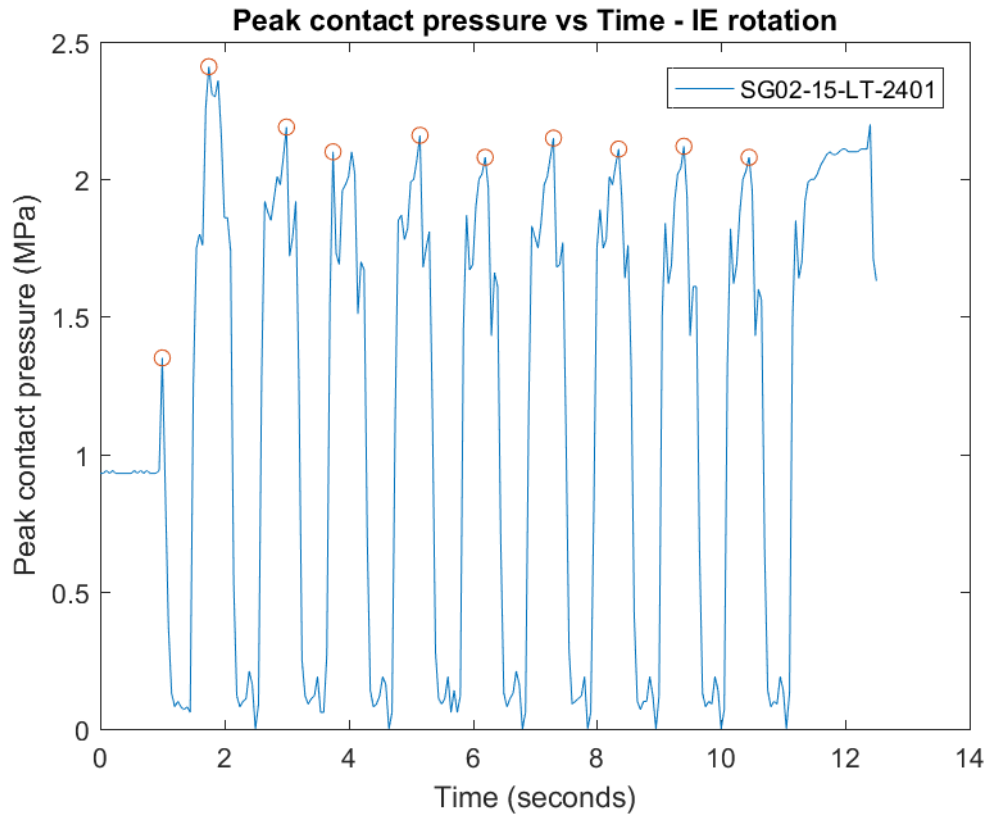
Appendix J:

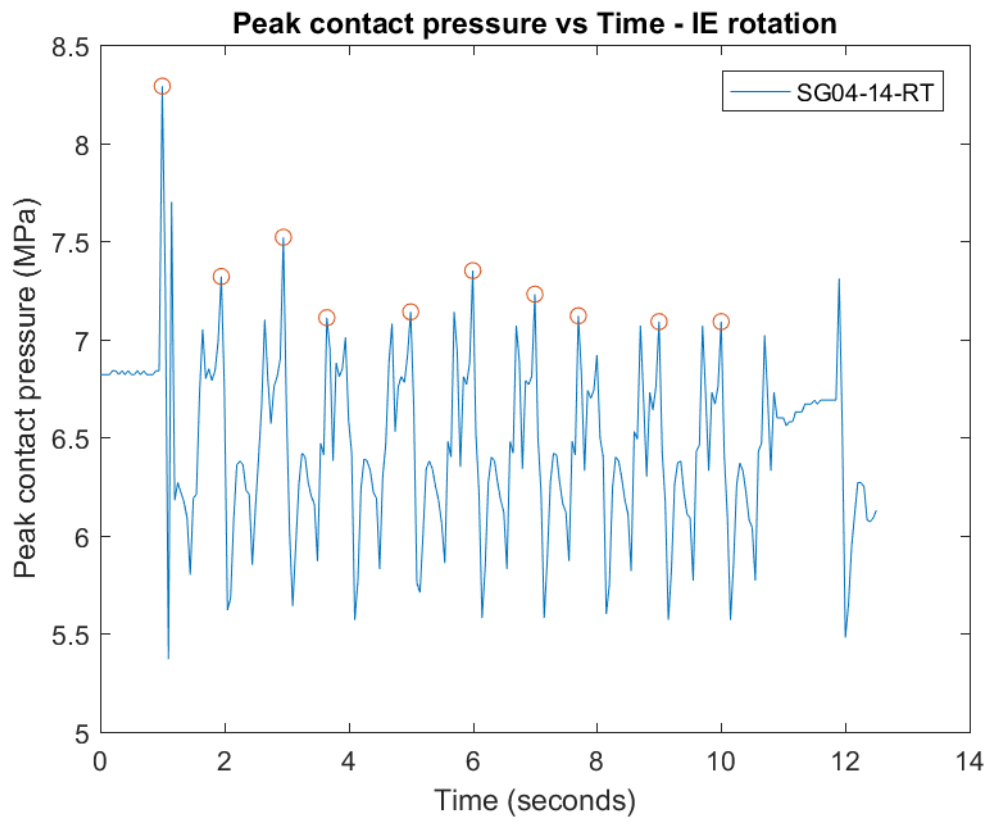
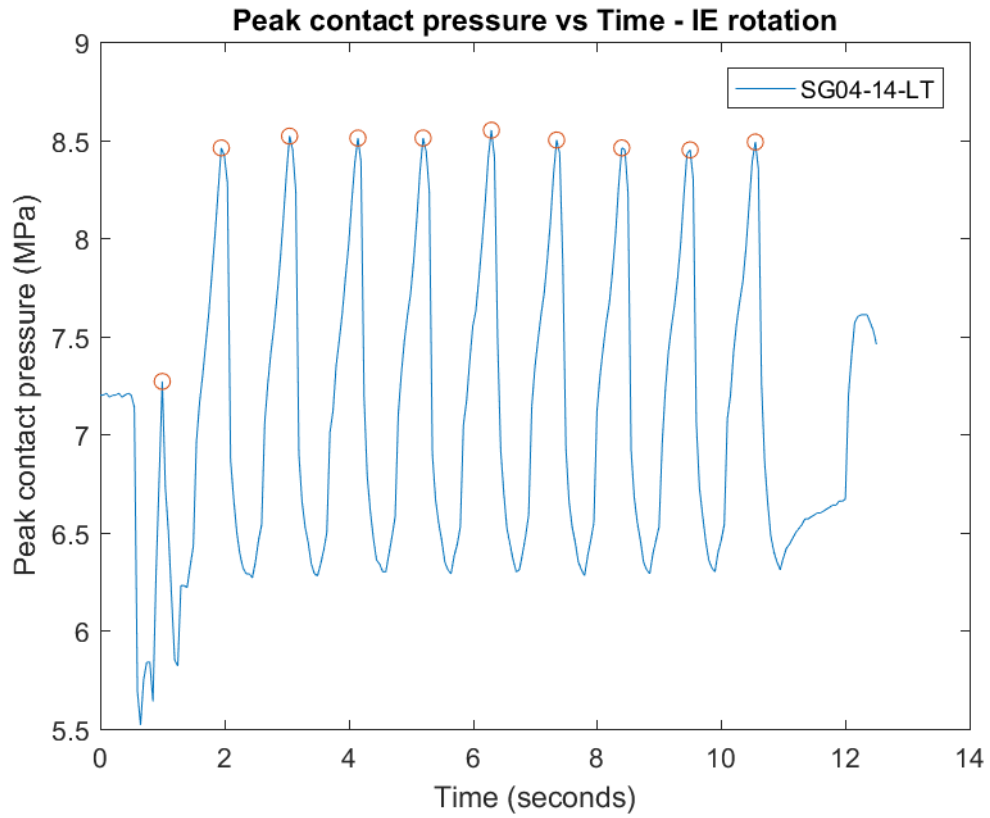
TekScan Graphs

i. Internal - External Rotation: Phase 1

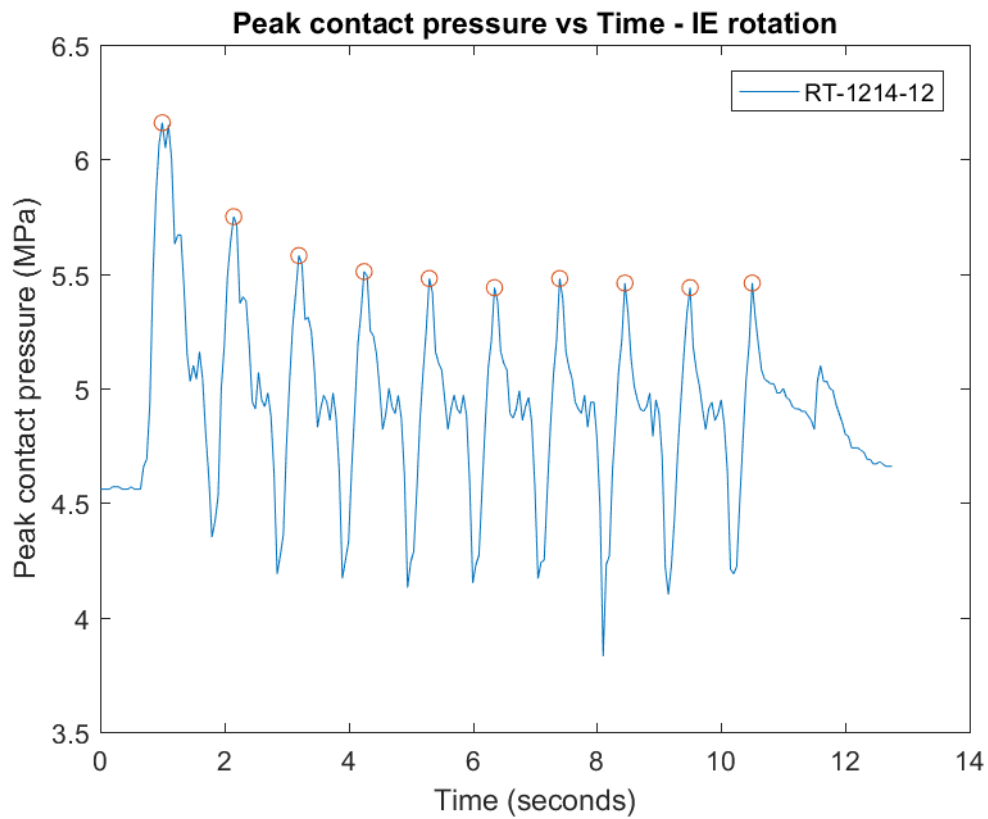
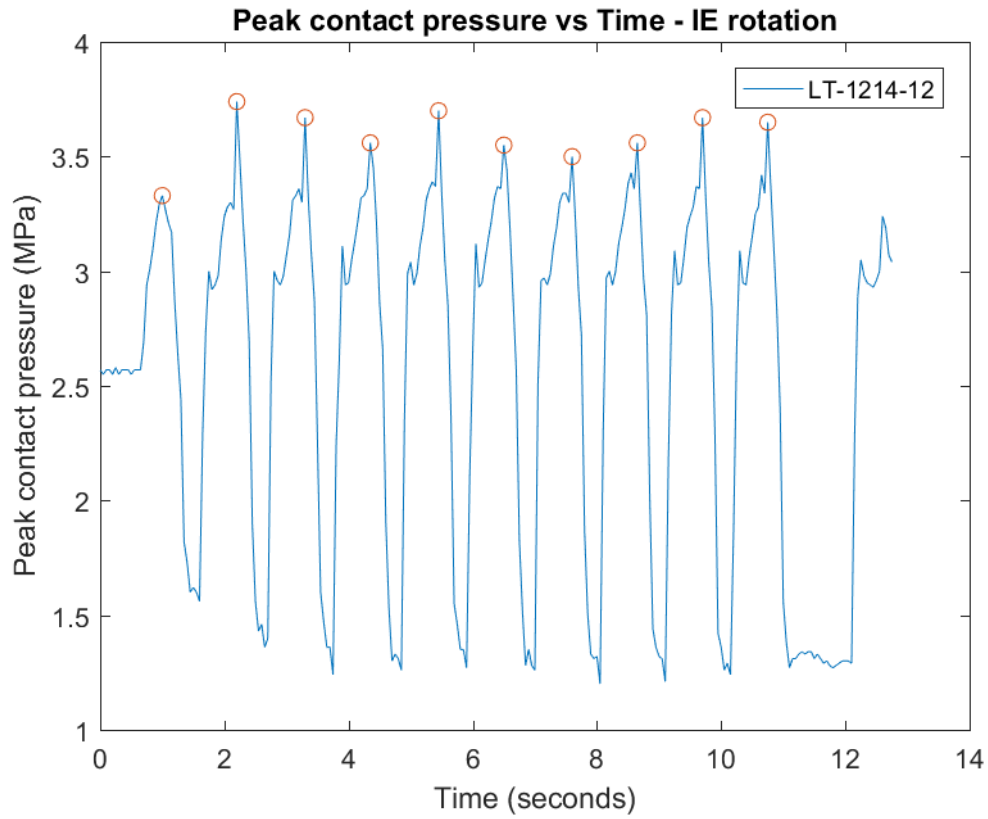


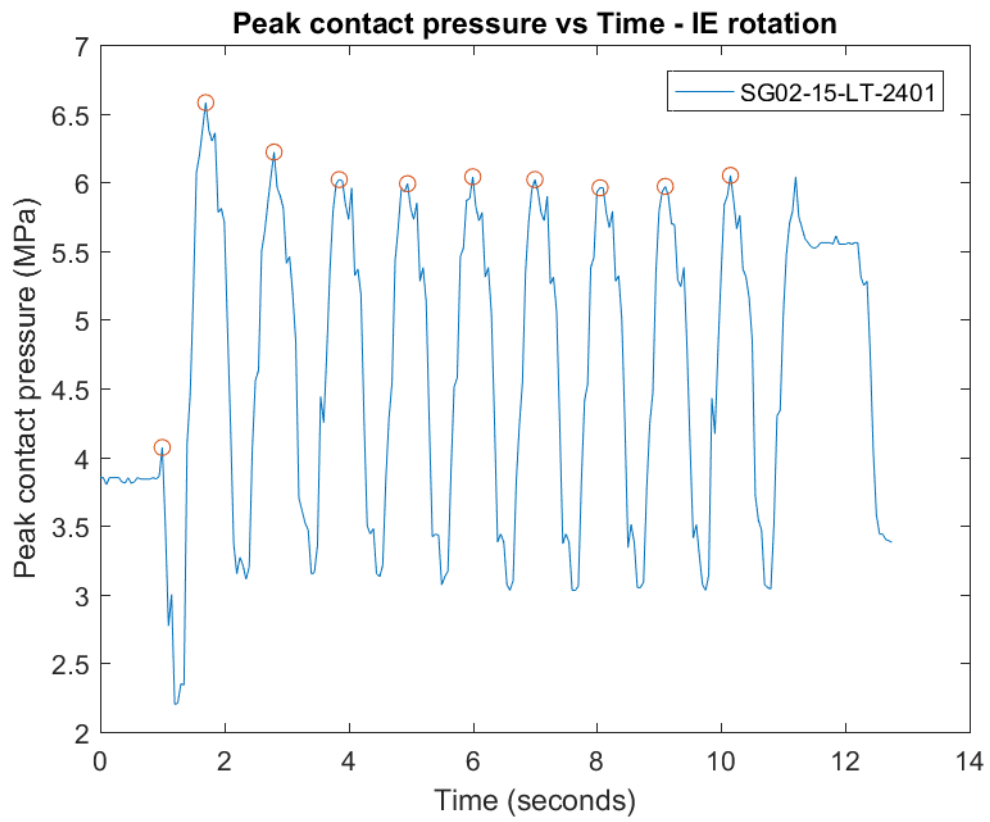
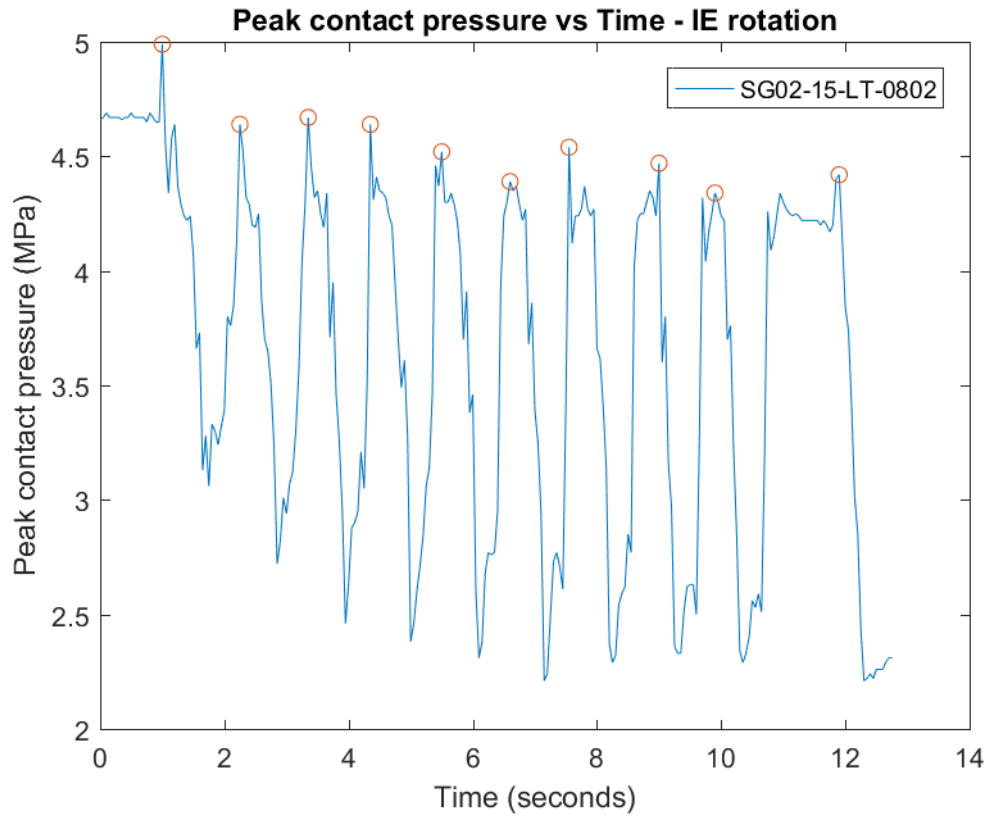


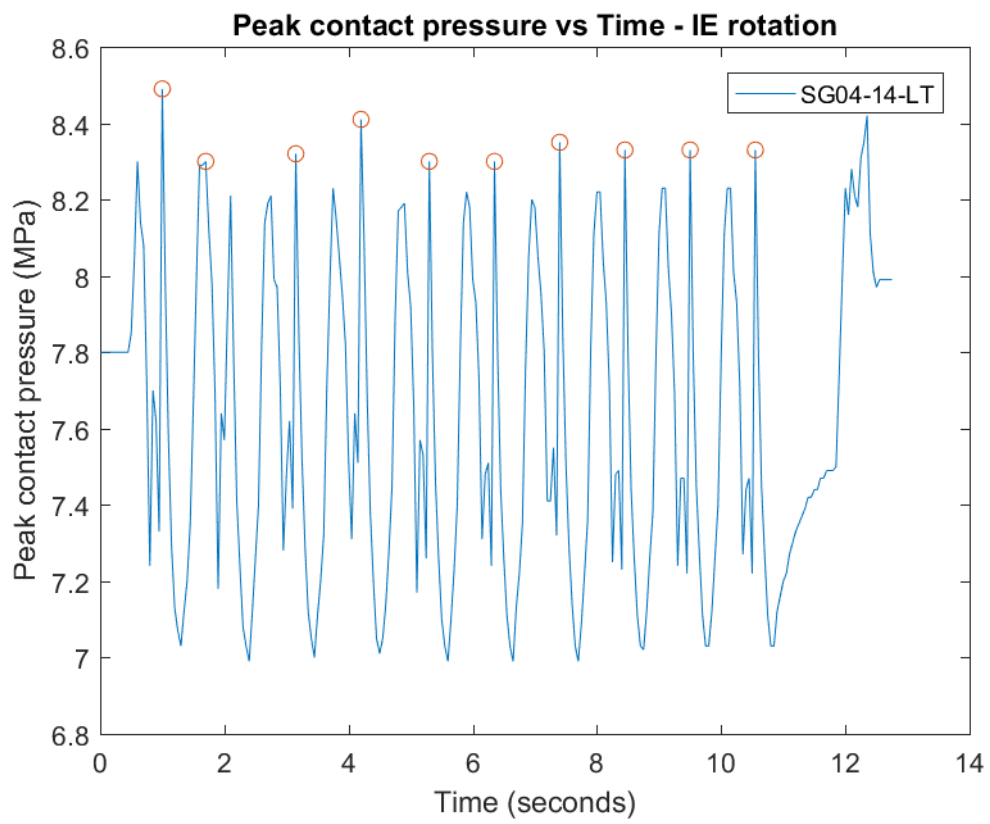
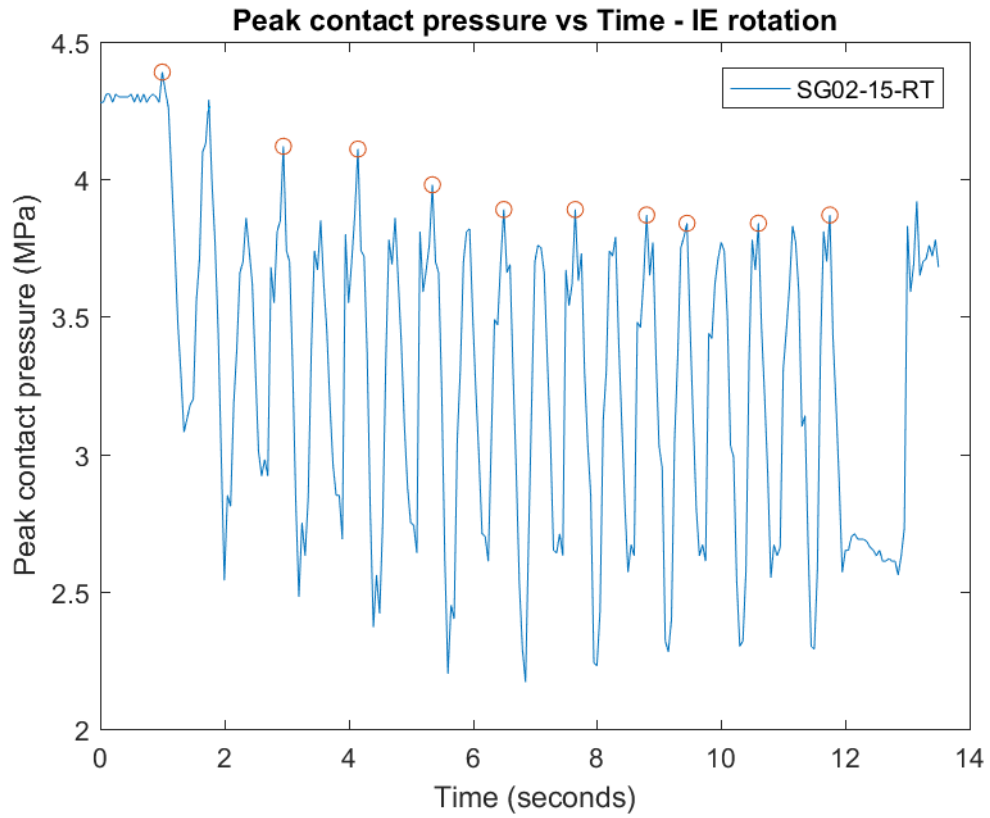


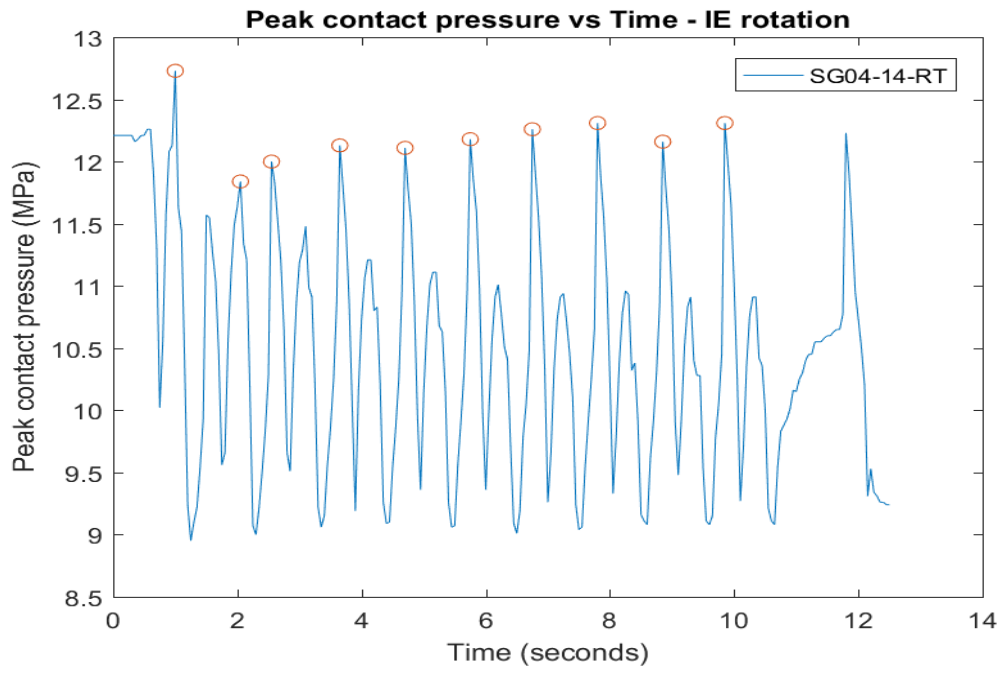


ii. Internal - External Rotation: Phase 3

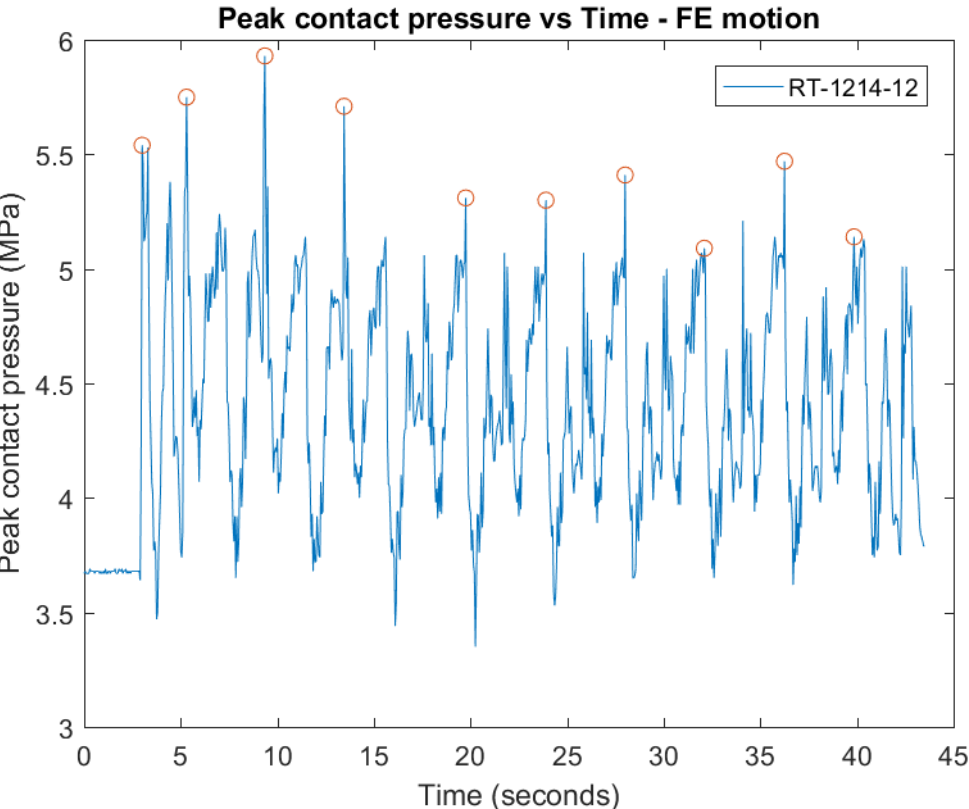
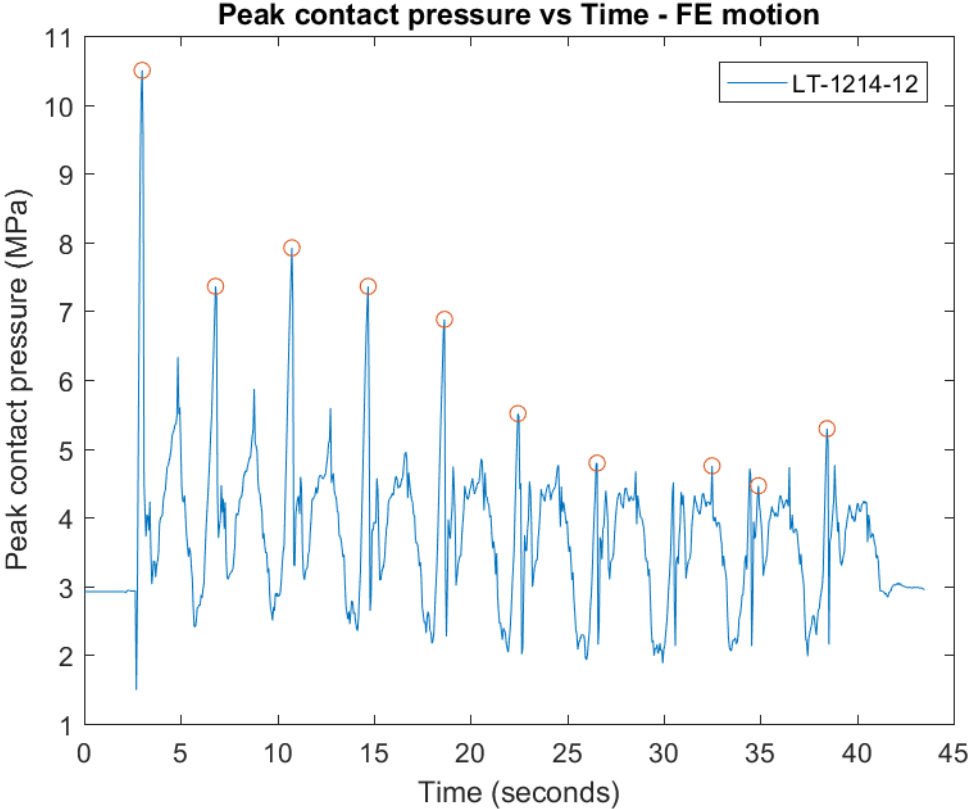


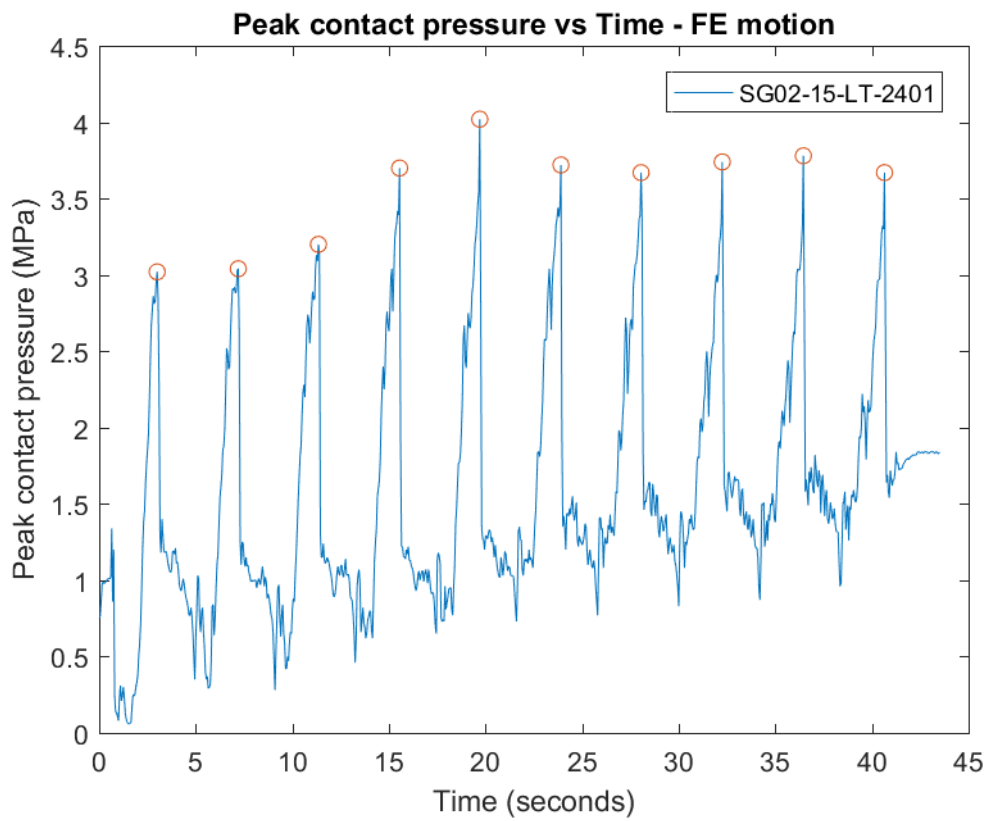
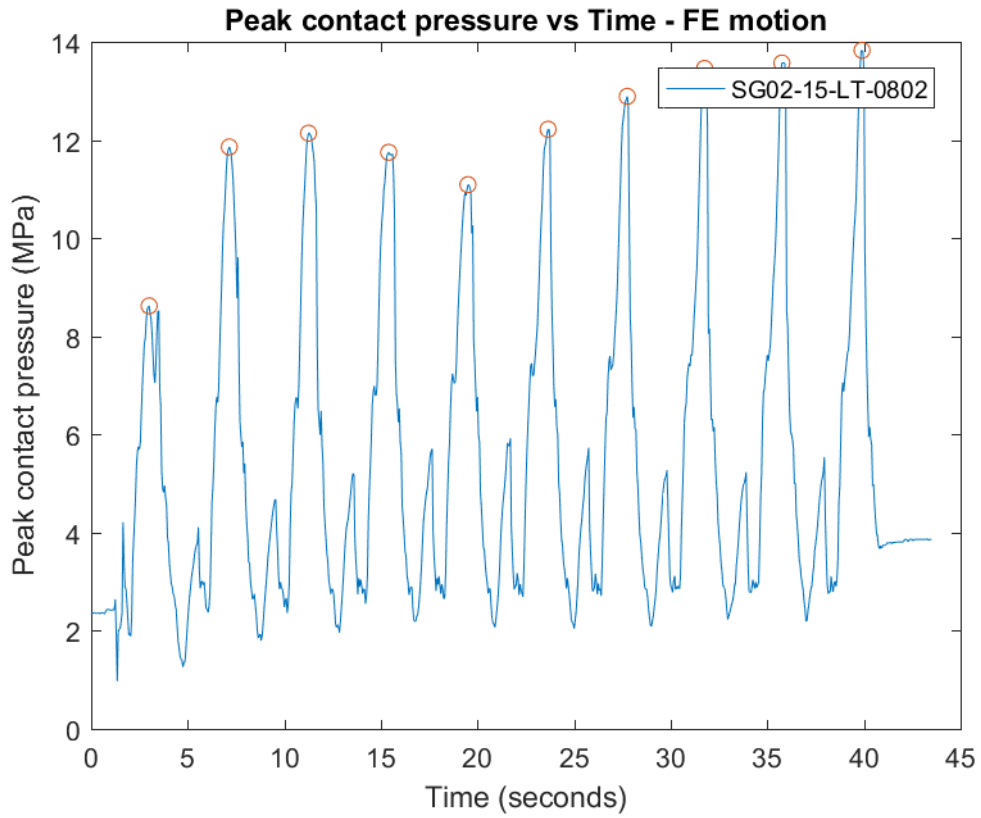


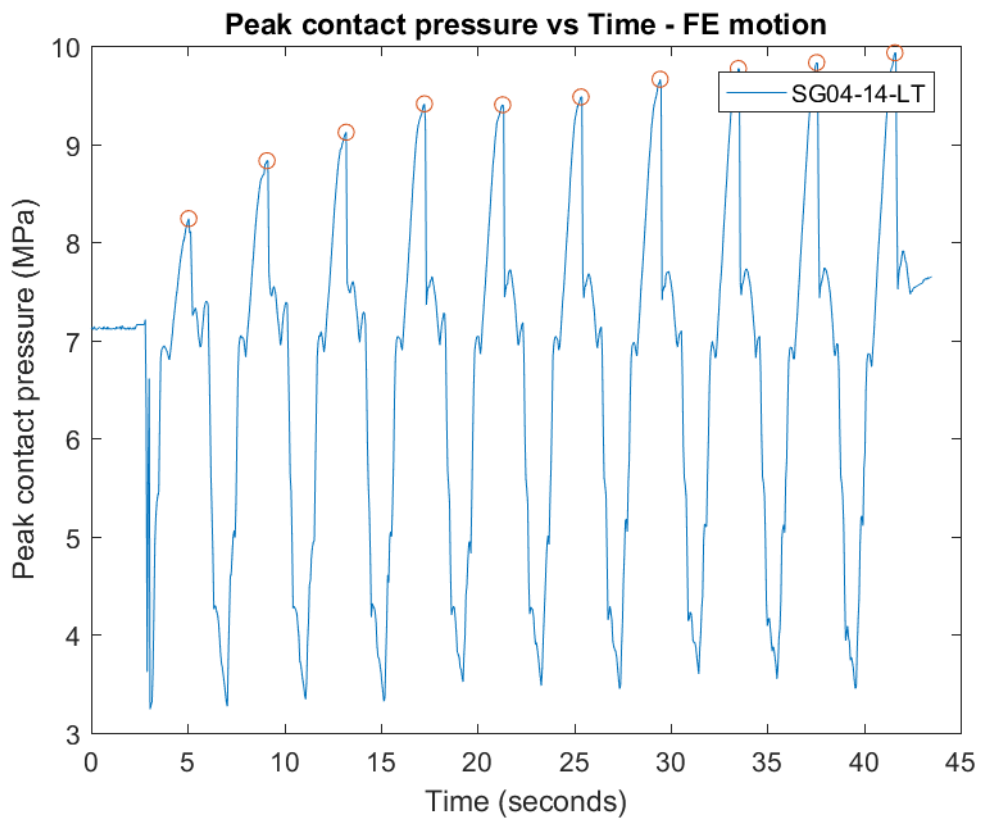
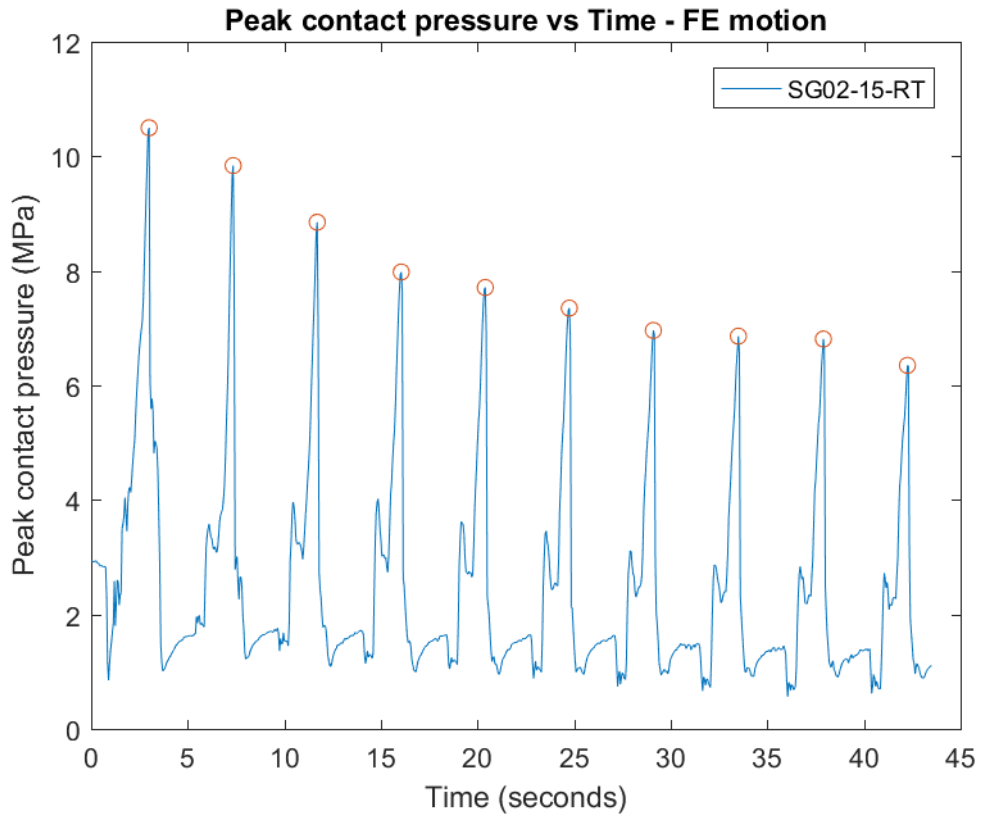


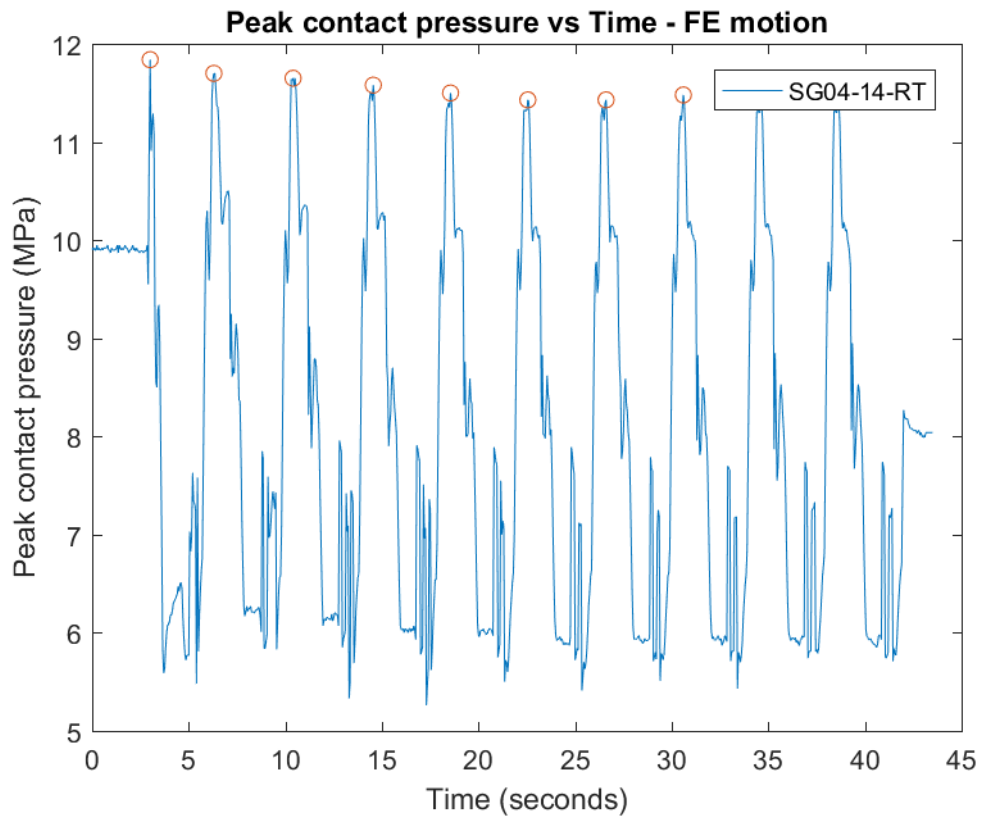


iii. Flexion-Extension Motion: Phase 1

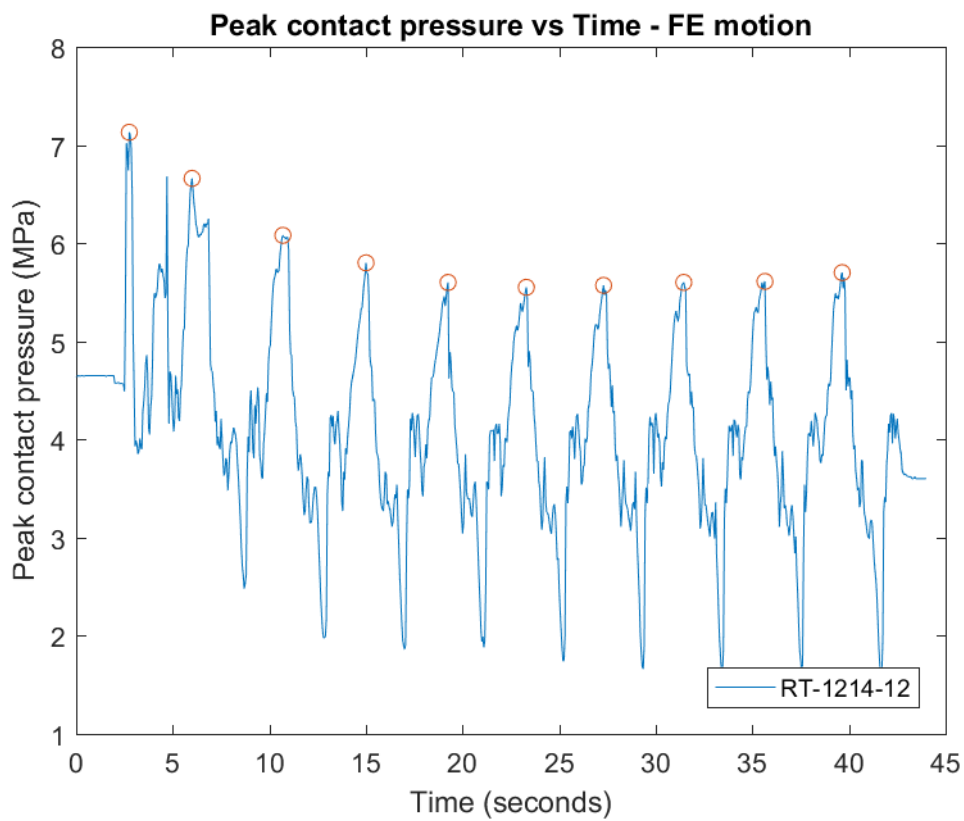
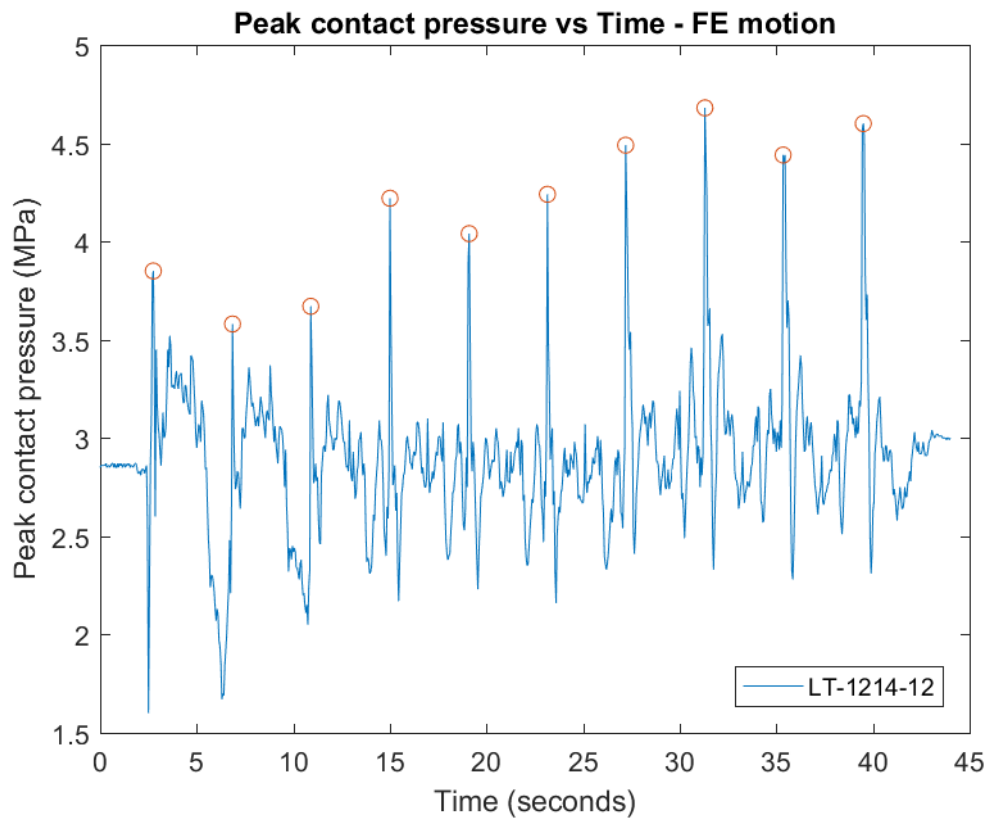


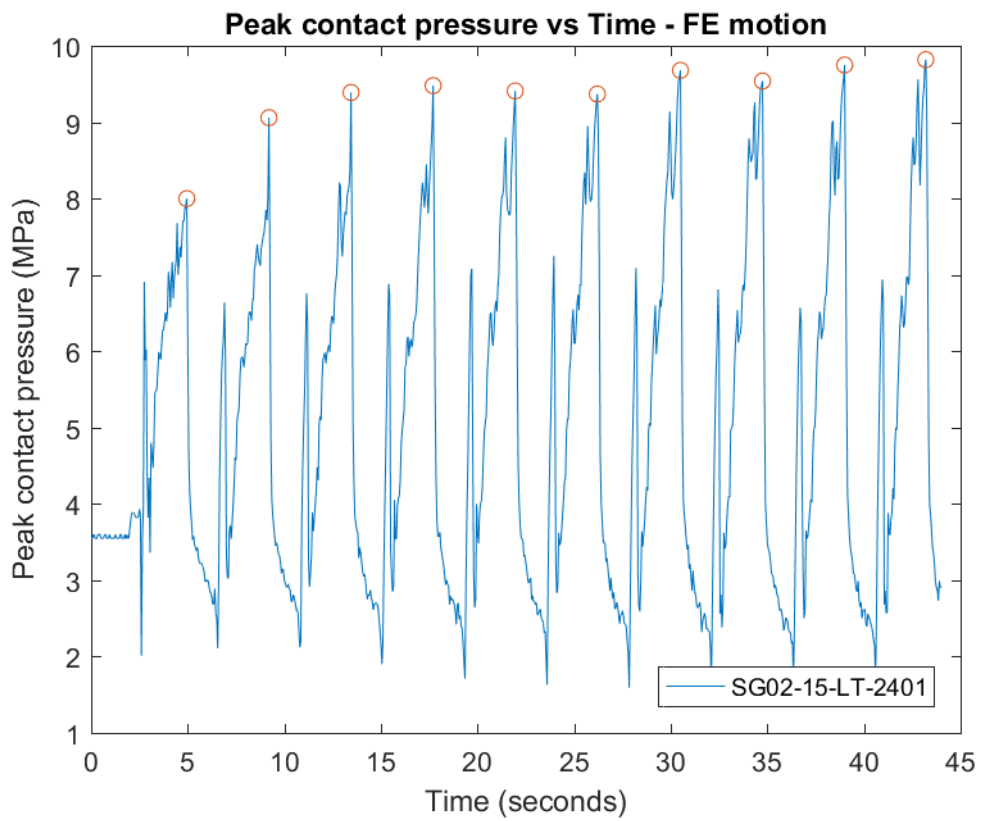
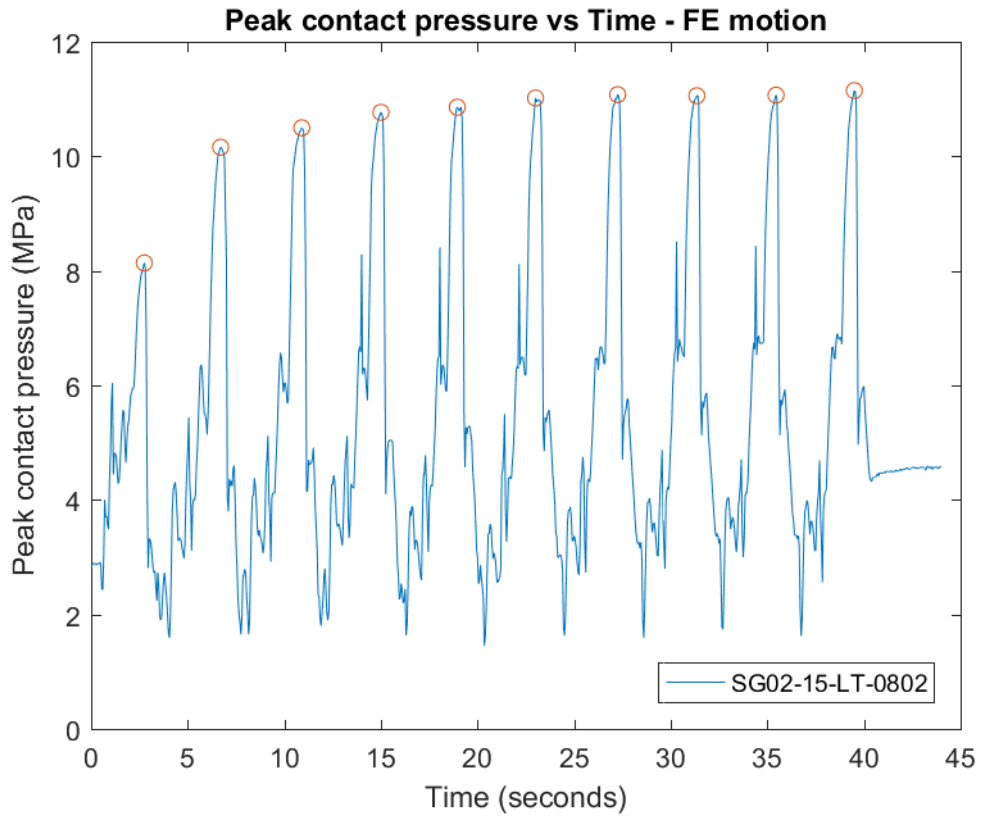


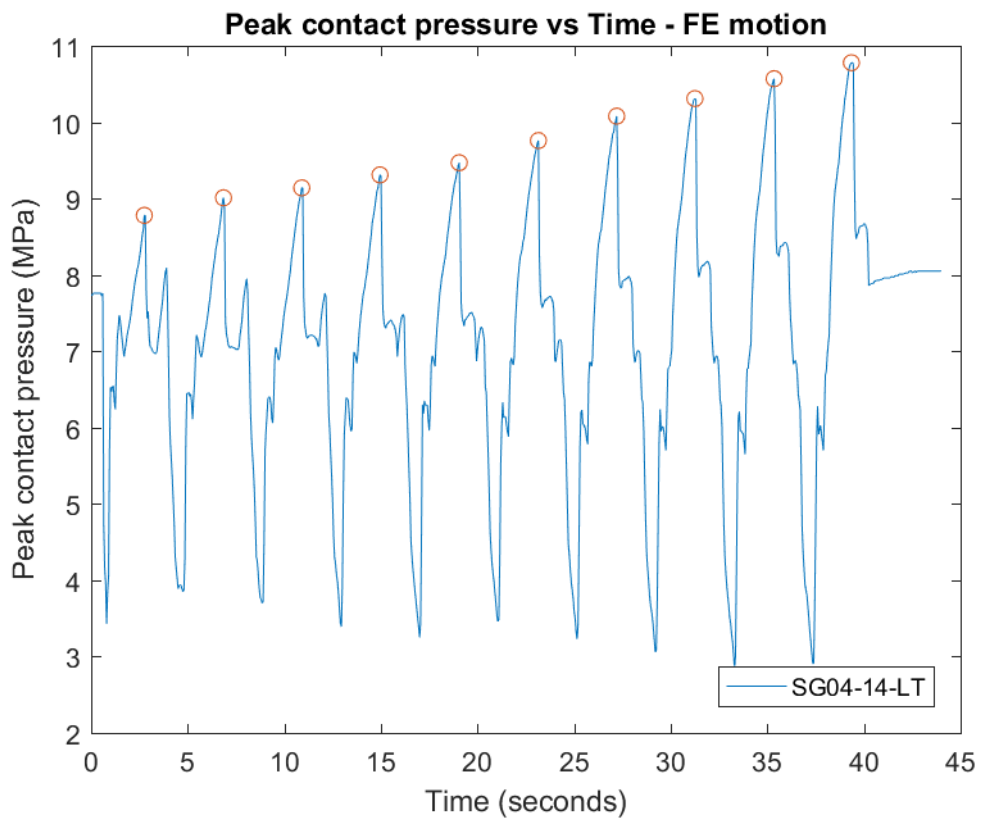
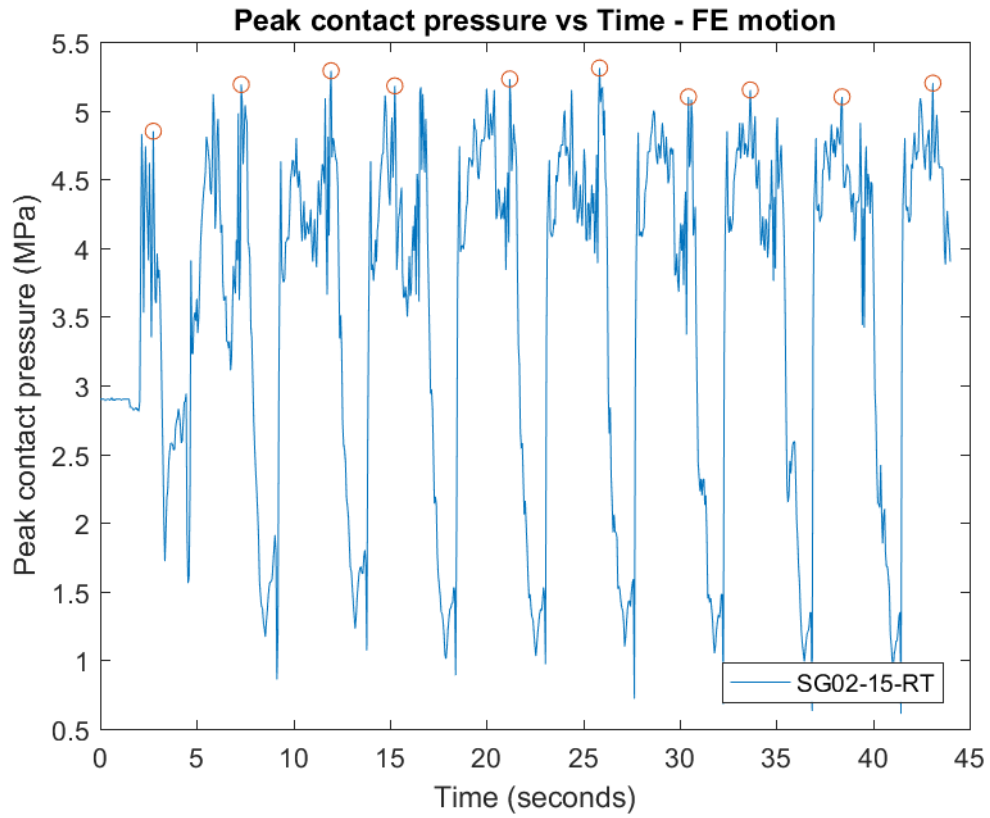


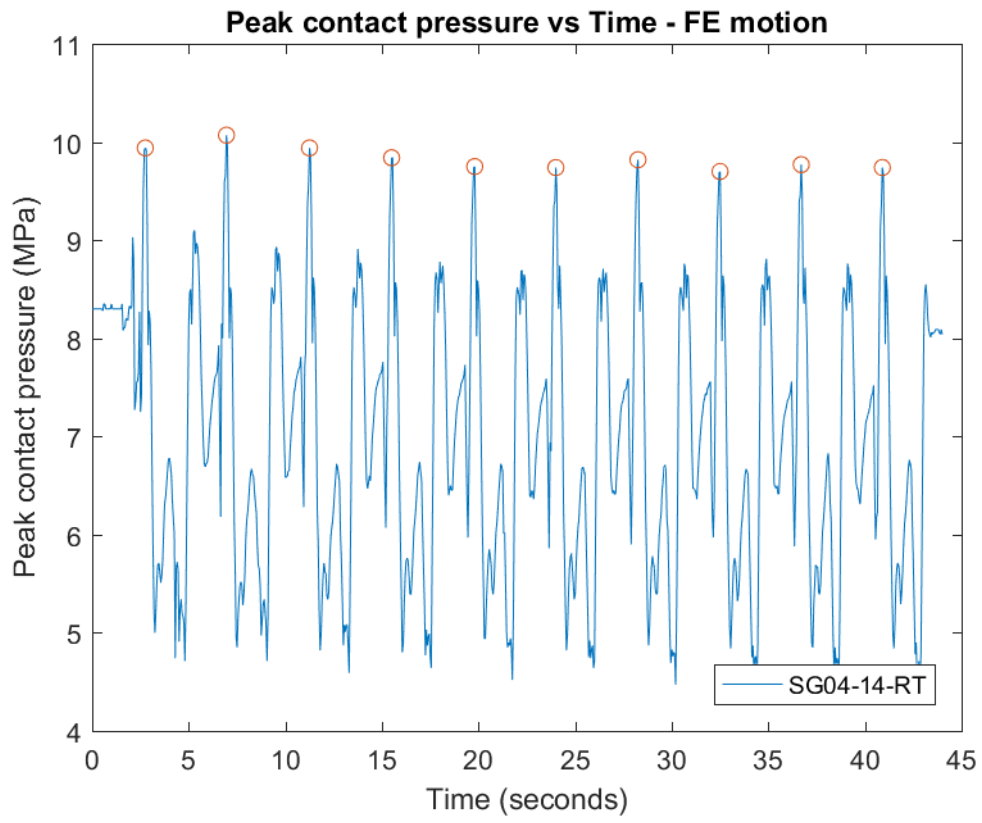


iv. Flexion-Extension Motion: Phase 3

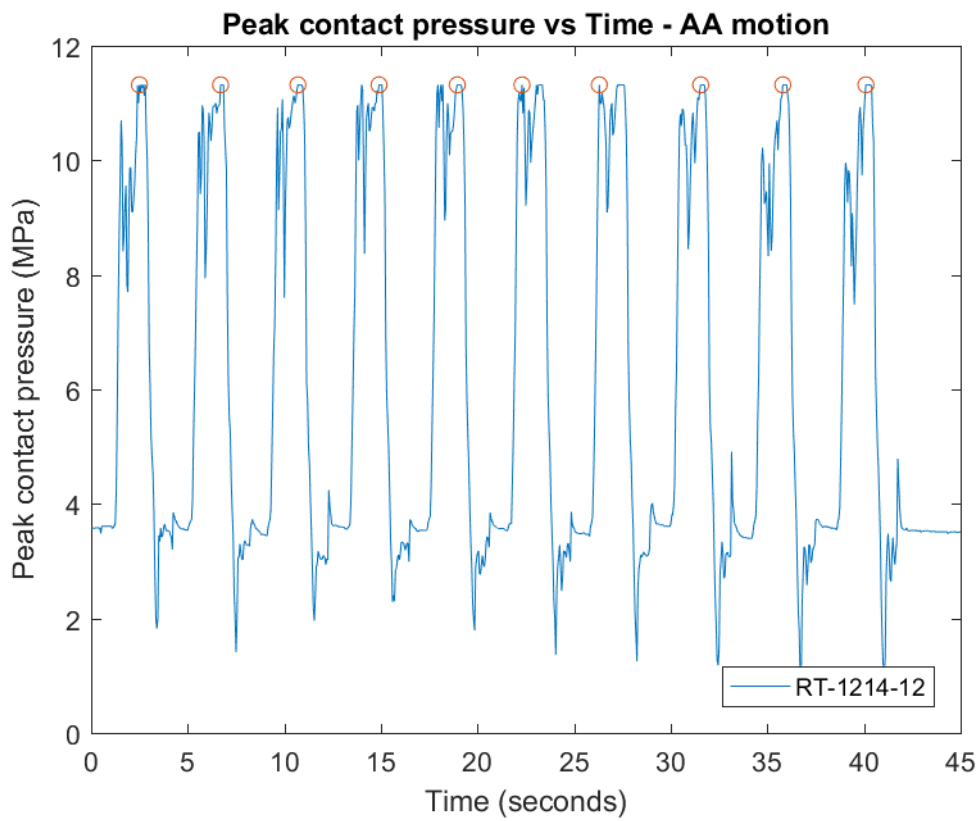
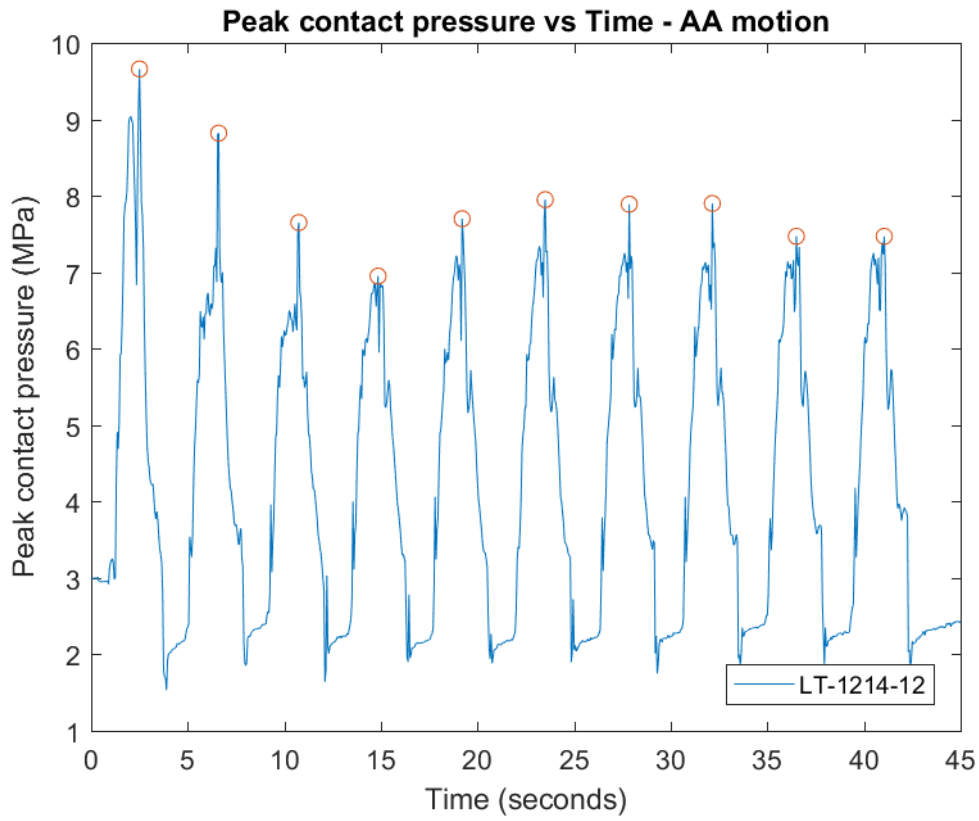


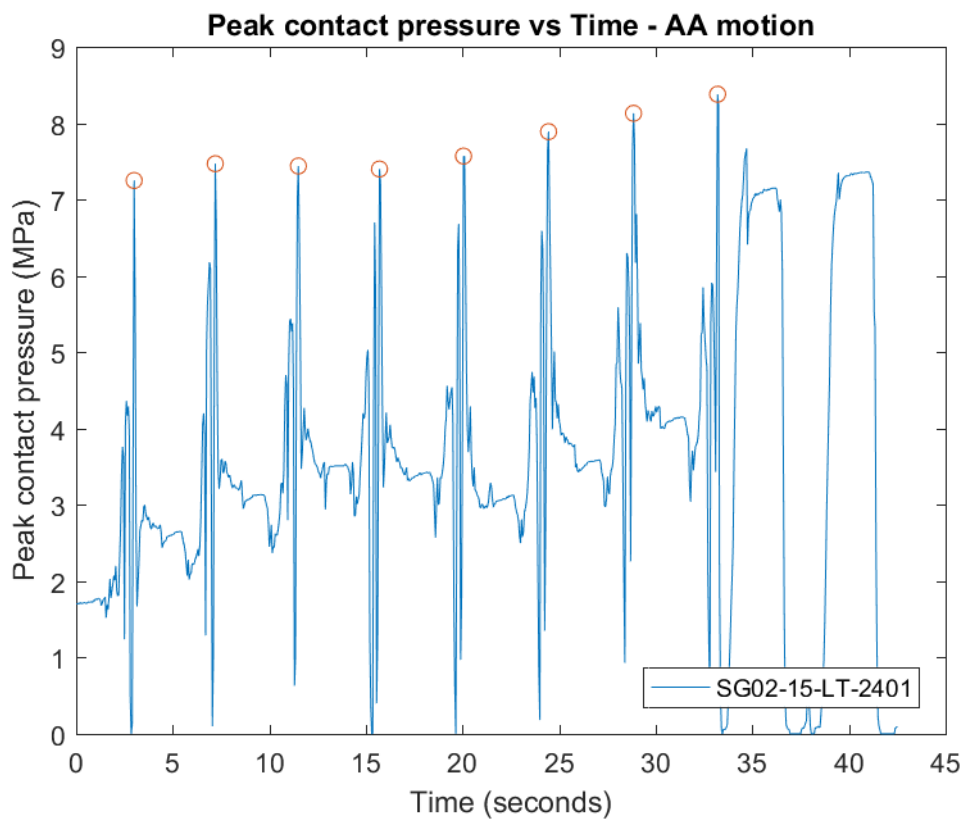
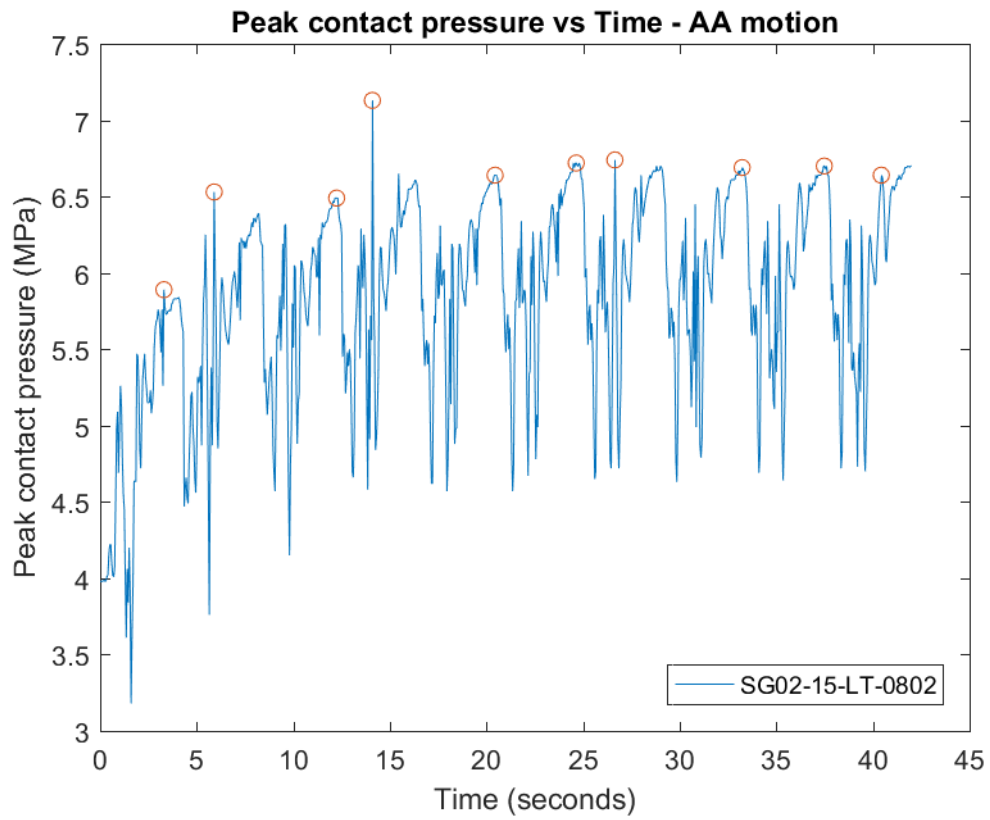


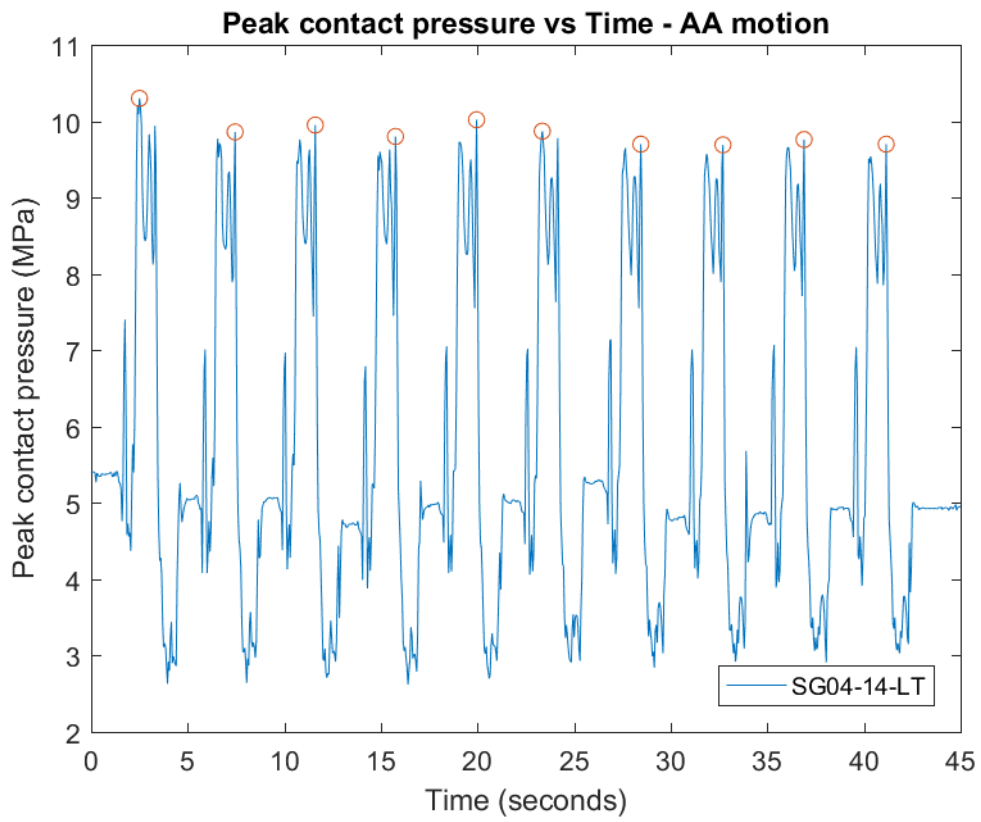
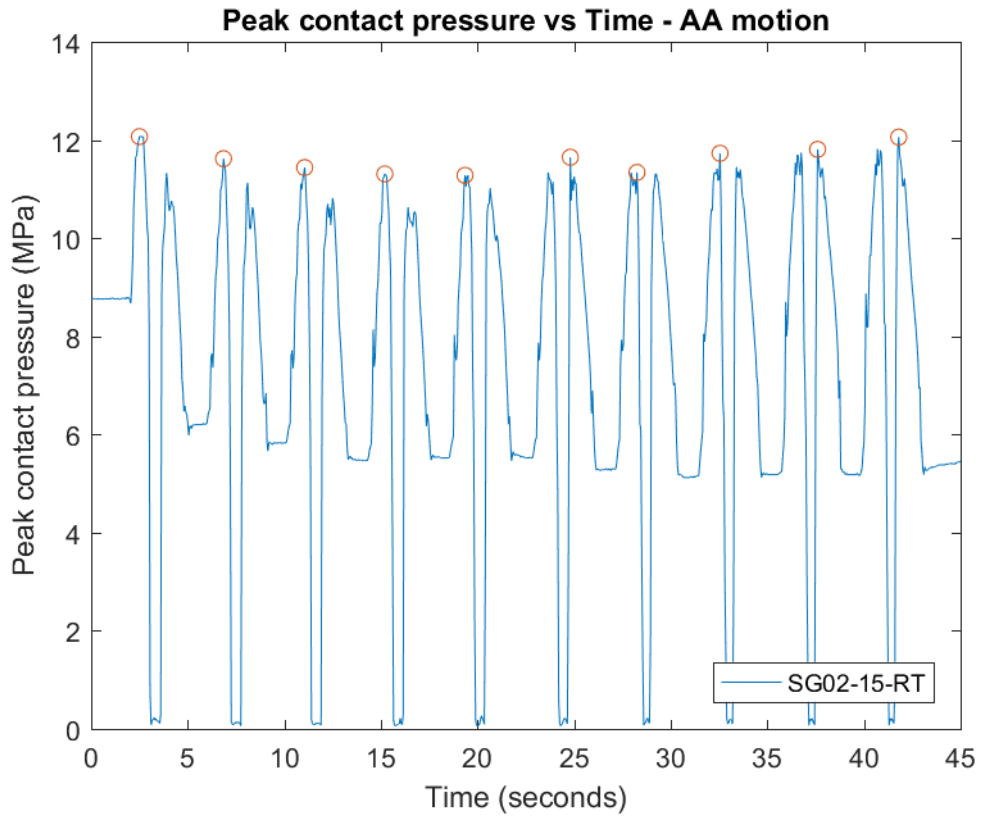


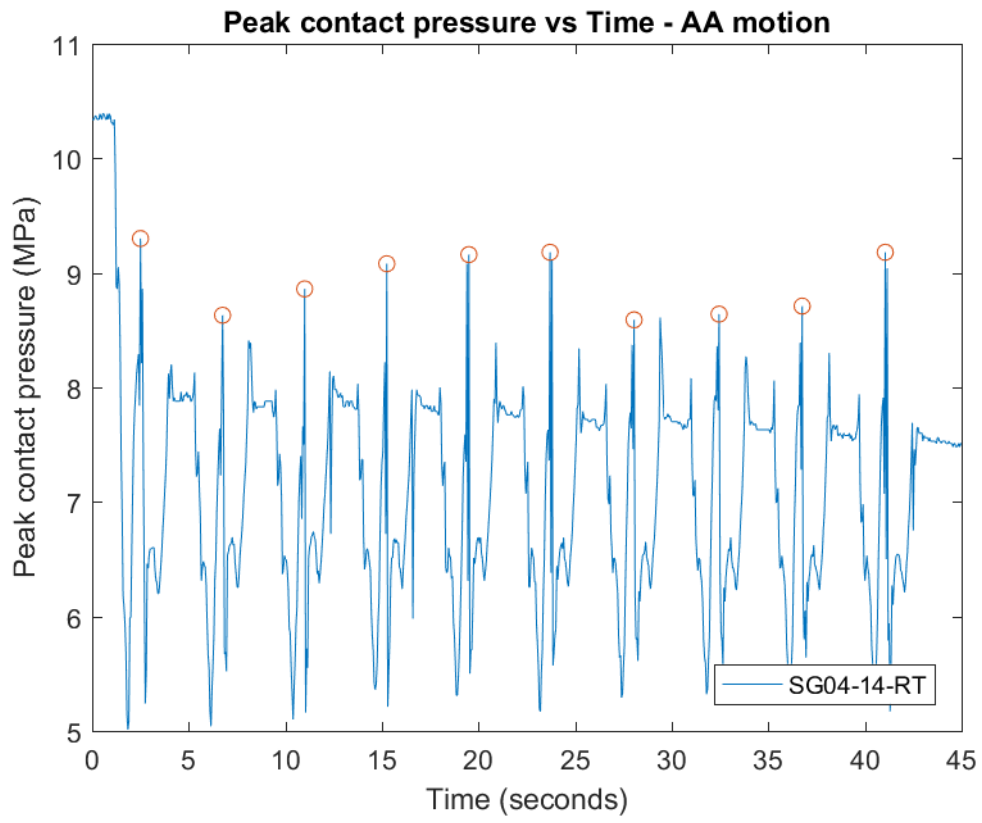


v. *Abduction-Adduction Motion: Phase 1*

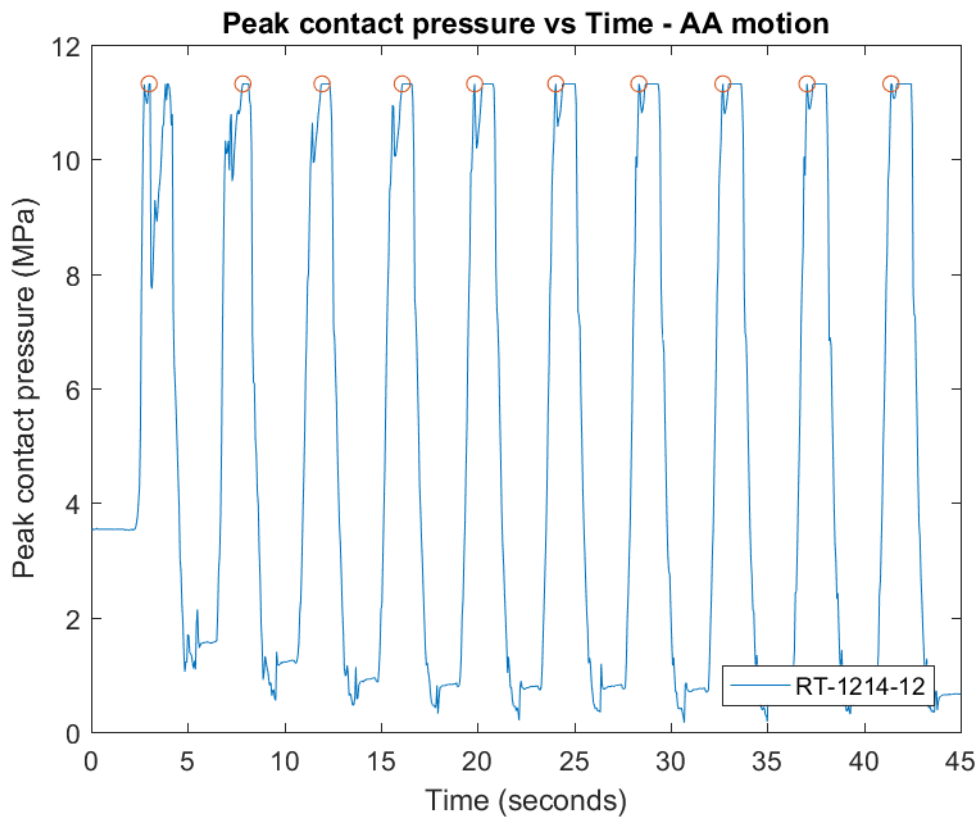
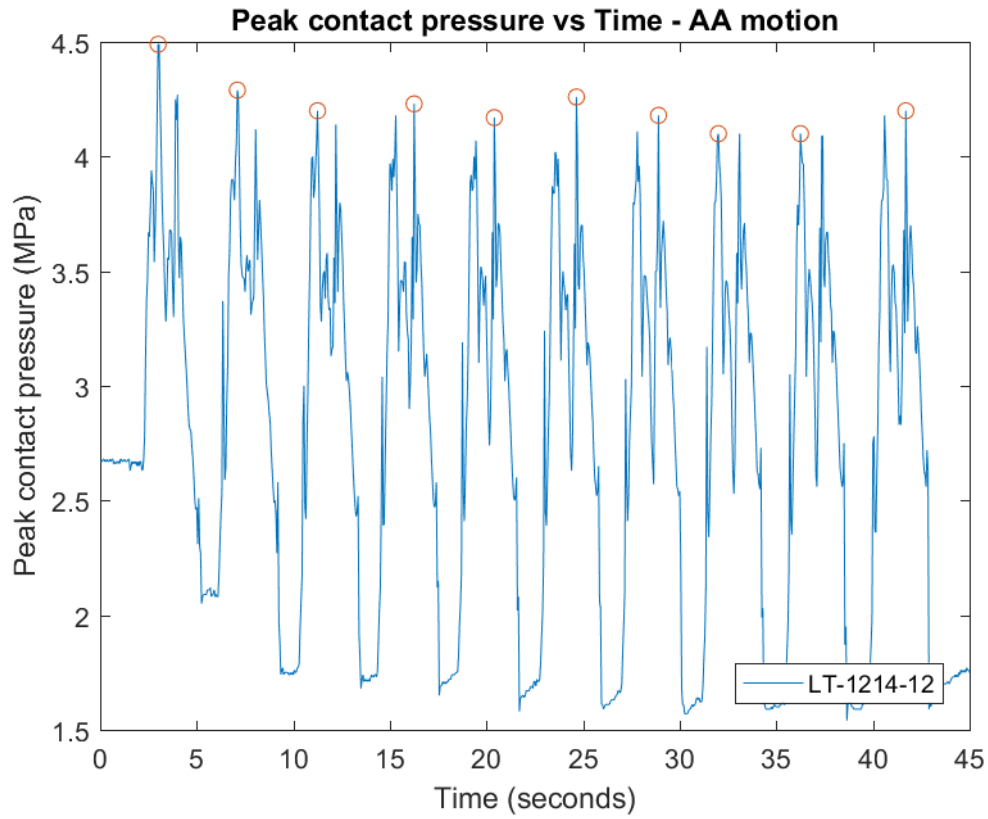


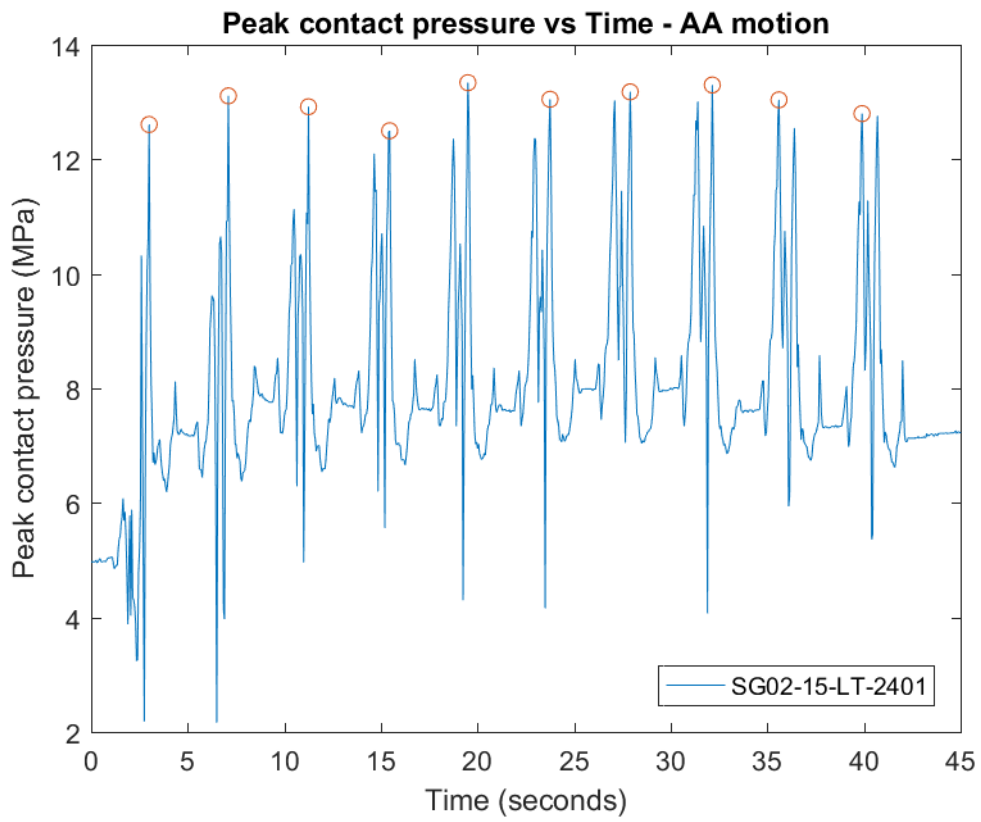
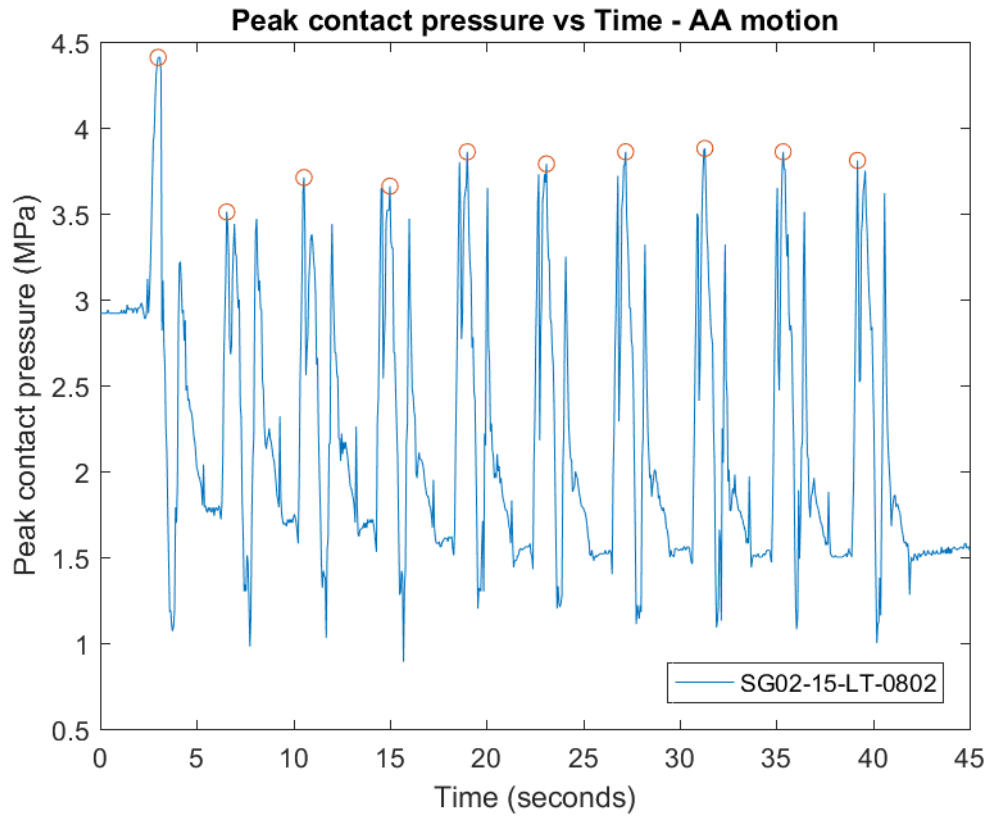


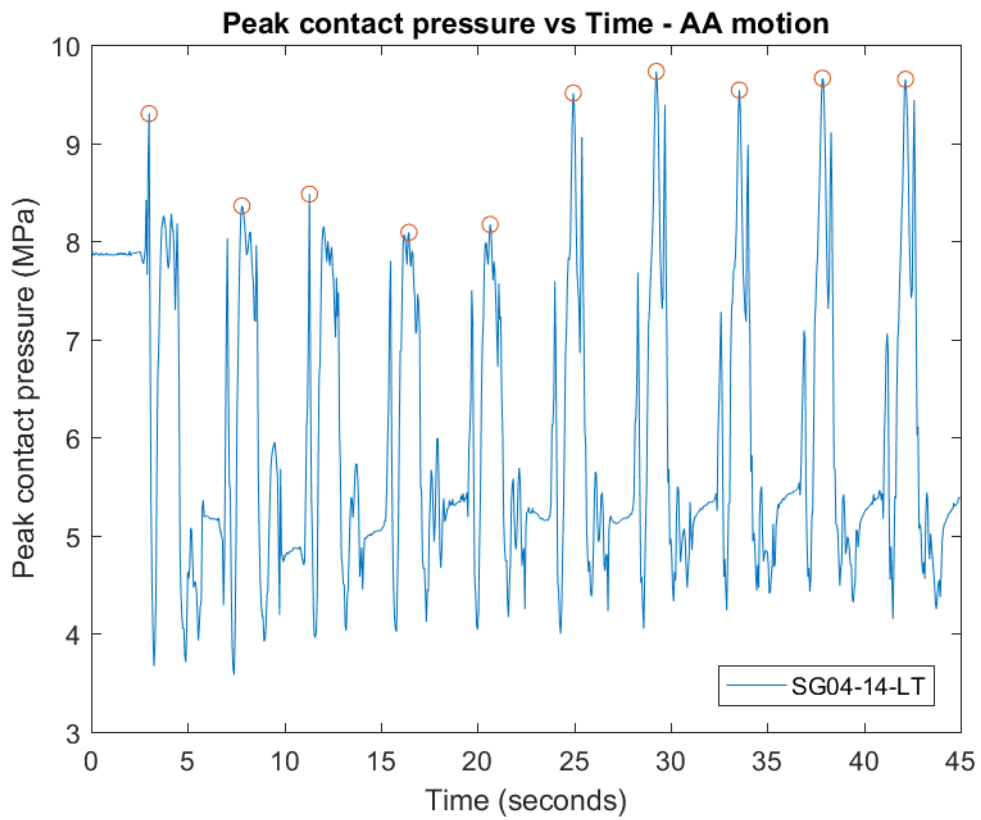
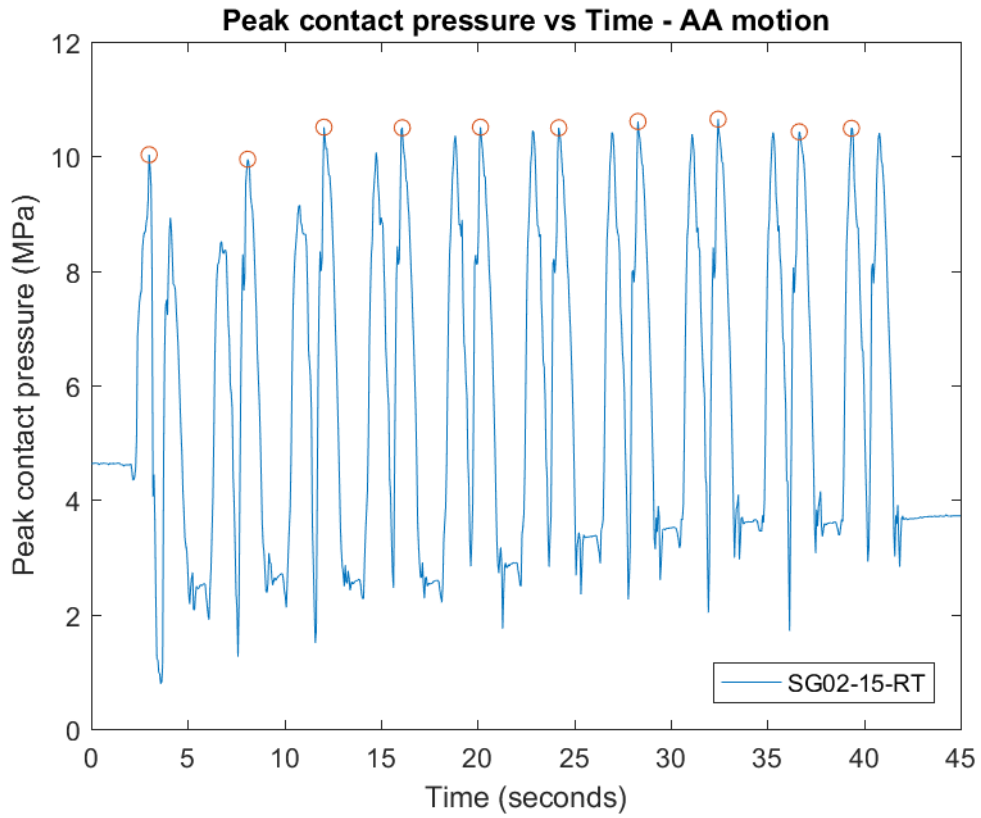


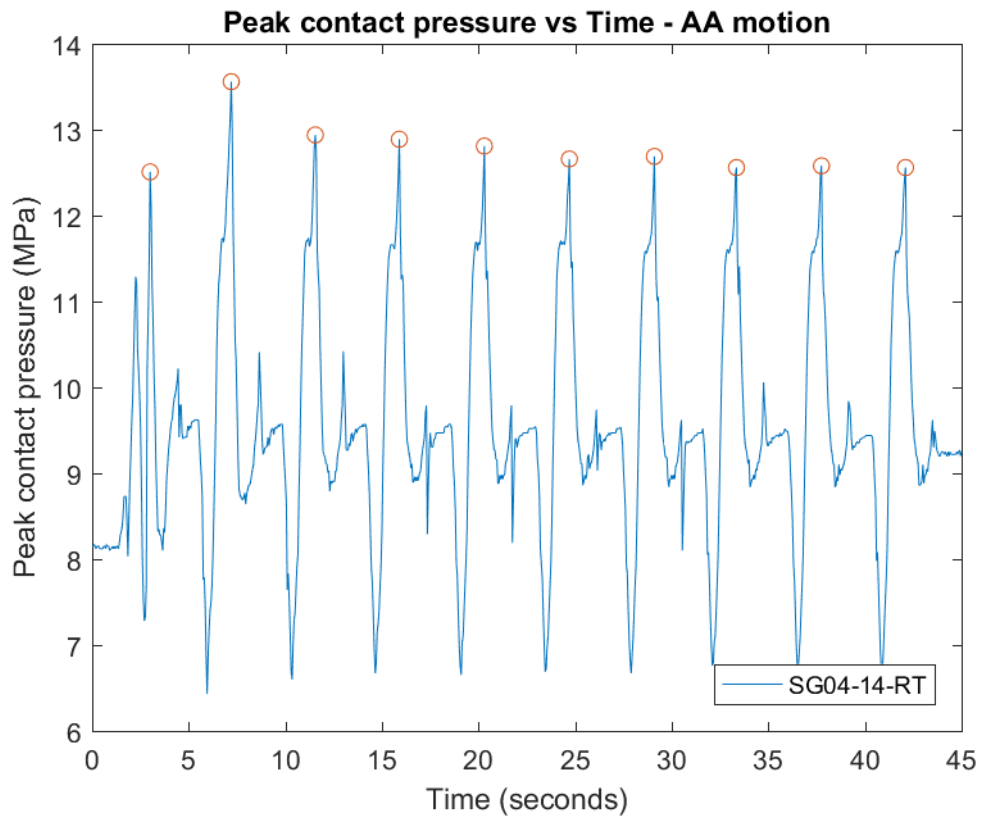


vi. Abduction-Adduction Motion: Phase 3









Appendix JJ:

Pioneers of Shoulder Arthroplasty

1. Prof. Dr. Themistocles Gluck (1853-1942)



Figure 1: Prof. Dr. Themistocles Gluck (1853-1942), the first arthroplasty surgeon, (DOI: 10.1007/s11999-011-1836-8) & (DOI: 10.1007/s11999-011-1837-7).

Original Texts Abstracted Without Modifications:
(DOI 10.1007/s11999-011-1837-7) & (DOI 10.1007/s11999-011-1836-8)

1.1. Biography;

The innovative and brilliant German surgeon, Themistocles Gluck, was born in Iasi, Moldavia (now, in Romania) in 1853. His well-known father was an attending physician for the royal family during a period when there was a large ethnic German population in the region. Gluck began his university studies in Leipzig in 1873, studying under the Swiss Anatomist, Wilhelm His, and continued his medical studies in Berlin in 1875. His professors in Berlin included Bernhard von Langenbeck (founder in 1860 of von Langenbeck's Archiv für Klinische Chirurgie, now Langenbeck's Archives of Surgery) and

the eminent pathologist, Rudolf Virchow. Gluck was evidently an excellent student and won a prize for research on nerve regeneration that he had conducted under the supervision of Virchow. He completed his degree in 1882, but, according to Eynon-Lewis et al., was unable to continue a university career because von Langenbeck retired and his replacement, von Bergmann, evidently found no position for him. He returned to his homeland and worked for a short time in Bucharest, but then practiced industrial medicine in Berlin until 1890, when he was appointed as head of surgery at the Emperor and Empress Friederich Paediatric Hospital [1.2.1].

Gluck had a remarkable career and was judged by Eynon-Lewis et al. as an “unrecognized genius”. He was most likely the first to implant artificial joints in the 1880s. According to Surin, he was responsible for many other remarkable concepts and developments: stress shielding, joint allografts (although he reportedly never performed any such transplants), intramedullary fixation (with ivory cylinders), biocompatibility (again, with ivory, a material he considered better than others). His interest in bone defects was almost certainly encouraged by his work as a wartime surgeon in the Balkans in 1877 and 1885, during which he first successfully used steel plates to fix a broken femur and replace part of a mandible. He also experimented with bone cements, including copper amalgam, plaster of Paris, and a stone putty (resin with pumice or gypsum). Thus, he antedated 20th Century pioneers, such as Haboush (1953), Wiltse (1957), and Charnley (1964), in the use of implantable cements by more than 50 years. He described a number of surgical procedures for the larynx, trachea, lung, and inguinal hernias. It is interesting to note that he performed vessel sutures and venous grafts in the 1880s, which predated by many years the work of the American surgeon Alexis Carrel who received the Nobel prize for vascular repair in 1912. He anticipated Küntscher’s popularization of intramedullary fixation of fractures by 50 years. Gluck’s pioneering work was often dismissed, but in his later life he

was honored for his accomplishments, being listed on the honor roll of the German Surgical Society. Gluck died at age 88 in Berlin in April 1942 [1.2.1].

The earliest dates of his implantations of artificial joints are variously reported as the mid-1880s to 1890. Gluck believed that preliminary animal experiments were essential, and implanted his ivory devices in animals before attempting them in humans. In May 1890, Gluck inserted a hinged ivory joint into the knee of a 17-year-old girl; this design was not dissimilar from those of the early constrained total knee arthroplasty prostheses introduced in the second half of the 20th Century. He reported performing 14 arthroplasties in that year, including a hip, but only provided details on five cases: three knees, a wrist, and an elbow. The procedures appeared successful over the short term; however, all of the five patients in the report suffered from tuberculosis, and all developed complications because of the chronic infection. Three of the five prostheses were removed (the wrist and one of the knees were left in situ). He later realized that prior joint infection was a contraindication to joint arthroplasty [1.2.1].

In order to help those in attendance better visualize his concepts, Gluck apparently fitted a human skeleton with his artificial joints, including a hip, knee, ankle, wrist, elbow, and shoulder. According to Eynon- Lewis et al., von Bergmann, forbade him from presenting his results: he wrote to Gluck, "As the leader of German surgery I cannot allow that you discredit German science in front of a platform of international surgical specialists. My pupils and I will fight you with all means." The most lasting evidence of his work, the display he created, reportedly became known as "The Skeleton of Paris" and was shown in multiple venues around Europe until it, along with the rest of the Berlin Medical Collection, was taken to the Soviet Union by the Red Army after World War II [1.2.1].

Gluck had no overly optimistic view of surgery of the day: "Surgery on the whole retains a destructive character, but despite this unavoidable aspect, this last decade has brought to full blossoming and development, conservative and reparative approaches." He realized that part of the success of his operations had to do with the biological reactions to his implants. He anticipated wear of the parts. He observed the immediate pain relief after fixation: "In clinical cases, it is surprising that besides the immediate functional effect, the part has been absolutely free of pain immediately after the surgery. There is a total lack of fracture pain because of the absence of motion of the fragment." He had a humanitarian view: "...going through life, the surgeon is always motivated and guided by the wish to alleviate suffering and to avert danger and on occasion is encouraged, by means of a new interpretation of known scientific facts, usually not previously discussed and therefore not utilized for a long time and facts with meaning that should not be underestimated." Presciently, Gluck commented; "We can certainly make the observation in medicine, as often also in other scientific disciplines, that certain facts have been known as such for a long time before their value is truly recognized." Although today he is largely unrecognized, we should appreciate that his accomplishments in the field of endoprostheses alone should enable him to be remembered as the first "arthroplasty surgeon." [1.2.1].

1.2. References

- 1.2.1. Brand A. MD, Mont M. MD, Manring M. PhD. *Biographical Sketch: Themistocles Gluck (1853-1942)*. *Clin Orthop Relat Res*. 2011 Jun; 469(6): 1525-1527.

2. Dr. Jules-Émile Péan (29 Nov. 1830 – 20 Jan. 1898)



Figure 2: Jules-Émile Péan (29 Nov. 1830 – 20 Jan. 1898), ([https://en.wikipedia.org/wiki/Jules-Émile Péan](https://en.wikipedia.org/wiki/Jules-Émile_Péan)).

**Original Texts Abstracted With Slight Modifications:
(Wikipedia & Faqs.org/Health)**

2.1. *Biography:*

Dr. Jules-Émile Péan (29 November 1830 – 20 January 1898) was one of the great French surgeons of the 19th century [2.2.1] and one of the founders of modern gynecology, Pean was so famous in his homeland for his advances in gynecological surgery and other innovations, so that Henri Toulouse-Lautrec (1864-1901) painted the surgeon's portrait [2.2.2].

Péan was born in 1830 in Chateaudun, in France [2.2.1] [2.2.2]. He studied at the college of Chartres and then studied medicine at age 19 at the university of Paris under Auguste Nélaton [2.2.1] [2.2.2], where he insisted on using aseptic surgical techniques throughout the 1850s despite his colleagues' general lack of concern about this crucial factor [2.2.2]. He disputed the discoveries of Louis Pasteur and refused to dissect corpses and operated preferably in residence. He was appointed a doctor in 1861 and worked at St. Antoine and

St. Louis up to 1893. He then created with his expenses the international hospital [2.2.1].

*Pean wrote the first of his many books, *The Splenectomy*, in 1860. He was instrumental in developing the arterial clamp in 1862 [2.2.2]. He wrote two volumes of private clinics (1876 and 1890). He was elected to the French Académie Nationale de Médecine on November 22, 1887, and was awarded the rank of Commander of Legion of Honor in 1893 [2.2.1].*

Although a teacher, he was never named professor [2.2.1]. He was the first to perform a successful surgical ablation of one cyst of the ovary in 1864. He was also a pioneer in performing a vaginal hysterectomy for carcinoma in 1890. He is believed to have performed the first surgery to correct diverticula of the bladder in 1895. In 1893, he attempted the first known total joint arthroplasty, implanting in the shoulder of a French waiter in 1893; it had to be removed two years later due to infection [2.2.1] [2.2.2].

*In 1874, Pean was appointed chief of services at St. Louis Hospital. He wrote *The Elements of Pathological Surgery* the following year, *Lessons in Clinical Surgery* in 1876 [2.2.2], and in 1877 a book on the use of hemostatic forceps, which he had invented in 1868 [2.2.1] [2.2.2]. He died on January 20, 1898 in Paris. A street, Rue Péan, in Châteaudun was named after him [2.2.1] [2.2.1].*

2.2. References:

2.2.1. (https://en.wikipedia.org/wiki/Jules-Émile_Péan)

2.2.2. (<http://www.faqs.org/health/bios/85/Jules-mile-Pean.html>)

3. *Dr. Charles S. Neer MD (1917-2011)*



Figure 3: Dr. Charles S. Neer, II, MD (1917-2011), (Reprinted by Permission from the American Shoulder and Elbow Surgeons) (DOI: 10.1007/s11999-011-1943-6) & (DOI 10.1007/s11999-011-1944-5).

Original Texts Abstracted Without Modifications:
(DOI: 10.1007/s11999-011-1944-5) & (DOI: 10.1007/s11999-011-1943-6)

3.1. *Biography:*

Dr. Charles Neer, II, was born and raised in Vinita, Oklahoma in 1917, the son and grandson of physicians. He graduated from Dartmouth College and obtained his MD degree from the University of Pennsylvania. He began a residency at Presbyterian Hospital, New York City, but his training was interrupted by WWII, where he served in three theaters. After the war, he returned to Columbia University to complete his residency, and then joined the faculty, where he remained throughout his career. He retired as an Emeritus Professor in 1990 and returned to his hometown [3.2.1].

Dr. Neer was a prolific writer, having published his first paper on hip fractures in 1948, and his last full paper in 1992. While he wrote on many topics, the majority related to the shoulder. In 1968, Dr. Neer organized a symposium for CORR titled "The Clavicle". Those papers reviewed the development and anatomy of the clavicle, and the treatment of various injuries. He was a founding member and the first president of the American Shoulder and Elbow Surgeons in 1982, and served on the American Board of

Orthopaedic Surgery, the Board of Trustees of The Journal of Shoulder and Elbow Surgery, and the International Board of Shoulder and Elbow Surgery. Among his best-known works is a classification of shoulder fractures reported in 1970 and still widely used today. However, he made many other contributions, including an understanding of the impingement syndrome and a procedure to alleviate the impingement. One of his legacies is the large number of individuals he trained, many of whom actively contribute to orthopaedic surgery in general, and shoulder surgery in particular [3.2.1].

Neer was a pioneer in shoulder arthroplasty, and developed the first practical and widely used prosthesis for the shoulder. (Gluck in 1891 and Péan in 1897 reported the use of shoulder arthroplasty, but neither of their approaches appear to have been subsequently used by others.). Neer described his rationale: Patients with comminuted fractures of the proximal humerus treated by open reduction and internal fixation, or resection arthroplasty, or arthrodesis all had “unsatisfactory” outcomes. He reasoned replacement of the humeral articular surface provided better pain relief and function, and designed a device and surgical technique for implantation. Neer reported 12 patients in his initial series, all of whom had acute or long standing “extra-articular extrusion and detachment of the humeral head or a long-standing painful incongruity of the humeral articulation.” Eleven of the 12 patients had pain relief, the exception being a patient with “improper seating of the prosthesis.” [3.2.1].

3.2. References:

- 3.2.1. Brand R. MD, Bigliani L. MD. Biographical Sketch; Charles S. Neer, II, MD (1917-2011) *Clin Orthop Relat Res.* 2011 Sep; 469(9): 2407-2408.

4. Prof. Dr. Paul-Marie Grammont (1940-2013)



Figure 4: Prof. Dr. Paul Grammont is shown in 2011, (Photographs courtesy of Dr. Grammont) (DOI: 10.1007/s11999-011-1959-y) & (DOI 10.1007/s11999-011-1960-5).

Original Texts Abstracted Without Modifications:
(DOI: 10.1007/s11999-011-1960-5) & (DOI: 10.1007/s11999-011-1959-y)

4.1. *Biography:*

Paul Grammont was born on April 1940 in Salins-les-Bains, in the northeastern part of France. His father was a teacher and his mother, who chose to raise the children, was trained as a physicist. During his primary and secondary school years, he lived in various cities as his father taught in different schools. After graduation from secondary school, he began medical studies in Lyon. Very quickly he became interested in surgery, and more specifically in orthopaedic surgery. He first became the fellow and then assistant of Professor Albert Trillat, head of the orthopaedic department in Lyon that was particularly well-known for knee and shoulder surgery. He did his military service overseas, in French Guiana where he had the opportunity to operate on many difficult cases. Encouraged by Albert Trillat, he became a Professor of Orthopaedic Surgery and Traumatology in 1974 at the age of 34. He then moved to Dijon in eastern France, where he became the Chairman of the Orthopaedic Department of the University Hospital [4.2.1].

While he had few laboratory resources, he was a skilled handyman and began many of his biomechanical experiments on the knee and the shoulder in his own garage before having the opportunity to work in the anatomical and biomechanical labs in the Medical University of Dijon. Grammont was creative: besides developing the reverse shoulder prosthesis, he also developed an early patellofemoral prosthesis and one of the first nails with a self-advancing mechanism designed to lengthen long bones like the tibia and the femur (Albizia nail). In 1997, at 57-years-old and in the prime of his career, he had a stroke with right hemiplegia and aphasia. Despite residual deficits, he remained active with carpentry and plumbing in his home, and began a second career as a painter using his left hand. He used to travel with his wife, Françoise. His successors in Dijon have stayed faithful to his teachings. [4.2.1]. Prof. Paul-Marie Grammont died on March 30th, 2013 [4.2.2].

In 1985, Grammont designed a reverse prosthesis for arthritic shoulders with severe destruction of the cuff, in which standard anatomic prostheses could not solve the problem of restoring both joint stability and mobility. He published his first paper on the reverse prosthesis in the French literature in 1987. Six years later, in 1993, he summarized the results of his biomechanical studies in English language. The concept of the reverse prosthesis developed by Grammont was a major step forward in the field of shoulder arthroplasty. Previous constrained prostheses (ball and socket or reverse ball and socket designs) all failed because their center of rotation remained lateral to the scapula, which limited motion and produced excessive torque on the prosthesis-bone interface of the glenoid component, leading to early loosening [4.2.1].

The reverse shoulder prosthesis designed by Grammont, unlike any previous reverse ball and socket design, introduced two major innovations which led to its success: (1) a large metal hemisphere with no neck on the glenoid side, and (2) a small polyethylene cup (covering less than half of the hemisphere),

oriented with a nonanatomic inclination of 155°, on the humeral side. This original and totally new design provided a fixed and medialized center of rotation, minimizing torque on the glenoid component, and aided the recruitment of more of the anterior and posterior deltoid to act as abductors. Furthermore, the humerus was lowered in relation to the acromion, increasing the tension of the deltoid fibers. This retensioning of the deltoid, together with the improved lever-arm for the abduction of the anterior and posterior deltoid, allowed the deltoid to compensate for the absent or deficient rotator cuff muscles. In fact, Grammont's reverse prosthesis imposed a new biomechanical environment for the deltoid muscle. The first generation of the Grammont reverse prosthesis had a large sphere all-cemented on the glenoid side and an all-polyethylene flute on the humeral side. The second generation (Delta reverse prosthesis, DePuy Inc., Warsaw, IN) has been used in France since 1997 and gained increasing popularity throughout Europe. Despite the encouraging early results in Europe, FDA approval for the Delta III prosthesis was not acquired until 2003 in the United States [4.2.1].

The Grammont reverse prosthesis offers a new surgical option in several situations where the rotator cuff and/or the proximal humerus are destroyed or absent, and where previously only limited options were available. Such indications include shoulder pseudo-paralysis due to a massive and irreparable cuff tear with or without osteoarthritis, severe fracture sequelae, failed prosthesis, and tumor surgery [4.2.1].

4.2. References:

- 4.2.1. Boileau P. MD. Biographical Sketch; Paul M. Grammont, MD (1940). *Clin Orthop Relat Res.* 2011 Sep; 469(9): 2422-2423.
- 4.2.2. Baulot E. MD. Paul-Marie Grammont. *Orthopaedics & Traumatology: Surgery & Research*, 2013 Jul., (DOI: 10.1016/j.otsr.2013.07.011). (Service d'orthopédie-traumatologie, hôpital du Bocage, 14, rue Paul Gaffarel, BP 77908, 21079 Dijon cedex, France).

وَقَالُوا الْحَمْدُ لِلَّهِ الَّذِي هَدَانَا لِهَذَا وَمَا كُنَّا لِنَهْتَدِيَ لَوْلَا أَنْ هَدَانَا اللَّهُ
لَقَدْ جَاءَتْ رَسُولُ رَبِّنَا بِالْحَقِّ وَتُودُوا أَنْ تُلَكُمُ الْجَنَّةَ أُورَثْتُمُوهَا بِمَا كُنتُمْ
تَعْمَلُونَ

الحمد لله الواحد الأحد الذي أعانني على إتمام هذا العمل بعد أن حيل
بينى وبينه وسدت إليه الطرق وتقطعت بى الأسباب وظننت أن لا سبيل إلى
تحقيقه فله الحمد والمنة، رب السماوات ورب الأرض رب العالمين، سبحانه غالب
على أمره ولكن أكثر الناس لا يعلمون.

محمد محمود

منتصف ليلة الإثنين لثمان ليالٍ بقين من شوال لعام ١٤٣٨، الموافق ليلة

السابع عشر من يوليو/تموز لعام ٢٠١٧

ميونيخ ألمانيا

